

UNIVERSITY OF SOUTHAMPTON

FIELD STUDIES, ANALYSIS AND NUMERICAL MODELLING OF  
RETAINING WALLS EMBEDDED IN WEAK ROCK

by

Toby Hayward

A dissertation submitted for the degree of Doctor of Philosophy

Department of Civil and Environmental Engineering

December 2000

UNIVERSITY OF SOUTHAMPTON

ABSTRACT

FACULTY OF ENGINEERING

CIVIL AND ENVIRONMENTAL ENGINEERING

Doctor of Philosophy

**FIELD STUDIES, ANALYSIS AND NUMERICAL MODELLING OF  
RETAINING WALLS EMBEDDED IN WEAK ROCK**

**By Toby Hayward**

This research has generated a high-quality case record of wall movements, bending moments, temporary prop loads, and vertical contact stresses under the permanent stabilising base of a retaining wall embedded in weak rock (Bromsgrove Sandstone). The field data have been used to investigate suitable geotechnical parameters and models for use in the design of walls embedded in weak rock.

The work presented in this thesis comprises of four major areas:

- Field monitoring and interpretation of the performance of a case study retaining wall, located on the Coventry North-South Road.
- Comparison of geotechnical parameters obtained in different ways for the weak rock involved at the site.
- A series of analyses comparing the discontinuous and continuum approach to modelling retaining wall behaviour.
- Back-analysis of the monitored section of retaining wall.

The results of the work presented in this thesis show:

- The necessities of recording temperatures in the field, when the measurements being made are temperature sensitive.
- The selection of a design approach for a retaining wall in weak rock should depend primarily on the presence and nature of the discontinuities.
- From all the stiffness parameters obtained from the different test methods, it would appear that the most suited stiffness parameters for calculating wall movements and bending moments, are those derived from geophysical tests.
- The back analysis has suggested that the lateral earth pressure coefficient tends to move towards unity in the ground adjacent to the wall, during the construction of a bored pile wall. This is also the assumption used in many soil mechanics problems. It would appear that this assumption might also be used in weak rock problems, if wall installation is not modelled.
- For stabilising base retaining walls, it has been demonstrated that pre-loading the temporary props will help to reduce the wall movements into the excavation. However, pre-loading results in wall movements away from the excavation and greater bending moments during the construction phase. These impacts should also be taken into consideration at the design stage.

## ACKNOWLEDGEMENTS

I am extremely grateful to my supervisors, William Powrie and David Richards, for their help, encouragement and patience throughout this period of research.

I would also like to thank Harvey Skinner and TRL for their technical expertise and help with the installation and monitoring of the field instrumentation.

My thanks further extend to a great many others who have, in various ways and at various times, helped me over the last four and a half years at the University of Southampton, in particular Richard Harkness, Max Barton, Xing Zhang, Chris Clayton, and my family.

Finally, I owe an enormous debt of gratitude to my wife Helen whose love and support has kept me going throughout.

# LIST OF CONTENTS

**List of contents**

**List of figures**

**List of tables**

**Notation**

## **Chapter 1: Introduction**

1.1 Preface	1
1.2 Objectives	2
1.3 Structure of thesis	2

## **Chapter 2: Background**

2.1 Introduction	5
2.2 Weak rock in the geotechnical spectrum	6
2.3 Significance of discontinuities	10
2.4 Summary	15

## **Chapter 3: Case study – Coventry North-South road**

3.1 Introduction	17
3.2 Project details	18
3.3 Ground conditions	20
3.3.1 Geology	20
3.3.2 Discontinuities	22
3.4 Ground water	26
3.5 Geotechnical parameters	26
3.6 Construction sequence	26
3.7 Instrumentation	31
3.7.1 Wall movements	34
3.7.2 Wall and base bending moments	35

3.7.3 Temporary prop loads	36
3.7.4 Vertical contact stress beneath stabilising base	36
3.8 Results and discussion	37
3.8.1 Base line readings	37
3.8.2 Wall movements	37
3.8.3 Temporary prop loads	42
3.8.4 Wall and base bending moments	45
3.8.5 Vertical contact stresses beneath the stabilising base	55
3.9 Simple assessment of wall and base bending moments	60
3.10 Summary	61

#### **Chapter 4: Geotechnical parameters for weak rock at study site**

4.1 Introduction	63
4.2 Field <i>in situ</i> tests	64
4.2.1 Weak rock self boring pressuremeter tests	64
4.2.2 Geophysical tests	76
4.2.3 Standard penetration tests	79
4.3 Laboratory tests	80
4.3.1 Unconfined compressive tests	80
4.3.2 Direct shear tests	85
4.4 Laboratory results from site investigation	86
4.5 Original design values	88
4.6 Comparison and discussion of stiffness values	88
4.7 Summary	93

#### **Chapter 5: Modelling weak rock masses**

5.1 Introduction	95
5.2 Distinct element analyse (UDEC)	96
5.3 Programme of analyses	96
5.4 Geometry of numerical models	97
5.5 Input parameters	99
5.5.1 Weak rock & joints properties used in discontinuous analyses	99

5.5.1.1 Joint properties	100
5.5.1.2 Intact rock properties	101
5.5.2 Weak rock properties used in equivalent continuum analyses	101
5.5.3 Concrete	107
5.5.4 <i>In situ</i> stress state	108
5.6 Results of discontinuous analyses	108
5.7 Results of equivalent continuum analyses	108
5.8 Discussion	109
5.9 Summary	119
<b>Chapter 6: Back-analysis of the instrumented wall</b>	
6.1 Introduction	121
6.2 Finite element program CRISP	122
6.3 Selection of elements, boundary conditions & number of load increments	123
6.4 Idealised geometry for each construction phase	125
6.5 Selection of constitutive model	127
6.6 Input parameters	133
6.6.1 Structural components	134
6.6.2 Material properties	136
6.6.3 Ground water	138
6.6.4 <i>In situ</i> lateral stresses	138
6.7 Results of analyses	151
6.8 Construction sequence	159
6.9 Comparison of measured and back calculated stiffness	166
6.10 Comparison of measured and back calculated <i>in situ</i> earth stresses	170
6.11 Summary	173
<b>Chapter 7: Conclusions</b>	
7.1 Introduction	175
7.2 The objectives	176
7.3. Field monitoring	176
7.4 <i>In situ</i> field tests	177
7.5 Significance of results for engineering practice	178

7.6 Construction sequence effects	180
7.7 Further research	180
<b>8.0 References</b>	<b>182</b>

## LIST OF FIGURES

- Figure 2.1. The contribution of weathering to properties of geotechnical materials as the change from hard rock towards particulate soil
- Figure 2.2. ISRM classification for geotechnical materials
- Figure 2.3. Influence of scale on stability
- Figure 2.4. Approaches for analysis in weak rock
- 
- Figure 3.1. Location of instrumented section
- Figure 3.2. Cross section through monitored section of road
- Figure 3.3. Ground conditions at the instrumented cross section
- Figure 3.4. Weak rock debris clinging to face of the piles at the instrumented wall
- Figure 3.5. Typical jointing for the area
- Figure 3.6. Highly weathered Sandstone
- Figure 3.7. Highly weathered Mudstone
- Figure 3.8. Moderately weathered Sandstone
- Figure 3.9. Bulk excavation, leaving behind temporary earth berms
- Figure 3.10. Temporary props pre-loaded & earth berms excavated
- Figure 3.11. Stabilising base constructed & temporary props being removed
- Figure 3.12. Road open to traffic
- Figure 3.13. Cross section through field instrumentation
- Figure 3.14. Plan of instrument locations
- Figure 3.15. Change in distance at span between Bay W69 and E71
- Figure 3.16. Change in wall crest movements
- Figure 3.17. Development of lateral movements of the wall
- Figure 3.18. Change in axial load measured in temporary prop P1
- Figure 3.19. Change in axial load measured in temporary prop P2
- Figure 3.20. Typical change in axial load with temperature
- Figure 3.21. Development of wall bending moments at 1.73m below top of wall
- Figure 3.22. Development of wall bending moments at 2.73m below top of wall
- Figure 3.23. Development of wall bending moments at 3.73m below top of wall
- Figure 3.24. Development of wall bending moments at 5.03m below top of wall
- Figure 3.25. Development of wall bending moments at 6.33m below top of wall



Figure 3.26. Development of wall bending moments at 7.63m below top of wall  
 Figure 3.27. Development of wall bending moments at 9.43m below top of wall  
 Figure 3.28. Development of wall bending moments at 10.23m below top of wall  
 Figure 3.29. Development of wall bending moments at 12.03m below top of wall  
 Figure 3.30. Development of wall bending moments at 13.33m below top of wall  
 Figure 3.31. Development of wall bending moments  
 Figure 3.32. Change in bending moment in the stabilising base  
 Figure 3.33. Bending moments in stabilising base  
 Figure 3.34. Vertical contact stresses beneath the stabilising base  
 Figure 3.35. Typical change in cell pressure with temperature  
 Figure 3.36. Temperature corrected vertical contact stresses  
 Figure 3.37. Variation of vertical stress beneath the stabilising base with distance  
                     from the wall  
 Figure 3.38. Assumed vertical contact stresses  
 Figure 3.39. Comparison of measured and calculated base bending moments

Figure 4.1. Pressuremeter test data plotted as cavity pressure versus cavity strain  
 Figure 4.2. Shear modulus determined from pressuremeter tests  
 Figure 4.3. Unload/reload shear modulus plotted against cavity strain  
 Figure 4.4. Normalisation method  
 Figure 4.5 Normalised unload/reload shear modulus  
 Figure 4.6. Typical stress-strain data from weak rock self boring pressuremeter test  
 Figure 4.7. Typical stress-strain data from high pressure dilatometer test  
 Figure 4.8. *In situ* horizontal stresses  
 Figure 4.9. Geophysics shear modulus profile  
 Figure 4.10. Shear modulus determined from standard penetration tests  
 Figure 4.11. Influence of weathering on SPT shear modulus  
 Figure 4.12. Typical rock stress-strain curve  
 Figure 4.13. Reduction factor  
 Figure 4.14. Comparison of geophysical and intact stiffness values  
 Figure 4.15 Comparison of pressuremeter, intact and geophysical stiffness values  
 Figure 4.16. Comparison of SPT, intact and geophysical stiffness values  
 Figure 4.17. Comparison of geophysical and London Clay stiffness values

Figure 5.1. Idealised geometry

Figure 5.2. Single discontinuity set rock mass model

Figure 5.3. Three orthogonal discontinuity sets rock mass model

Figure 5.4. Modulus reduction factor versus discontinuity spacing

Figure 5.5. Calculated wall movements from discontinuous analyses

Figure 5.6. Calculated wall movements from discontinuous analyses

Figure 5.7. Comparison between discontinuous analyses

Figure 5.8. Calculated wall movements from equivalent continuum analyses

Figure 5.9. Calculated wall movements from equivalent continuum analyses

Figure 5.10. Comparison between discontinuous and equivalent continuum analyses

Figure 5.11. Comparison between discontinuous and equivalent continuum analyses

Figure 5.12. Effect of scale

Figure 6.1. Finite element mesh

Figure 6.2. Comparison of calculated lateral wall movements

Figure 6.3. Comparison of calculated wall bending moments

Figure 6.4. Mobilised angle of friction

Figure 6.5. Stress-deformation behaviour of hard rock joints

Figure 6.6. Stress-deformation behaviour of hard rock masses

Figure 6.7. Typical deformation curve for chalk

Figure 6.8. Pressure distributions for a circular foundation on rock masses with different discontinuity set orientations

Figure 6.9 One combination of stiffness and  $K_i$  that will produce, a given set of movements

Figure 6.10. Comparison of calculated and measured wall movements (STIFF1)

Figure 6.11. Comparison of calculated and measured wall bending moments (STIFF1)

Figure 6.12. Comparison of calculated and measured wall movements ( $K_i0.75$ )

Figure 6.13. Comparison of calculated and measured wall bending moments ( $K_i0.75$ )

Figure 6.14. Comparison of calculated and measured wall movements (STIFF2)

Figure 6.15. Comparison of calculated and measured wall bending moments (STIFF2)

Figure 6.16. Comparison of calculated and measured wall movements ( $K_i1.5$ )

Figure 6.17. Comparison of calculated and measured wall bending moments ( $K_i1.5$ )

Figure 6.18. Comparison of calculated and measured wall movements  
(prop load = 140 kN/m)

- Figure 6.19. Comparison of calculated and measured wall bending moments  
(prop load = 140 kN/m)
- Figure 6.20. Comparison of calculated and measured toe bending moments  
(prop load = 140 kN/m)
- Figure 6.21. Comparison of calculated and measured vertical contact stresses  
(prop load = 140 kN/m)
- Figure 6.22. Comparison of calculated and measured wall movements  
(prop load = 180 kN/m)
- Figure 6.23. Comparison of calculated and measured wall bending moments  
(prop load = 180 kN/m)
- Figure 6.24. Comparison of calculated and measured toe bending moments  
(prop load = 180 kN/m)
- Figure 6.25. Comparison of calculated and measured vertical contact stresses  
(prop load = 180 kN/m)
- Figure 6.26. Shear strains around retaining wall (prop load=140kM/m)
- Figure 6.27. Comparison of calculated wall movements
- Figure 6.28. Comparison of calculated wall bending moments
- Figure 6.29. Comparison of calculated toe bending moments
- Figure 6.30. Comparison of calculated vertical contact stresses
- Figure 6.31. Comparison of horizontal stresses
- Figure 6.32. Comparison of calculated vertical contact stresses
- Figure 6.33. Comparison of calculated toe bending moments
- Figure 6.34. Comparison of calculated wall movements
- Figure 6.35. Comparison of back calculated and geophysical stiffness values
- Figure 6.36. Comparison of back calculated and initial pressuremeter stiffness values
- Figure 6.37. Comparison of back calculated and unload/reload pressuremeter stiffness  
Values
- Figure 6.38. Comparison of back calculated and SPT stiffness values

## LIST OF TABLES

Table 2.1. The rock mass rating system

Table 2.2. A classification of chalk for the prediction of settlement

Table 3.1. Mean orientation for each discontinuity set

Table 3.2. Main stages of construction at the instrumented cross section

Table 3.3. Installation of instruments

Table 4.1 Pressuremeter test data

Table 4.2 Unconfined compressive stiffness of highly weathered mudstone

Table 4.3 Unconfined compressive stiffness of moderately weathered sandstone

Table 4.4 Summary of parameters from direct shear tests

Table 4.5 Summary of geotechnical properties – Highly weathered mudstone

Table 4.6 Summary of geotechnical properties – Moderately weathered mudstone

Table 4.7 Summary of geotechnical properties – Highly weathered sandstone

Table 4.8 Summary of geotechnical properties – Moderately weathered sandstone

Table 4.9 Design geotechnical parameters

Table 4.10 Summary of shear modulus properties

Table 4.11 Summary of shear strength properties

Table 4.12 Summary of *in situ* stresses

Table 5.1 Joint stiffness properties

Table 5.2 Intact rock properties

Table 5.3. Strength failure criteria

Table 5.4 Equivalent stiffness properties

Table 5.5 Concrete properties

Table 6.1. Idealised geometry

Table 6.2. Material properties of wall

Table 6.3. Made ground parameters

Table 6.4. Bromsgrove sandstone parameters

Table 6.5. Design stiffness parameters

Table 6.6. Geophysical stiffness parameters

Table 6.7. Parameters back calculated using a 140kN/m prop pre-load

Table 6.8. Parameters back calculated using a 180kN/m prop pre-load

Table 6.9. Summary of back calculated properties

## NOTATIONS

$\alpha$	dip angle
$c'$	Intersection with $\tau$ -axis of extrapolated straight line joining peak strength states in $(\tau, \sigma')$ space
$\phi'$	Strength or angle of shearing resistance
$\varepsilon_c$	Cavity strain in pressuremeter test
$\rho$	Bulk density
$\sigma, \sigma'$	Total and effective stress, respectively
$\tau$	Shear stress
$\gamma$	Bulk unit weight
$\nu$	Poisson's ratio
$E$	Intact Young's Modulus
$E_i$	Equivalent Young's Modulus
$E_{50}$	Tangent modulus at 50% of the uniaxial compressive strength
$EI$	Bending stiffness of a retaining wall
$E_y$	Post-yield modulus
$G$	Shear modulus
$G_i$	Initial shear modulus from pressuremeter tests
$G_s$	Dynamic shear modulus
$G_{ur}$	Unload/reload shear modulus from pressuremeter test
$G_m$	Mass modulus
$k_n$	Joint normal stiffness
$k_s$	Joint shear stiffness
$K_0$	<i>In situ</i> earth pressure coefficient
$M$	Bending moment
$N$	SPT blowcount
$P$	Prop load
$P_0$	Cavity pressure
RMR	Rock mass rating
$s$	joint spacing
$V_s$	Shear wave velocity

# ***CHAPTER 1***

## ***INTRODUCTION***

### **1.1. Preface**

The engineering behaviour of soils has given rise to the science of soil mechanics. This area of study has concentrated on the various forms of sands and clays, and has led to the development of a range of methods of ensuring safe design and construction on and with these materials. Rocks, on the other hand, are the principal subjects of study in the science of rock mechanics. In contrast to the soil mechanics approach wherein geotechnical materials are regarded as a continuum, rock mechanics, because of the dominant influence of discontinuities, is primarily a study of discontinua, with the properties of the intact rock perhaps of little consequence when compared with the much weaker defects.

Both these traditional branches of geotechnical engineering often encounter geotechnical materials described as weak rock, which appear at the upper fringe of soil mechanics or at the lower fringe of rock mechanics. While each of the areas of geotechnical engineering have to consider some of the design aspects of weak rock engineering, little effort has been made to correlate or unify the different approaches of soil and rock mechanics to the solution of engineering problems involving weak rock.

It is timely that some consideration should be given to the position of weak rock engineering with respect to the more traditionally accepted design methods for soils and rocks. Clearly, in this research it would be impossible to consider all aspects of weak rock engineering design and therefore this thesis has concentrated on some of the aspects of the behaviour of retaining walls embedded in weak rock.

## 1.2 Objectives

The overall aim of the research was to investigate suitable models, geotechnical parameters and methods of analysis for use in the design of walls embedded in weak rock. The specific objectives of the research were:

- i. To monitor in detail the performance of a retaining wall embedded in weak rock, during and shortly after construction.
- ii. To obtain geotechnical parameters for the weak rock involved, using conventional *in situ*, seismic and laboratory testing techniques.
- iii. To compare the range of stiffness parameters obtained using *in situ*, seismic and laboratory techniques, with those suggested by a back analysis of the behaviour of the wall.
- iv. To investigate suitable models, geotechnical parameters and methods of analysis for use in the design of walls embedded in weak rock, with reference to the data obtained from the case study.

## 1.3. Structure of the thesis

The work presented in this thesis comprises of four major areas:

- Field monitoring and interpretation of the performance of a case study retaining wall, located on the Coventry North-South Road.
- Comparison of geotechnical parameters obtained in different ways for the weak rock involved at the site.



- A series of analyses comparing the discontinuous and continuum approach to modelling retaining wall behaviour.
- Back-analysis of the monitored section of retaining wall.

The thesis is divided into chapters as follows:

### ***Chapter 2: Background***

The meaning of the term “weak rock” is outlined and relevant aspects of weak rock engineering are reviewed.

### ***Chapter 3: Case study – Coventry North-South road***

The ground conditions, construction sequence and field instrumentation at the case study site are described and the results of the field monitoring are presented and discussed.

### ***Chapter 4: Geotechnical parameters for weak rock at study site***

Geotechnical strength and stiffness parameters obtained from field tests carried out at the case study site and laboratory tests on samples from the site are presented and discussed.

### ***Chapter 5: Numerical modelling***

Numerical parametric studies are then used to evaluate which approach is best suited to back analysing the instrumented wall. A brief overview of the distinct element program UDEC (Cundall 1971) is also included in this chapter.

## ***Chapter 6: Coventry: back analyses and discussion***

Back-analysis of the Coventry wall is used to assess the operational effective stiffness parameters and *in situ* stresses for the case study, using the finite element program CRISP (Britto & Gunn 1987). The back-calculated parameters are also compared with the values obtained from the *in situ* and laboratory tests in this chapter.

## ***Chapter 7: Conclusions***

The major conclusions drawn from the findings presented in the thesis are summarised and recommendations for further work are made.

## ***CHAPTER 2***

### ***BACKGROUND***

#### **2.1. Introduction**

The study of weak rock falls within the largely undefined interface between soil and rock mechanics. Recent work has attempted to address this and bring these two disciplines closer (Chandler 1969, Clayton, 1990, Matthews 1993, Johnston and Novello, 1994, Cuccovillo and Coop 1997, Tatsuoka *et al.*, 1993). Similarities in behaviour have been observed across the spectrum of geomaterials (Leroueil and Vaughan 1990). The behaviour of intact weak rock has been analysed within the Critical State Soil Mechanics framework (Burland, 1990; and Cuccovillo, 1995), although this research has been limited to the study of intact material and has not been extended to include discontinuities.

The main difference between soil and rock mechanics is that soil mechanics tends to view a soil as being a relatively homogeneous continuum. On the other hand, the rock

mechanics view is that the behaviour of the rock mass is governed principally by the discontinuities within it.

Careful consideration needs to be given to weak rocks, since they fall in the middle ground between soils and rocks mechanics. Matthews and Clayton (1992) have shown that the deformation of intact chalk differed from that of a chalk rock mass containing discontinuities. This might suggest that the presence of discontinuities in weak rock masses is just as important as in hard rocks and therefore the methods of design and analysis in the rock mechanics literature would be directly applicable to discontinuous weak rock masses.

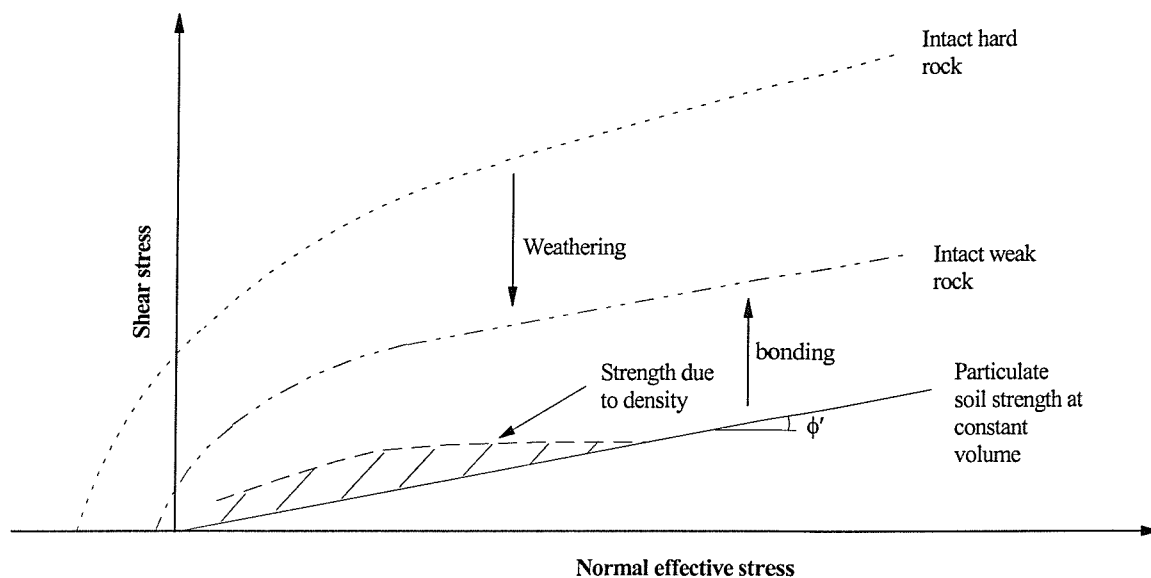
In clay soils the influence of fissures on the mass strength and stiffness has also long been recognised (Terzaghi 1936, Ward *et al.*, 1959, Skempton *et al.*, 1969, Lo 1970, Rowe 1972 and Marsland 1972). Johnson & Novello (1994) argue that soil discontinuities are very similar in character to those encountered in rock masses, and have the same general influence on mass strength and stiffness. It is simply that with soil, the difference between the intact and mass behaviour is not as marked as with rocks. Therefore, although the degree of influence of discontinuities may increase as the intact geotechnical material gets harder, the principles are the same. Weak rocks are no exception to the above progression as they display the same range of discontinuities encountered in soils and rocks.

The presence or absence of discontinuities may have a very important influence on the appropriate method used for the analysis of retaining walls embedded in weak rock. This chapter defines the meaning of the term “weak rock” and discusses the significance of discontinuities with respect to the design of retaining walls embedded in weak rock.

## **2.2. Weak rock in the geotechnical spectrum**

The uncemented particulate soils often considered in soil mechanics have a strength due only to angle of shearing resistance,  $\phi'$ , Figure 2.1. This strength can be also increased by density and dilation as indicated on Figure 2.1. The hard rocks we usually consider

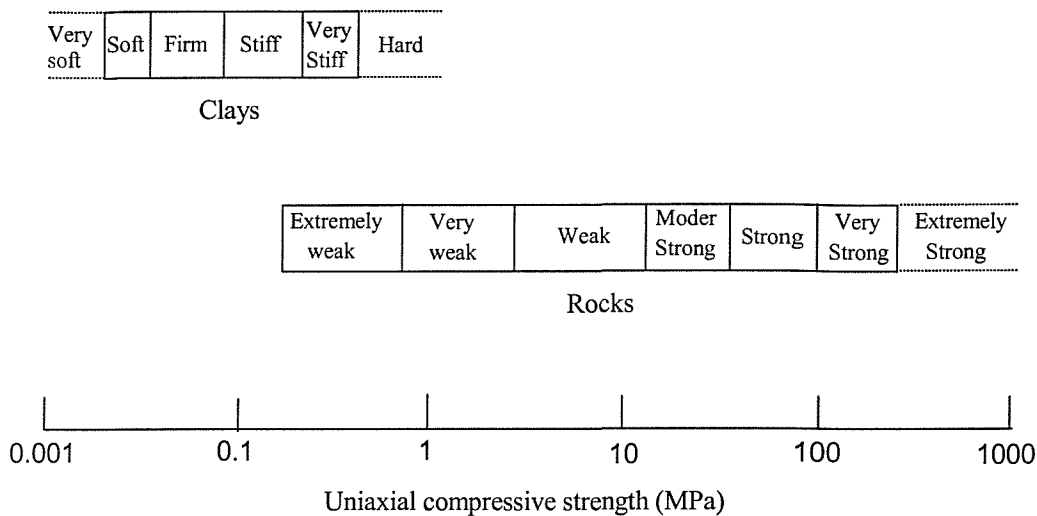
in rock mechanics have a very high strength in the engineering stress range due to bonding. Weak rocks of concern to engineers have often been subject to various weathering processes that weaken them from a hard rock towards the state of a particulate soil or are soils that have been slightly bonded. Weak rocks have a much lower strength than hard rocks, due to the weaker bonding.



**Figure 2.1. The contribution of weathering to the properties of geotechnical materials as they change from hard rock toward particulate soil**

Weak rock is conventionally accepted as a material that has an unconfined compressive strength in the range of 0.5 to 25 MPa, depending upon the classification scheme used. Figure 2.2 shows the International Society for Rock Mechanics classification scheme for intact geotechnical materials. The classification scheme tends to distinguish weak rock as those materials forming the overlap between stiff clay and weak rock. The International Society for Soil Mechanics and Foundation Engineering Technical Committee Report (1985) suggests that weak rock is the group of geotechnical materials for which the intact uniaxial compressive strength falls approximately in the range 0.5-25 MPa. Under the ISRM rules, concrete would be classified as a weak material, yet it is doubtful whether a client would be happy with such a description. To avoid this difficulty the Geological Society of London (1970) adopted values of 1.25 to 5.0 MPa for its definition of weak. Yet, in doing so it has adopted a definition which disguises

the fact that rock masses containing materials with unconfined compressive strengths of less than 25 MPa are often described as weak.



**Figure 2.2. ISRM classification for geotechnical materials**

Bieniawski (1973 & 1989) has developed a system of classifying rock masses for design assessment, Table 2.1. In this system, five parameters are used to describe the quality of the rock mass and another factor is used to take account of the orientations of the discontinuities. The rating system clearly indicates that the presence of discontinuities reduces the overall strength of a rock mass, and that their spacing and orientation govern the degree of such reduction. Masses that would tend to be regarded as weak would usually fall into the very poor rock class, (i.e. V in Table 2.1).

It can be seen from the classification system that rock masses that classify as weak do so because of their joint structure and the weathering and infilling of joints that has taken place, rather than the weakness of the intact material.

Rock can be weak because the particles are only weakly cemented, or blocks of intact material are separated by significantly weaker discontinuities. As there is no rigid definition of what a weak rock is, in this thesis weak rock will be regarded as a generic term covering intact geotechnical materials that could be described as weakly bonded, with a uniaxial compressive strength in excess of 0.5 MPa. A weak rock mass will be regarded as lumps of intact weak rock, intersected by discontinuities.

Parameter		Range of values				
Strength of intact rock material	Point load strength (MN/m <sup>2</sup> )	>10	4-10	2-4	1-2	
	Uniaxial compressive strength (MN/m <sup>2</sup> )	>250	100-250	50-100	25-50	5-25 1-5 <1
	Rating	15	12	7	4	2 1 0
Drill core quality RQD (%)		90-100	75-90	50-75	25-50	<25
Rating		20	17	13	8	3
Spacing discontinuities		>2m	0.6-2m	200-600mm	60-200mm	<25
Rating		20	15	10	8	5
Condition of discontinuities		Very rough surfaces Not continuous No separation Unweathered	Slightly rough Separation < 1mm Slightly weathered	Slightly rough Separation < 1mm Highly weathered	Gouge < 5mm thk Or Separation 1-5mm Continuous	Soft gouge > 5mm thk Or Separation > 5mm Continuous
Rating		30	25	20	10	0
Groundwater		Completely dry	Damp	Wet	Dripping	Flowing
Rating		15	10	7	4	0

(a) Classification parameters and their ratings

Strike and dip orientations of discontinuities	Very favourable	Favourable	Fair	Unfavourable	Very unfavourable
Ratings (slopes)	0	-5	-25	-50	-60

(b) Rating adjustment for discontinuity orientations

Rating	100-81	80-61	60-41	40-21	<20
Class No	I	II	III	IV	V
Description	Very good rock	Good rock	Fair rock	Poor rock	Very poor rock

(c) Rock mass classes determined from total ratings

**Table 2.1. The rock mass rating system (after Bieniawski 1989)**

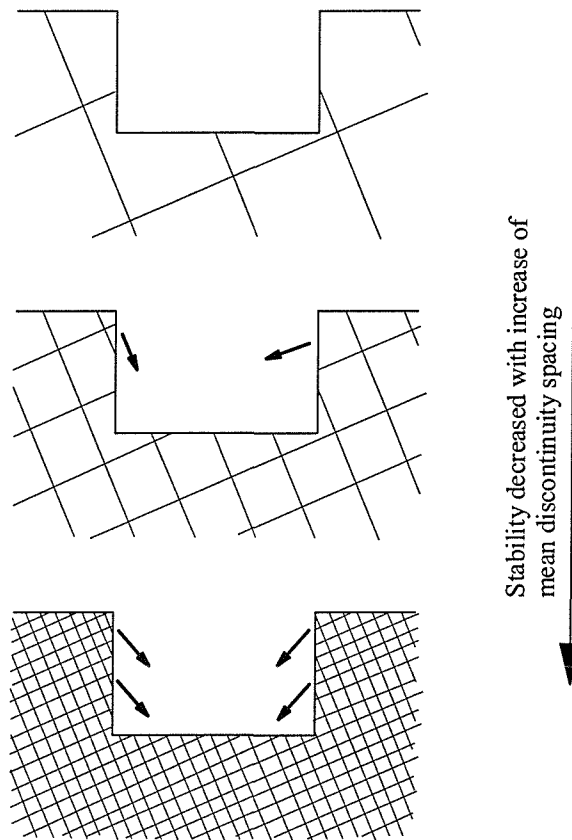
### **2.3. Significance of discontinuities**

The rock masses which we are required to analyse are generally heterogeneous, anisotropic and contain discontinuities. The anisotropy and the presence of discontinuities play a dominant role in the deformational behaviour and stability of rock masses. The influence of the discontinuities therefore must be incorporated in the model used for analysis.

Soils and rocks both contain discontinuities, the major difference between rock masses and soil masses are that in a rock the discontinuities can be on the same scale as the excavation. With the exception of large pre-existing slip surfaces, this is not in general the case for soils because the discontinuities tend to be several orders of magnitude smaller than the engineering dimensions of the excavation. The effect of scale is therefore an important factor in design. Figure 2.3 illustrates this effect. In the figure the excavation dimensions are considered to be the same; yet as the discontinuity spacing is decreased, it becomes less stable as more blocks are free to fall into it. In other words, stability depends on the ratio of the excavation dimension to the discontinuity spacing (see Hoek & Bray 1981 or Hudson 1989). Another factor that will influence the performance of the rock mass is the orientation of the discontinuities.

British Standard 8002 (BSI 1994) recognises that the extent and orientation of the discontinuities within the weak rock mass control the engineering properties relevant to the design of retaining walls. General guidance is not given because of the widely varying nature of weak rocks. However, BS 8002 suggests that for minor structures it is generally adequate to take a conservative approach and treat weak rocks as being composed of interlocking granular fragments, with an effective angle of friction. For major structures an examination of exposures of the weak rock type should be carried out to determine the stable slope angle. This is not very helpful for a designer.





**Figure 2.3. Influence of scale on stability**

In hard rock cuttings discontinuities generally govern mass failure, giving rise to the commonly recognised mechanisms of planar, wedge and toppling failure modes. However in very closely jointed material, failure is less constrained by individual defects and mass failures involving circular or general soil mechanics type failure surfaces are also possible (see Hoek & Bray 1981). The overall behaviour of a closely jointed material is often thought to be similar to that of a continuum and is often analysed as an equivalent-continuum with the properties of the rock mass defined in terms of some combination of the properties of the intact rock and those of the discontinuities.

In heavily jointed weak rock masses, it is difficult to obtain geological field information in sufficient detail to permit accurate modelling of every discontinuity. Therefore, it would appear that there might be considerable practical merit in treating a closely jointed discontinuous weak rock mass as an equivalent continuum. This can lead to criticism since in hard rock mechanics it is often emphasised that a rock mass is not a

continuum and that its behaviour is dominated by discontinuities. This of course, is quite true. However, in hard rock mechanics, it is also recognised that the contribution of discontinuities to rock mass behaviour depends very much on the size of the structure relative to the discontinuity spacing. This has always been the general case in soil mechanics, with discontinuities usually considered to be small on the global scale (unless a large pre-existing shear plane is being considered). Discontinuities in weak rocks are no exception as they display the same range of scales encountered in soils and rocks.

Another material that would be classified as weak rock under the uniaxial compressive strength classification system is concrete. In the stress analysis of concrete the engineer will use continuum theories without hesitation. The success of such an approach is justified by the smallness of imperfections compared with the size of the constructed object.

In rock mechanics the problems are of an identical nature, the main difference being that of scale. The granular-crystalline structure of the intact rock with its irregularities is evident in dimensions ranging from microns to millimetres. The discontinuous rock mass exhibits its properties in dimensions varying from millimetres to metres. Clearly, the applicability of a continuum analysis will have to be assessed by means of the spacing of the discontinuities in relation to the overall dimensions of the problem.

Rocks vary widely in their competence to carry loads. At one extreme the rock mass can be virtually free from any discontinuities, while at the other it may have highly fragmented and crushed rocks. In both these cases, it would appear that the rock mass can be analysed as a continuum.

Hoek and Brown (1980) have presented an empirical failure criterion for characterising the strength of an equivalent homogeneous isotropic continuum for heavily jointed rock masses. There are limitations in the use of the criterion (see Hoek and Brown 1988). In particular, the designer should evaluate the applicability of the criterion to the rock mass at the site, taking into account the effects of relative scale in relation to the size of the structure being designed, and anisotropy. Other authors (Goodman *et al.* 1968, Duncan

and Goodman 1968, Gerrard, 1982, Singh 1973, and Zienkiewicz and Pande, 1977) have also justified using the continuum method in particular situations.

In general, the nature of a rock mass is such that the assumption of homogeneous and isotropic properties will not be valid. This can occur, for example, where discontinuities are preferentially oriented or widely spaced. In practice, a simplified wedge analysis is often used for design in such cases (Goodman 1989). As in all methods of limit equilibrium analysis, the shape of the slip surface is assumed at the outset. Since the kinematics of a rock mass at failure are ignored, any shape may be taken for this slip surface. The actual surface will, of course, depend upon the spatial distribution of the discontinuities and the shearing resistance available along them. Limit equilibrium methods of analysis therefore employ a trial and error procedure to find the most critical slip surface. However, more refined analytical techniques are available for identifying failure mechanisms (e.g. discrete element method, see Williams 1990).

The weak rocks in which retaining walls are built can be classified into three groups: (i) continuous, (ii) discontinuous and (iii) equivalent-continuous types, (see Figure 2.4). Type (i) classification may be used for ground consisting of intact rock without discontinuities. Type (ii) represents jointed weak rock masses. Type (iii) classification is for highly fractured and weathered weak rock masses where the orientation and inclination of discontinuities is such that simple sliding is not possible.

The mechanical behaviour of Type (i) ground can be analysed by means of the theory of continuum mechanics, while discontinuous approaches can be used for analysing the behaviour of type (ii) ground.

A discontinuous approach similar to that used for type (ii) can be adopted for type (iii) ground. However, it is almost impossible to explore the location, dimension and mechanical characteristics of all the joint systems. This means that a discontinuous approach is not normally feasible in engineering practice. Moreover, it seems that this type of ground behaves, in general, as a continuous body. A continuum mechanics approach may therefore be suitable for Type (iii).

Although there are arguments for three basic models to be used in particular situations, there is currently no guidance on when they should be used.

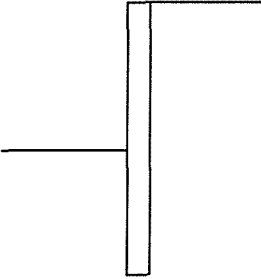
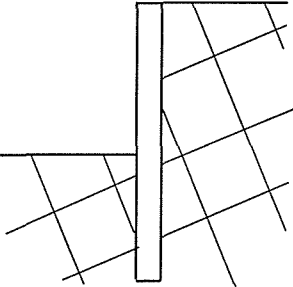
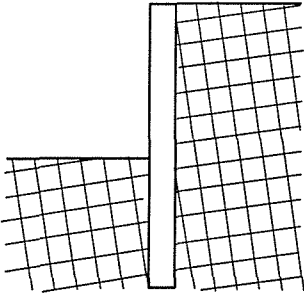
Option	Schematic	Approach
<p>i. Treat as uniform. (continuum)</p>		<p>Parameters from laboratory or in-situ tests considered representative of mass properties.</p>
<p>ii. Treat as discontinuous due to structural control. (discontinuum)</p>		<p>Discontinuity controlled.</p>
<p>iii. Treat as uniform but mass weakened by discontinuities. (continuum)</p>		<p>Allowance made for influence of discontinuities on mass properties.</p>

Figure 2.4. Approaches for analysis in weak rock

The other major difficulty in the numerical modelling of weak rock is the determination of the input parameters. In the case of determining parameters for equivalent continuum analyses, results from laboratory tests are not always relevant to the weak rock *in situ*. Attempts have been made to overcome these problems by the scaling of input parameters, e.g. Rock mass classification schemes (Deere 1967, Serafim and Pereira 1983, Kulhawy 1978) have been used to infer input parameters relevant to *in situ* conditions. In recent years, there has been a firm move towards *in situ* field tests to determine mass parameters.

Determining the properties for the joints is one of the main limitations of discontinuous analyses. The joint properties are conventionally derived from small scale laboratory tests (Goodman 1989). Published data on stiffness properties for rock joints are limited; summaries of data can be found in Kulhawy (1975) and Bandis *et al.* (1983).

#### **2.4. Summary**

To qualify as a weak rock, the geotechnical material must be weakly cemented and have a uniaxial compressive strength in excess of 0.5 MPa.

The difficulties of making predictions of the engineering response of weak rock masses derive largely from their variable nature. The stability of excavations and the mechanical response of a weak rock mass during an excavation sequence both depend on the material encountered, and any structure inherited from the parent rock. The presence of discontinuities in the excavation might provide planes of low shear strength along which slip may occur or a reduction in the overall shear strength and stiffness properties of the weak rock mass.

At present, there appear to be two different approaches to the problem of understanding and analysing the effects of discontinuities on the behaviour and properties of rock masses. The first approach seeks to assess the aggregate effects of many discontinuities, so as to make a continuum analysis of the problem. The other approach is to treat joints, particularly the dominant sets, as discrete entities.

Currently there are no universal standard solutions for designing retaining walls embedded in weak rock, because each solution is specific to the circumstances. Nonetheless, recognising and applying the basic geomechanic principles may help to optimise design and clarify whether it is appropriate or not to use a continuum analysis. It is this possibility that is explored in this thesis.

## ***CHAPTER 3***

### ***CASE STUDY – COVENTRY NORTH-SOUTH ROAD***

#### **3.1. Introduction**

The two key uncertainties facing the designer of a retaining wall embedded in weak rock are the characterisation of the geotechnical properties of the ground, and the way in which these should be incorporated into an appropriate design procedure. The aim of this research was to investigate these issues with reference to an instrumented case study, located on Phase II of the Coventry North-South road scheme in Warwickshire. In this chapter, the ground conditions, construction sequence and field instrumentation are described and the results of the monitoring exercise are presented.

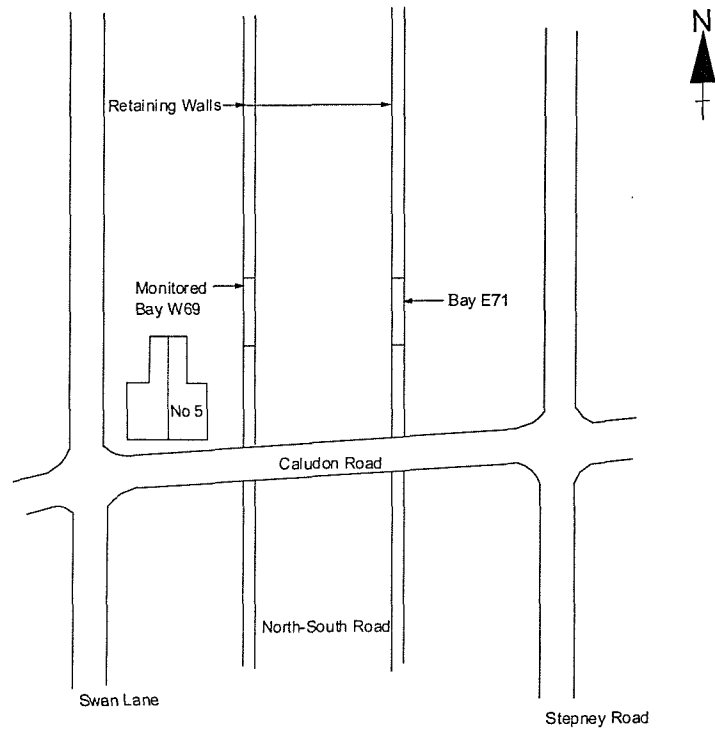
### 3.2 Project details

In 1988, Coventry City Council commissioned Broadgate Consultants (now Babbie Group) to act as consulting engineers for Phase II of the Coventry North-South road. Mott MacDonald were engaged to design the highway structures. John Mowlem Civil Engineering were appointed as main contractor and commenced work on the project in June 1995.

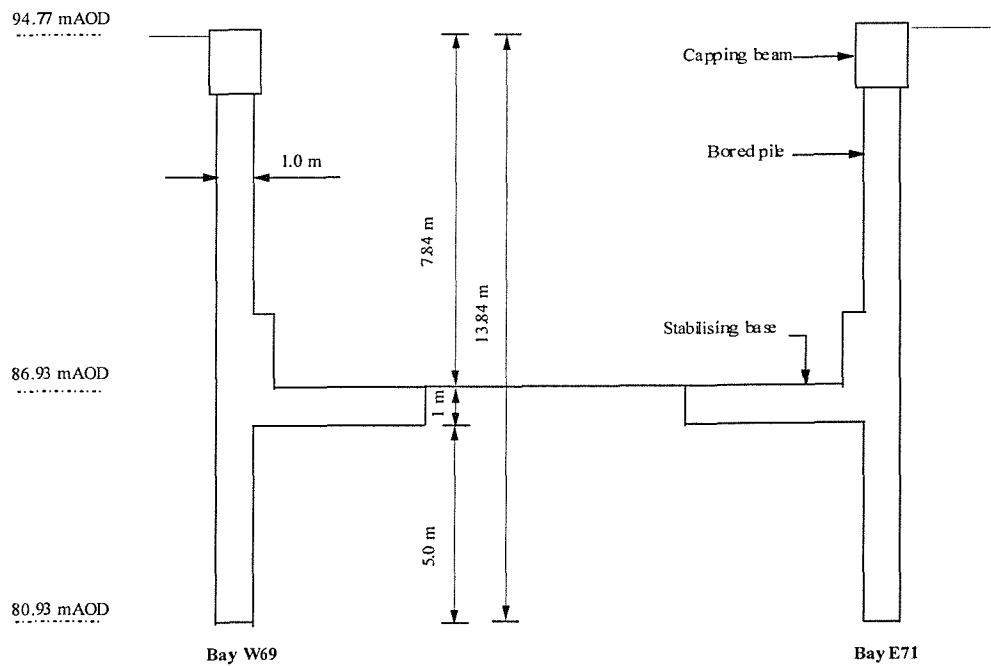
The Coventry North-South road links the M6 north of Coventry to the A45 to the south. The route is intended to divert through traffic away from the centre of Coventry, and to improve access to a deprived area to stimulate regeneration. Phase II comprised the construction of approximately 1.8km of dual carriageway, east of Coventry city centre. Over the majority of its length the route passes through a densely populated urban area with the site boundary being formed by the rear fences of existing private gardens. The route generally follows the line of an abandoned railway cutting, which was widened and deepened to construct the new carriageway. The road was kept in cutting as much as possible to minimise the impact on local residents. The widening scheme involved the installation of retaining walls having an approximate total length of 2.2km. The instrumented section of wall, Bay W69, lies on the west side of the cutting just north of the Caludon Road footbridge (Figure 3.1).

The instrumented wall section was formed from 14m deep  $\times$  1m diameter contiguous bored piles spaced at 1.1m centres, with a retained height of 7.8m. A stabilising base was located 1.45m below the finished carriageway level, extending 5m from the face of the pile beneath the verge and a short distance under the carriageway (Figure 3.2).





**Figure 3.1. Location of instrumented section**



**Figure 3.2 Cross section through monitored section of road**

### 3.3 Ground conditions

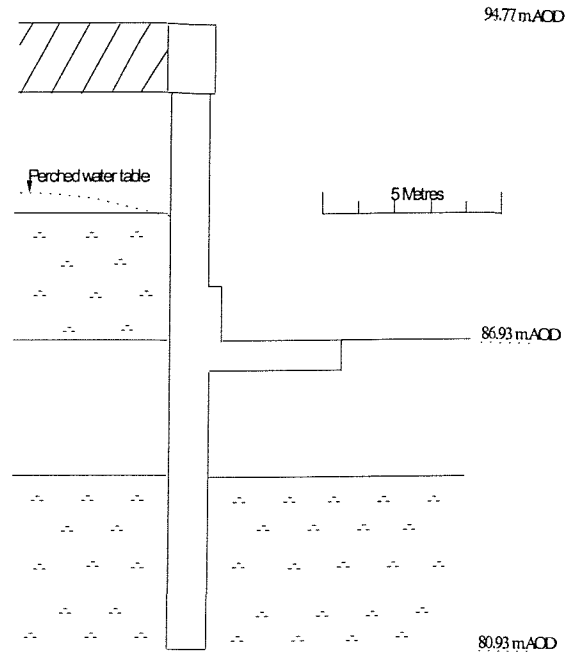
#### 3.3.1. Geology

An account of the geological sequence of the Coventry area can be found in three BGS Reports, (Old *et al.* 1990). Old *et al.* (1990) indicate that the Caludon Road area is underlain by the Bromsgrove Sandstone Formation, part of the Sherwood Sandstone Formation which is Triassic in age. This sequence of the solid geology lies unconformably upon the Coventry Sandstone Formation, which is part of the Enville Group and is Carboniferous in age. Below this formation lie the Keele, Halesowen and Etruria Marl Formations respectively; these formations are underlain by the Productive Coal Measures.

Exploration Associates carried out site investigations on behalf of Coventry City Council in 1989, 1993 and 1994. The geology at the instrumented section was deduced from borehole records obtained during these site investigations, together with field observations during construction of the road (Figure 3.3). The top 1.5m of the cutting at the instrumented section was made ground; below this the Bromsgrove Sandstone Formation was encountered. Weak rock debris clinging to the face of the piles indicates the stratigraphy at the instrumented wall, Figure 3.4

The Bromsgrove Sandstone Formation consists of sandstone layers interbedded with mudstone layers. The sandstone layers are grey to buff in colour. The mudstone layers are generally 2 to 3m thick, and of a dark red-brown colour. The formation exhibits cyclic sedimentation, with the sandstone often passing upward into mudstone. The strata at the top of the cutting are frequently highly weathered and extremely weak. The lower strata are typically slightly to moderately weathered and weak. Davies and Barton (1998) give further details of the geology at the instrumented wall section.

Level (m.AOD)	Description
94.7 – 93.2	Made Ground
93.2 – 90.5	Highly weathered Bromsgrove sandstone
90.5 – 87.4	Highly – moderately weathered Bromsgrove mudstone
87.4 – 84.2	Moderately weathered Bromsgrove sandstone
84.2 –	Moderately – slightly weathered Bromsgrove mudstone



Level (mAOD)	Joint spacing (mm)	Infill (mm)	Description
94.7 – 93.2			Made Ground
93.2 – 90.5	H 100 – 200 V 150 - 300	10 - 30	Extremely weak light brown fine to coarse SANDSTONE with close spaced discontinuities ( <i>Highly weathered Sandstone</i> ).
90.5 – 88.3	Intact lumps, with no regular orientation		Very stiff/Extremely weak red brown structureless CLAY/MUDSTONE ( <i>Highly weathered Mudstone</i> ).
88.3 – 87.4	H 150 – 300 V 300 - 500	5 - 10	Very weak red brown MUDSTONE with close spaced discontinuities ( <i>Moderately weathered Mudstone</i> ).
87.4 – 84.2	H 150 – 300 V 300 - 500	3 - 10	Very weak grey brown fine to coarse SANDSTONE with close spaced discontinuities ( <i>Moderately weathered Sandstone</i> ).
84.2 – 81.9			Very weak red brown MUDSTONE with very medium spaced discontinuities ( <i>Moderately weathered Mudstone</i> ).
81.9 -			Weak red brown MUDSTONE/SILTSTONE with medium spaced discontinuities ( <i>Slightly weathered Mudstone</i> ).

**Key: Description of weathered bedrock**

**Figure 3.3. Ground conditions at the instrumented cross section (Bay W69)**

### 3.3.2. Discontinuities

Davies and Barton (1998) identified the main joints at a location adjacent to the instrumented section of retaining wall (Table 3.1). The weak rock at this location was considered to be similar to the weak rock at the instrumented section and the jointing was considered typical for the area (Figure 3.5).

Joint spacing in the highly weathered sandstone at the top of the excavation is typically in the range of 100 to 300mm, (close spaced discontinuities, BS 5930: 1981). The joints are moderately open and infilled with sand. The amount of infilling is usually around 10mm although as much as 30mm occurs in some joints (Figures 3.6). The highly weathered mudstone is structureless and comprised of intact lumps of weak rock, with no regular orientation surrounded by clay (Figure 3.7). The joint spacing in the moderately weathered weak rock is also typically in the range of 150 to 500mm. But, the joints are tighter (open) and therefore infilled with less material (Figure 3.8). Bedding at the top of the monitored section of retaining wall is around 50mm (very thinly bedded); lower down the cutting it is around 300mm (medium bedded).

<b>Discontinuity</b>	<b>Orientation</b>	<i>Note: Orientations are quoted in degrees as dip direction / dip amount followed by a compass orientation of the dip direction.</i>
Joint Set 1	236/85 SW (near vertical)	
Joint Set 2	139/85 SE (near vertical)	
Joint Set 3	235/23 SW (sub horizontal)	
Bedding	068/07 ENE (near horizontal)	
Random	Random fissuring	

**Table 3.1. Mean orientation for each discontinuity set (after Davies & Barton 1998)**

Using the Bieniawski (1989) system of classifying rock masses, the RMR for the highly weathered weak rock at the case study is 8, the moderately weathered weak rock is 12 and the slightly weathered weak rock is 19, (note the orientation adjustment factor has not been used).



**Figure 3.4. Weak rock debris clinging to face of the piles at the instrumented wall**



**Figure 3.5. Typical jointing for the area**



**Figure 3.6. Highly weathered Sandstone**



**Figure 3.7. Highly weathered Mudstone**



**Figure 3.8. Moderately weathered Sandstone**

Davies and Barton (1998) carried out a slope stability assessment using stereographic projection and the data obtained from the discontinuity survey. The method used for identifying important pole concentrations is the one developed by Markland (1972). Markland's test was designed to establish the possibility of a failure occurring in which sliding takes place along the line of intersection of two planer discontinuities.

The stability of the weak rock mass at the case study was considered without the support of the retaining wall. Davies and Barton (1998) concluded that no major instability was envisaged due to the favourable orientation of the discontinuity sets, but there was a possibility that small minor wedges might form.

### **3.4 Ground water**

The sandstone unit at the top of the instrumented section of the retaining wall contains a localised perched water table, the level of which varies seasonally. Below final carriageway level there is some evidence of a water table in the lower aquifer, but owing to a lack of deep piezometers, its exact level is unclear, but it probably lies around 82.0m.AOD. Data obtained from a piezometer located next to the retaining wall at a depth of 80.0 mAOD, (which remained dry during monitoring), suggests that the ground water level at the instrumented section is below the toe of the retaining wall.

### **3.5. Geotechnical parameters**

Geotechnical strength and stiffness parameters obtained from field tests carried out at the case study site and laboratory tests on samples from the site are presented and discussed in Chapter 4.

### **3.6 Construction sequence**

Prior to the installation of the piled retaining wall, the railway cutting was backfilled to provide a platform for the pile rig.

The retaining wall was constructed using the contiguous bored pile system. During boring, the top 2m of each pile shaft was supported by a casing. A steel reinforcing cage was then lowered into each pile shaft and the concrete poured. Following pile installation, a stiff concrete capping beam was cast on top of the wall.

Bulk excavation of the backfill was then carried out in phases to a maximum of 6.3m depth in front of the wall along its entire length, leaving behind temporary earth berms of gradually decreasing cross section (Figure 3.9). Tubular steel temporary props were then installed at capping beam level at intervals of approximately 5 metres and preloaded to 1300kN (260 kN/m). The earth berms were then excavated to the approximate cutting profile (Figure 3.10).



Further excavation to stabilising base foundation level did not take place until immediately prior to construction of the stabilising base. Polystyrene void formers had been cast into the front face of the bored piles at toe level. These were exposed by the excavation and removed to reveal the pile longitudinal reinforcement. Couplers cast into the pile shaft were used to provide reinforcement continuity with the stabilising base and provide the pile/base moment connection. Following construction of the stabilising base, the temporary props were removed to leave the finished structural wall, (Figure 3.11). After a period of several months had elapsed, to allow any immediate wall movement to occur, the non-structural brickwork facing was erected (Figure 3.12).

The principal stages of retaining wall construction at the instrumented section, (Bay W69), are summarised in Table 3.2.



**Figure 3.9. Bulk excavation, leaving behind temporary earth berms**



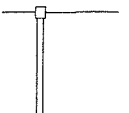
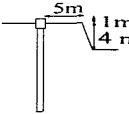
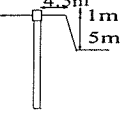
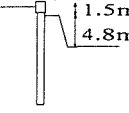
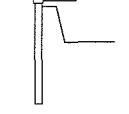

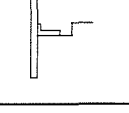
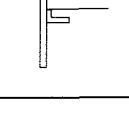
**Figure 3.10. Temporary props pre-loaded and earth berms excavated**



Figure 3.11. Stabilising base constructed and temporary props being removed



Figure 3.12. Road open to traffic

Stage	Description	Schematic	Date	Day
I	Installation of contiguous pile wall.		03/02/96	
II	First stage excavation.		14/05/96	0
III	Second stage excavation.		24/09/96	133
IV	Third stage excavation.		16/10/96	155
V	Temporary props installed and pre-loaded to 1300 kN.		22/11/96	192
VI	Earth berm removed.		25/11/96	195
VII	Excavation to stabilising base blinding level and construction of stabilising base.		11/12/96	211
VIII	Temporary props removed.		28/02/97	290
IX	Road opened to traffic		12/12/97	577

**Table 3.2. Main stages of construction at the instrumented cross section (Bay W69)**

### 3.7 Instrumentation

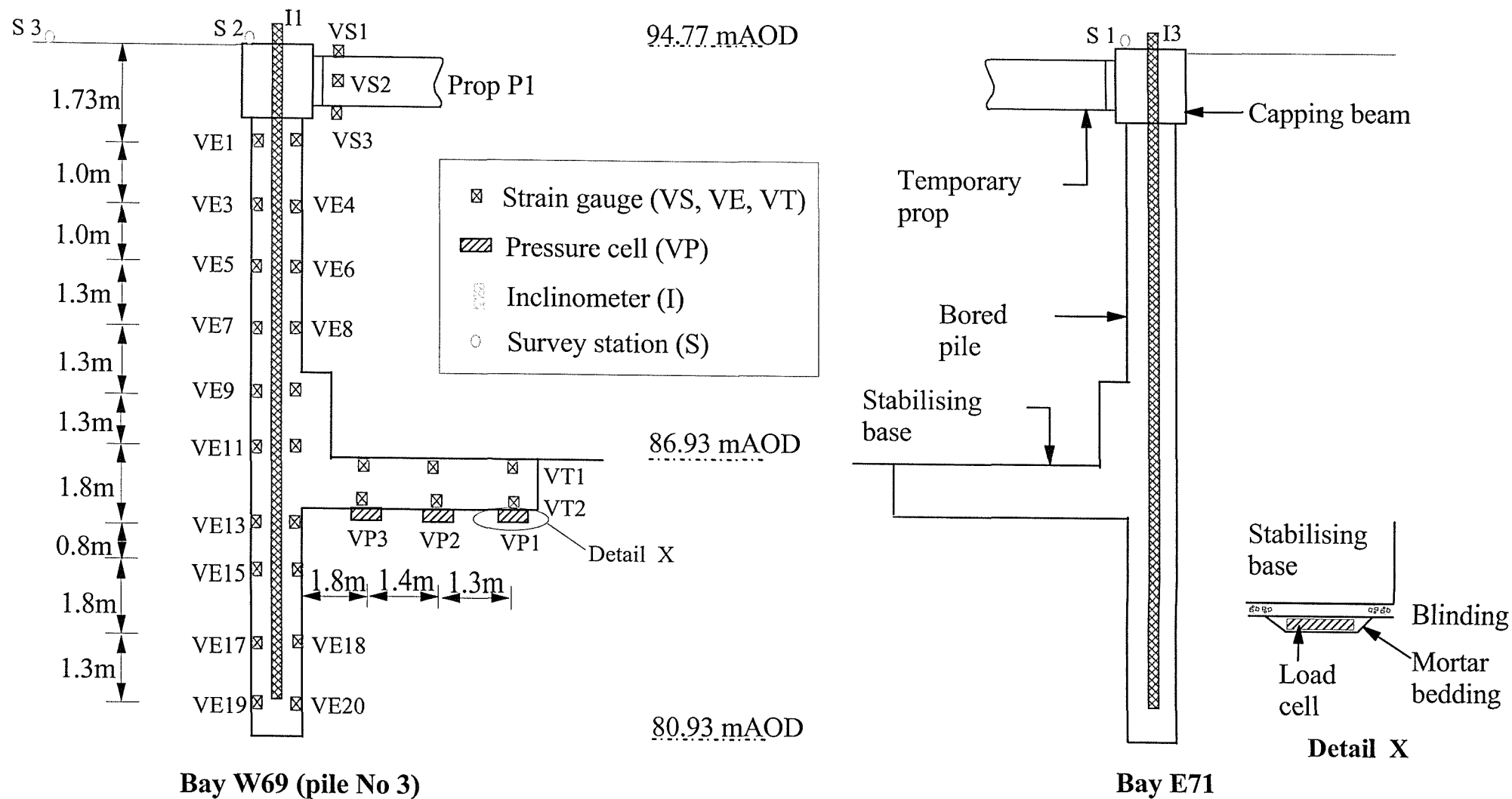
Instruments were installed to monitor wall movements, bending moments, temporary prop loads and stresses under the permanent stabilising base. Table 3.3 gives the dates of installation of the various instruments and Figures 3.13 and 3.14 show a cross section and plan of the instrumentation layout, which comprised:

- vibrating wire strain gauges installed in the pile shaft and stabilising base, to measure bending moments;
- pressure cells installed at the underside of the stabilising base, to measure vertical contact stresses;
- vibrating wire strain gauges attached to the temporary props, to determine prop loads; and
- inclinometers and survey stations, to monitor wall movements.

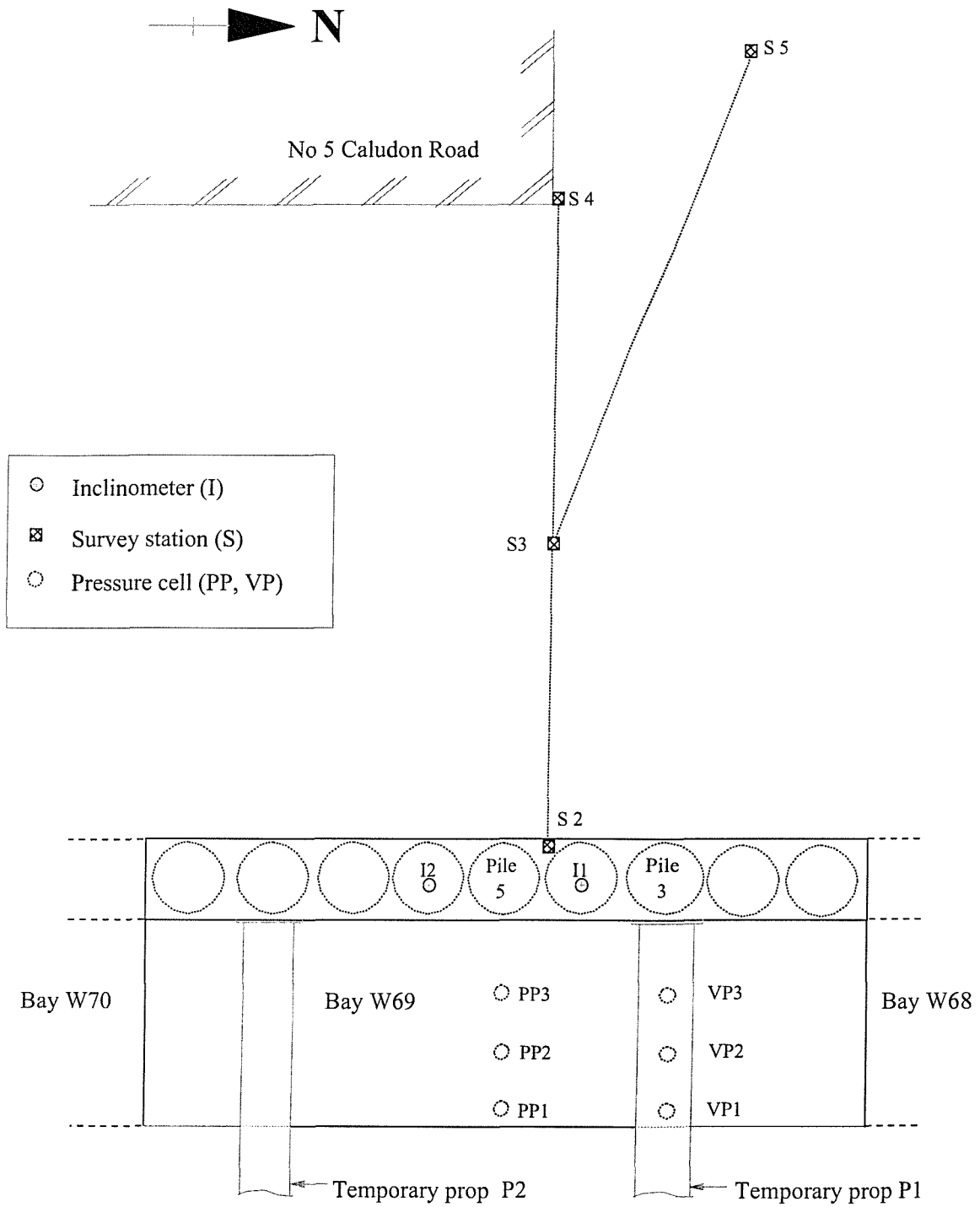
A Campbell Scientific CR10 data logger was used to obtain a continuous record of the strain gauge and pressure cell output.

Dates	Vibrating wire strain gauges		Inclinometers		Surface movement stations		Pressure cells	
	Nos	Location	Nos	Location	Nos	Location	Nos	Location
Feb 1996	VE1-40	Bored pile	I1-3	Bored pile				
May 1996					Sm1-5	Retained ground		
Nov 1996	VS1-8	Temporary Props						
Dec 1996							VP1-3 & PP1-3	Beneath stabilising base
Feb 1997	VT1-12	Stabilising base						

**Table 3.3. Installation of instruments**



**Figure 3.13. Cross section through monitored cross section, showing location of instrumentation**



**Figure 3.14. Plan showing instrument locations**

### 3.7.1 Wall movements

The instrumentation used for monitoring the wall movements was installed and monitored by the University of Southampton and TRL (Transport Research Laboratory). Wall movements were monitored by three independent methods:

- A tape extensometer system was used to measure the crest level movements at the instrumented Bay (W69). Measurement lines were extended from an eyebolt fixed into the capping beam to survey stations S4 and S5 (Figure 3.14). Each of the survey stations consisted of a concrete block founded about 0.3m below ground level, fitted with a stainless steel socket designed to accept pillars to which the measuring tape was attached. Readings were corrected for the effects of temperature and sag on the steel tape. The survey stations were assumed to be located outside the possible movement zone (12m away from the wall). The accuracy of the measured wall crest movements was estimated to be within  $\pm 0.5\text{mm}$  (Carder 1998).
- Three 13m long inclinometer tubes were installed in the retaining walls, two in the instrumented Bay (W69) and one in the opposite Bay (E71). Relative horizontal displacement profiles for the walls were determined by means of inclinometer surveys carried out at suitable intervals. The repeatability of the measurements was found to be better than  $\pm 1.0\text{mm}$  (Carder 1998).
- A Geomensor electronic distance measuring system was used to monitor the change in span at crest level between the instrumented Bay (W69) and the opposite Bay (E71). A tribracket to accept the Geomensor system was fixed onto the capping beam of Bay W69 and a machined socket for a target reflector into the capping beam of Bay E71. The estimated accuracy of the measured change in span at crest level was  $\pm 0.2\text{mm}$  (Carder 1998).



### 3.7.2 Wall and base bending moments

Gage Technique TEST/5.5 concrete embedment strain gauges with temperature measurement were used for monitoring the bending moments in the wall. These were installed by the University of Southampton and Gage Technique Ltd and monitored by the University of Southampton.

Two sets of twenty vibrating wire embedment strain gauges, incorporating thermistors, were cast into the retaining wall. Two separate sets of six gauges were installed in the stabilising base. Gauges were placed in pairs at the intervals shown in Figure 3.10, to enable bending moments to be determined. A Campbell Scientific CR10 data logger was used to obtain a continuous record of the strain gauge output. Standard engineering beam theory (Equation 3.1) was used to convert the longitudinal strains  $\varepsilon_1$  and  $\varepsilon_2$  measured by the vibrating wire strain gauges near the back and front of the wall at the same depth into bending moment (M).

$$M = E.I \left( \frac{\varepsilon_1 - \varepsilon_2}{y} \right) \quad 3.1$$

Where E is the Young's Modulus of concrete, I is the second moment of area, and y is the distance from the gauge to the neutral axis. Composite flexural rigidities, EI, of  $1.4 \times 10^6$  kNm<sup>2</sup> per pile and  $2.2 \times 10^6$  kNm<sup>2</sup> per m run of base were calculated using E =  $25 \times 10^6$  kN/m<sup>2</sup> for concrete (BS 8110). The repeatability of the measurements was found to be  $\pm 7$  kNm/m.

Estimating the bending moment using equation 3.1. is not straightforward, because the flexural rigidity (EI) varies with bending moment when the wall is in a partly cracked state. In the analysis of field observations of retaining walls, generally uncracked behaviour is assumed (Tedd *et al.* 1984 and Wood and Perrin, 1984). This assumption has also been made in interpretation of the field measurements in this thesis.

### 3.7.3 Temporary prop loads

Gage Technique TEST/5.5 concrete embedment strain gauges with temperature measurement were used for monitoring the bending moments in the wall. These were installed by the University of Southampton and Gage Technique Ltd and monitored by the University of Southampton.

Axial loads and temperatures in the two temporary props in the instrumented bay were measured using surface mounted vibrating wire strain gauges incorporating thermistors. The gauges were located at quarter points around the circumference, 3m from the end of the prop. The data logger was used to obtain a continuous record of the strain gauge and temperature output every half hour. The axial load (P) was calculated using Equation 3.2. The repeatability of the measurements was found to be  $\pm 25$  kN.

$$P = \epsilon_{av} \cdot A \cdot E \quad 3.2$$

Where  $\epsilon_{av}$  is the average of all four gauges, A is the nominal net cross-sectional area of the prop, ( $A = 0.0192\text{m}^2$ ), and E is the Young's Modulus of the prop steel.

### 3.7.4 Vertical contact stresses beneath the stabilising base

Soil instruments 300 mm diameter oil filled pneumatic and vibrating wire pressure cells, with temperature measurement were used for monitoring the vertical contact stresses beneath the stabilising base. These were installed by the University of Southampton and Soil instruments Ltd and monitored by the University of Southampton.

Six pressure cells were installed beneath the stabilising base, in two rows of three as shown in Figure 3.12. All cells were fluid filled, with three of the cells having a pneumatic pressure transducer (PP) and three having a vibrating wire transducer (VP). Prior to casting the blinding concrete for the stabilising base, each cell was placed in a carefully trimmed pocket in the ground and surrounded with mortar bedding (Figure 3.12). The vibrating wire cells were monitored continuously using the CR10 data logger, while readings from the pneumatic cells were taken at appropriate intervals.

### **3.8. Results and discussion**

In this section the results of the field monitoring are presented, both for the main stages of construction and an eight-month period after the road was opened.

#### **3.8.1 Base line readings (wall movements and bending moments)**

The baseline readings were taken when the construction phase was at stage II (Table 3.3). This means that movements and bending moments that occurred during the first stage of excavation are not represented in the field data presented in this thesis. This possibly did not matter, as first stage excavation was the removal of the backfill to expose the existing cutting profile, it is therefore likely that the wall movements that occurred during this initial stage would have been small and within the accuracy of the measured wall movement readings.

#### **3.8.2 Wall movements**

Figure 3.15 shows the change in span at crest level between the monitored Bay W69 and the opposite Bay E71 as determined from the Geomensor measurements. Figure 3.13 also includes data on the span calculated from the inclinometer surveys assuming base fixity of the wall<sup>#</sup>. Geomensor datum readings were taken slightly after the first stage of excavation (Table 3.3). During further excavation of the berm there was a slight decrease of between 1-2mm in the closure of the retaining walls. On pre-loading the props, the distance between the retaining walls increased by approximately 10mm. Subsequent construction events caused small changes in the measured distance, until removal of the props when the distance between the retaining walls decreased by an increment of 15mm, or 5mm relative to the datum reading. During the main construction period close agreement was obtained between the two techniques, indicating that movements at the toe during this stage were small. The possible exception to this is the reading on day 379 where a small discrepancy is apparent in

---

<sup>#</sup> The assumption of base fixity may not always be correct due to small movements at the toe.

Figure 3.15. It may be that this Geomensor measurement was in error, but the reading could not be repeated because the line of sight was lost after day 379 due to the construction of a boundary wall.

Lateral movements of the crest of the retaining wall relative to the tape extensometer stations are shown in Figure 3.16, together with data from inclinometer I1 (assuming base fixity) and the semi-span of the underpass measured by the Geomensor. During the initial period of monitoring, the extensometer eyebolt in the capping beam was obstructed and had to be re-installed at a new location. A new datum reading for the replacement mount was established on day 155, and corrected to the Geomensor reading. A similar procedure was carried out on day 469 when the eyebolt had to be moved from the capping beam to the parapet when topsoil was placed over the retained ground.

Figure 3.16 shows close agreement between the various measuring techniques. Small differences are apparent between the movements of the crest of the wall as measured by the tape extensometer and those determined by the Geomensor (readings halved in order to estimate movements at Bay W69), when the temporary props in bay 69 were released on day 290. This indicated that an outward movement of the wall toe of no more than 2mm may have occurred at this time. Wall movements appear to have stabilised by day 632, with no indication of any seasonal variations during the following year's monitoring.

The horizontal deformations measured in the three inclinometer tubes are shown in Figure 3.17 for several stages during and shortly after construction of the underpass. These movements have been calculated assuming fixity at the base of the inclinometer tubes and as discussed previously, this assumption is not valid as it is possible that small (< 2mm) outward movements of the toe of the wall occurred, but these are not included in Figure 3.17. Little or no movement occurred during excavation in front of the wall up to day 155 (Table 3.3). More significant movements are apparent by day 196, after the props had been pre-loaded, with the crest of the wall at both Bays W69 and E71 being pushed about 5mm into the retained ground. By day 279 the movement profiles indicate that the temporary props had restricted the crest movements, but berm excavation for stabilising base construction had induced a 2mm outward movement of the wall at about

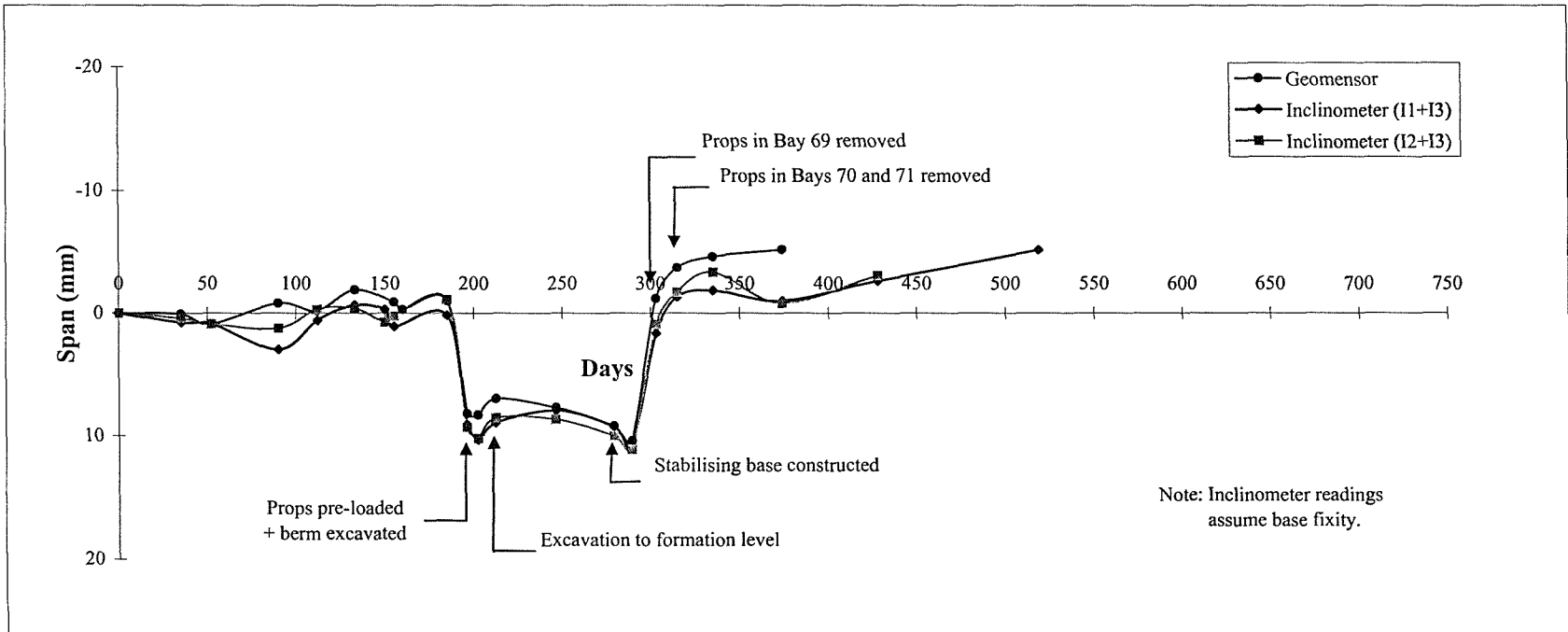


Figure 3.15. Change in distance at span between Bay W69 and E71

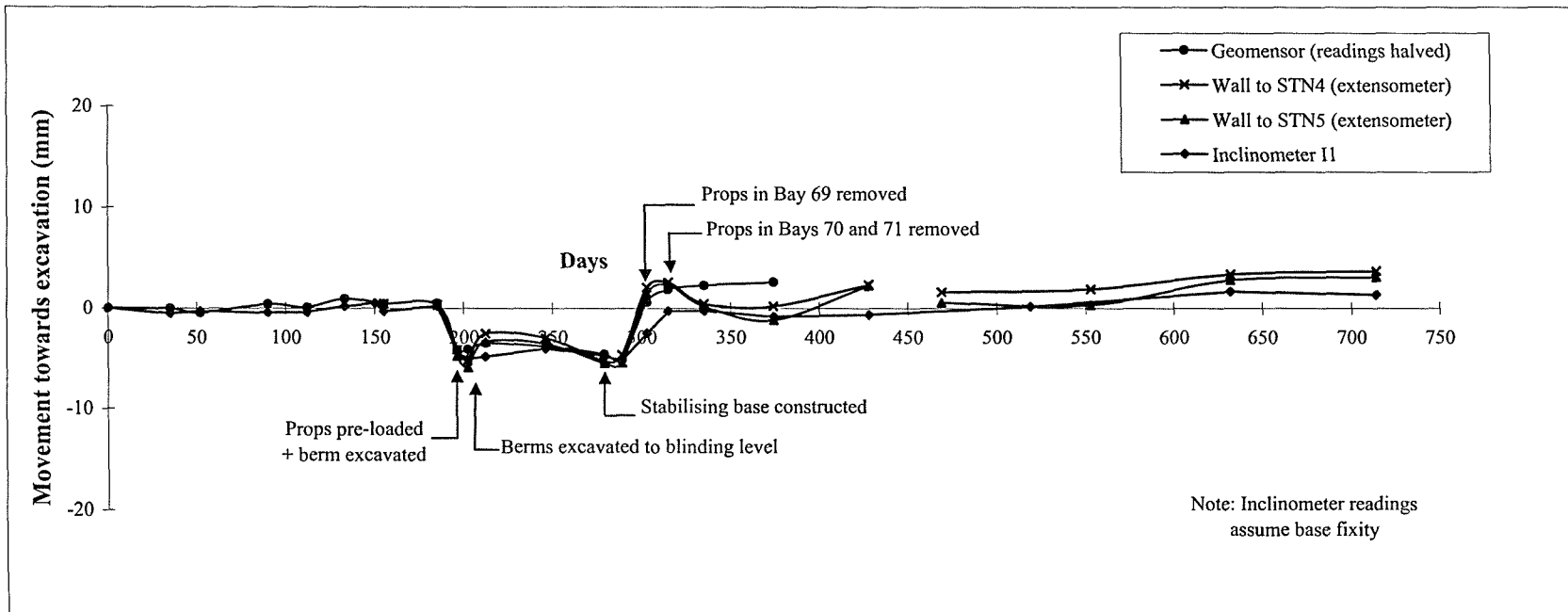


Figure 3.16. Change in wall crest movements (Bay W69)

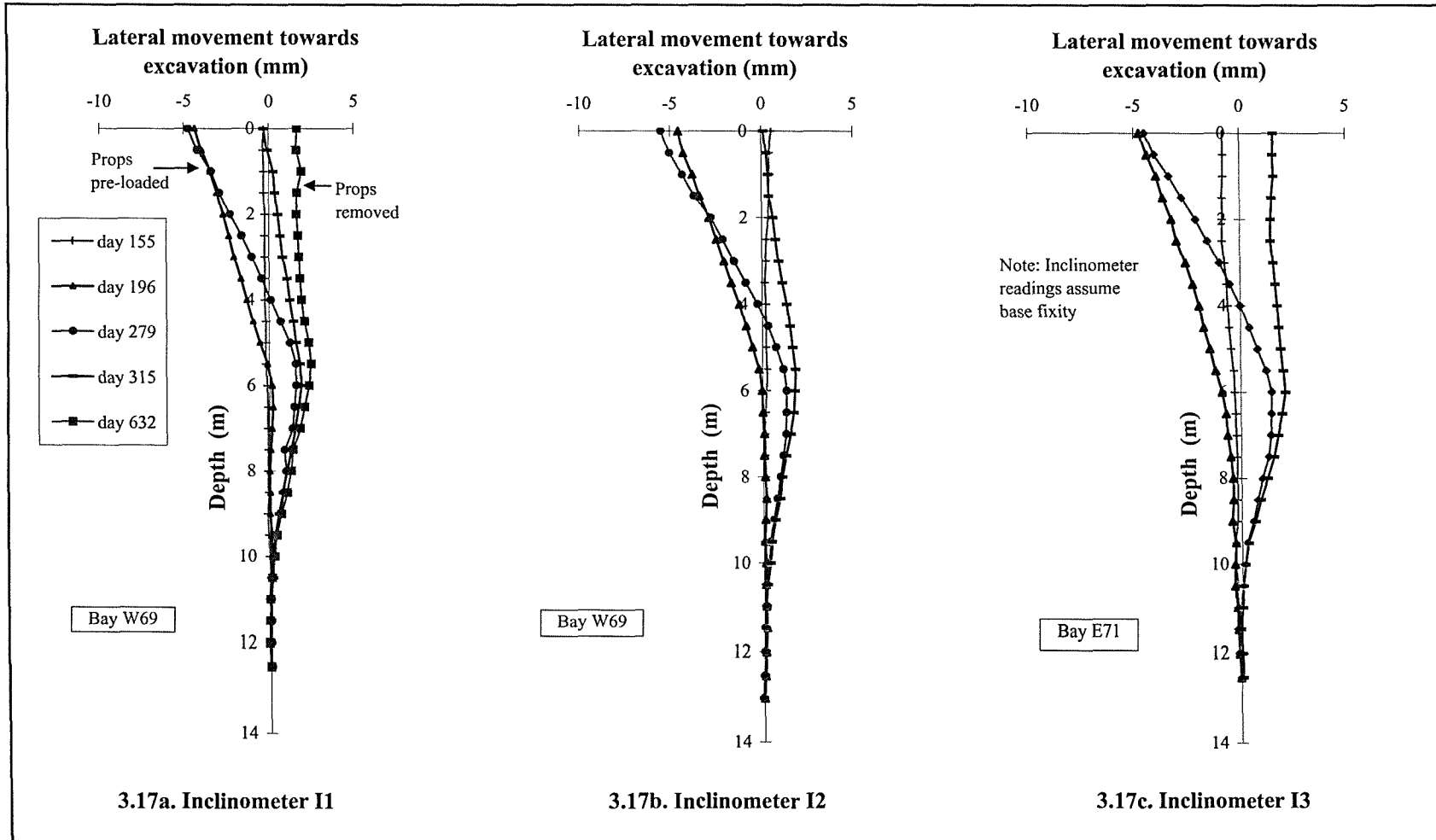


Figure 3.17. Development of lateral movements of the wall

6m depth. On removal of the props, the top of the wall moved towards the excavation. By day 632 the crest of the wall was about 2mm beyond its original position and most of the short term movement due to the construction work had probably taken place.

### 3.8.3. Temporary prop loads

Continuous records of the prop axial load and temperature against time are given in Figures 3.18 and 3.19 for temporary props P1 and P2 respectively. Figures 3.18a and 3.19a show the characteristic effects of restrained thermal expansion. These are typical of those identified at other sites where steel props have been used (Batten 1998; Twine and Roscoe 1999; Richards *et al.* 1999). Figures 3.18b and 3.19b show the calculated loads in both props due only to construction activity, i.e. with axial loads due to variations in prop temperature removed using the method described by Batten (1998). The temperature compensation factor was determined by monitoring prop loads and temperatures over a period when no construction activity took place on site (Figure 3.20).

Figures 3.18 and 3.19 show the changes in prop loads in the monitored bay as the construction sequence progressed. Prop P1 was the first prop in the monitored bay to be pre-loaded. When prop P2 was pre-loaded, the axial load in the Prop P1 fell as some of the load previously carried by the prop P1 was redistributed onto prop P2. Similar changes in loads on the props in monitored bay occurred when the props in the adjoining bay were pre-loaded. On excavation of the earth berms in front of the retaining wall, a very slight increase in axial loads in the props was observed (Figures 3.18b and 3.19b). Subsequent construction events did not cause any notable changes in the magnitude of the measured prop loads, until the loads fell to zero on prop release.

After all the props had been pre-loaded, the typical loads recorded in P1 and P2 were 900kN (180 kN/m) and 700kN (140 kN/m) respectively.



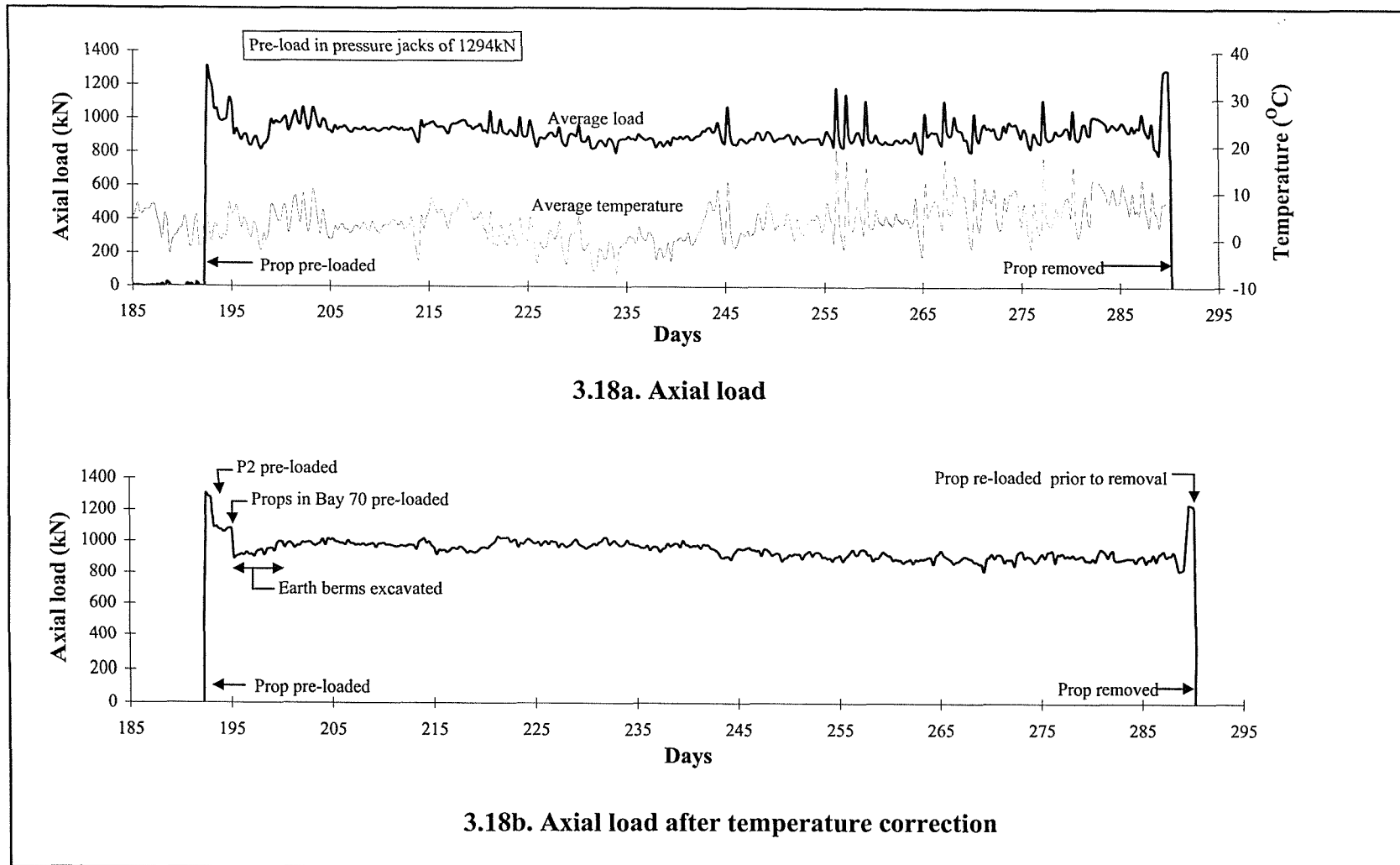
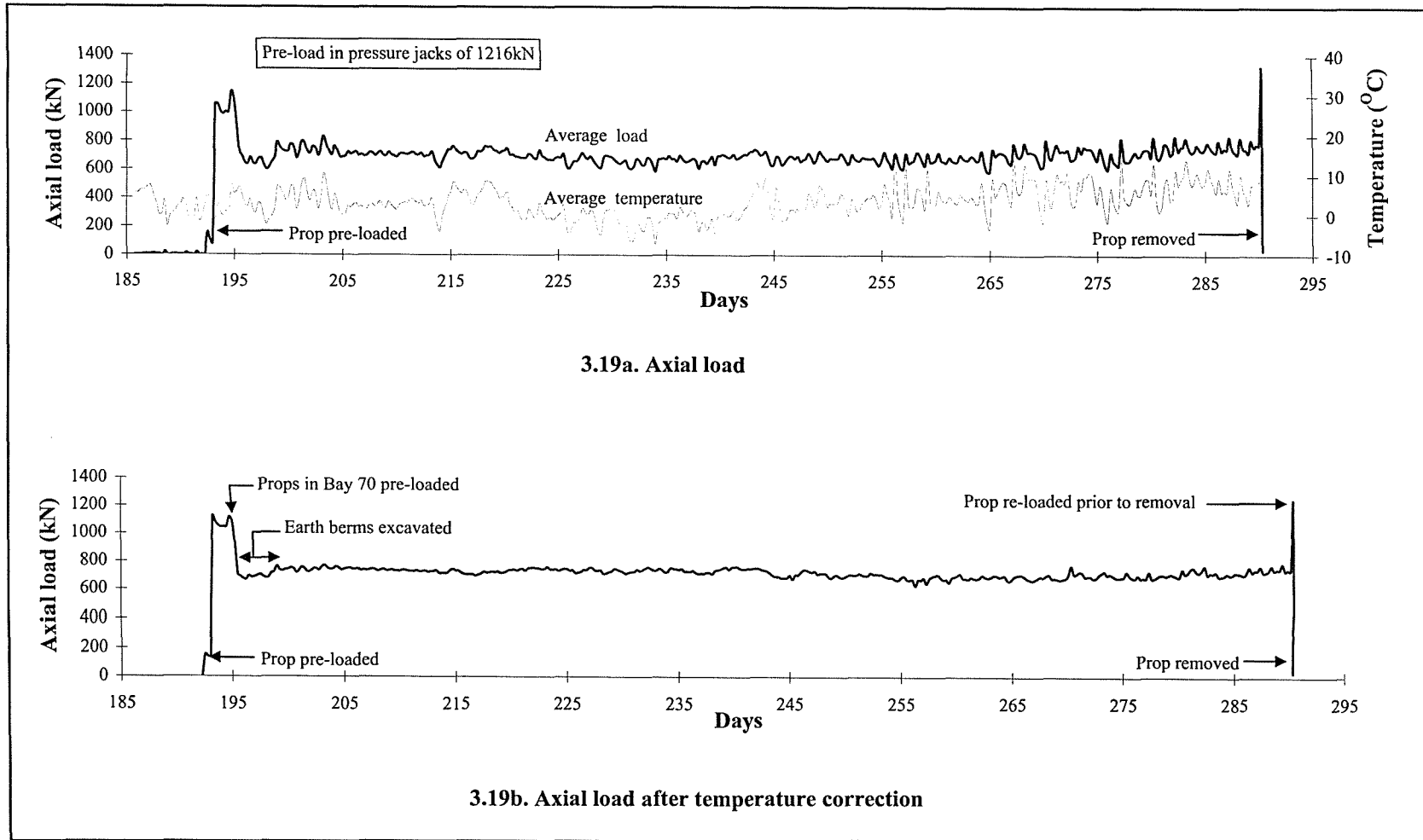


Figure 3.18. Change in axial load measured in temporary prop P1



**Figure 3.19. Change in axial load measured in temporary prop P2**

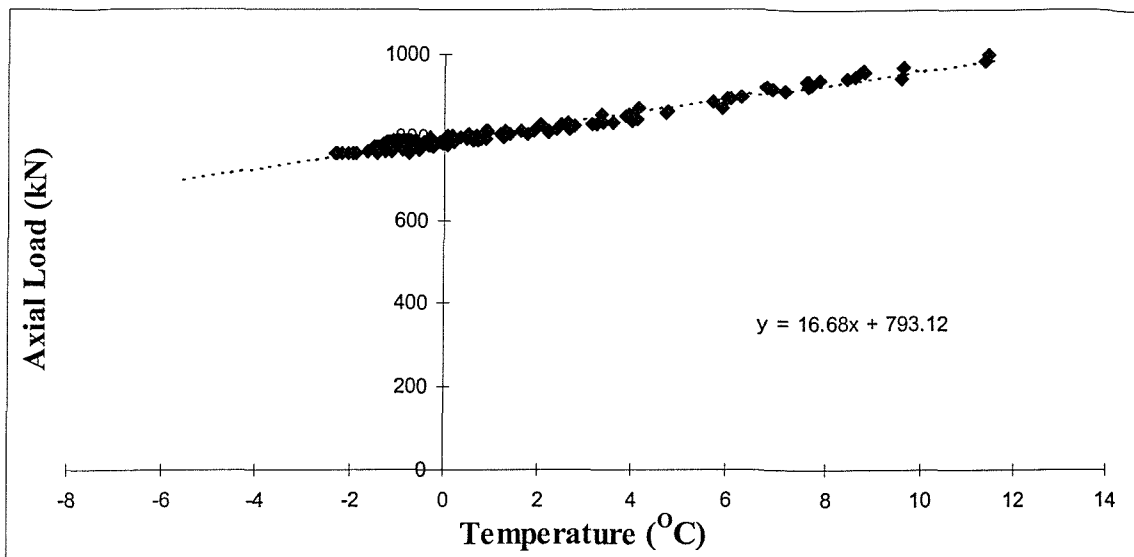


Figure 3.20. Typical change in axial load with temperature

#### 3.8.4. Wall and base bending moments

Continuous records of bending strain, and hence bending moment, were obtained from the vibrating wire gauges in the wall. Plots of bending moment against time for the gauges are shown in Figures 3.21 to 3.30. In all cases a sharp change in values occurred when the temporary props were pre-loaded and subsequently released. These changes are particularly noticeable at depths just above base formation level. Below formation level, the changes are not so pronounced.

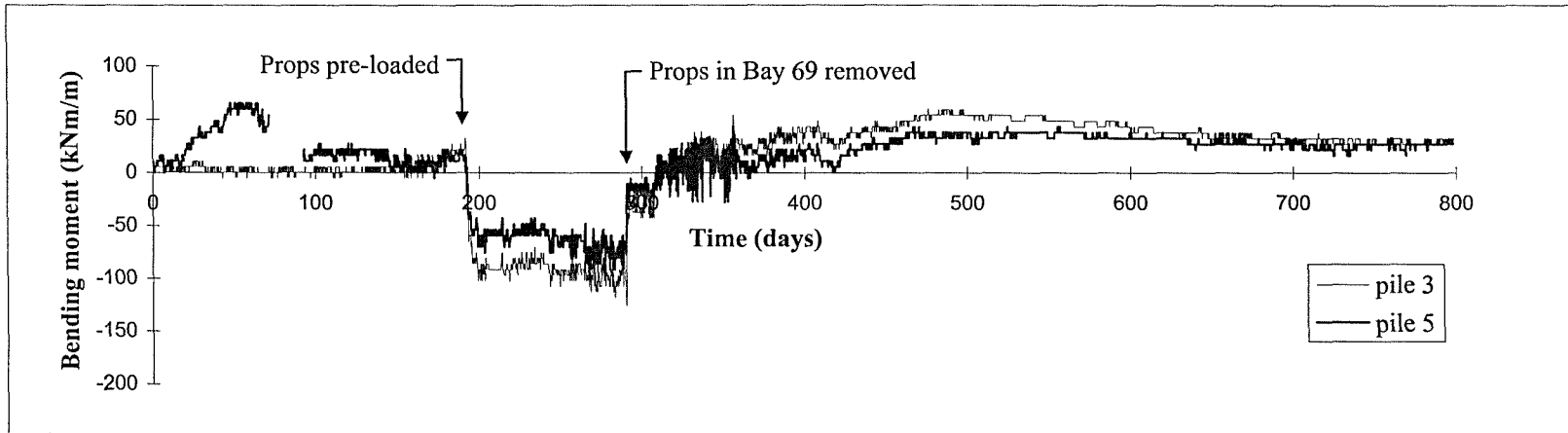
Figures 3.21 to 3.30 suggest that bending moments have stabilised by day 632. This is consistent with the wall movement observations.

Bending moments determined from the vibrating wire strain gauges in the wall at key stages of the construction sequence, corresponding to the days the wall movement readings were taken, are shown in Figure 3.31. Prior to the pre-loading of the temporary props on day 192, monitored bending moments in the wall were very small. After pre-loading the temporary props the bending moment profile was typical of a propped cantilever, with a maximum bending moment of around 215 kNm per pile. Removal of the berm induced an outward wall movement at about 6m depth, increasing the maximum bending moment at this level to 280 kNm per pile. On releasing the props,

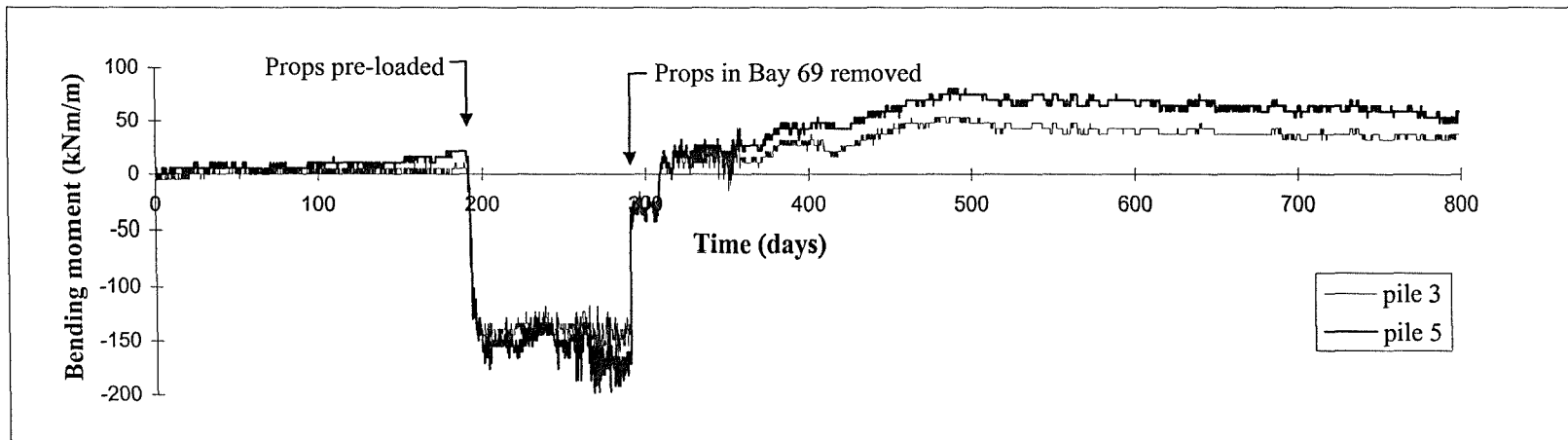
the rotation of the wall towards the excavation generated a bearing pressure on the underside of the stabilising base, which imparted a restoring moment to the retaining wall. The results in Figure 3.31 demonstrated that the maximum bending moment over the retained part of the wall for design purposes is likely to occur after excavation to full depth with the temporary props in place. Also, the pre-loading of the temporary props allowed the development of a significant base bearing pressure as the wall rotated back to its initial position, and thus probably reduced the overall wall movement towards the excavation.

Figure 3.32 shows continuous records over time of bending moments developed in the stabilising base at two locations in front of piles 3 and 5. These confirm that on releasing the temporary props, bending moments were developed immediately in the stabilising base as the outward rotation of the wall was resisted. As would be anticipated the largest bending moment of about 100kNm/m was measured using the strain gauges closest to the wall (Figure 3.32c) with the moment reducing to about 40kNm/m at 4.5m away (Figure 3.32a). A reduction in the bending moment in the base with time was initially recorded, although by day 632, readings have stabilised.

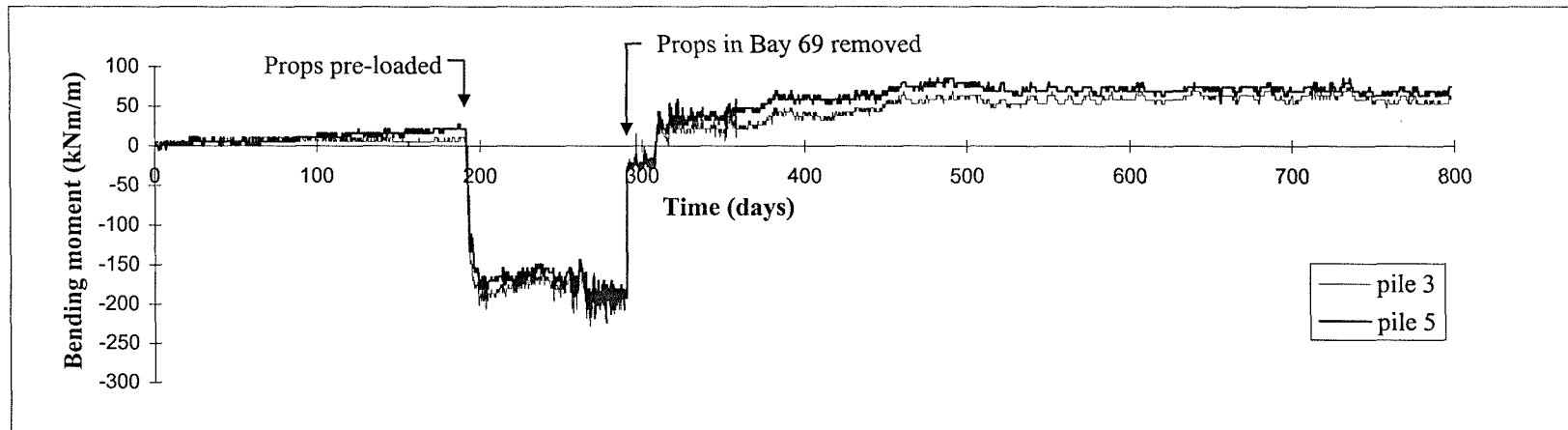
The results in Figure 3.33 show variation of stabilising base bending moments with distance from the wall.



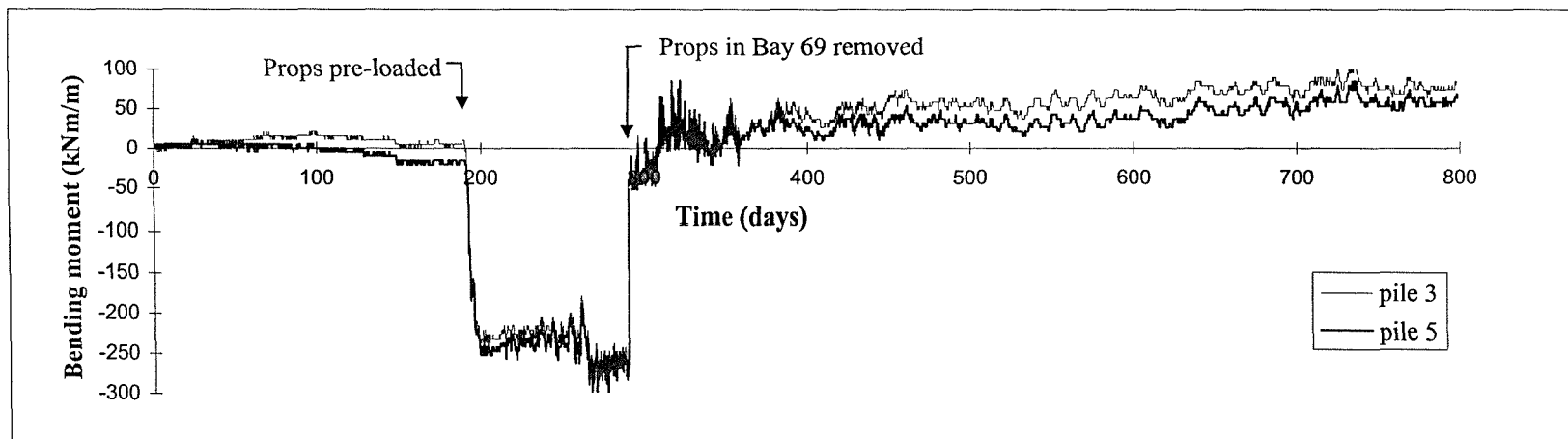
**Figure 3.21. Development of wall bending moments at 1.73m below top of wall**



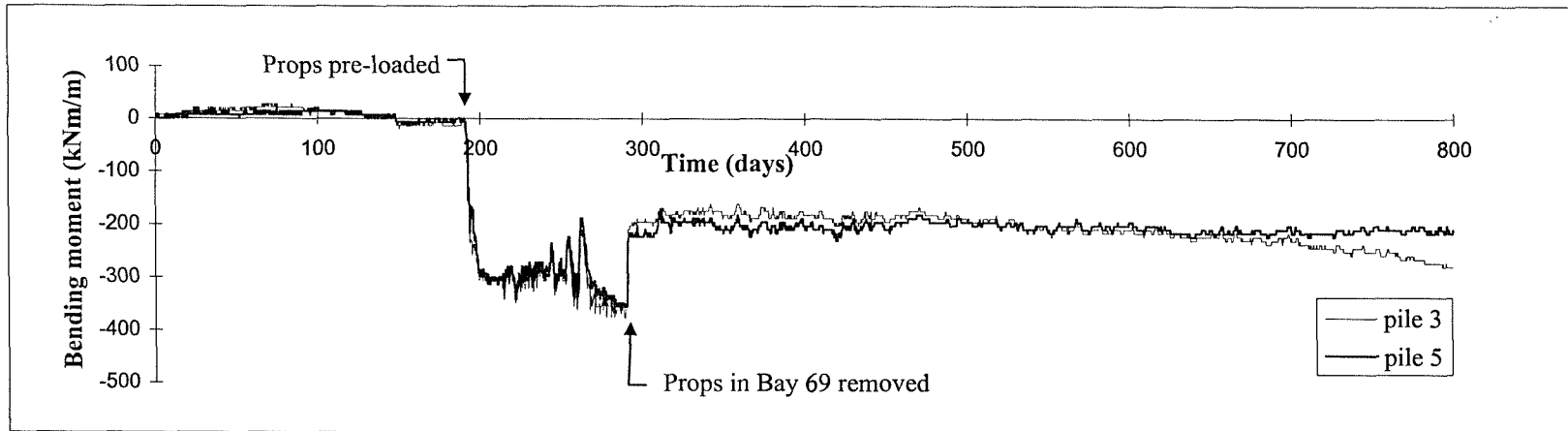
**Figure 3.22. Development of wall bending moments at 2.73m below top of wall**



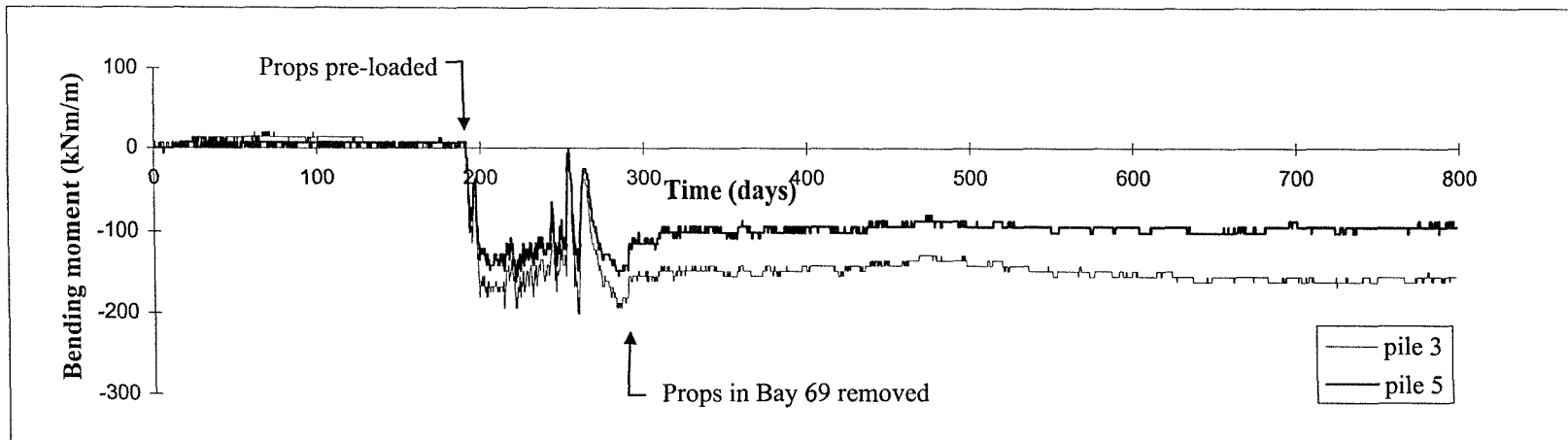
**Figure 3.23. Development of wall bending moments at 3.73m below top of wall**



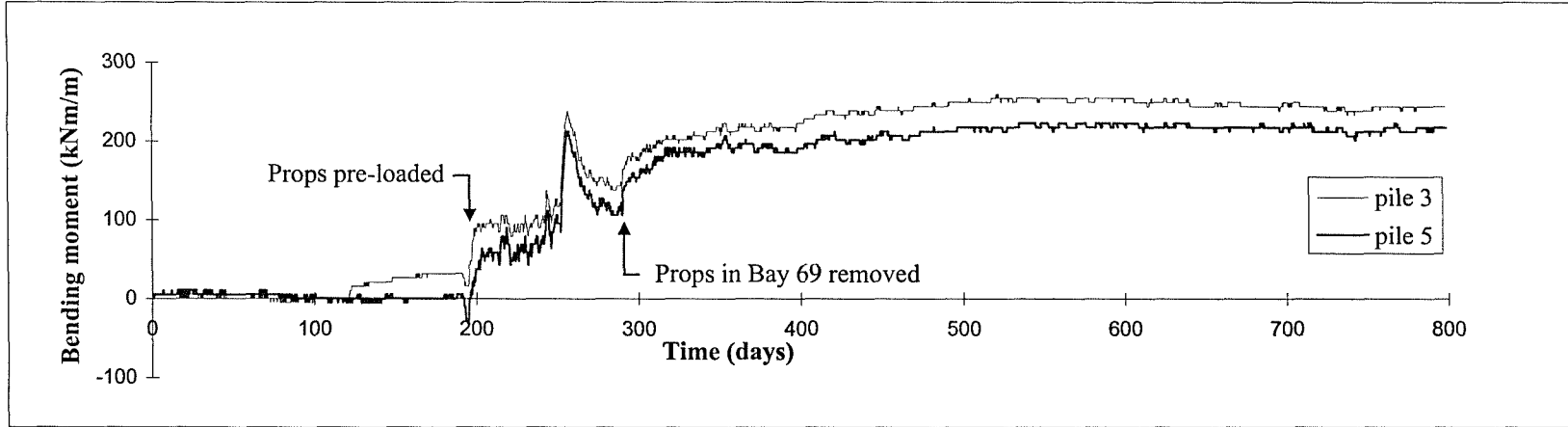
**Figure 3.24. Development of wall bending moments at 5.03m below top of wall**



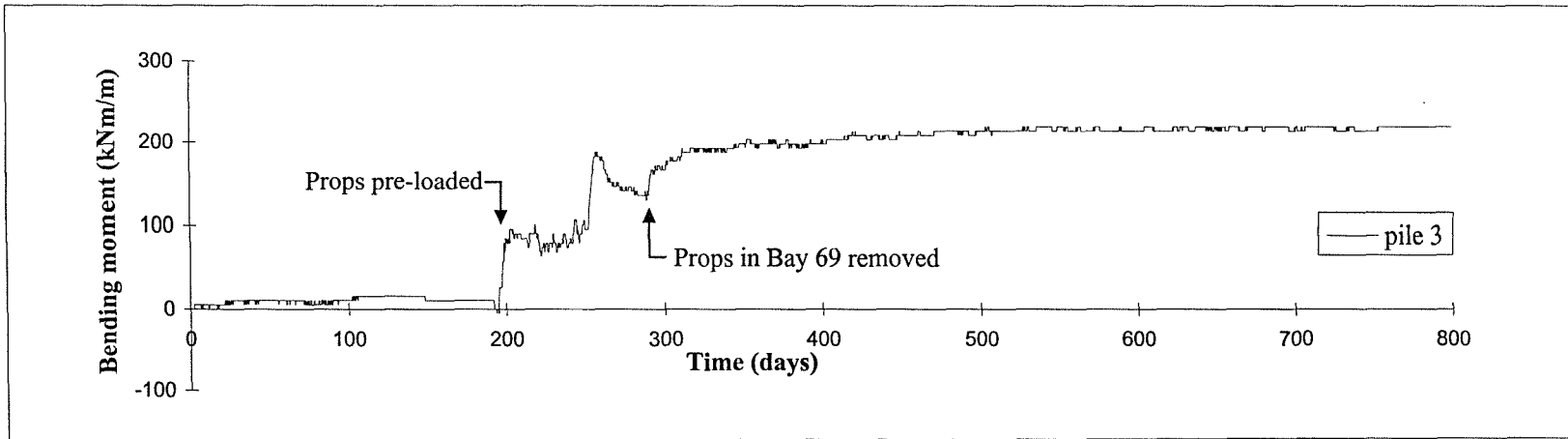
**Figure 3.25. Development of wall bending moments at 6.33m below top of wall**



**Figure 3.26. Development of wall bending moments at 7.63m below top of wall**

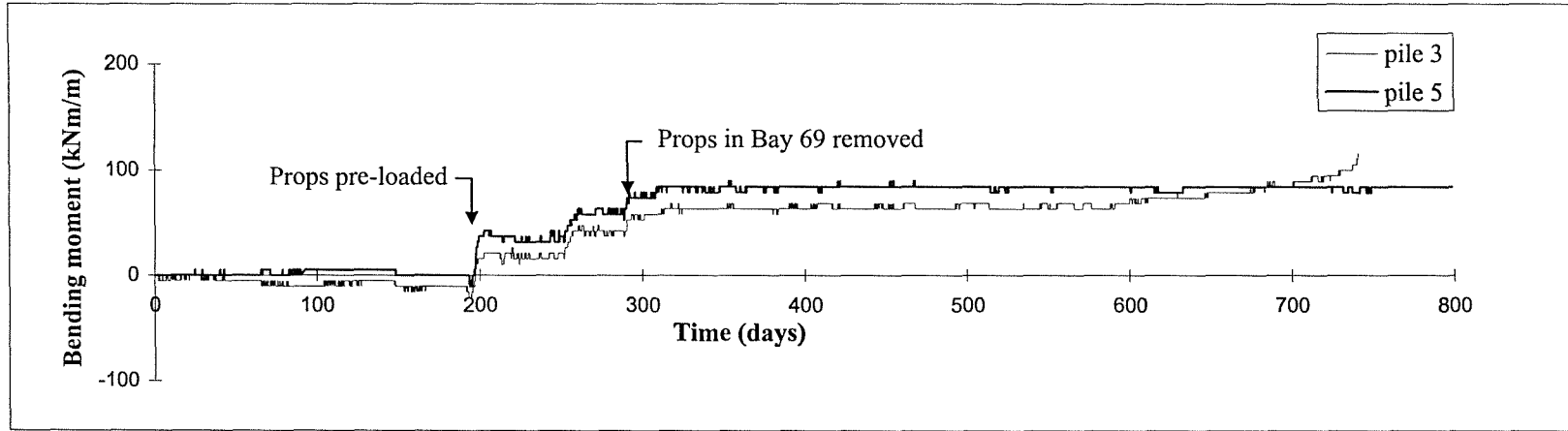


**Figure 3.27. Development of wall bending moments at 9.43m below top of wall**

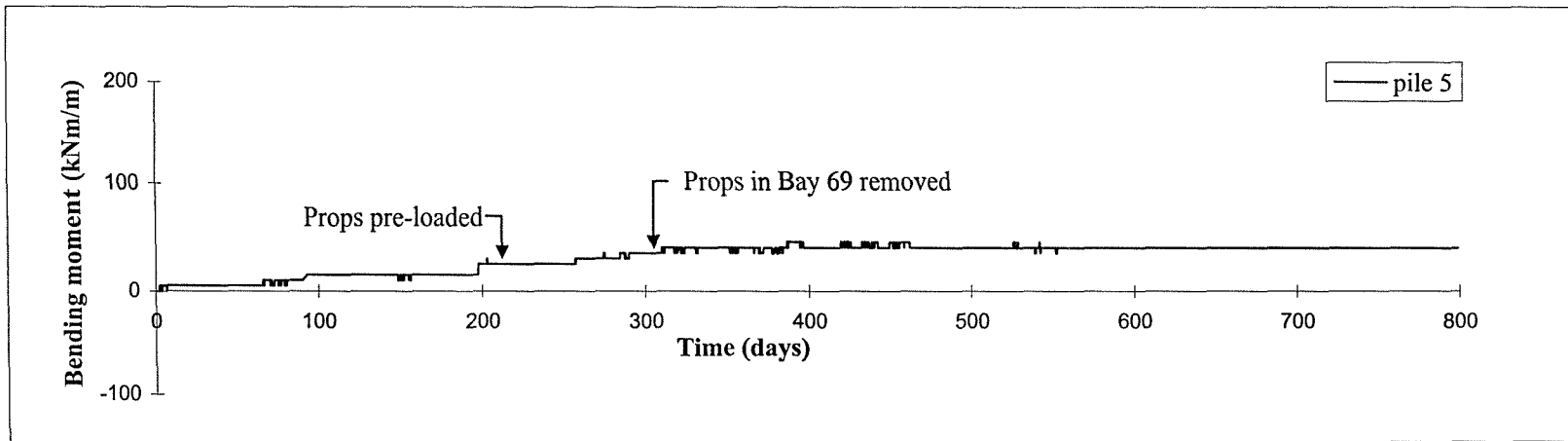


**Figure 3.28. Development of wall bending moments at 10.23m below top of wall**

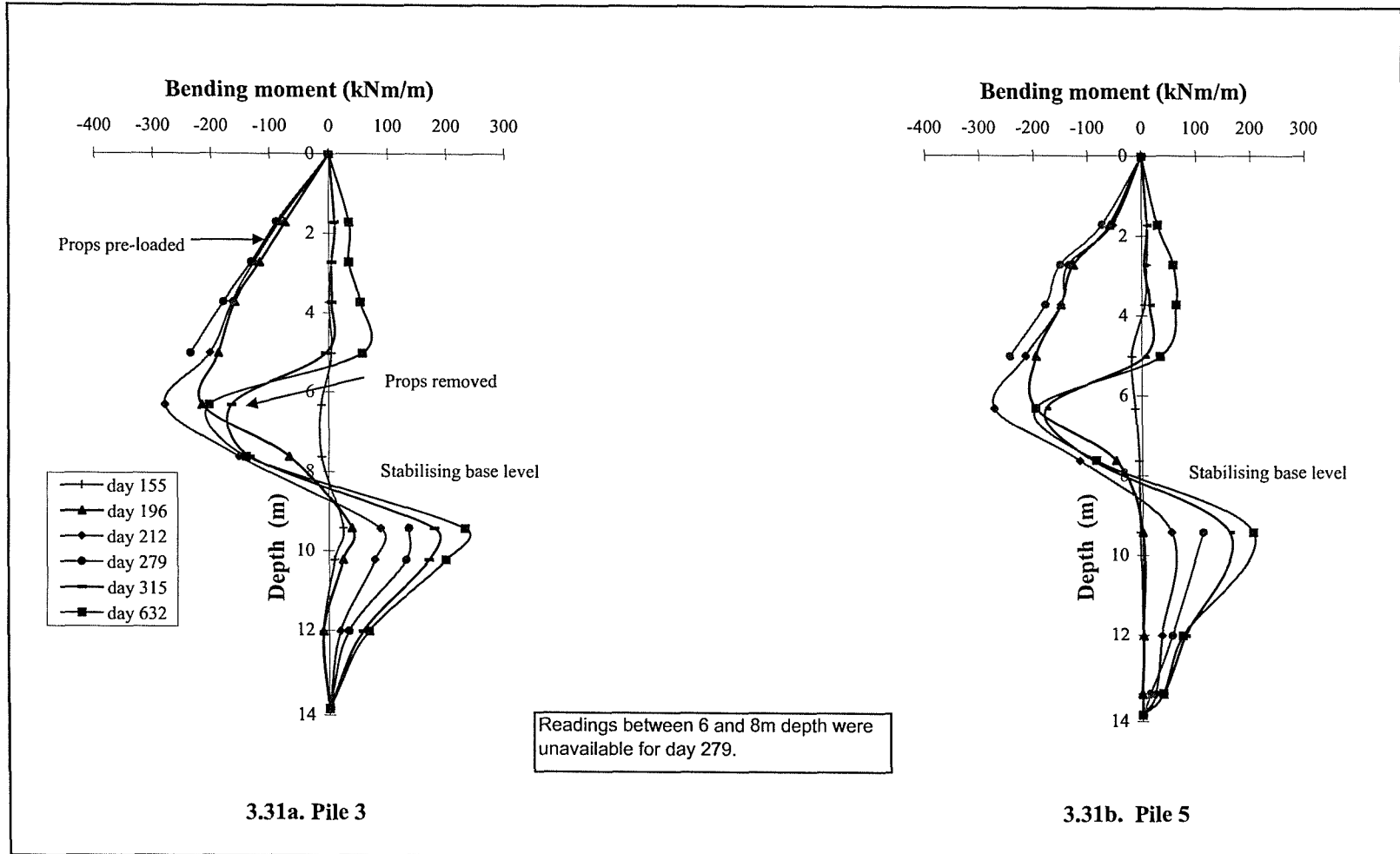




**Figure 3.29. Development of wall bending moments at 12.03m below top of wall**



**Figure 3.30. Development of wall bending moments at 13.33m below top of wall**



**Figure 3.31. Development of wall bending moments (Bay W69)**

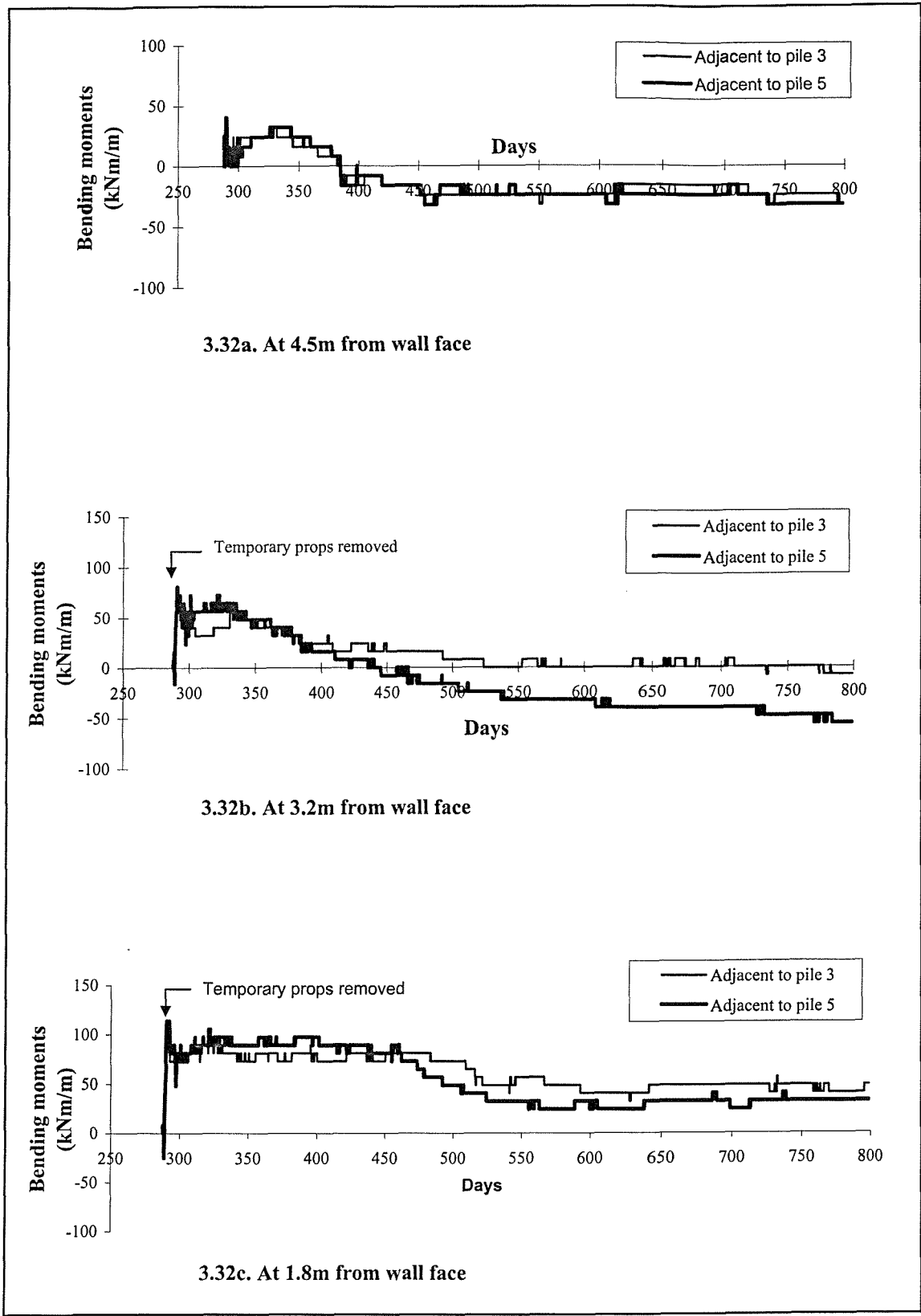


Figure 3.32. Development of stabilising base bending moments

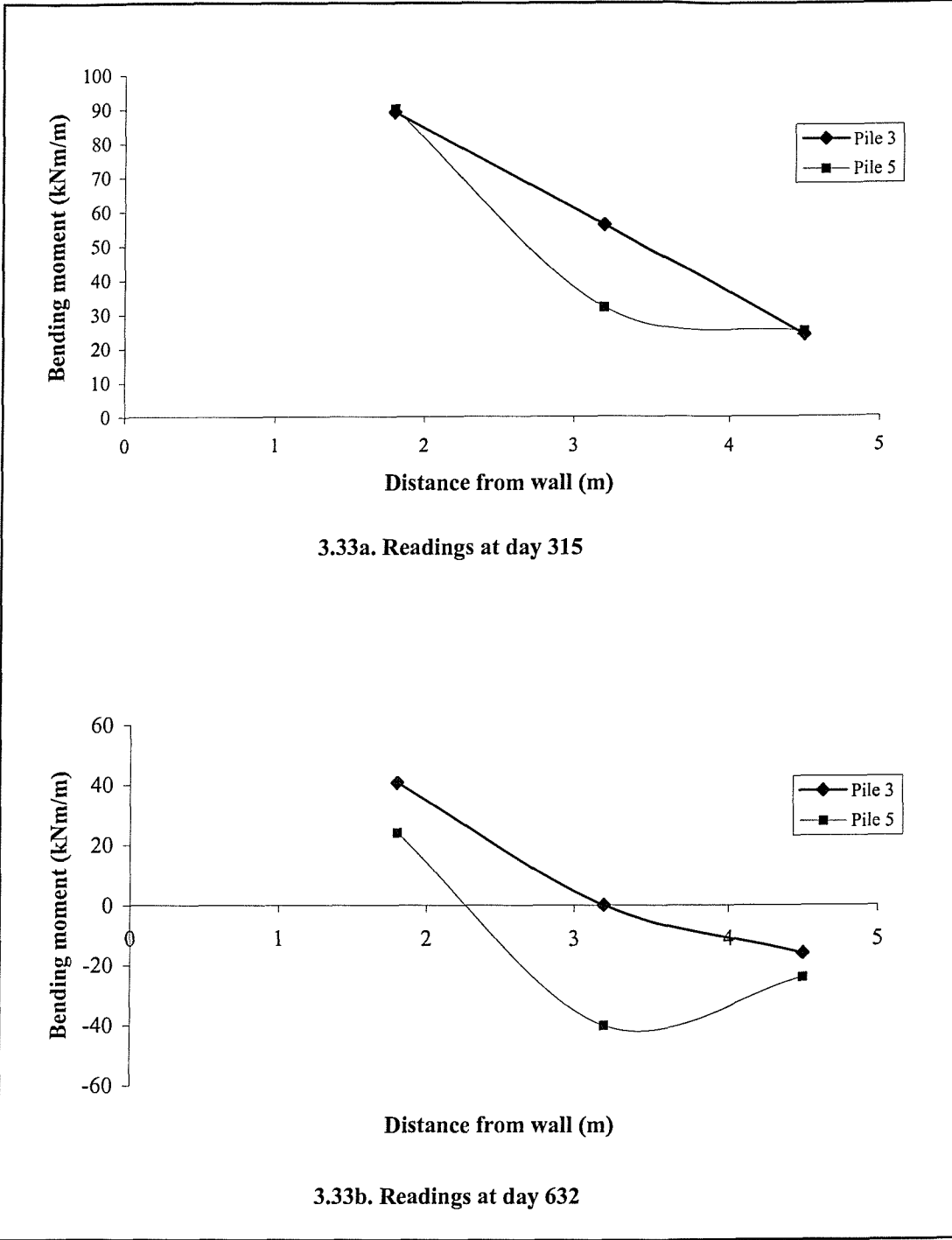


Figure 3.33. Bending moments in stabilising base

### 3.8.5. Vertical contact stresses beneath the stabilising base

Boundary total stress cells need to be calibrated, like any measurement equipment. Calibrations under fluid pressure will usually produce easily repeatable results, but when the cell is inserted into the ground the stress field in the vicinity of the cell is modified and this may lead to unrepresentative values being recorded. Total stress cells have therefore been the subject of considerable research and discussion, which has shown that cells will under-read if care is not taken in the selection of the cell (see Taylor, 1947, Askegaard, 1961, Trollope and Lee, 1961, Carder and Krawczyk, 1975, and Clayton and Bica, 1993).

The cell action factor (CAF) has been proposed to quantify the measurement error; this is the ratio between the value of normal stress measured by the cell and the value that would have existed in its absence (Taylor 1947). The nearer to 1 is the CAF value, the more accurate is the measurement of normal stress. The CAF depends on the Young's modulus of the soil and the Young's modulus of the diaphragm material (see Askegaard 1961 and Clayton and Bica, 1993) and can be as low as 0.25 if the incorrect type of cell is used in a specific soil type. The readings from the pressure cells presented in this thesis have not been corrected for any possible under-read. It is therefore possible that the results presented for the vertical contact stress under the stabilising base are an underestimate of the actual results. However, experience has shown that the under-read for this type of cell is likely to be less than 10% (Carder 2000).

Figure 3.34 shows the development of vertical contact stress as measured by the pressure cells under the stabilising base. Figure 3.34a gives the readings taken manually from cells with pneumatic transducers beneath the base in front of pile 5. Figure 3.34b shows the continuously logged data from the cells with vibrating wire transducers in front of pile 3. In both cases, a significant increase in the pressure was recorded when the temporary props were removed. The average temperature variations at both locations are also shown. The pressures show some thermal fluctuation, as the cells are fluid-filled and therefore have some temperature susceptibility. These have been corrected by obtaining a change in cell pressure with temperature equation, from data that was measured during a period when there was no measurable wall movement, Figure 3.35.

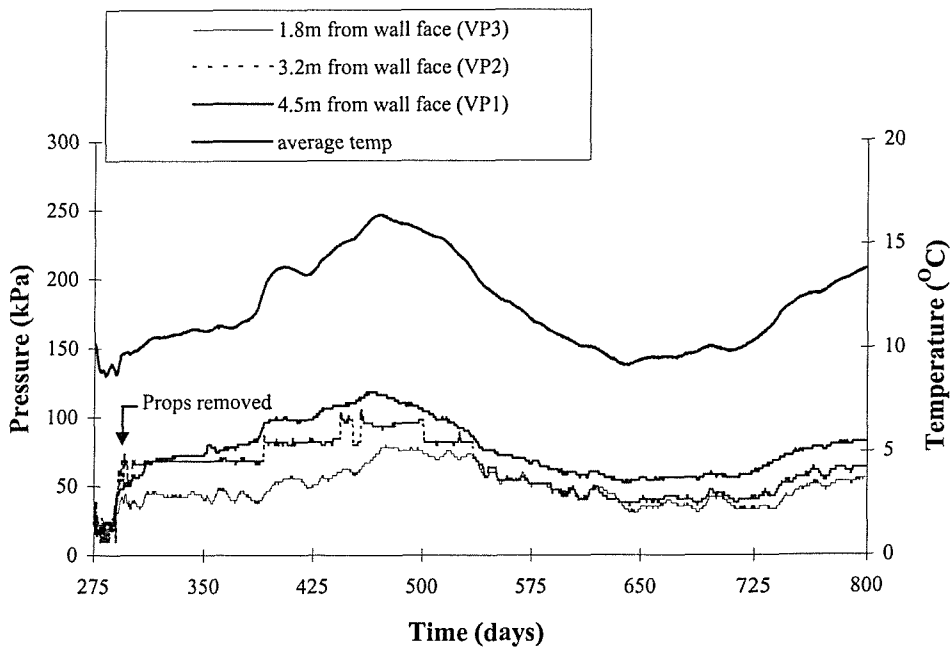
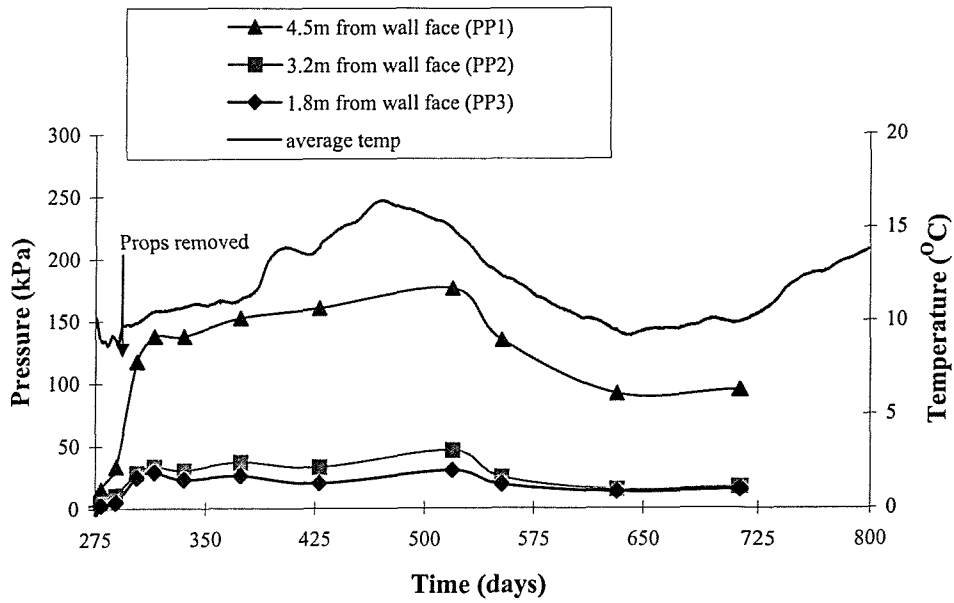
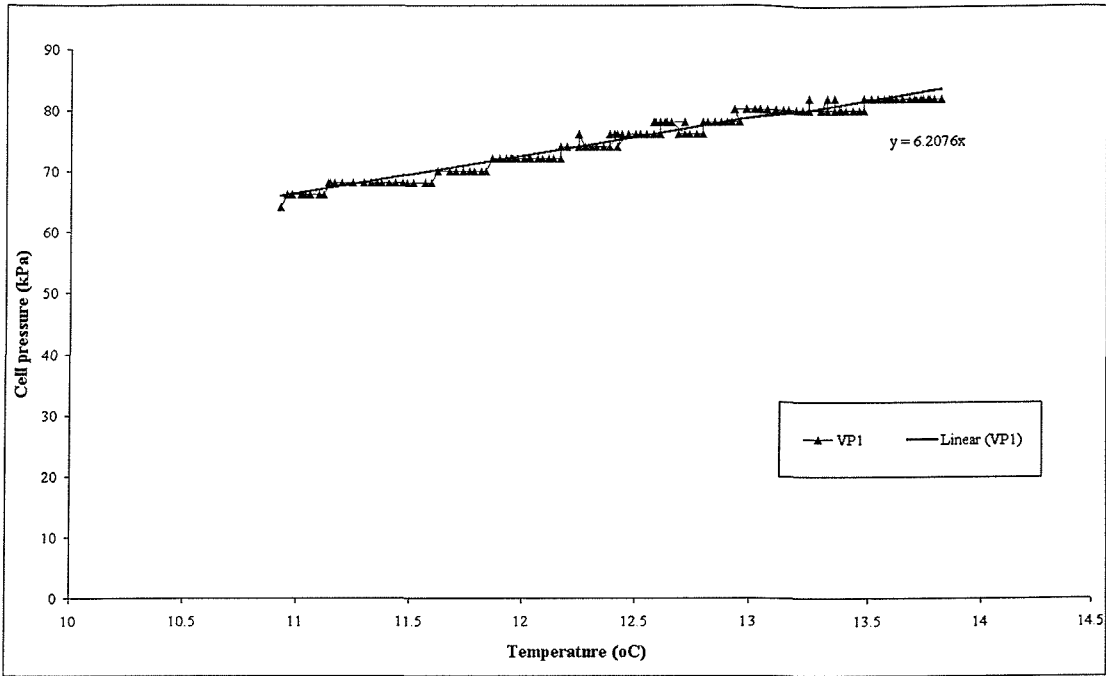


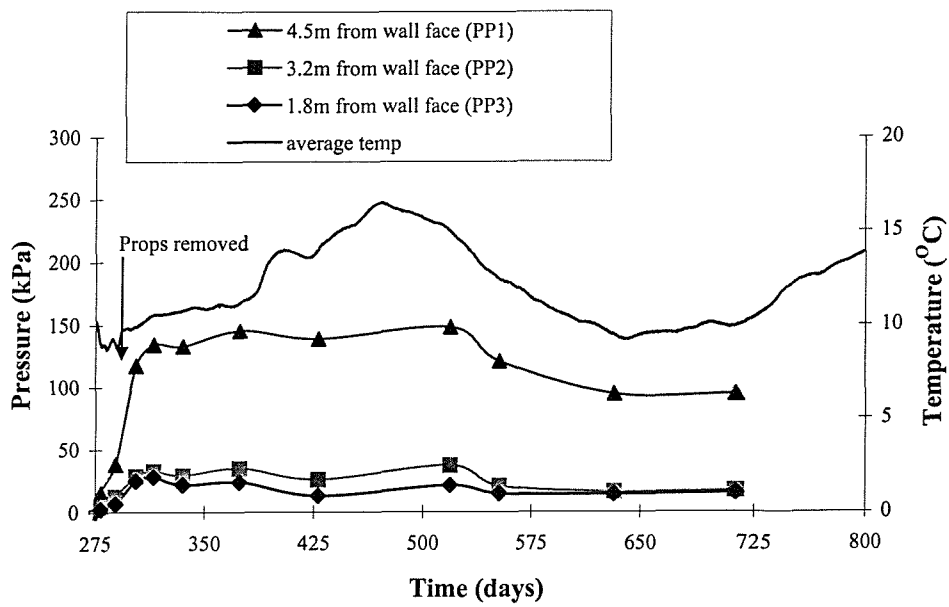
Figure 3.34. Vertical contact stresses beneath the stabilising base



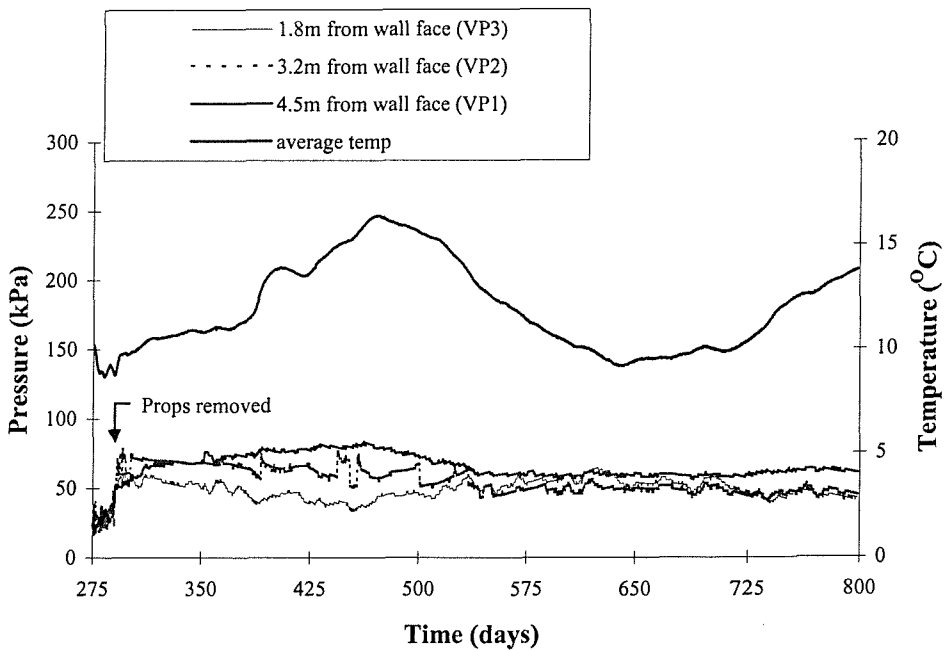
**Figure 3.35. Typical change in cell pressure with temperature**

Figure 3.36 shows the vertical contact stresses corrected for temperature. It indicates a slight reduction in vertical stress with time.

The results in Figure 3.37 show a variation in the vertical contact stress with distance from the wall. These dates, (day 315 and 632), correspond to the days the wall movement readings were taken. Generally the vertical contact stresses beneath the base increase with distance from the wall in front of pile 5, although this trend is less evident in front of pile 3.



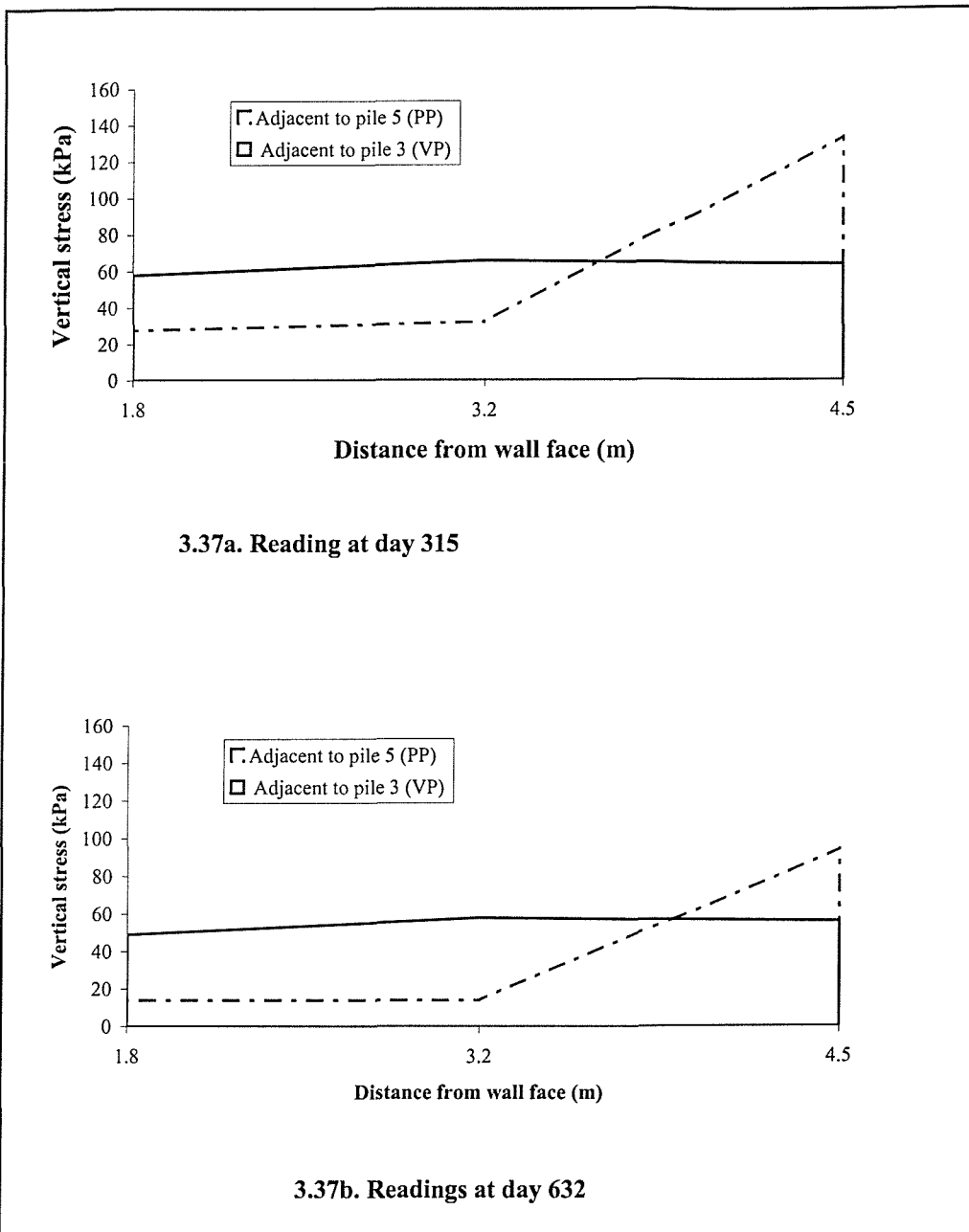
3.36a. Stresses beneath the base adjacent to pile 5



3.36b. Stresses beneath the base adjacent to pile 3

Figure 3.36. Temperature corrected vertical contact stresses





**Figure 3.37. Variation of vertical contact stress beneath the stabilising base with distance from the wall**

### 3.9. Simple assessment of instrument performance

Attempts were made to calculate the wall movements of the retaining wall from the measured bending moment profiles. This proved to be unsuccessful, as it was difficult to fit a curve to the measured bending moment data.

The bending moments in the stabilising base have been calculated using the measured vertical contact stresses beneath the stabilising base. It was assumed that the vertical contact stresses beneath the stabilising base, just after the props have been removed, day 315, are as given in Figure 3.38. This distribution has been taken from Figure 3.37, but has removed the self weight of the stabilising base. The measured stress under the base, (180 kN/m at pile 3 and 129 kN/m at pile 5), approximates to the pre-load (160 kN/m) applied to the temporary prop. Using the vertical contact stresses shown in Figure 3.38 the bending moments were calculated over the stabilising base and these are shown in Figure 3.39. Also shown is the measured profile of the stabilising base bending moment at this stage reproduced from Figure 3.33. The shapes of the measured and calculated moments are similar, although the calculated moments are slightly higher.

This simple assessment of the wall suggest that there is a consistency between the different measurements of prop load, vertical contact stress and base bending moments and any under-read of the load cells may not be very significant.

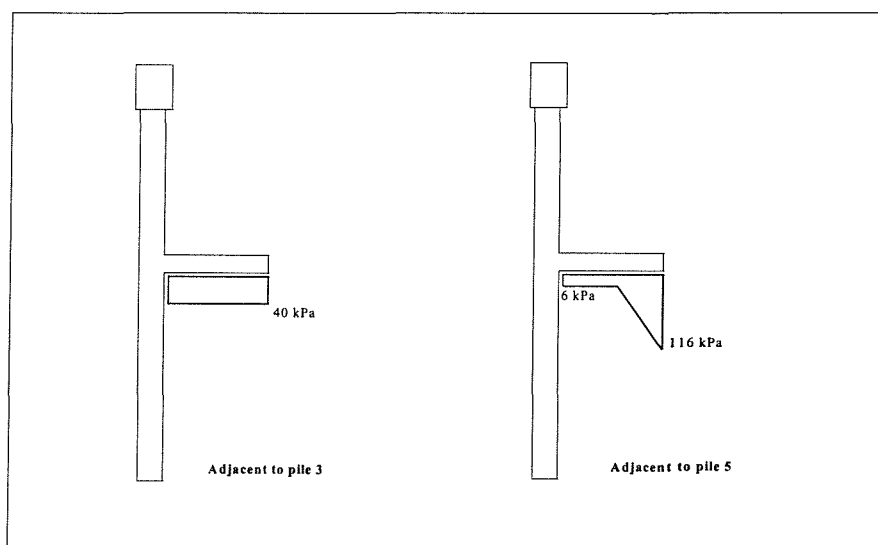


Figure 3.38. Assumed vertical contact stresses

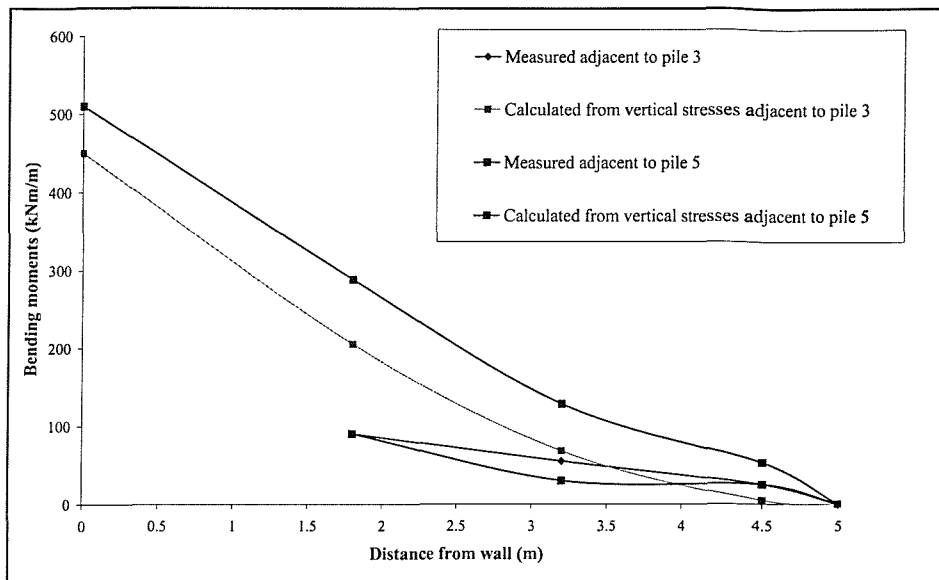


Figure 3.39. Comparison of measured and calculated base bending moments

### 3.10. Summary

Field monitoring has been carried out to investigate the behaviour of a contiguous bored pile retaining wall founded in weak rock during and immediately after its construction as part of the Coventry North-South Road scheme in Warwickshire. The following key features were observed.

- i. Pre-loading of the temporary props used to support the wall during excavation to formation level pushed the top of the wall about 5mm into the retained Bromsgrove Sandstone Formation. After final excavation and construction of the stabilising base, the temporary props were removed and the wall cantilevered towards the excavation until its top was 2mm beyond its original position. During the later stages of construction, it is likely that a small outward movement of the toe, and hence a translation of the wall, of up to 2mm, occurred.
- ii. The axial loads in the temporary steel props varied with temperature. Normalisation of the loads to a constant temperature showed that only small changes in load from the original pre-load values occurred due to construction activities over the construction period.

- iii. Prior to pre-loading the temporary props, measured wall bending moments were small. After pre-loading, the bending moment profile was typical of a propped cantilever, with a maximum moment of around 215kNm/m. Excavation of the berm induced an outward wall movement at about 6m depth, increasing the maximum bending moment at about this level to 280kNm/m. On removing the temporary props, a bearing pressure was developed on the underside of the stabilising base which imparted a restoring moment to the wall.
- iv. Measurements of vertical pressures beneath and bending moments in the stabilising base confirmed their immediate development on removal of the temporary props. As would be anticipated the largest bending moment (about 100kNm/m) was measured closest to the wall with the moment reducing to 40kNm/m at 4.5m away. Generally the vertical stresses beneath the base increased with distance from the wall in front of pile 5, although this trend was less evident in front of pile 3.
- v. All measurements indicate that by day 634 short-term movements due to the construction work had probably ceased.

Temperatures changes have an influence on the readings taken from fluid filled pressure cells. This can be compensated for if a temperature compensation factor is obtained over a period of time when no construction activity is taking place.

The field monitoring has reaffirmed

- the desirability of datalogging the output from field instrumentation, which enables a continuous record to be obtained; and
- the necessity of recording temperatures when the measurements being made are temperature sensitive.

Independent wall movement measuring techniques ensured that consistent sets of wall movements were obtained for the case study. In addition, lines of instruments at different locations confirm the agreement between the measurements. Simple assessments of the wall suggest that there is a consistency between the different measurements of prop load, vertical contact stress and base bending moments.

## CHAPTER 4

### **GEOTECHNICAL PARAMETERS FOR WEAK ROCK AT STUDY SITE**

#### **4.1. Introduction**

Discontinuities have a significant effect on the mechanical properties of a rock mass. Discontinuities also influence mechanical behaviour of soil, with the difference between the properties of intact and fissured clays widely acknowledged (Terzaghi 1936, Skempton *et al.* 1969, Rowe 1972 and Marsland 1972). In hard rocks the stiffness of the discontinuities is generally significantly less than that of intact rock. It is therefore difficult to make accurate estimates of mass compressibility from laboratory stiffness measurements made on intact rock if the rock mass is any way fractured. In chalk and London Clay the interrelationships between discontinuity spacing and the dimensions of the loaded area has also been demonstrated to be important (see Matthews 1990 and Marsland 1972). Because the discontinuities can play an important role in controlling the mass compressibility it is preferable to perform *in situ* tests to assess the mass compressibility parameters. Nevertheless, Kulhawy (1978) suggests that the intact stiffness can be used in conjunction with the rock mass rating to obtain rock mass stiffness parameters.

In this chapter, parameters obtained from field tests carried out at the research study site and laboratory tests on samples collected from the site are compared and discussed.

## 4.2 Field *in situ* tests

The first set of parameters discussed in this chapter are those obtained from *in situ* field tests. These include profiles obtained from weak rock self boring pressuremeter tests (RSBP) and high pressure dilatometer tests (HPD), geophysical tests and Standard Penetration Tests (SPT). Parameters obtained from the field tests should represent mass parameters if a representative volume of the rock mass is tested for its performance, but as will be seen in the discussion this is not always the case.

### 4.2.1. Weak rock pressuremeter tests

The principles of pressuremeter testing can be found in various publications (Mair and Wood 1987), with details of the weak rock self boring pressuremeter in particular given by Clarke and Allen (1989). The pressuremeter is a cylindrical device designed to apply a uniform radial pressure to the sides of a borehole. There are two basic types used at Coventry:

- the high pressure dilatometer (HPD), which is lowered into a pre-formed borehole
- the weak rock self-boring pressuremeter (RSBP), which forms its own borehole and thus causes much less disturbance to the weak rock prior to testing.

In both cases, the pressuremeter test involves the application of known stresses to the weak rock and the measurement of the resulting weak rock deformation. The interpretation of pressuremeter test data in engineering terms does not, therefore, rely on empirical correlations. Therefore, theoretically the pressuremeter is a good method for determining the stiffness parameters for a weak rock.

Pressuremeters are normally inserted vertically at various depths in the ground. The sides of the borehole are loaded by pressurising a fluid contained within a flexible rubber membrane. The expansion of the cavity is determined either by measuring the volume of fluid needed to pressurise the membrane, and/or by measuring the movement of the material at the cavity wall directly using displacement transducers. The

interpretation of pressuremeter data is based on the analysis of an expanding cylindrical cavity, with deformation in the horizontal plane.

Corrections must be made to the measured pressure, volume change and cavity deformation in order to account for the compressibility of the fluid and pipework, differences in elevation between the instruments and pressure transducer, and the stiffness of the membrane. The calibration procedures that are carried out in order to quantify these effects are described by Mair and Wood (1987).

In general, some disturbance of the borehole wall is inevitable in a pressuremeter test where the probe is lowered into a pre-formed borehole. At the early stages of the test this disturbance influences the stress strain curve, (Figure 4.1a). In a HPD test the stress-strain curve should steepen sharply at a point such as A, as the device comes into contact with the pre-formed borehole wall and compresses any softened rock. The relationship between the increase in pressure and the increase in cavity strain will then be approximately linear and elastic until point B is reached. At B, the rock at the borehole wall starts to deform plastically. In a high-quality self boring pressuremeter test, the stress strain curve should start with the pressuremeter in contact with the sides of the borehole.

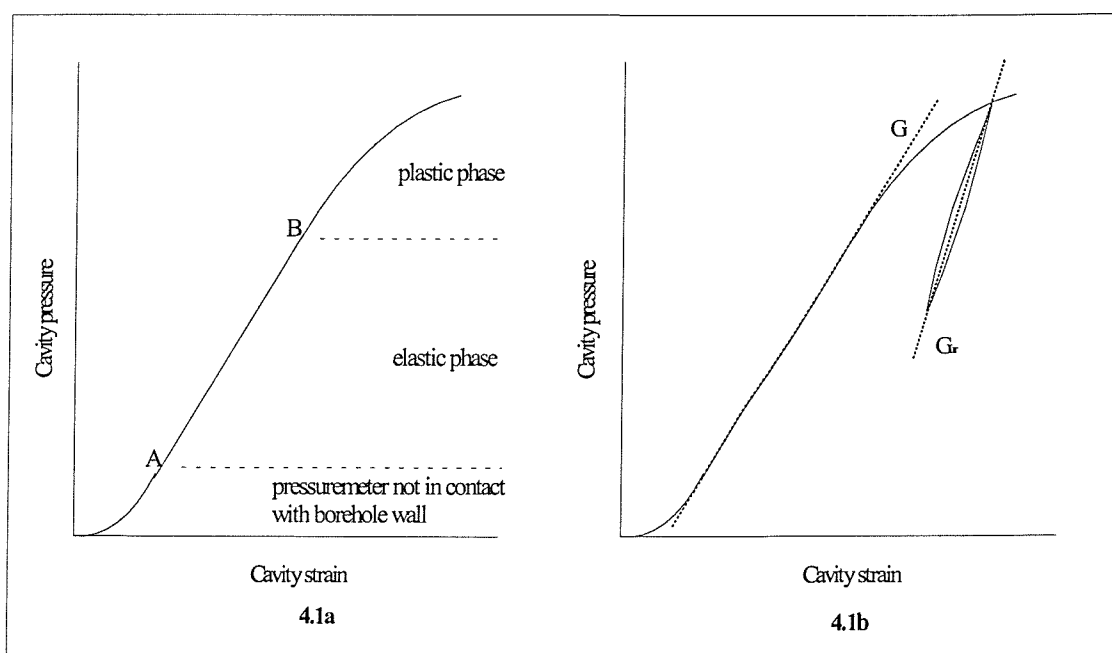


Figure 4.1. Pressuremeter test data plotted as cavity pressure versus cavity strain

If the ground around the pressuremeter is behaving truly elastically, the shear modulus can be calculated from the slope of the pressure-expansion curve. The initial slope can thus be used to estimate an initial,  $G_i$ , using the following expression (Figure 4.1b):

$$G_i = \frac{1}{2} \frac{dp}{d\varepsilon_c} \quad (4.1)$$

where

$dp$  = change in applied stress

$d\varepsilon_c$  = change in cavity strain

In clays, in order to ensure that the soil is responding elastically, it is more satisfactory to determine the shear modulus of the clay from the slope of an unload-reload cycle performed after the expansion has clearly reached a plastic phase (Figure 4.1b). In clay, the installation of the pressuremeter is generally accompanied by some disturbance, and therefore the initial modulus may give a low estimate of the true *in situ* modulus. It is therefore preferable to obtain the unload/reload modulus (Mair and Wood 1987). Jewell and Fahey (1984) found that for tests in moderately weak siltstone the ratio between the unload/reload and initial shear modulus,  $G_{ur}/G_i$ , varied between 1.2 and 7. The values of  $G_i$  in the weak rock were also found to vary widely as a result of disturbance, whereas  $G_{ur}$  values were much more repeatable.

In weak rocks the prime requirement for a high quality test is the formation of a good quality test pocket with minimum disturbance. Ideally the wall of the test pocket should be reasonably smooth. Irregularities in the borehole wall will result in limited contact between the membrane and the wall resulting in non-uniform distribution of stresses and strains. The inclusion of discontinuities in the borehole may cause the pressuremeter to deform asymmetrically due to movements along the joints (Ervin *et al.* 1980). Also, Haberfield & Johnston (1990) have demonstrated that tensile failure/ radial cracking can occur in pressuremeter tests carried out at low *in situ* horizontal stresses in weak rock. Based on their findings, Haberfield & Johnston (1993) argue that if radial cracking has occurred the modulus obtained from the initial loading curve bears little resemblance to the modulus of the intact weak rock. It would appear that the only



parameter that can be determined from a pressuremeter test in weak rock with any reliability is the unload/reload shear modulus.

Fourteen tests were carried out by Exploration Associates at the case study site as part of the main site investigation. The tests were carried out in highly and moderately weathered weak rock (graded from visual descriptions given in the borehole records), at various locations across the site. Typically, the unload/reload shear moduli,  $G_{ur}$ , were measured over increments of 0.05 to 0.8% cavity strain.

The initial shear moduli,  $G_i$ , along with the unload/reload shear moduli,  $G_{ur}$ , are listed in Table 4.1 and plotted in Figure 4.2. It can be seen from this figure that the initial shear moduli,  $G_i$ , tend to be lower than the unload/reload shear moduli,  $G_{ur}$ . Drilling disturbance/radial cracking is a possible reason for this. The question then arises as to which of these moduli are the more representative of *in situ* conditions relevant to a structure such as an embedded retaining wall. As discussed, the initial loading modulus is usually assumed to be representative of a disturbed modulus, while the unload/reload modulus is more representative of an undisturbed modulus. In addition, if the spacing of the discontinuities is greater than the diameter of the pressuremeter probe the unload/reload modulus is considered to represent an intact modulus.

As drilling disturbance/radial cracking is likely to have influenced the moduli data obtained from the initial loading curve, this would suggest that the unload/re-load moduli are the only useful data obtained from the pressuremeter tests carried out at the Coventry site. However, as the joint spacing was greater than the diameter of the pressuremeter probe, the unload/reload moduli are most likely to represent an intact modulus of the weak rock.

Even though Figure 4.2 indicates an increase in stiffness with depth and reduced degree of weathering, there is still a wide scatter in the data. It was thought that in the case of Figure 4.2b the scatter might be due to strain level dependency as the shear moduli values were obtained over different cavity strain increments. To investigate this the unload/reload shear moduli were plotted against cavity strain (Figure 4.3). Representing the data in this way did not reduce the scatter, and so the different stress levels in each test were then taken into account by normalising the unload/reload shear modulus,  $G_{ur}$ ,

with respect to the cavity pressure,  $P_o$ , at the start of the unload/reload loop, (see Figure 4.4). The normalised shear modulus,  $G_{ur}/P_o$ , was then plotted against the cavity strain that occurred during the unload/reload loop, Figure 4.5. Figure 4.5 shows that by representing the data in this way, the amount of scatter is considerably reduced.

Elevation mAOD		Description	G <sub>i</sub> MPa	G <sub>ur</sub> MPa	ε <sub>c</sub> %	P <sub>o</sub> kPa	G <sub>ur</sub> MPa	ε <sub>c</sub> %	P <sub>o</sub> kPa	G <sub>ur</sub> MPa	ε <sub>c</sub> %	P <sub>o</sub> kPa
No												
		Loop 1			Loop 2			Loop 3				
P1	88.57	RSBP in MWM	80	194	0.05	307	297	0.07	642	382	0.14	2050
P2	82.57	RSBP in MWM	112	164	0.19	1089	146	0.35	1743	222	0.22	2306
P3	85.36	HPD in MWM	39	223	0.12	1239	234	0.22	1921	241	0.34	3203
P4	89.01	RSBP in HWM	31	54	0.17	401	36	0.37	543			
P5	92.99	RSBP in MWS	21	58	0.11	241	66	0.16	358			
P6	91.69	RSBP in MWS	64	153	0.09	472	166	0.13	778			
P7	89.79	RSBP in MWS	88	348	0.07	925	175	0.19	1276			
P8	89.56	RSBP in HWS	14	55	0.18	453	61	0.19	585	60	0.18	707
P9	87.76	RSBP in HWS	21	26	0.29	382	26	0.34	463			
P10	85.06	RSBP in HWS	25	92	0.11	448	68	0.22	634			
P11	86.57	HPD in MWS	22	102	0.51	2208	123	0.8	3520			
P12	83.84	HPD in MWS	77	266	0.11	1053	323	0.18	2002			
P13	82.16	HPD in MWS	100	270	0.2	2397	402	0.23	4908	527	0.31	7363
P14	85.61	HPD in MWS	75	260	0.15	1585	276	0.2	3053	326	0.34	5010

**Table 4.1. Pressuremeter test data**

Key

HWM - Highly weathered mudstone

MWM - Moderately weathered mudstone

HWS - Highly weathered sandstone

MWS - Moderately weathered sandstone

G<sub>i</sub> - Initial shear modulus

G<sub>ur</sub> - Unload/reload shear modulus

ε<sub>c</sub> - Cavity strain during unload/reload loop

P<sub>o</sub> - Cavity pressure at start of unload/reload loop



Figure 4.5 clearly indicates the stress and strain level dependency of the modulus obtained from the unload/reload loop of a pressuremeter test. Also, the figure suggests that there is no clear difference between the stiffness of the different degrees of weathered sandstone and mudstone. This would suggest that the bonding has been destroyed during testing, and that the data presented in Figure 4.5, represents data for a de-structured material typical of an uncemented soil, not a bonded weak rock. This is somewhat unexpected, as the unload/reload loops were performed during the elastic phase of the curve, prior to any plastic behaviour (see typical test data plots from the pressuremeter tests carried out at Coventry given in Figures 4.6 RSBP test and 4.7 HPD test). It is therefore unlikely that the bonding in the weak rock has been de-structured. The question is what do the data in Figure 4.5 represent?

As already discussed, the initial loading modulus is usually assumed to be representative of a disturbed modulus, because of disturbance to the borehole wall during drilling. As the unload/reload loop were also performed during the same phase of the test as the initial modulus is determined from, it is therefore likely that the unload/reload modulus has also been influenced by the disturbance. The reason for the pressure dependency is therefore due to bedding.

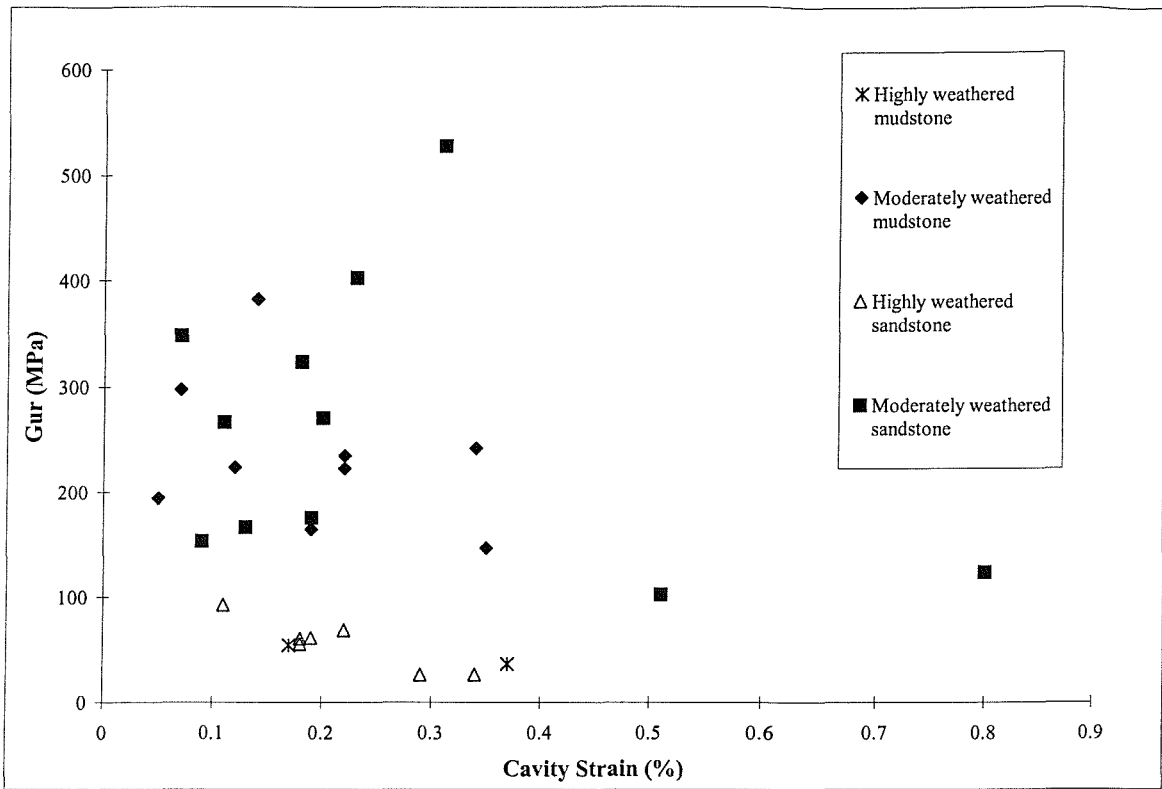


Figure 4.3. Unload/reload shear modulus plotted against cavity strain

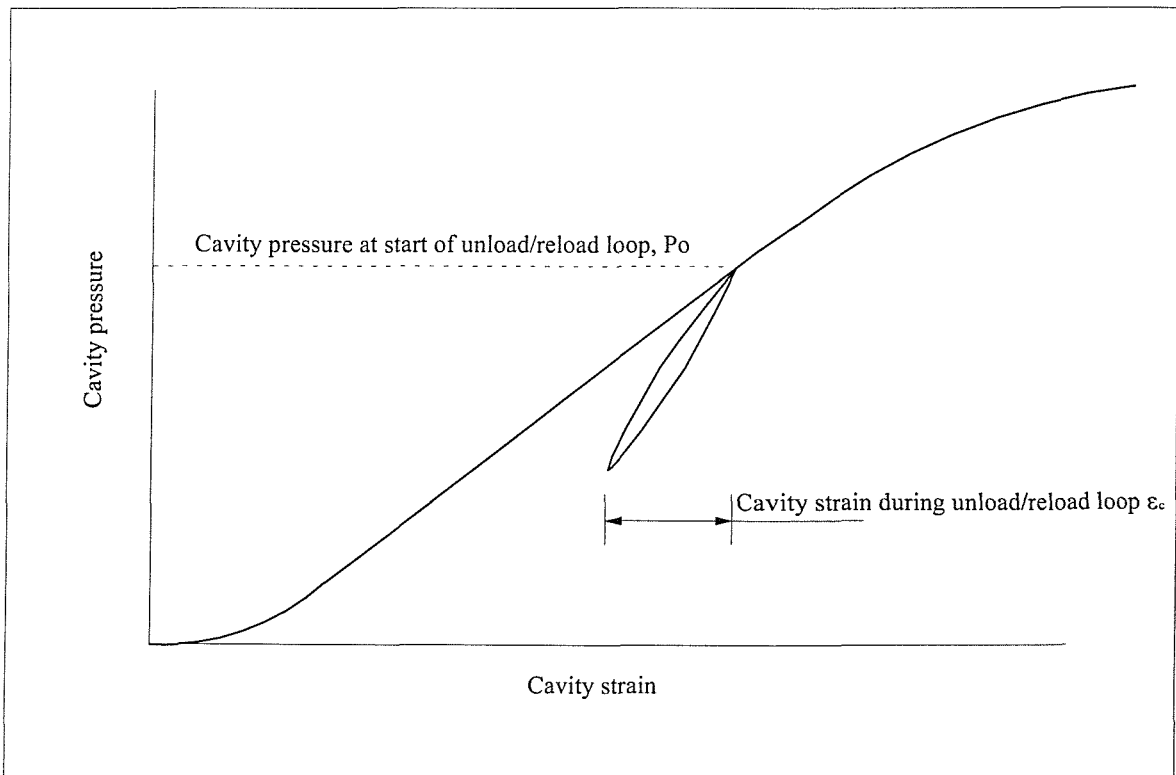


Figure 4.4. Normalisation method

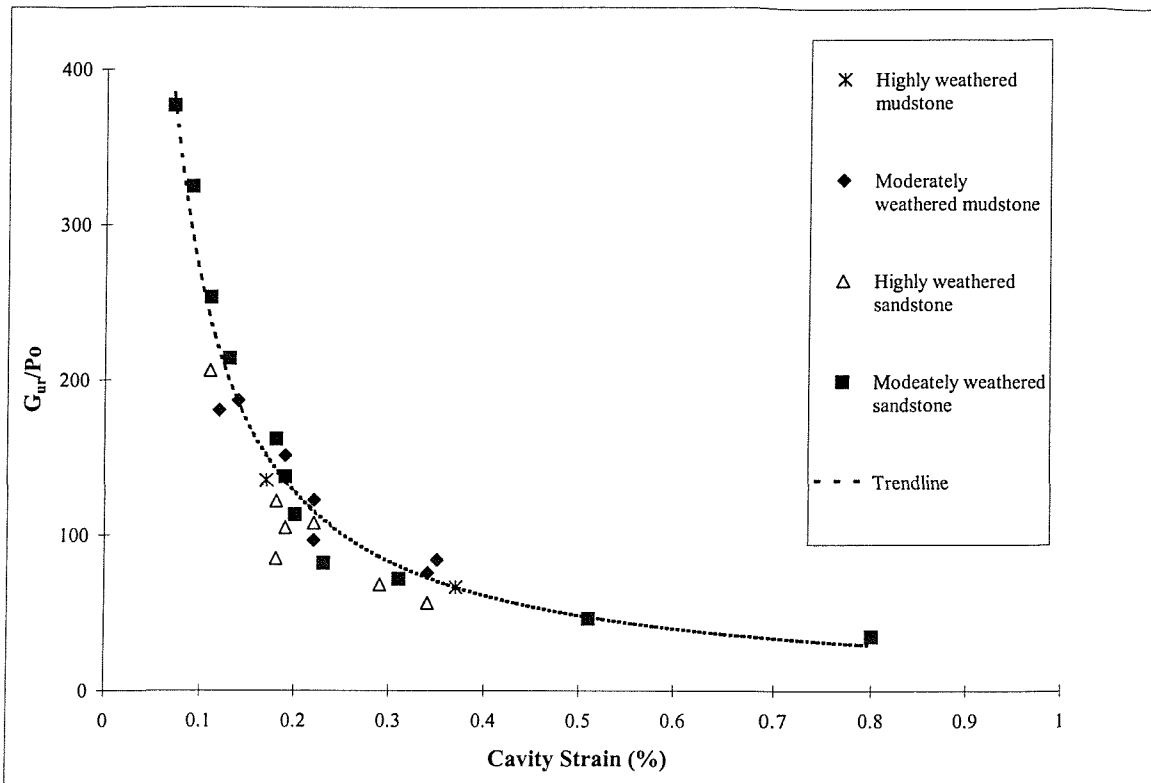


Figure 4.5. Normalised unload/reload shear modulus

The *in situ* horizontal stresses indicated by lift off pressure are presented in Figure 4.8 (calculated using the Marsland and Randolph method). These indicate that the *in situ* earth pressures coefficients,  $K_0$ , within the Bromsgrove Formation are generally in the range 0.8 to 2.0. However, the validity of using the lift off pressure method for weak rocks is questionable (e.g. Clarke 1995, Haberfield & Johnston 1993), particularly as the results have probably been influenced by borehole disturbance.

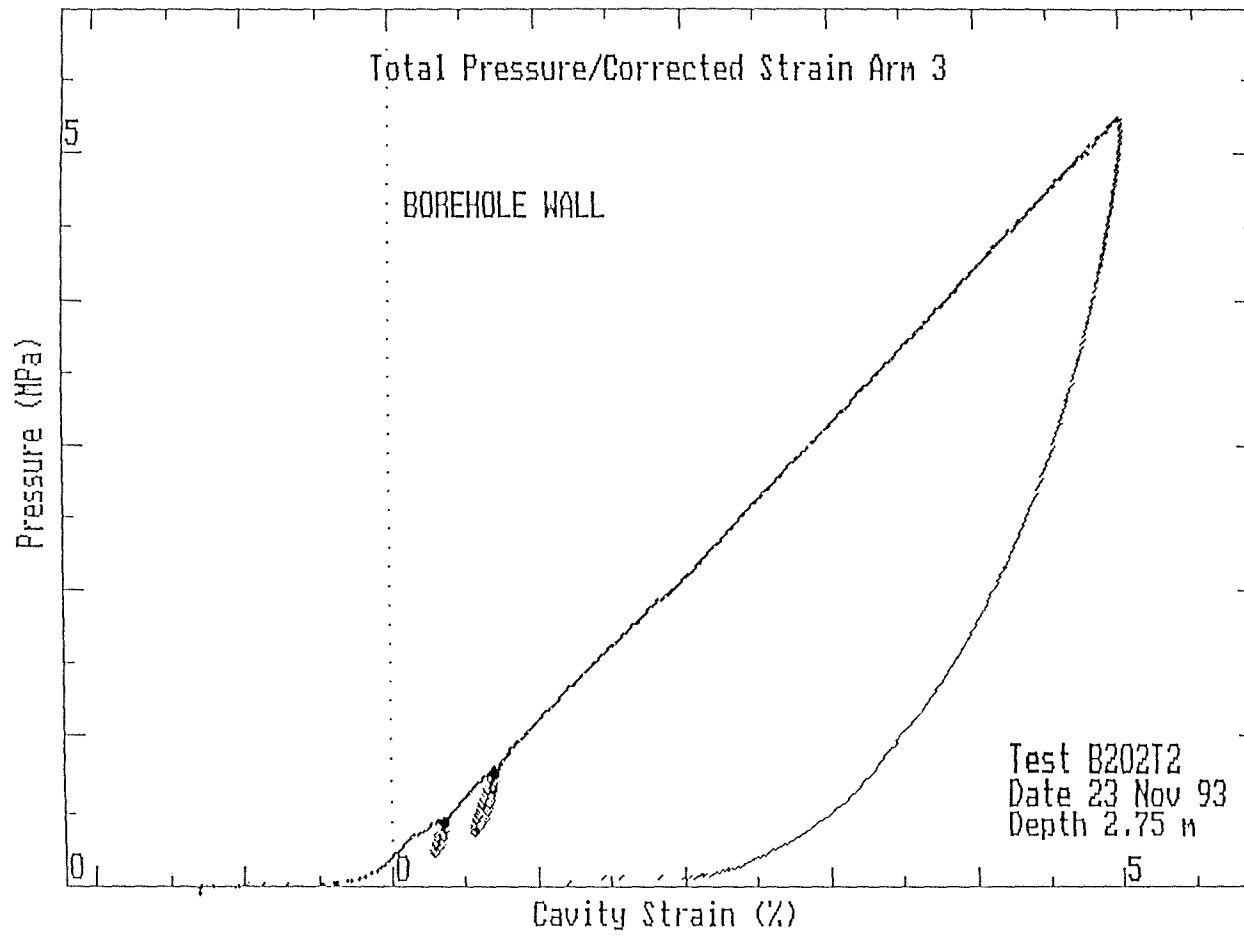


Figure 4.6. Typical stress-strain data from weak rock self boring pressuremeter test (PT6)

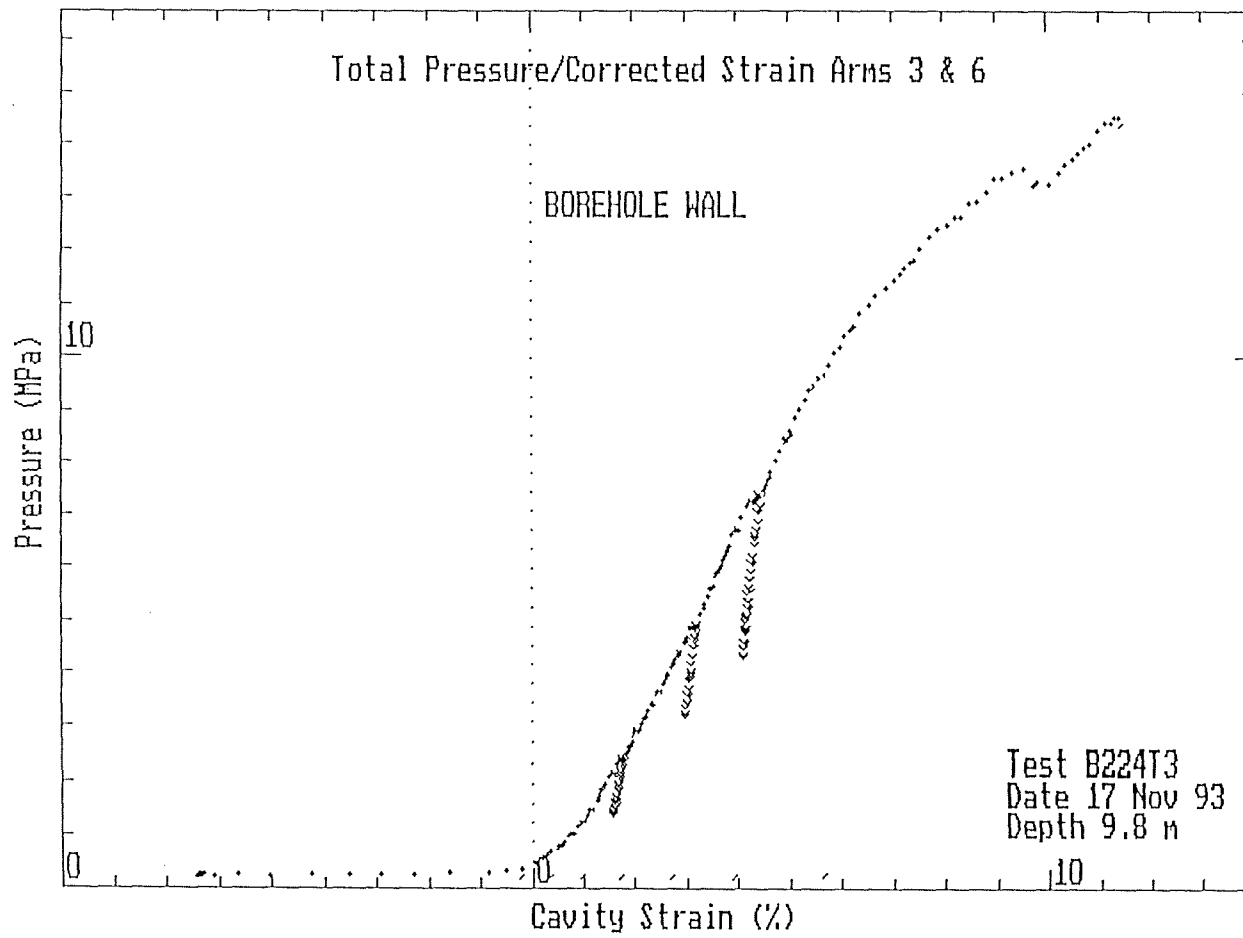


Figure 4.7. Typical stress-strain data from high pressure dilatometer test (PT13)



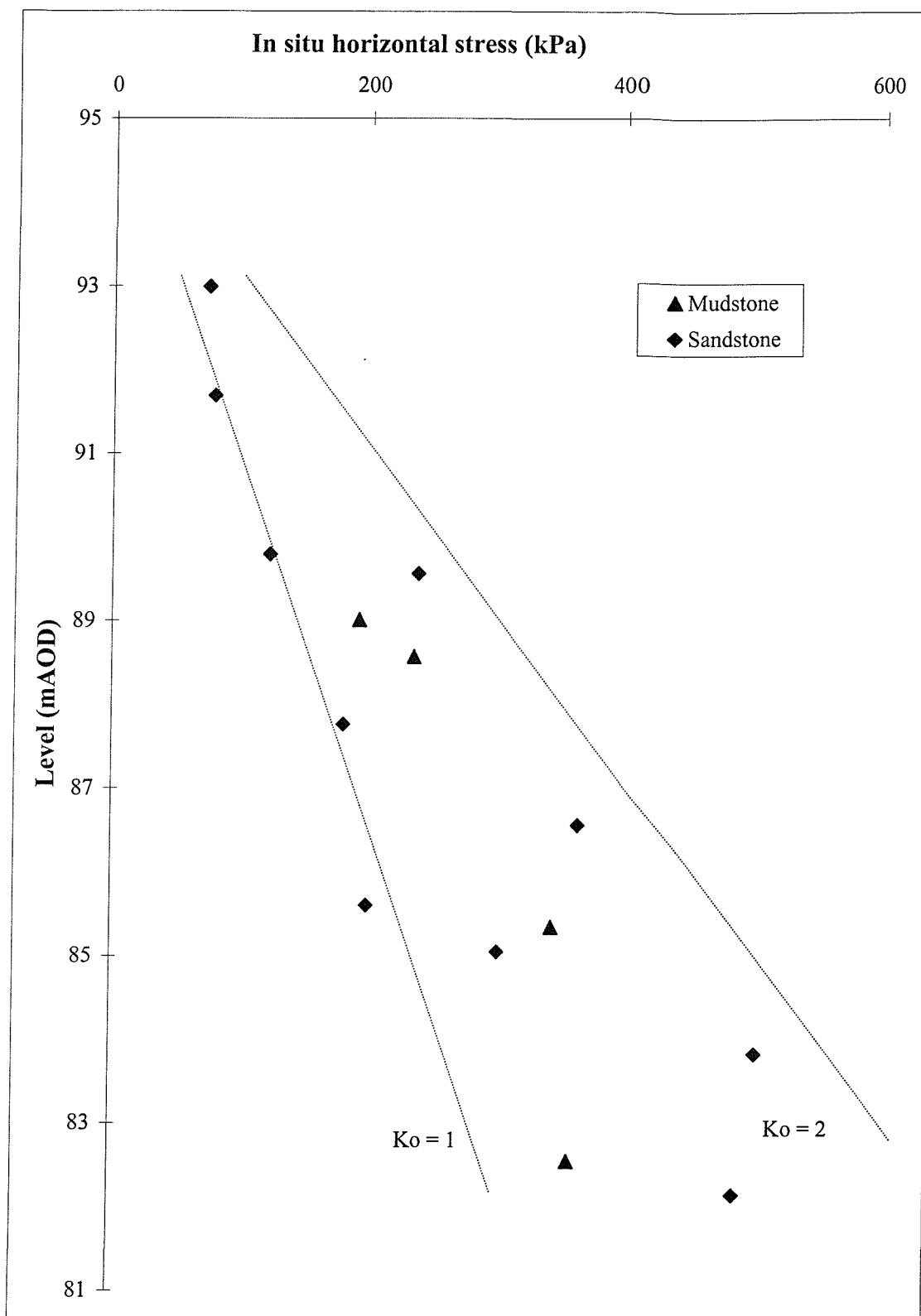


Figure 4.8. *In situ* horizontal stresses

#### 4.2.2. Geophysical tests

Geophysics provides a number of indirect methods of determining ground stiffness. Such indirect methods do not involve the direct measurement of stress and strain but make use of mathematical relationships to determine stiffness parameters.

There are a number of different seismic techniques that are used to obtain a modulus depth profile. Two seismic geophysical techniques were used to obtain a shear modulus profile of the weak rock behind the retaining wall at the monitored section:

i Continuous Surface Wave (CSW)

Surface waves (Rayleigh waves) are generated by a controlled vibratory energy source. The surface waves are detected by a series of geophones placed in line with the vibrator.

ii Down-hole Seismic Profiling.

In this type of survey the transit of shear waves are travelling between points in a borehole and a point on the ground surface near the top of the borehole. The term down-hole refers to the general direction in which the seismic waves are travelling.

Seismic methods utilise the propagation of elastic waves through the ground. The waves propagate at velocities that are a function of the density of the ground. In an isotropic elastic medium the velocity of a shear wave,  $V_s$ , is:

$$V_s = \sqrt{\frac{G_s}{\rho}} \quad (4.2)$$

Where  $G_s$  is the shear modulus and  $\rho$  the density. Thus  $G_s$  can be obtained from measurements of  $V_s$  and density.

Further details of the testing techniques and most of the data obtained from the tests at the monitored retaining wall are described in Hope *et al.*, (1998). A summary of the findings is given in Figure 4.9.

Theoretically, the stiffness profile in Figure 4.9 represents the mass stiffness at very small strains, and is an intrinsic profile that incorporates the effects of weathering and discontinuities on the overall behaviour of the material. The stiffness profile in Figure 4.9 tends to indicate that there is an increase in stiffness as the weak rock becomes less weathered, with no evident difference between the stiffness of the sandstone and the mudstone. Low values of shear modulus were measured close to the ground surface at Coventry (30 MPa), as a result of the loose fracture block system which is characteristic of the weathering style of this weak rock. The shear modulus was seen to increase by about 150 MPa over a distance of 4 to 5m indicating a significant reduction in the looseness of the fractured block system with depth and increased discontinuity spacing. The stiffness was more or less uniform over the next 7m with values between 180 and 270 MPa. This reflects the tighter nature and increased discontinuity spacing of the fracture block system of the moderately weathered weak rock. These features are confirmed by the description of the rock mass given in Chapter 3.



### 4.2.3. Standard Penetration Tests

Standard penetration tests were carried out by Exploration Associates as part of the main site investigation. The test involves measuring the number of blows necessary to drive a standard penetrometer through a given distance (300mm) into the base of a borehole using a standard mass falling through a given distance. The number of blows required to drive the penetrometer the standard distance is referred to as the SPT 'N' value. The test is described in detail in BS 1377:1990.

The mass compressibility of weak rock is a function of the discontinuity spacing and the mechanical properties of the intact weak rock. In order for there to be a unique correlation between elastic modulus and SPT 'N' value these factors must be reflected in the penetration resistance. In highly fractured weak rock a large proportion of the test volume may be through open discontinuities, whereas in weak rock where discontinuities are wide apart the intact rock will dominate the penetration resistance.

A number of correlations between 'elastic modulus' and SPT 'N' value have been proposed for weak rock. Generally these are based on moduli determined from pile load tests (Leach and Thompson 1979, Stroud 1988 and Thompson *et al.* 1988).

Correlations between SPT 'N' value and weak rock properties are wholly empirical. Because the SPT is not completely standardised (see Clayton 1995), these correlations can be also influenced by variations in the test apparatus and disturbance created by boring the hole.

Using the empirical relationship  $E' = N$  (MPa) given by Stroud (1988) and Thompson *et al.* (1988) and equation 4.3 the shear stiffness profiles for the sandstone and mudstone were estimated, Figure 4.10.

$$G = \frac{E}{2(1+\nu)} \quad (4.3)$$

where:  $\nu = 0.2$

The stiffness profiles in Figure 4.10 indicate no clear difference in the stiffness of the sandstone and mudstone, but there is a considerable scatter in the data.

The SPT values have been re-plotted in Figure 4.11, and this time a description of the degree of weathering of the material at the SPT location is also included. The description of the degree of weathering is taken from the borehole records, so there might be some variation due to different borehole loggers. Although there is some scatter, it would appear that the SPT stiffness values increase as weathering decreases. Figure 4.11b suggest that this is also the case at the monitored section of retaining wall. This would suggest that the SPT N value could be used to establish whether there was any general improvement in the quality of the rock mass with depth.

Although the SPT is a popular *in situ* test for providing stiffness parameters for weak rock, it is perhaps not a very accurate method. The empirical nature of the correlations between N value and E together with the small penetration area of the test should cause the results to be treated with caution when used for the determination of design parameters for discontinuous rock masses.

### **4.3. Laboratory tests**

#### **4.3.1. Unconfined compressive tests**

The unconfined compressive strength test is the most common laboratory test undertaken for rock mechanics. It is used generally used to determine the unconfined compressive strength, but it can also be used for estimating the intact stiffness of a rock.

Bieniawski (1967) has described the typical features of a rock stress-strain curve, Figure 4.12. It shows an initial stage of increasing gradient, due to closure of micro-cracks, followed by a phase of linear deformation prior to a phase of non-linear deformation. This means that a laboratory stress-strain curve is invariably non-linear. In the unconfined compressive test it is quite common practice to quote the tangent modulus at a stress close to 50% of the unconfined strength, so that the initial crack closure is not

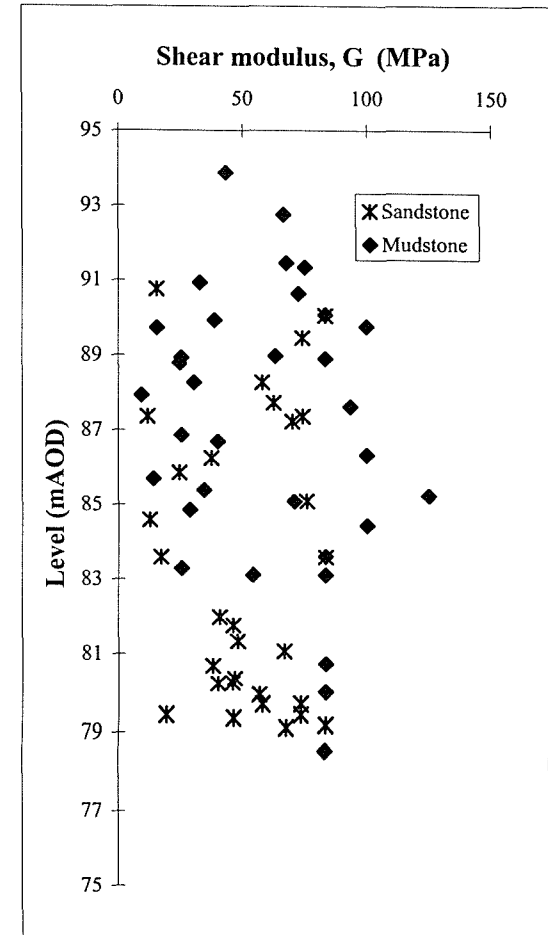
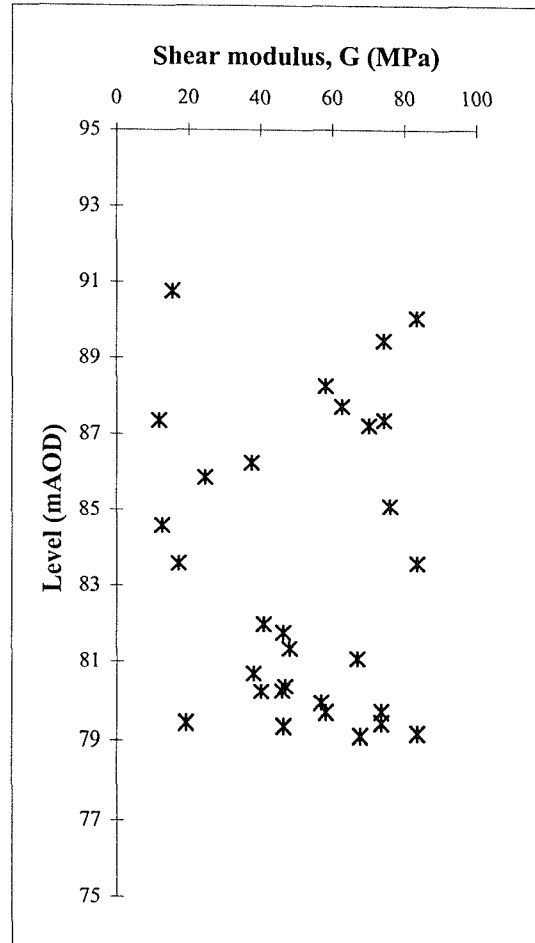
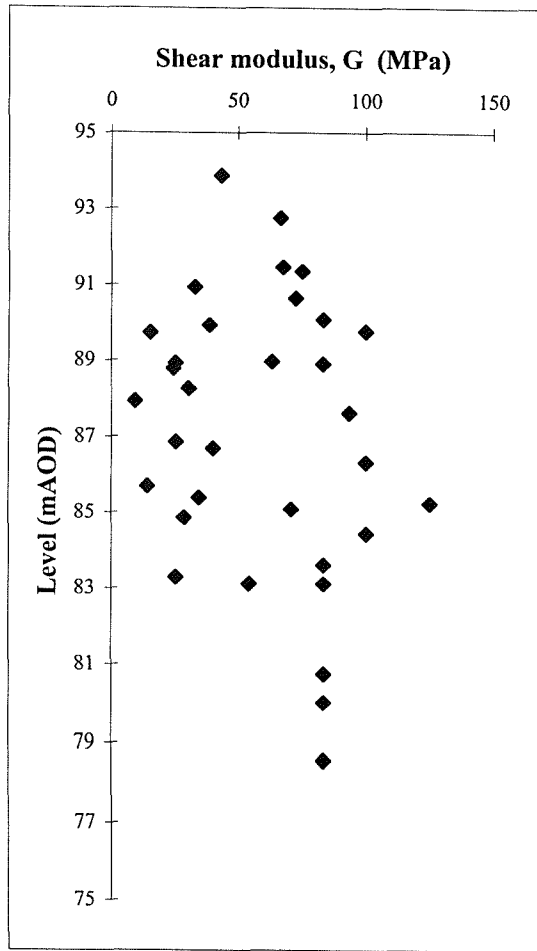
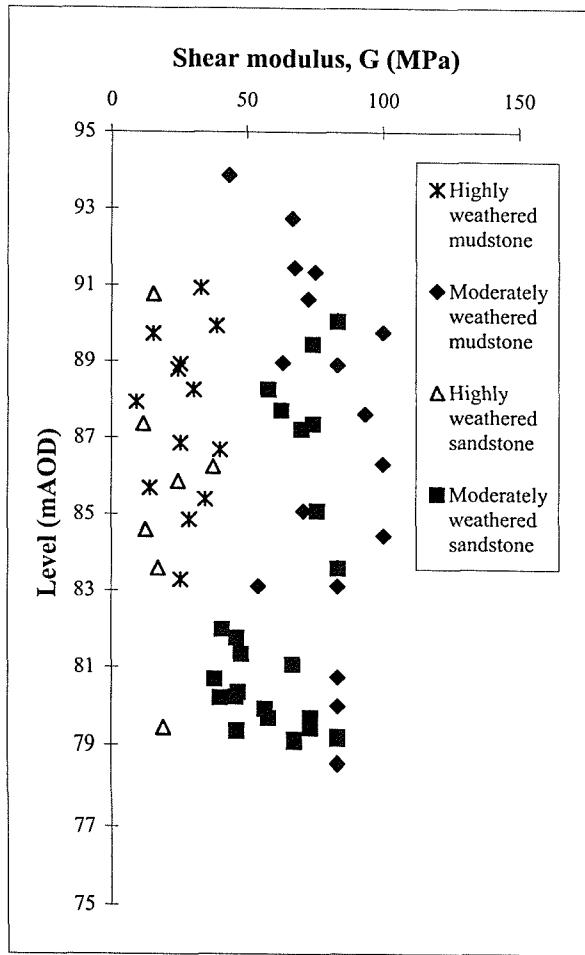
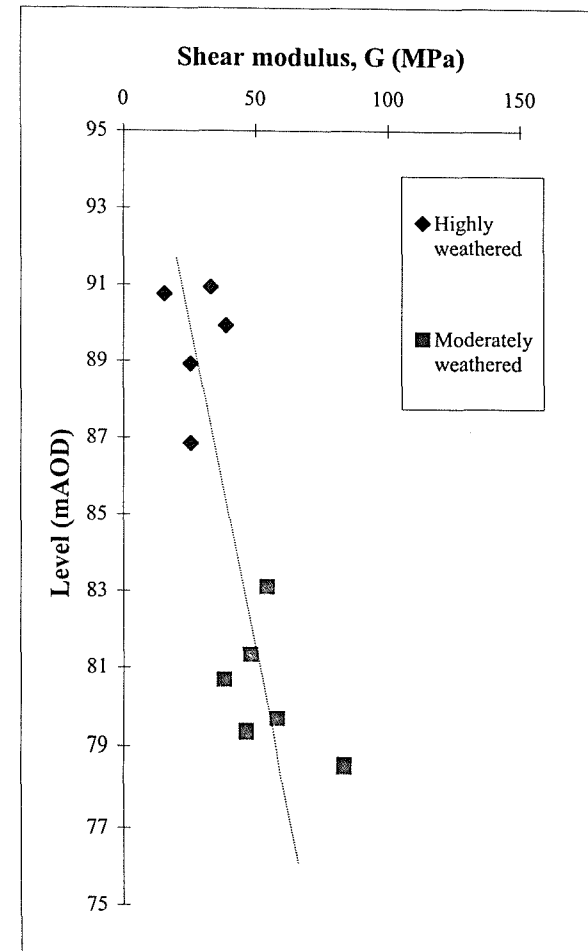


Figure 4.10. Shear modulus determined from standard penetration tests



4.11a. All SPT data

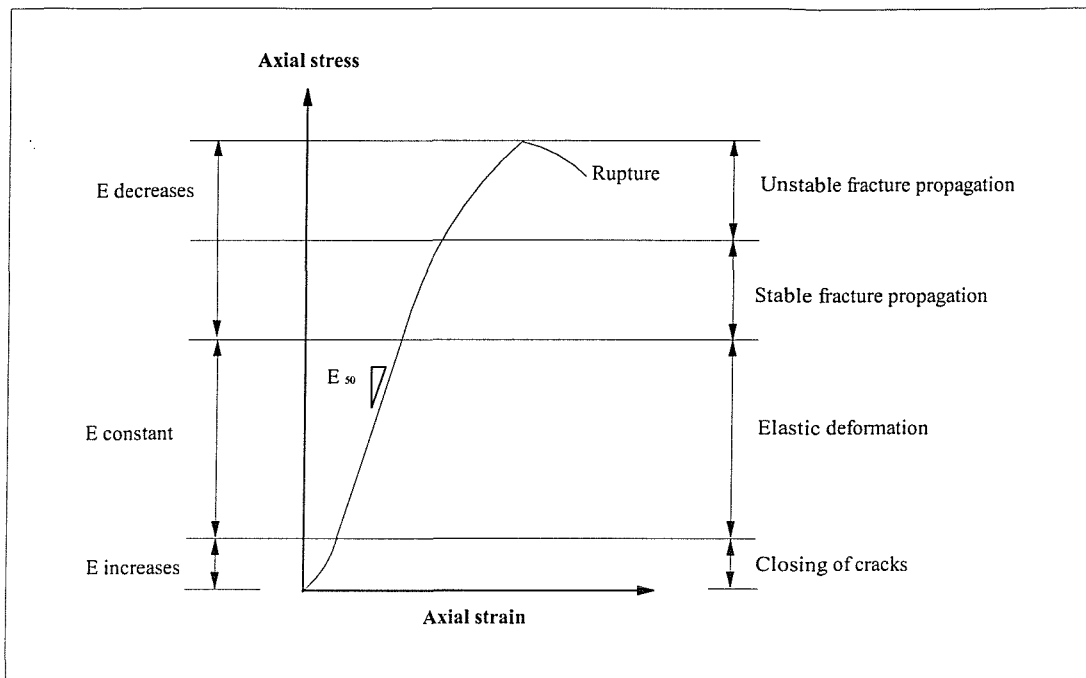


4.11b. SPT data from boreholes close to monitored section

Figure 4.11. Influence of weathering on SPT shear modulus



included (see Figure 4.12).



**Figure 4.12. Typical rock stress-strain curve after Bieniawski (1967)**

Twelve tests were carried out according to ISRM (1972) recommendations. The stiffness was determined by measuring axial strains locally using a pair of miniature linear variable differential transformers (LVDTs), which measured strains over the central length of the sample. Suitable cores of highly weathered mudstone and moderately weathered sandstone measuring 38mm diameter by 76mm long were taken from blocks retrieved from in front of the instrumented section of retaining wall.

The unconfined compressive test stiffness moduli,  $E_{50}$ , (tangent value) obtained from tests on fissured highly weathered mudstone and intact moderately weathered sandstone are listed in Table 4.2 and 4.3, respectively.

Tests No	Sample	UCS (MPa)	Moisture content (%)	Young's Modulus, E <sub>50</sub> (MPa)	*Shear Modulus G <sub>50</sub> (MPa)
UCM1	Mudstone	0.71	10.3	24	10
UCM2	Mudstone	0.65	10.7	20	8
UCM3	Mudstone	0.58	10.5	30	13
	average	0.64		25	10

**Table 4.2. Unconfined compressive stiffness of highly weathered mudstone**

Tests No	Sample	UCS (MPa)	Moisture content (%)	Young's Modulus, E <sub>50</sub> (MPa)	*Shear Modulus G <sub>50</sub> (MPa)
UCS1	Sandstone	2.44	18	614	256
UCS2	Sandstone	2.08	17.6	775	323
UCS3	Sandstone	2.17	17.9	785	327
UCS4	Sandstone	2.12	18	643	268
UCS5	Sandstone	1.99	14	780	325
UCS6	Sandstone	1.94	13.7	733	305
UCS7	Sandstone	1.64	13.2	977	407
UCS8	Sandstone	1.62	13.8	661	275
UCS9	Sandstone	1.85	12.4	834	348
UCS10	Sandstone	1.86	16.5	401	167
	average	1.97		720	300

**Table 4.3. Unconfined compressive stiffness of moderately weathered sandstone**

\* Determined using a Poisson ratio of 0.2

For jointed rock masses, Kulhawy (1978) demonstrated from field data that a general correlation exists between a modulus reduction factor and the rock mass rating, RMR. The reduction factor, which is essentially the ratio of the rock mass modulus to the modulus of the intact material, is determined from unconfined compression testing of intact core and field plate tests, Figure 4.13.

The RMR for the moderately weathered sandstone at the case study was estimated to be about 12 (see Chapter 3, section 3.2.2). Using Figure 4.13, a reduction factor of around 0.12 is obtained. Therefore, the empirically determined Young's mass modulus would be about 90 MPa, (determined using the average modulus from the unconfined compressive tests, multiplied by the reduction factor).

The mass reduction factor has been based on unconfined compression tests on intact rocks. It is therefore not suitable for use with the highly weathered mudstone, which was fissured.

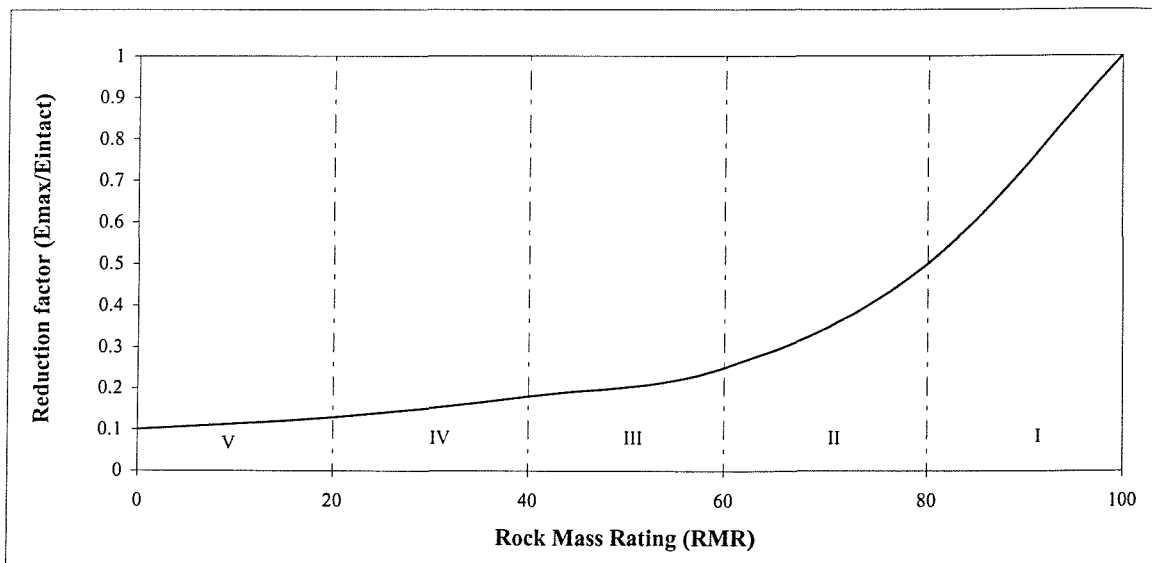


Figure 4.13. Reduction factor (after Kulhawy 1978)

#### 4.3.3. Direct shear test

Direct shear tests were undertaken on moderately weathered sandstone samples

collected from the site. Details of the testing techniques and most of the data obtained from the tests are described in Schuil-Brewer (2001). A summary of the findings is presented in Table 4.4.

Test description	Average strength envelope
Intact block	$c' = 53 \text{ (kPa)} \ \& \ \phi' = 33^\circ$
Natural discontinuity (residual)	$c' = 0 \ \& \ \phi' = 43^\circ$
Prepared discontinuity (residual)	$c' = 0 \ \& \ \phi' = 31^\circ$

**Table 4.4. Summary of parameters from direct shear tests**

#### 4.4 Laboratory results from site investigation

The interpretative report for the main site investigation (produced by Exploration Associates Ref 114080) lists typical geotechnical properties determined from the site investigation laboratory tests, these tests are summarised in Table 4.5 to 4.8

	Unit	Mean	Range	No of test results
<b>Index Tests</b>				
Moisture content	%	15	6-26	90
Liquid limit	%	31	23-41	35
Plastic limit	%	16	11-24	35
<b>Density</b>				
Bulk density	Mg/m <sup>3</sup>	2.12	1.71-2.26	26
Dry density	Mg/m <sup>3</sup>	1.89	1.75-1.99	3
<b>Undrained strength</b>				
Undrained strength	kN/m <sup>3</sup>	209	43-396	24
<b>Effective stress parameters</b>				
Cohesion intercept	kN/m <sup>2</sup>	22	19-25	2
Angle of shearing resistance	Degrees	17.5	15-20	2

**Table 4.5. Summary of geotechnical properties – Highly weathered mudstone**

	Unit	Mean	Range	No of test results
<b>Index Tests</b>				
Moisture content	%	9.7	1.6-20	19
Liquid limit	%	27	25-23	4
Plastic limit	%	15	12-17	4
<b>Density</b>				
Bulk density	Mg/m <sup>3</sup>	2.11	1.91-2.3	2
Dry density	Mg/m <sup>3</sup>	1.88	1.85-1.94	4
<b>Effective stress parameters</b>				
Cohesion intercept	kN/m <sup>2</sup>		5	1
Angle of shearing resistance	Degrees		34	1

**Table 4.6. Summary of geotechnical properties – Moderately weathered mudstone**

	Unit	Mean	Range	No of test results
<b>Particle size distribution</b>				
Clay	%	7	2-16	6
Silt	%	12	13-23	6
Sand	%	72	59-81	6
<b>Density</b>				
Bulk density	Mg/m <sup>3</sup>		2.01	1
Dry density	Mg/m <sup>3</sup>	1.9	1.87-1.91	4

**Table 4.7. Summary of geotechnical properties – Highly weathered sandstone**

	Unit	Mean	Range	No of test results
<b>Density</b>				
Bulk density	Mg/m <sup>3</sup>		1.71	1
Dry density	Mg/m <sup>3</sup>	1.74	1.67-1.87	4

**Table 4.8. Summary of geotechnical properties – Moderately weathered sandstone**

#### 4.5. Original design values

The parameters used for the original retaining wall design are listed in Table 4.9.

	Highly weathered rock	Moderately weathered rock
Strength parameters	$c' = 0$ and $\phi' = 35^\circ$	$c' = 0$ and $\phi' = 35^\circ$
Stiffness parameters	$G = 12.5 \text{ MPa} + 2 \text{ MPa/m}$	$G = 42 \text{ MPa} + 8 \text{ MPa/m}$
<i>In situ</i> stresses	$K_0 = 1$	$K_0 = 1$
$\gamma_{\text{bulk}}$	$22 \text{ kN/m}^3$	$22 \text{ kN/m}^3$

Table 4.9. Design geotechnical parameters

#### 4.6. Comparison and discussion

Figures 4.14 to 4.17 compare the stiffness values measured from the different tests and typical values for London Clay.

In Figure 4.14 the geophysical values are compared with the intact values,  $G_{50}$ , obtained from the unconfined compressive tests. The intact values have been plotted at the elevation that samples were taken from. The intact values from the unconfined compressive tests,  $G_{50}$ , yield higher stiffnesses than the geophysical values. The latter reflects the reduced stiffness of the rock mass that results from the compressibility of the discontinuities. Using the mass reduction factor suggested by Kulhawy (1978), the empirically determined shear mass modulus is lower than the seismic values. The difference is likely to be attributed to the correlation factor being site specific. Also, the correlation factor was obtained by comparing plate loading tests stiffness values and intact stiffness values, which are likely to have been obtained at much higher strains than those of the seismic tests.

It is the discontinuities that reduce the mass stiffness of the weak rock at the case study. Since discontinuity patterns in a weak rock often make the rock mass anisotropic. Such anisotropy is likely to give rise to mass modulus anisotropy with  $G_v < G_h$ . This may be

significant at the case study, as the frequency of the horizontal joints are greater than vertical joints.

Figure 4.15 compares the pressuremeter, geophysical and intact stiffness values. As the joint spacing at Coventry was greater than the diameter of the pressuremeter probe, the moduli determined from the pressuremeter data are most likely to represent an intact modulus. Figure 4.15 indicates that the stiffness values determined from the unconfined compressive tests,  $G_{50}$ , and seismic tests exceed those determined from the initial loading curve from the pressuremeter tests. This would suggest that the initial loading curves obtained from the pressuremeter tests were influenced by drilling disturbance. However, the unload/reload stiffness values are very scattered and as already discussed are dependent on cavity pressure and strain increment they were determined over. The majority of the unload/reload values are less than the intact,  $G_{50}$ , values. This would tend to confirm that the unload/reload have also been influenced by drilling disturbance and therefore are not representative of the intact value and are more likely to represent a disturbed value. However, a few unload/reload stiffness values are similar to the intact values. These stiffness values were obtained from unload/reload loops performed at high cavity pressures, (see Table 4.1). This would tend to suggest that if the pressure is taken high enough, the bedding no longer influences the results. Hence a higher modulus, typical of an intact response is obtained. Nevertheless, the results would suggest that it is difficult to obtain reliable data from pressuremeter tests performed in poorly formed holes in weak rock.

Figure 4.16 compares the SPT, geophysical and intact stiffness values. As it was anticipated that the intact rock would dominate the penetration resistance, it was therefore likely that stiffness values obtained from the SPT tests would be similar to the intact stiffness values. However, the values determined from the SPT are much lower than the intact stiffness from the unconfined compressive tests and are also lower than the geophysical stiffness values. There are several possible reasons for the difference in the values. The first is the assumption that the intact rock dominates the penetration resistance. It is possible that the joints could have had an influence on the SPT values. As the spacing of the vertical joints were closely spaced and open there is likely to be less resistance to penetration since the rock is able to deform laterally with ease ahead and around the SPT tool (see Matthew 1990). This could lead to significant lower N

values and an underestimation of the intact stiffness. Another reason for the low N values could be due to disturbance ahead of the bottom of the borehole produced by the drilling method. Alternatively the empirical nature of the correlations between N value and E could be site specific.

Figure 4.17 compares stiffness of the London Clay (Burland and Kalra 1986) to the geophysics stiffness values. The modulus values obtained at the weak rock are certainly higher than those of a stiff clay.

The properties presented in this chapter are compared and with those back calculated in chapter 6, and are therefore also discussed later in chapter 6.



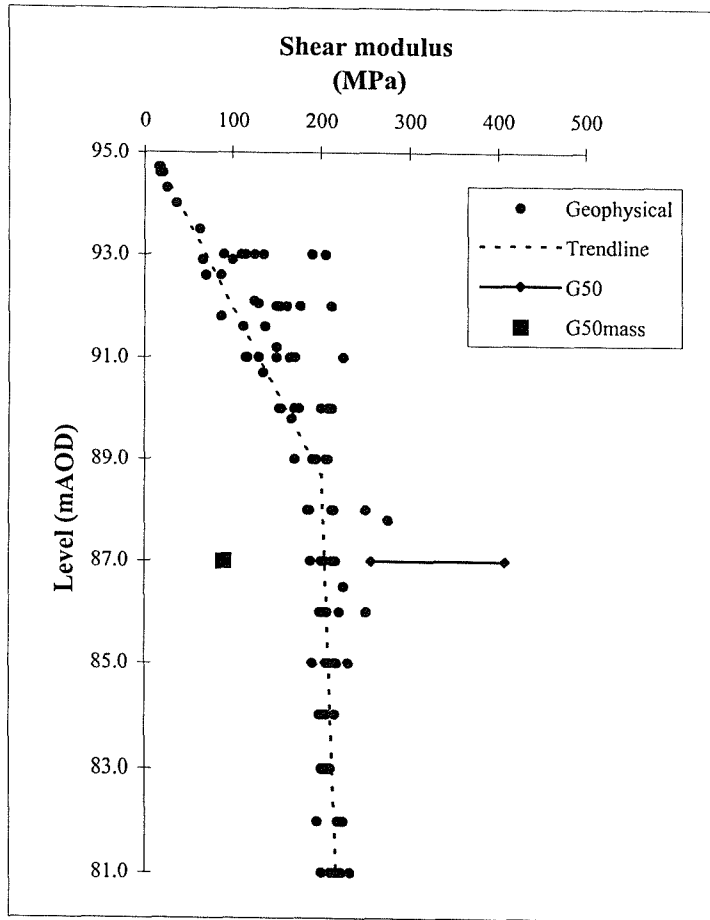


Figure 4.14. Comparison of geophysical and intact stiffness values

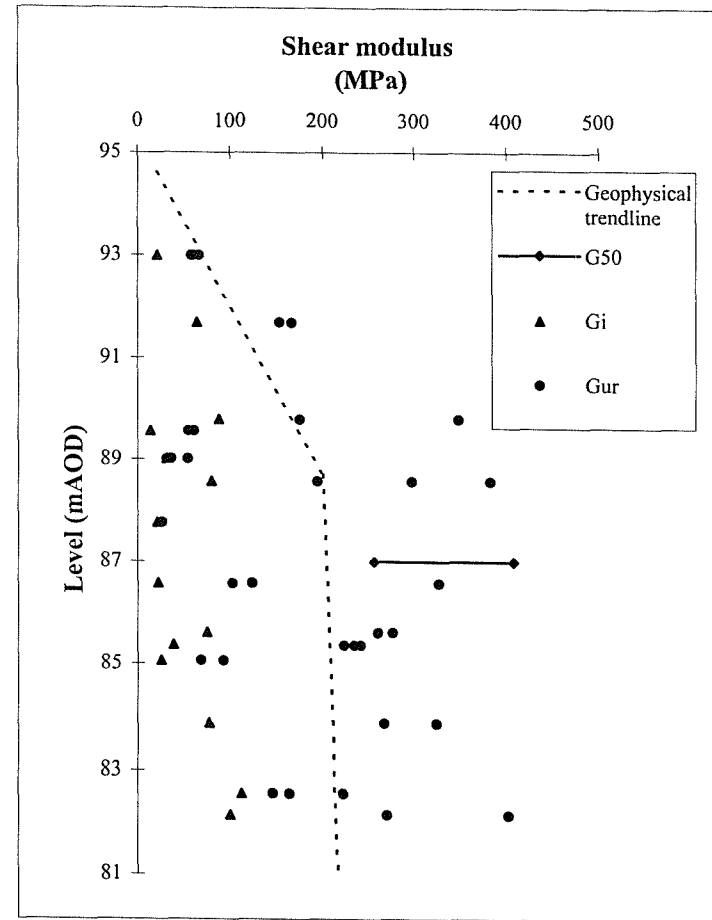


Figure 4.15. Comparison of pressuremeter, intact and geophysical stiffness values

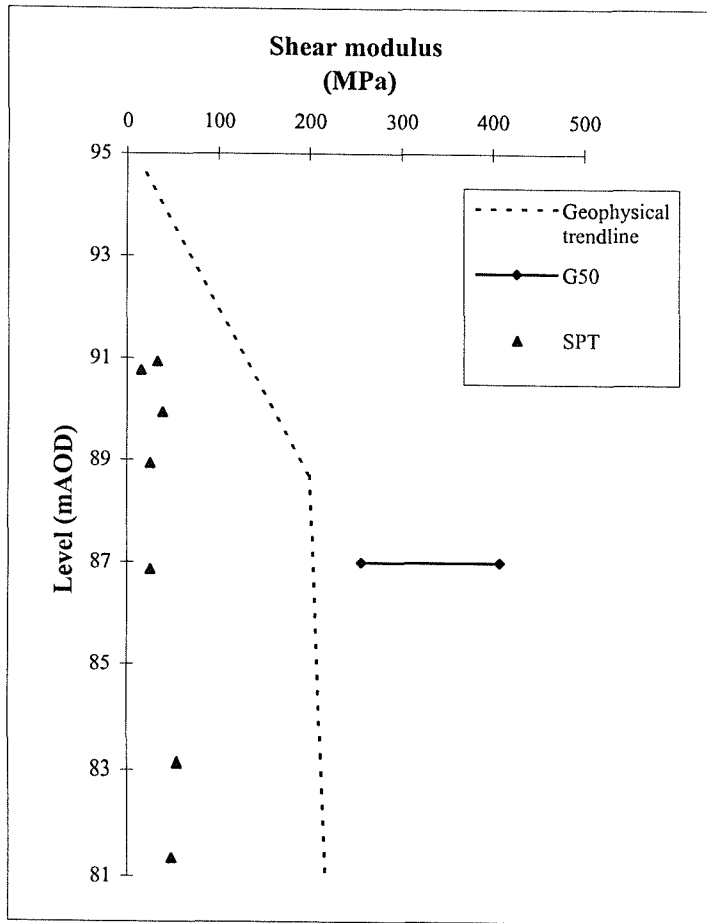


Figure 4.16. Comparison of SPT, intact and geophysical stiffness values

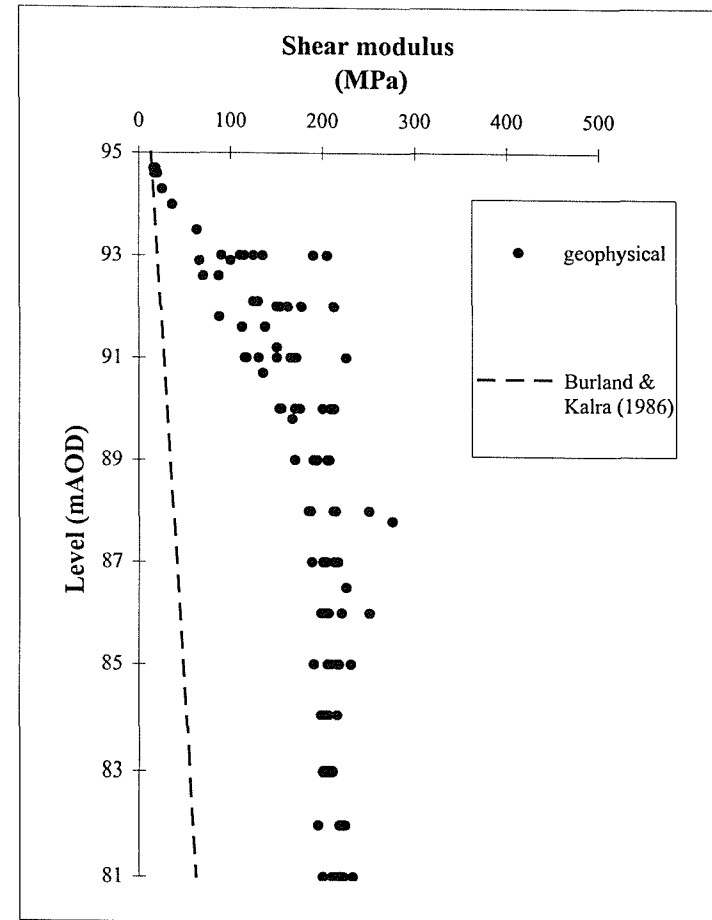


Figure 4.17. Comparison of geophysical and London Clay stiffness values (from Burland and Kalra 1986)

#### 4.7. Summary

The parameters presented in this chapter are summarised in Tables 4.10 to 4.12.

		Pressuremeter		SPT	Geoph	UCS	Design
		$G_i$ (MPa)	$G_{ur}$ (MPa)	$G$ (MPa)	$G_s$ (MPa)	$G_{50}$ (MPa)	$G$ (MPa)
<b>Highly weathered mudstone</b>	Ave	31	45	26		10	12.5+
	Range		36-54	9-38	62-210	8-13	2MPa/m
<b>Moderately weathered mudstone</b>	Ave	77	234	65			42+
	Range	39-112	146-382	43-83	180-285		8MPa/m
<b>Highly weathered sandstone</b>	Ave	20	56	20			12.5+
	Range	14-25	24-92	12-40	62-210		2MPa/m
<b>Moderately weathered sandstone</b>	Ave	64	240	50		300	42+
	Range	21-100	58-527	37-68	180-285	167-407	8MPa/m

Table 4.10. Summary of shear modulus properties

	Site Investigation	Laboratory tests	Design
<b>Highly weathered mudstone</b>	$c' = 22$ and $\phi' = 17.5^\circ$		$c' = 0$ and $\phi' = 35^\circ$
<b>Moderately weathered mudstone</b>	$c' = 5$ and $\phi' = 34^\circ$		$c' = 0$ and $\phi' = 35^\circ$
<b>Highly weathered sandstone</b>			$c' = 0$ and $\phi' = 35^\circ$
<b>Moderately weathered sandstone</b>		$c' = 53$ and $\phi' = 33^\circ$	$c' = 0$ and $\phi' = 35^\circ$

Table 4.11. Summary of shear strength properties for intact weak rock

	Pressuremeter	Design
In situ stresses $K_0$	0.8 - 2.0	1.0

**Table 4.12. Summary of *in situ* stresses**

The shear moduli determined from the initial loading stages of the pressuremeter tests are smaller than those determined from the unload/reload loops. This is not that unexpected, as generally the initial loading curve from a pressuremeter test is influenced by drilling disturbance. However, it would also appear that unload/reload parameters obtained from the pressuremeter tests at Coventry are also influenced by the initial drilling disturbance. The shear parameters obtained from the pressuremeter tests at Coventry are therefore not representative of the intact value of the weak rock, but are more likely to represent a disturbed value

The shear modulus parameters determined from the geophysics tests are the most likely values to represent the mass stiffness of the weak rock at Coventry.

The SPT stiffness parameters were very low. This was likely to be due to disturbance ahead of the bottom of the borehole produced by the drilling method and the empirical nature of the correlations between N value and E being site specific. The relationships between N and E are purely empirical and hence rely to a large extent on the scope of the database which forms the basis for the relationship. In general these database are too limited for weak rock to enable any reliable stiffness parameters to be obtained for use in weak rock.

## ***CHAPTER 5***

### ***MODELLING WEAK ROCK MASSES***

#### **5.1. Introduction**

The rock mass encountered at the instrumented section of retaining wall was of a discontinuous nature. As it was possible that the discontinuities might provide most of the weakness and instability of the weak rock mass, it was important that their influence was considered when back analysing the instrumented retaining wall. In hard rock mechanics, numerical modelling of discontinuous rock masses falls into two broad categories. The first aims at individually modelling the geometry and the behavioural response of every discontinuity, while in the second an equivalent-continuum is defined that is considered to behave in effectively the same way as the rock mass. The mechanical behaviour of the latter can be analysed by means of the theory of continuum mechanics, while discontinuous approaches are adopted for the former.

This chapter compares both these geomechanical models using the distinct element program UDEC (Cundall 1971).

## **5.2. Distinct element analysis (UDEC)**

UDEC can be used to treat a weak rock mass as a continuum or as a discontinuum. In the discontinuum case, the mass is represented as an assemblage of discrete blocks. Discontinuities are viewed as interfaces between distinct bodies – i.e. the discontinuity is treated as a boundary condition rather than a special element in the model. The contact forces and displacements at the interfaces of a stressed assemblage of blocks are found through a series of calculations that trace the movements of each individual block. Movements result from the propagation through the block system of a disturbance applied at the boundary. This is a dynamic process. The dynamic behaviour is described numerically by using a timestepping algorithm in which the size of the timestep is selected such that velocities and accelerations can be assumed constant within the timestep. This solution is identical to that used by the explicit finite difference method for continuum numerical analysis.

The calculations carried out in the distinct element method alternate between application of a force displacement law at the contacts and Newton's second law of motion at the blocks. The force displacement law is used to find contact forces from displacements. Newton's second law gives the acceleration motion of the blocks resulting from the forces acting on them. For further details of UDEC see Cundall (1971).

Although UDEC is a very powerful method for analysing discontinuous weak rock masses, there are possible drawbacks in using it as a standard engineering design tool. In addition to the difficulty of obtaining reliable data on the location and orientation of the discontinuities so that the element geometries can be described, there is usually a lack of information on material behaviour at the contacts. Nevertheless, UDEC can be extremely useful for providing an insight into discontinuous mass behaviour.

## **5.3. Programme of analyses**

The analyses presented in this chapter modelled the influence that discontinuities have on the behaviour of a retaining wall embedded in jointed weak rock. The results are

presented in terms of the influence of discontinuities on wall displacements during excavation. A summary of the analyses presented in this chapter is given in the following text.

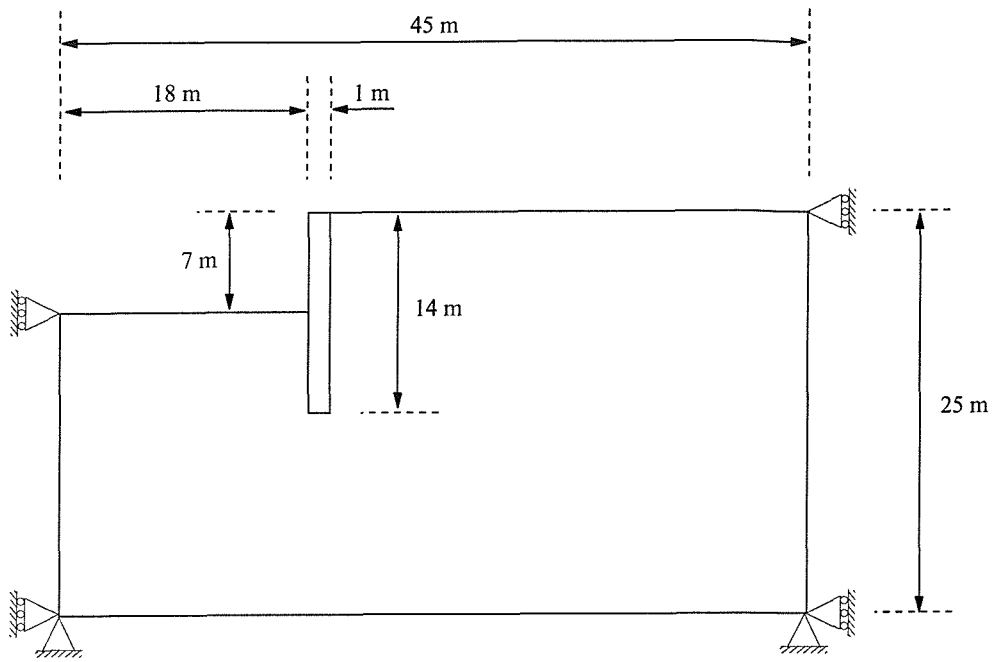
- Initially, discontinuous analyses were carried out modelling the joints. These analyses looked at the influence that joint spacing, joint stiffness, joint strength and dip direction have on wall behaviour.
- Equivalent continuum analyses were carried out, also accounting for the influence of joints on wall behaviour (Using the equivalent continuum model proposed by Goodman and Duncan 1971).

The geometry and input parameters used in the analyses presented in this chapter are described in section 5.4 and 5.5. The results from these discontinuous and equivalent continuum analyses are presented in section 5.6 and 5.7 respectively. These are then compared and discussed in section 5.8.

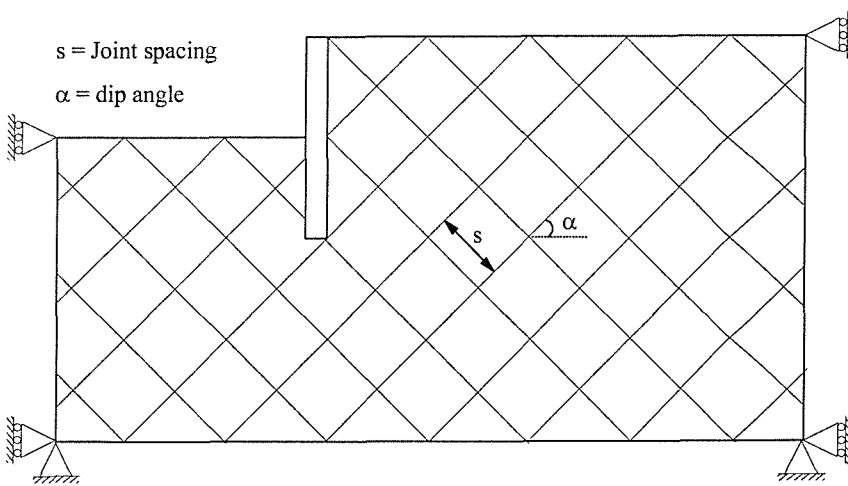
#### **5.4. Geometry used in the numerical models**

A simple cantilever wall was used as the basis for the numerical studies carried out in this chapter. The instrumented wall could not be modelled due to problems in replicating the small joint spacing (number of blocks used in the analysis) and the construction sequence (temporary propping could not be included). The idealised geometry, Figure 5.1a, is symmetrical about the centre line, so that the model represents one half of a cross-section through the cutting. The boundaries along the base of the mesh were modelled as fully pinned. The boundaries at the side of the model were modelled as being restrained in the horizontal direction only. The analyses commenced with the wall already in place.

In the analyses in which joints were modelled explicitly, the rock mass was divided into the appropriate number of blocks for the required joint spacing, Figure 5.1b.



**5.1a. Equivalent continuum analysis**



**5.1b. Discontinuous analysis**

**Figure 5.1. Idealised geometry**



## 5.5. Input parameters

Two geomechanical models are used in this chapter. The *in situ* stresses and the retaining wall properties were the same for both sets of analyses.

### 5.5.1. Weak rock and joints properties in discontinuous analyses

Parameters are required for both the joints, and the blocks that represent the intact rock. The parameters required depend on the model being used. The models used in the analyses presented in this thesis are

- **Joint model**

The joint model used in the analyses captures several of the features which are representative of the physical response of joints. In the normal direction, the stress-displacement relationship is assumed to be linear and governed by the stiffness  $k_n$  such that

$$\Delta\sigma_n = k_n \Delta u_n \quad (5.1)$$

where  $\Delta\sigma_n$  is the effective normal stress increment, and  $\Delta u_n$  is the normal displacement increment.

Similarly, in shear, the response is controlled by a constant shear stiffness,  $k_s$ . The shear stress,  $\tau_s$ , is limited by a combination of cohesive ( $c$ ) and frictional ( $\phi$ ) strength. Thus, if

$$\tau_s < c + \sigma_n \tan \phi = \tau_{\max} \quad (5.2)$$

then

$$\Delta\tau_s = k_s \Delta u_s^e \quad (5.3)$$

or if  $\tau_s > \tau_{\max}$  then the joint behaves as a plastic material.

where  $\Delta u_s^e$  is the elastic component of the incremental shear displacement.

This model is described as the Coulomb slip model.

- **Block model**

The deformable weak rock blocks are automatically discretized into triangular constant strain elements. These elements were modelled as elastic perfectly plastic with a Mohr Coulomb yield criterion.

#### **5.5.1.1. Joint Properties**

One of the limitations of UDEC is the difficulty of determining the properties of the joints. The joint friction angle, cohesion, and dilation angle, and joint normal and shear stiffnesses, are conventionally derived from laboratory tests.

Values for normal and shear stiffness for rock joints typically can range from 10 to 100 MPa/m for joints with clay in-filling, to over 100 GPa/m for tight joints in granite. Published data on stiffness properties for rock joints are limited; summaries of data are given by Kulhawy (1975) and Bandis *et al.* (1983).

It is important to recognise that joint properties measured in the laboratory are not representative of those for real joints in the field due to the scale dependence of the joint properties (Bandis *et al.* 1983). Because of this a parametric study was undertaken to investigate the influence of joint properties. To reduce the number of analyses, the ratio of shear stiffness to normal stiffness was taken to be one. The properties used are listed in Table 5.1.

Joint Stiffness, $k_n$ (MPa/m)	500	250	100	75	50
Joint spacing, $s$ (m)	4		2		1
Joint dip, $\alpha$ (degrees)	0		45		60
Joint strength, $c'$ (kPa) & $\phi'$ (degrees)	$c' = 0$ & $\phi' = 35^\circ$			$c' = 0$ & $\phi' = 25^\circ$	

**Table 5.1. Joint stiffness properties**

### 5.5.1.2. Intact rock properties

The discrete elements representing the intact weak rock were prescribed properties of an elastic perfectly plastic material, as already mentioned. These were kept the same for all the discontinuous analyses. The properties used were based on those obtained from the laboratory tests performed on the moderately weathered Bromsgrove Sandstone. The strength and stiffness parameters used are shown in Table 5.2.

Young's Modulus, $E$ , (MPa)	500
Shear strength, $c'$ (kPa) & $\phi'$ (degrees)	$c' = 50$ $\phi' = 35$
Poisson Ratio, $\nu$	0.2

**Table 5.2. Intact rock properties**

### 5.5.2. Weak rock properties in equivalent continuum analyses

The influence of discontinuity spacing upon mass compressibility may be explored mathematically by considering the anisotropic rock mass as an equivalent continuous material made up of joints and intact rock. For an anisotropic material, 21 independent elastic constants are needed to describe the stress-strain relationship. It is impossible to be able to evaluate this large number of constants for any rock. However, if the assumption of transverse isotropy is made, (i.e. the rock is regularly crossed by a single

set of joints Figure 5.2), there is only one set of elastic parameters for any direction along the plane of the stratification. Such a material has only 5 elastic constants and it is possible to calculate elastic constants for the equivalent continuous material representative of the rock mass. The equivalent parameters for a single, uniformly spaced joint set, were given by Goodman and Duncan (1971) as:

$$E_n = \left( \frac{1}{E} + \frac{1}{sk_n} \right)^{-1} \quad (5.4)$$

$$E_p = E \quad (5.5)$$

$$\nu_{np} = \nu E_n / E_p \quad (5.6)$$

$$\nu_{pn} = \nu \quad (5.7)$$

$$G_{np} = \left( \frac{1}{G} + \frac{1}{sk_s} \right)^{-1} \quad (5.8)$$

where

$E_n$  = equivalent rock mass Young's modulus in the n direction,

$E_p$  = equivalent rock mass Young's modulus in the p direction,

$E$  = intact rock Young's modulus,

$G_{np}$  = equivalent rock mass shear modulus,

$G$  = intact rock Young's modulus,

$k_s$  = joint shear stiffness,

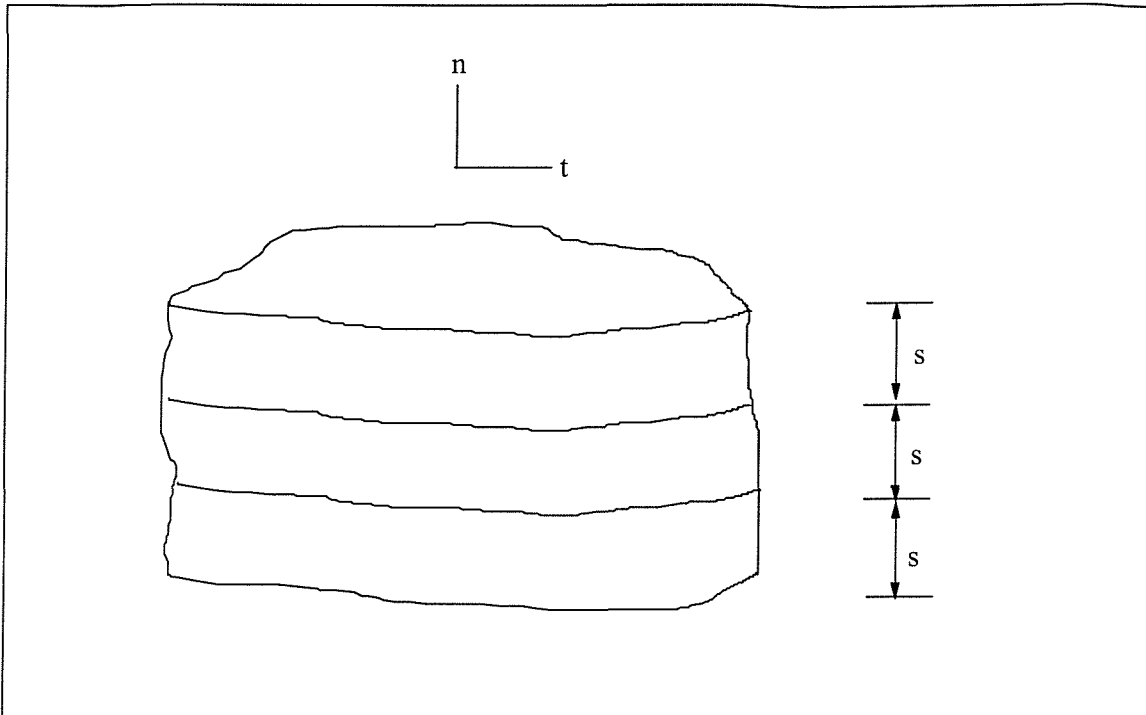
$k_n$  = joint normal stiffness,

$\nu_{pn}$  = Poisson's ratio giving strain in the n direction caused by a stress in the p direction,

$\nu_{np}$  = Poisson's ratio giving strain in the p direction caused by a stress in the n direction,

$\nu$  = intact rock Poisson's ratio, and

$s$  = joint spacing



**Figure 5.2. Single discontinuity set rock mass model**

The model indicates that if the joint stiffness is smaller in magnitude than the intact modulus  $E$  and the joints are orientated perpendicular to the direction of the applied load then it is the modulus of the joints which control the deformation of the rock mass. If however the joints are parallel to the direction of the applied load it is the intact modulus which tends to control the deformation of the rock mass.

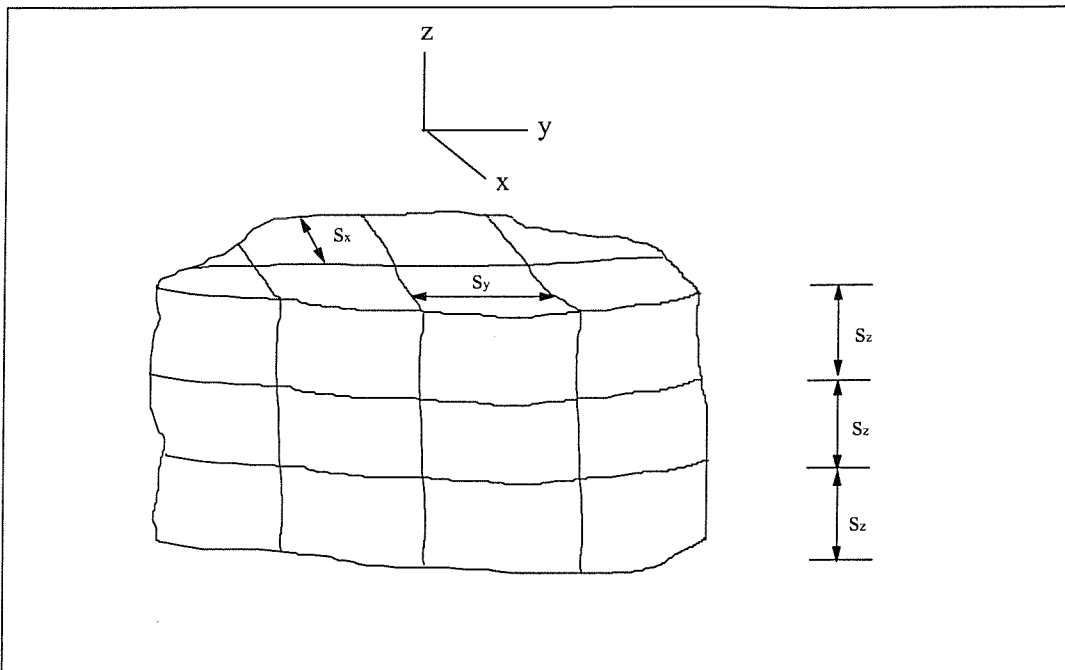
Discontinuities normally occur in sub-parallel sets, not a single set of joints as assumed in the above model. For this reason Goodman and Duncan (1971) have considered a rock mass with three orthogonal discontinuity sets Figure 5.3. Goodman and Duncan (1971) have shown the equivalent elastic properties for the model with three orthogonal discontinuity sets are:

$$E_i = \left( \frac{1}{E} + \frac{1}{sk_{ni}} \right)^{-1} \quad (5.9)$$

$$G_{ij} = \left( \frac{1}{G} + \frac{1}{s_i k_{si}} + \frac{1}{s_j k_{sj}} \right)^{-1} \quad (5.10)$$

$$\nu_{ij} = \nu_{ik} = \nu E_i / E \quad (5.11)$$

for  $i = x, y, z$  with  $j = y, z, x$  and  $k = z, x, y$ . The single discontinuity model is a special case of the above in which  $s_x = s_y = \infty$ .

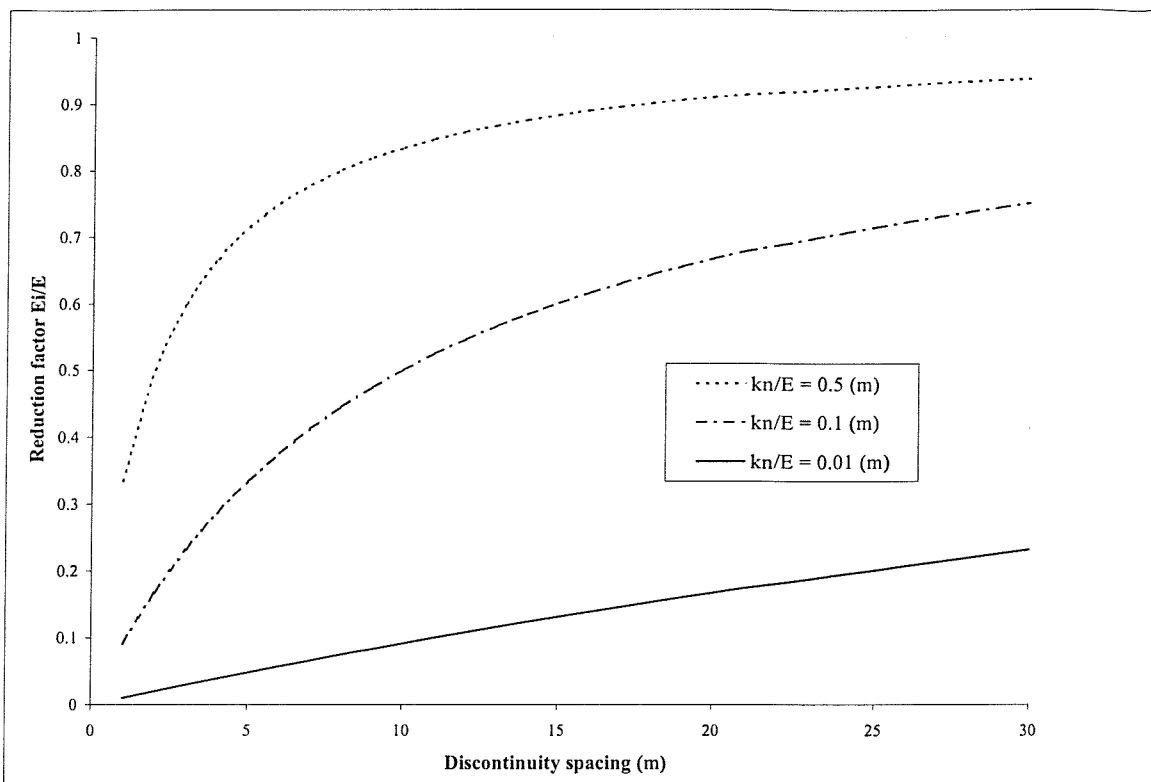


**Figure 5.3. Three orthogonal discontinuity sets rock mass model**

These equations show that the equivalent rock mass properties are functions of the elastic properties of the rock material,  $E$ ,  $\nu$ ,  $G$ , the deformation of the rock discontinuities,  $k_n$ ,  $k_s$ , and the discontinuity spacing,  $s$ .

The effect of discontinuity spacing on the mass modulus may be depicted by comparing the equivalent rock mass Young's modulus,  $E_i$ , to the intact rock Young's modulus,  $E$ , Figure 5.4. Figure 5.4 shows that when the modulus of the joint is much lower than that of the intact rock ( $k_n/E = 0.01$ ), the number of joints has little effect on the ratio of mass modulus to intact modulus. Again, as the modulus of the joint approaches that of the intact material ( $k_n/E = 0.5$ ) the number of joints has little effect on the ratio of mass

modulus to intact modulus. The implication is that for hard rock masses with soft joints there is an appreciable difference between the mass modulus and intact modulus. However, for the softer type of materials such as soils, the joint system does not cause an appreciable difference between the mass modulus and intact modulus.



**Figure 5.4. Modulus reduction factor versus discontinuity spacing**

These simple models relating joint frequency to mass modulus assume that the ratio  $k_n/E$  remains constant for the system of joints under consideration. However tests on individual fractures (Goodman, 1976 and Bandis *et al.* 1983) have shown that  $k_n$  is highly stress dependent. In reality the stiffness of the joints beneath a loaded area is likely to change with depth as a result of the distribution of applied stresses. The situation is further complicated by the fact that the orientation of the joints will have a strong influence on the distribution of stresses within the rock mass associated with an applied load (Gazier and Erlikhman, 1971).

The Goodman and Duncan (1971) model with three orthogonal discontinuity sets has been used to estimate the equivalent rock mass stiffness. The estimated equivalent rock mass stiffnesses are based on the intact rock modulus, joint stiffness and joint spacing used in the discontinuous analyses (see Table 5.1 and 5.2). The resulting equivalent stiffness and strength parameters are listed in Tables 5.3 & 5.4. Generally the model with three orthogonal discontinuity sets would behave as an anisotropic system. But when all three values of  $s$ ,  $k_n$  and  $k_s$ , are equal in each direction (as with the parameters used in the equivalent continuum analysis presented in this chapter), an isotropic system occurs. There are arguments against using an isotropic deformation model for a discontinuous hard rock mass, because of the influence on the distribution of stresses within the rock, (see Gazier and Erlikhman, 1971). However, fissured soils are generally treated as an isotropic material. The modulus values obtained for the weak rock at the case study (see chapter 4) are certainly closer to those that would be expected in a soil, rather than a hard rock. So the deformation behaviour of the weak rock at the case study might be expected to behave more like a soil, rather than a rock.

In the equivalent continuum model the weak rock is represented as an isotropic elastic material and as a perfectly plastic material with a Mohr Coulomb yield criterion.

Analysis set	Strength, $c'$ & $\phi'$
1	$c' = 0$ $\phi' = 35$ (joint strength)
2	$c' = 0$ $\phi' = 25$ (joint strength)
3	$c' = 50$ (kPa) $\phi' = 35$ (intact strength)
4	Elastic (no friction)

**Table 5.3. Strength failure criteria**



Joint spacing, $s$ , (m)	Joint stiffness $k_n$ or $k_s$ , (MPa/m)	Equivalent mass modulus, $E_i$ , (MPa)	Equivalent mass modulus, $G_i$ , (MPa)
1	500	250	109
1	250	167	76
1	100	83	40
1	75	65	31
1	50	45	22
2	500	333	139
2	250	250	109
2	100	142	66
2	75	115	54
4	500	400	161
4	250	333	139
4	100	220	98
4	75	188	84

**Table 5.4. Equivalent stiffness properties**

### 5.5.3. Concrete

The discrete element representing the concrete wall was prescribed the elastic material properties shown in table 5.5, where the Young's modulus is an uncracked value taken from BS 8110.

Young's modulus, $E$ (MPa)	Shear Modulus, $G$ (MPa)	Poisson's Ratio, $\nu$
$2.5 \times 10^4$	$1.09 \times 10^4$	0.15

**Table 5.5. Concrete properties**

#### 5.5.4. *In situ* stress state

As with soils, the selection of the *in situ* lateral stresses is not straightforward. For simplicity a pre-excavation lateral stress profile corresponding to  $K_o = 1$  was used in both sets of analyses. As all the analyses were carried out with the wall installed at the start of the analysis, a  $K_o = 1$  is considered to be a reasonable representation of the lateral stress distribution imposed by the concrete during placement (Tedd *et al.* 1984 and Powrie and Li, 1991).

#### 5.6. Results of discontinuous analyses

Figures 5.5 to 5.7 show the normalised wall displacement at the top of the retaining wall after excavation plotted against a normalised stiffness for joint frictional strengths of  $35^\circ$  and  $25^\circ$ , respectively. The wall displacements have been normalised by dividing the wall displacements by the wall displacement of an analysis that did not contain any discontinuities, (i.e. in which the weak rock mass was modelled as intact rock). The stiffness has been normalised by dividing the intact stiffness by the joint stiffness and joint spacing,  $(E/sk_n)$ .

#### 5.7. Results of equivalent continuum analyses

Figures 5.8 and 5.9 show the normalised wall displacement at the top of the retaining wall after excavation plotted against a normalised stiffness. The wall displacements in these Figures have been normalised the same way as in Figures 5.5 to 5.7. Originally, the stiffness in Figures 5.8 and 5.9 was normalised by dividing the intact rock stiffness,  $E$ , by the Equivalent continuum stiffness,  $E_i$ , but this has been changed so it can be compared to Figures 5.5 to 5.7. So Equation 5.9 has been re-arranged to give:

$$\frac{E}{sk_n} = \frac{E}{E_i} - 1 \quad (5.12)$$

## 5.8. Discussion

Figures 5.5 and 5.6 indicate the influence that the discontinuities have on the calculated wall displacements. It can be seen that the wall displacements increase with increasing  $E/sk_n$ . This is not unexpected, as the overall rock mass stiffness is reducing as  $E/sk_n$  increases. In addition, it can be seen that as the dip direction increases, so do the wall displacements. This is consistent with the yielding that occurred in the joints, once the dip direction exceeded the joint strength. In the case of the  $0^\circ$  dip direction, no yielding was noted in the joints.

Figure 5.7 is a comparison of the discontinuous analyses data from Figures 5.5 and 5.4. It indicates that the wall displacements are not only dominated by the dip direction of the joints, but also by the joint strength.

Again, Figures 5.8 and 5.9 show that the wall displacements increase with increasing  $E/sk_n$ . However, this time the wall displacements are dominated by the specified failure criteria. It can be seen that if a failure criterion corresponding to the joint strength is specified, the wall displacements are greater than those calculated when using the intact rock failure criterion. The calculated results using the intact strength agree with those calculated using the elastic model, indicating that there is no yield when the intact rock friction is used.

Figures 5.10 and 5.11 are a comparison of the discontinuous and equivalent continuum analyses. For clarity, 2<sup>nd</sup> order polynomial trendlines have been used to represent the equivalent continuum data.

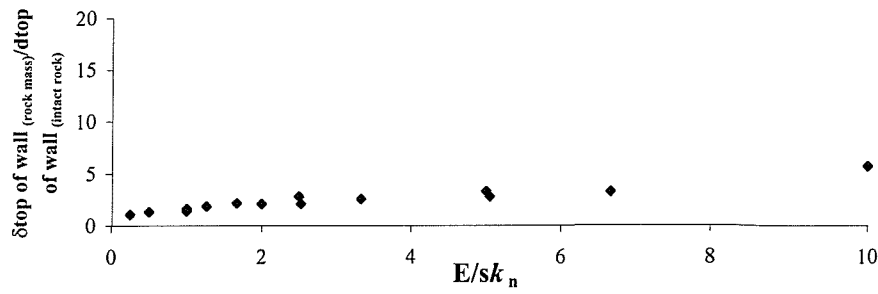
It would appear from Figures 5.10 and 5.11 that there is a reasonable agreement between the calculated displacements from the equivalent continuum analyses (using the rock strength) and the discontinuous analyses where the dip direction is  $0^\circ$ . This would indicate that the discontinuous analyses were dominated by the elastic behaviour of the intact rock and joints and this corresponds with the fact that no yielding in the joints was noted for this particular set of analyses.

In the cases where the joint dip direction exceed the joint strength, the wall displacements are greater than those calculated by the rock strength analysis; but less than those calculated from the analyses where the failure criterion was specified to match the joints. This would suggest that once the joint dip direction exceeds the joint strength the calculated wall displacements were dominated by a combination of the plastic behaviour of the joints and the elastic behaviour of the intact rock.

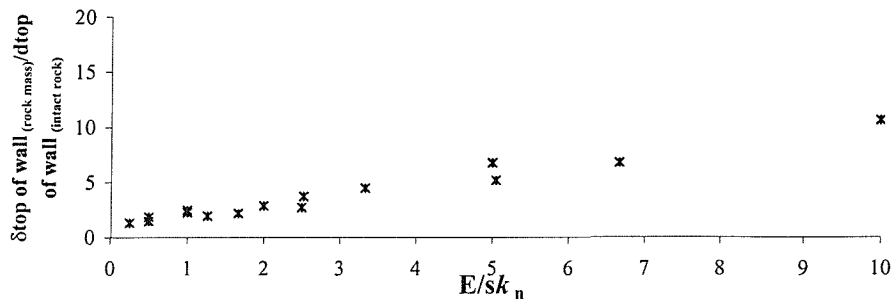
Based on the above results, it could be argued that the method of modelling a retaining wall in weak rock should depend primarily on the presence and nature of the discontinuities. It follows that a detailed discontinuity survey should form part of the site investigation for an excavation in weak rock. The pattern and nature of the discontinuities would then influence the design methodology as follows

- where discontinuities are included in a rock mass with a dip angle that is small in relation to the shear strength of the discontinuity, an equivalent continuum analysis may be used
- where discontinuities are included in a rock mass with a dip angle that is significant to the shear strength of the discontinuity, the discontinuities will control the design and a method that explicitly takes into account the properties of the discontinuity (e.g. a discrete element/limit equilibrium analysis) should be used.
- where discontinuities are included in a rock mass with a dip angle that is significant to the shear strength of the discontinuity a simple method to take account for this is to use the joint strength in an equivalent continuum analysis which will provide upper bound estimates of wall displacements.

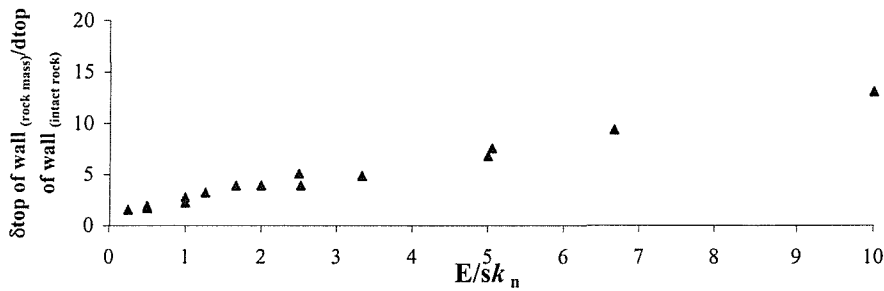
Although, analyses were attempted to investigate the influence of small scale joint spacing, problems arose with modelling the resulting large number of blocks. It could be argued that if the joint spacing were close enough, the dip direction of the blocks would have no influence on the wall behaviour, as the critical block would find its own path (see Figure 5.12). Where the discontinuities are closely spaced, it is possible that the ground will behave as a granular material and the wall movements might be similar to those calculated using a Mohr-Coulomb failure criterion (see Hoek and Brown 1980).



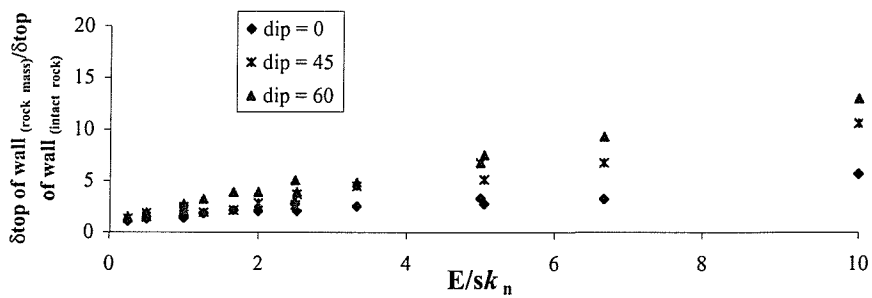
5.5a. Dip = 0°



5.5b. Dip = 45°



5.5c. Dip = 60°



5.5d. All

Figure 5.5. Calculated wall movements from discontinuous analyses (joint strength  $\phi' = 35^\circ$ )



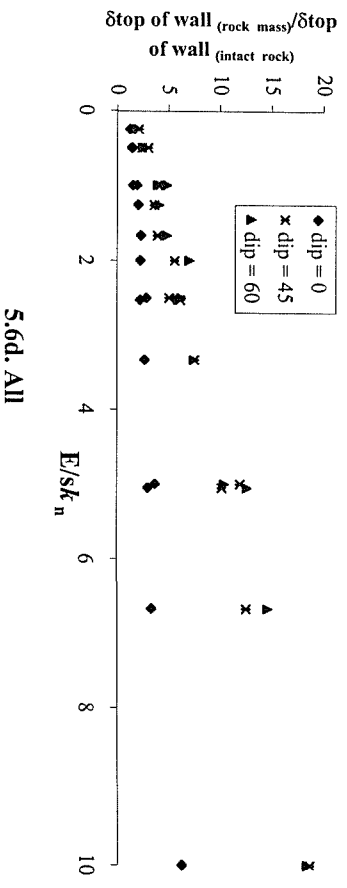
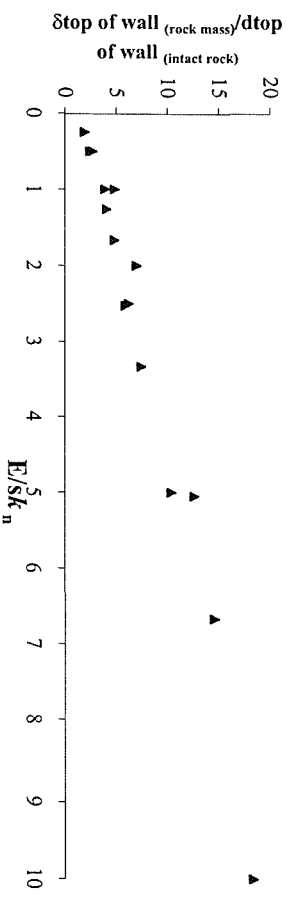
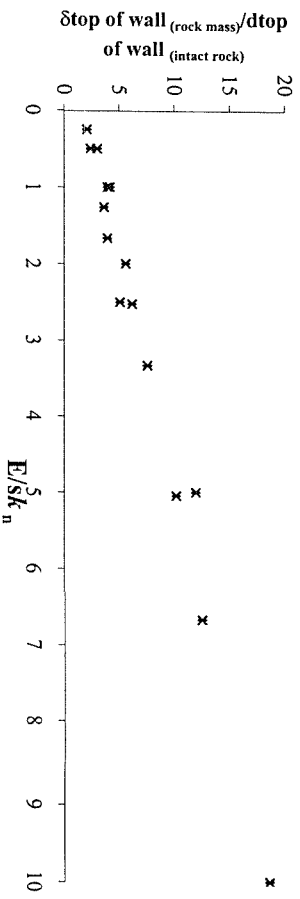
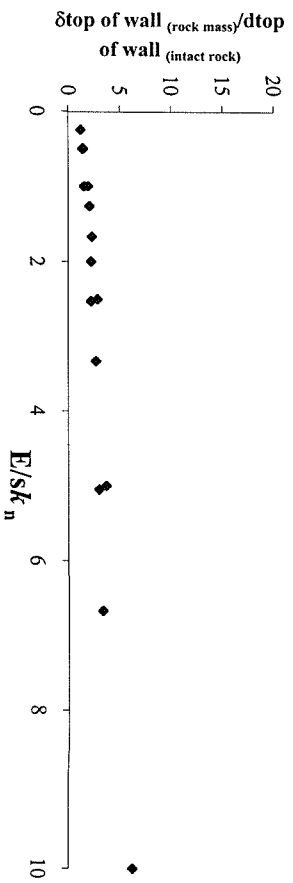


Figure 5.6. Calculated wall movements from discontinuous analyses  
(joint strength  $\phi' = 25^\circ$ )

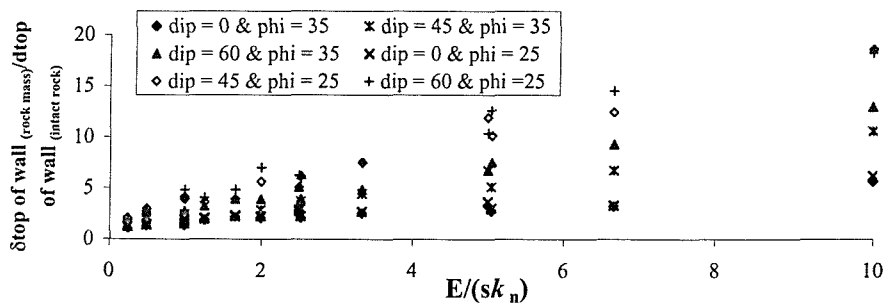
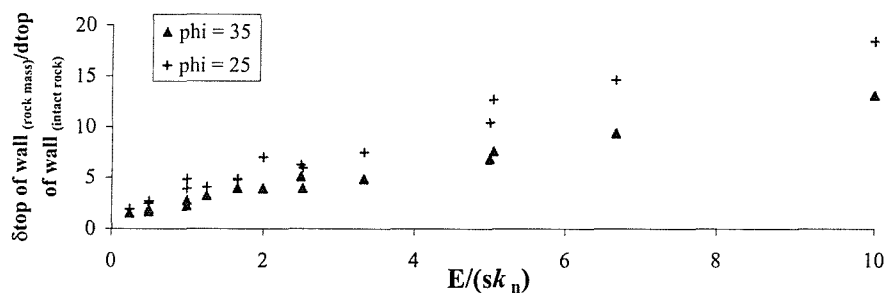
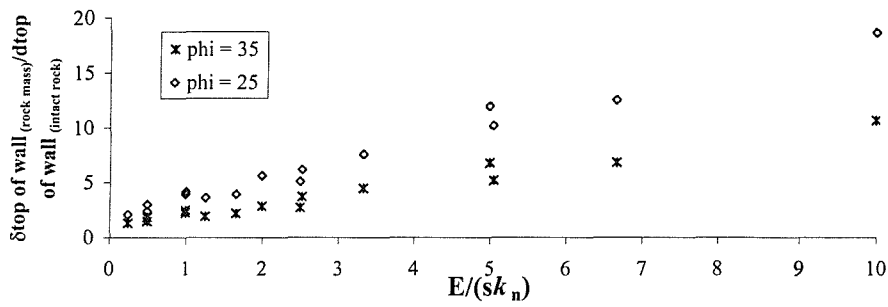
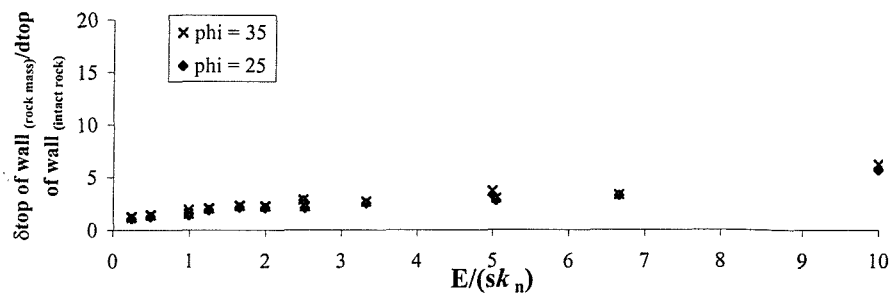
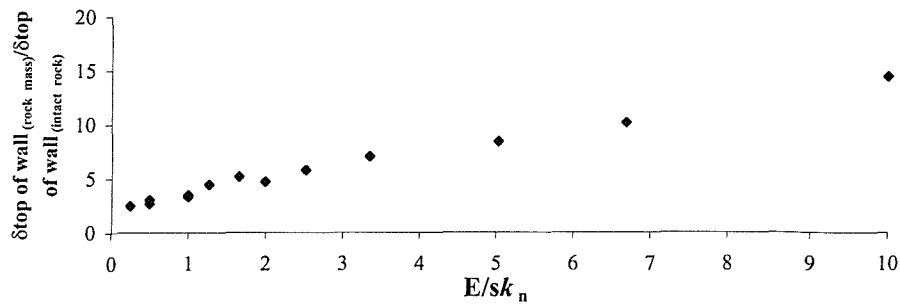
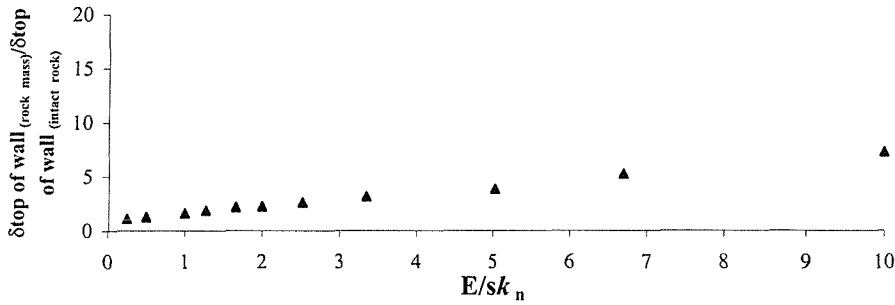


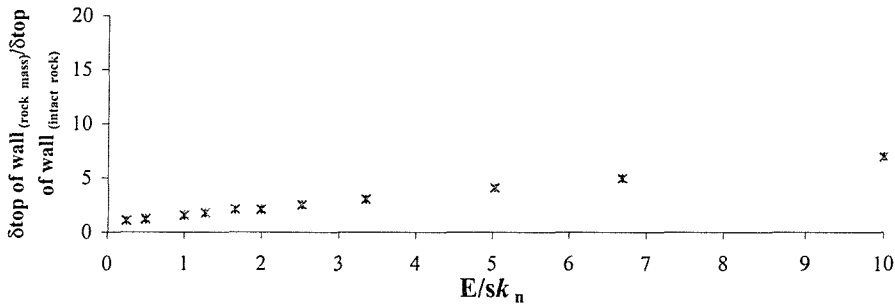
Figure 5.7. Comparison between discontinuous analyses



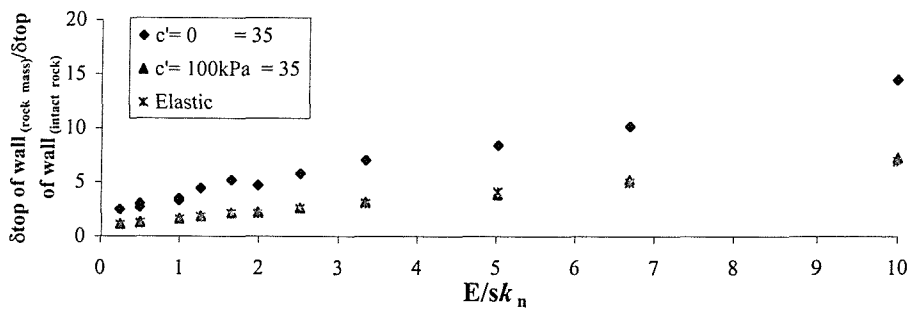
5.8a.  $c' = 0$  &  $\phi = 35^\circ$



5.8b.  $c' = 50 \text{ kPa}$  &  $\phi = 35^\circ$



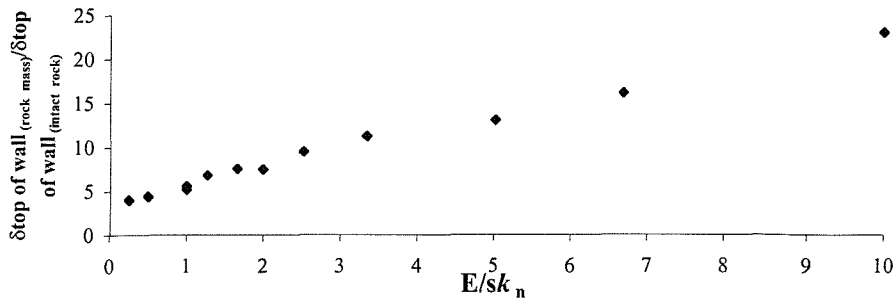
5.8c. Elastic



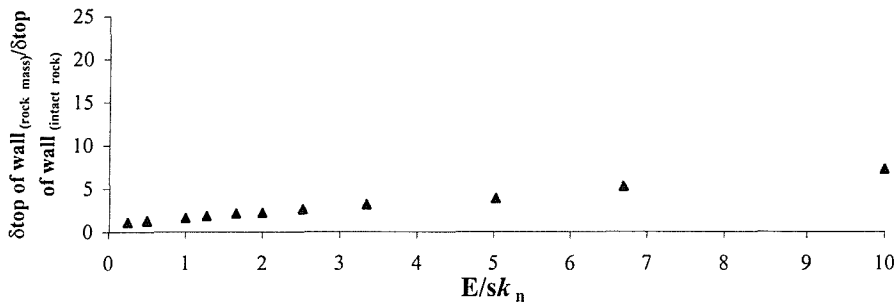
5.8d. All

Figure 5.8. Calculated wall movements from equivalent continuum analyses (joint strength  $\phi'=35$ )

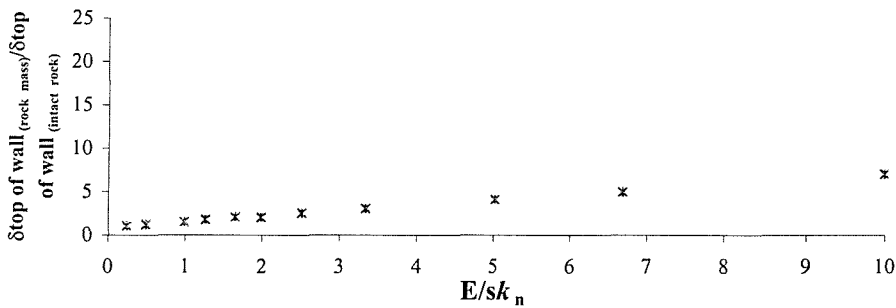




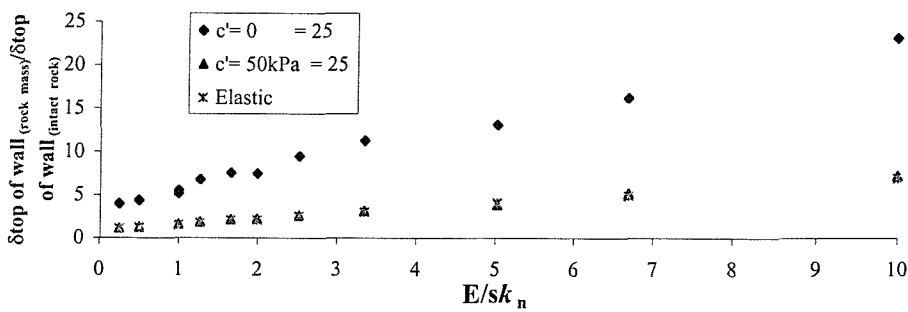
5.9a.  $c' = 0$  &  $\phi = 25^\circ$



5.9b.  $c' = 50 \text{ kPa}$  &  $\phi = 25^\circ$

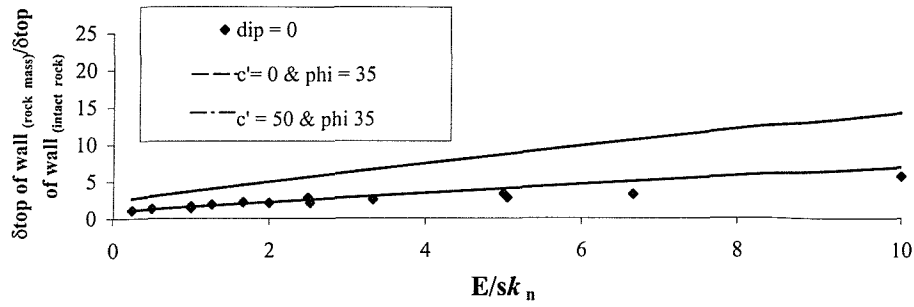


5.9c. Elastic

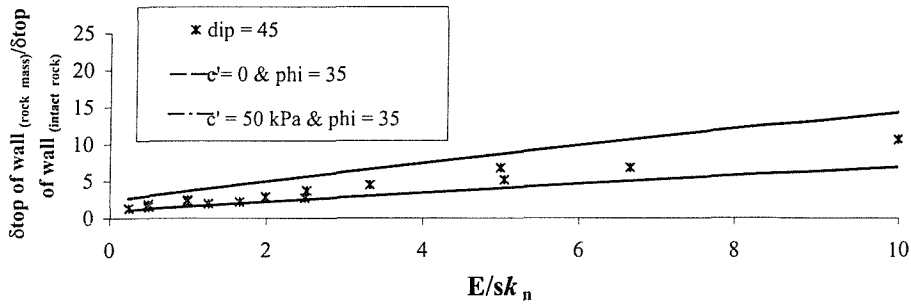


5.9d. All

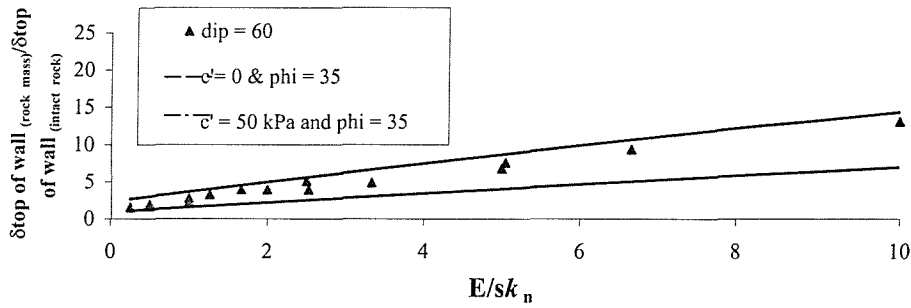
Figure 5.9. Calculated wall movements from equivalent continuum analyses (joint strength  $\phi'=25$ )



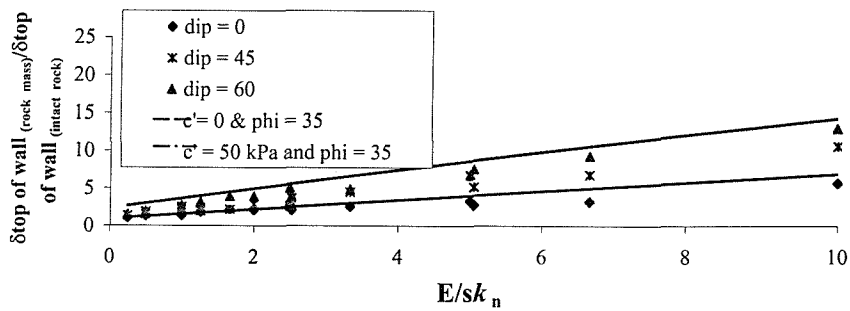
5.10a. Dip =  $0^\circ$



5.10b. Dip =  $45^\circ$

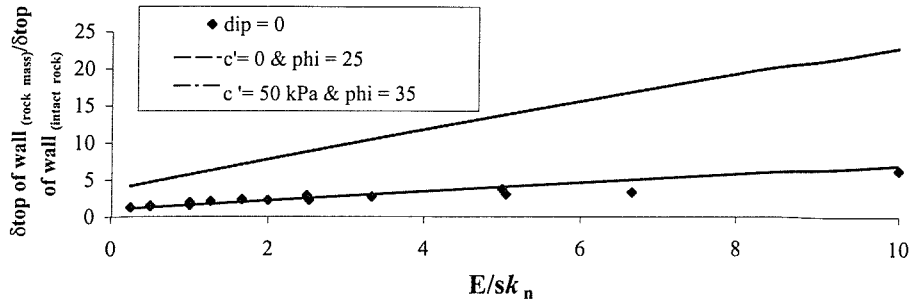


5.10c. Dip =  $60^\circ$

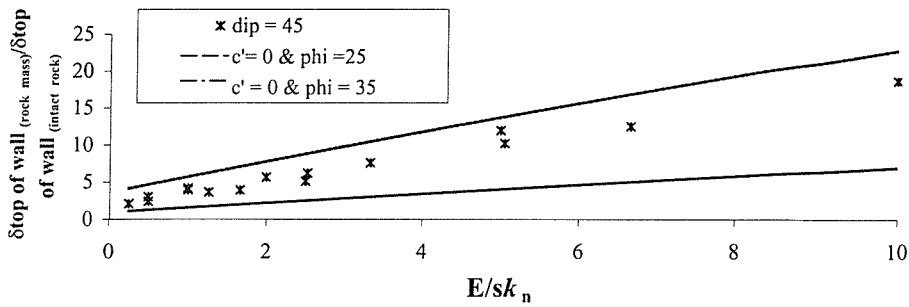


5.10d. All

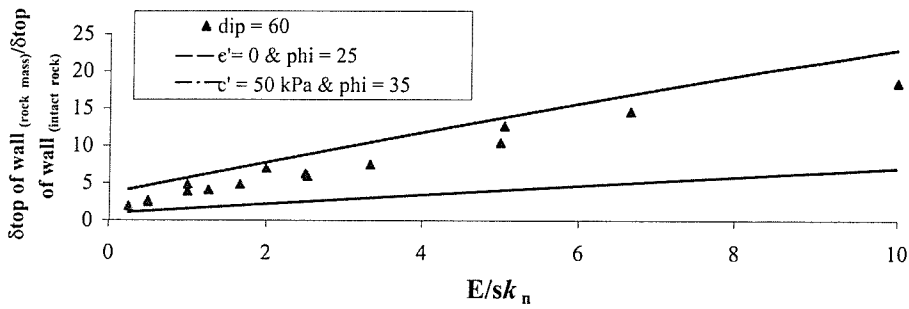
Figure 5.10. Comparison between discontinuous and equivalent continuum analyses (joint strength  $\phi'=35$ )



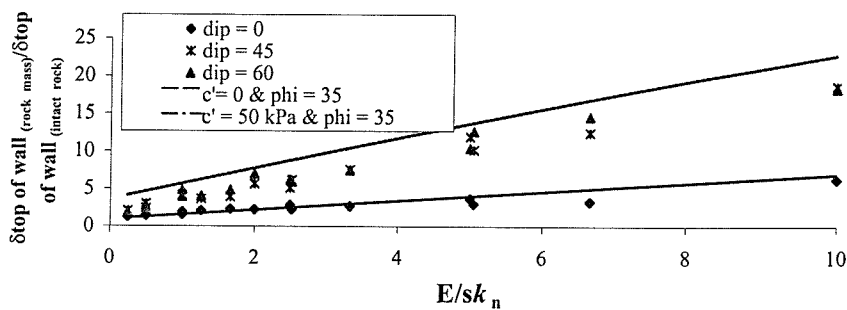
5.11a. Dip =  $0^\circ$



5.11b. Dip =  $45^\circ$

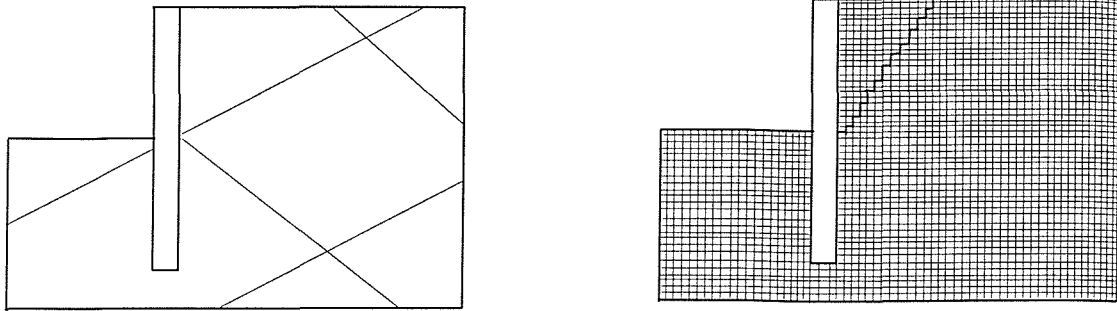


5.11c. Dip =  $60^\circ$



5.11d. All

Figure 5.11. Comparison between discontinuous and equivalent continuum analyses (joint strength  $\phi'=25$ )



**Figure 5.12. Effect of scale**

When using an equivalent continuum model for carrying out a retaining wall analysis in weak rock, the calculated wall movements will depend on how the mass strength is taken into account. But the question is how should the mass strength be modelled. Models like the modified Mohr-Coulomb model proposed by Hoek and Brown (1983) for quantifying the strength of a jointed rock might be more suitable, as this type of model estimates a failure envelope based on both the intact strength and joint strength. Nevertheless, the simple approach would be to use the intact strength if the dip direction of the joints is less than the joint strength and the joint strength when the dip direction exceeds the joint strength.

In the case of the instrumented retaining wall, where the joints are near vertical and horizontal, this would indicate that the best approach for back-analysing the wall as an equivalent continuum model is to take the mass strength as the intact strength of the weak rock.

It would appear that both geomechanical models have a potential for determining the serviceability of retaining walls embedded in weak rock. However, the real question is what method best represents the field behaviour. A further consideration is the practicability of any model for routine use in weak rock engineering. Should a model include as much geological detail as possible, or should it focus primarily on simplified analysis? The main arguments against the inclusion of as much geological detail are:

- i. it is currently unrealistic ever to expect to have sufficient data to model a jointed rock mass in every detail,
- ii. the computer hardware requirements quickly exceed what is typically available, and
- iii. most importantly, a controlled engineering understanding of the model results becomes less effective as more detail is added.

On the other hand, the perceived difficulty with the continuum approach is the concern that the problem will become over simplified, and that essential features may have not been included. This is at the heart of all engineering models, be they conceptual or quantitative. An engineering model must include the important aspects of real behaviour, and discard the unimportant detail that makes all real problems complex. It is this question that the rest of this thesis will attempt to solve.

## 5.9. Summary

It is clear that the method of modelling a retaining wall in weak rock should depend primarily on the presence and nature of the discontinuities. It follows that a detailed discontinuity survey should form part of the site investigation for an excavation in weak rock. The pattern and nature of the discontinuities would then influence the design methodology as follows

- where discontinuities are included in a rock mass with a dip angle that is small in relation to the shear strength of the discontinuity, an equivalent continuum analysis may be used in which the stiffness profile is determined from field tests involving a volume of material sufficient to represent the behaviour of the mass. This has been demonstrated to be the case at the monitored section of wall.
- where discontinuities are included in a rock mass with a dip angle that is significant relative to the shear strength of the discontinuity, the discontinuities will control the design and a method that explicitly takes into account the properties of the discontinuity (e.g. a discrete element/limit equilibrium analysis) should be used.
- where discontinuities are included in a rock mass with a dip angle that is significant relative to the shear strength of the discontinuities a simple method to take account

for this is to use the joint strength in an equivalent continuum analysis which will provide upper bound estimates of wall displacements.

In the case of the instrumented retaining wall, the discontinuity orientation is such that it should be possible to model the wall as an equivalent continuum, where the mass strength is represented by the intact strength.

It would appear that both geomechanical models have a potential for determining the serviceability of retaining walls embedded in weak rock. However, the real question is what method best represents the field behaviour and is it correct to model the rock mass as an isotropic elastic material. It is this question that the rest of this thesis will attempt to solve.

## **CHAPTER 6**

### ***COVENTRY: BACK-ANALYSIS AND DISCUSSION***

#### **6.1. Introduction**

A reasonable knowledge was gained of the distribution of the discontinuities throughout the weak rock mass at the case study site, revealing that no major instability was envisaged due to favourable orientation of the discontinuity sets (Davies and Barton 1998). The joint spacing was relatively small in comparison to the monitored retaining wall, and in view of the findings presented in Chapter 5 it was decided to use an equivalent continuum approach to back calculate the operational stiffness profile for the monitored retaining wall.

In this chapter, wall behaviour calculated in a plane strain finite element analysis replicating site conditions as closely as possible at the case study site is compared with those observed. The mesh geometry, material properties and the sequence of the analysis are first described.

## 6.2. Finite element program CRISP

The CRISP (Critical State Package, Britto and Gunn 1987) finite element program was used to back analyse the instrumented wall. CRISP is a finite element program developed principally for soil mechanics. As the program name suggests, this program incorporates the critical state concepts of soil mechanics into a finite element program. However other constitutive models are also incorporated that are more suitable for weak rock.

Since the program was written as a research tool, with a structure that facilitates amendments by users, many variations of the program exist. In its basic form the program can be used for drained, undrained or fully-coupled consolidation analyses of two-dimensional plane strain, axi-symmetric and three-dimensional problems. The constitutive models available include anisotropic elasticity, non-homogeneous elasticity (Young's Modulus varies with depth), elastic-perfectly plastic models incorporating various failure criteria, and critical state models.

For strains that vary linearly within an element, 6 noded triangles and 8 noded quadrilaterals are available. Higher order elements such as the 15 noded cubic strain triangles can also be used. To model soil/structure interaction effects, an interface element is available, together with discrete bar and beam elements.

CRISP uses an incremental or tangent stiffness approach to model a non-linear stress-strain response. For this reason, the change in the loading of the elements due to some event such as excavation is divided into a number of smaller increments and the program applies each of these incremental loads in turn. In each increment the stiffness properties appropriate to the current stress level are used in the computation. This has the disadvantage that if too few increments are used in the analysis, the stiffness is over predicted and displacements are under predicted.

One of the distinguishing features of CRISP is the ability to model construction processes such as excavation and backfilling. To model excavation the element is not actually removed from the mesh but its stiffness and self weight are reduced



to zero and the force interaction between the element to be removed and the elements which remain is calculated. To model construction the elements to be added are included in the initial mesh and prescribed with zero values of stiffness and self weight. The user then specifies a point in the analysis at which to assign the intended material properties of the elements.

Loading can be applied without the addition or removal of elements by specifying an individual or a series of point loads at nodes over load increments. Nodes can also be fixed in position or displaced by the user at any stage of an analysis to represent a real activity causing a stress change in the surrounding elements.

### **6.3. Selection of elements, boundary conditions and number of load increments**

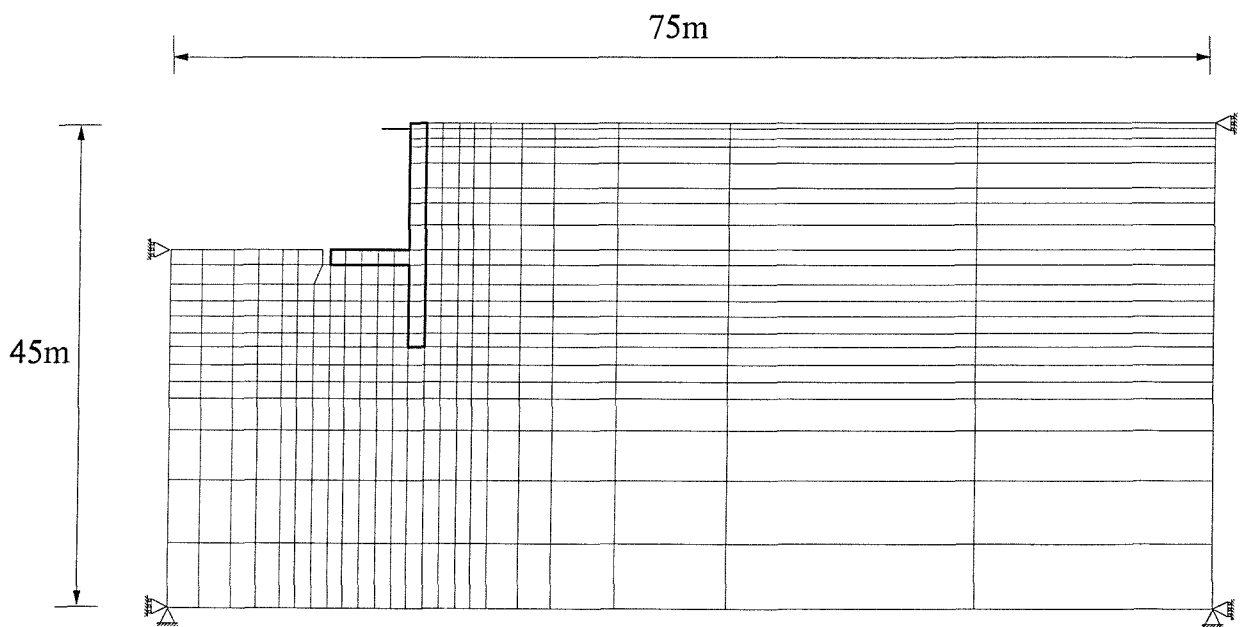
Mesh boundaries must be placed sufficiently remote from the area of the mesh in which external loads are applied that changes in the stress at the boundaries are negligible, or roller supported boundaries positioned to represent an intended plane of symmetry. Remote boundaries fixed on roller supports have by definition zero shear strength, so that even a small shear stress at the boundary will cause significant displacement. These points were taken into consideration in determining the location of the mesh boundaries.

It is not only the location of the mesh boundaries that is important in ensuring a realistic representation of stresses and strains within a finite element mesh: the number, size and distribution of elements are also critical. Theoretically as a mesh is progressively refined there is convergence of the numerical solution to the exact solution. It is most important to have smaller elements in regions where the rate of change of stress with distance is expected to be greatest. In regions where the changes in stress are expected to be small, larger elements can be used with little loss of accuracy. In many cases, the results that can be achieved with a mesh of few elements concentrated in the critical regions can be just as accurate as those with a mesh with more elements distributed inefficiently.

The mesh used in the analyses, shown in Figure 6.1, comprised 491 linear strain quadrilateral elements. The wall and stabilising base were modelled using linear strain quadrilateral elements. The prop was modelled using a 2-noded beam element. Smaller elements were concentrated around the wall, where the most significant changes in stress were expected to occur.

In the analysis, the prop pre-load was applied at the bar element node furthest from the wall. Once the pre-load had been applied, the node was then fixed.

Before the mesh in Figure 6.1 was eventually adopted, an analysis was carried out using twice the number of elements used in the adopted mesh. No difference in the results was indicated, so the smaller mesh was adopted.



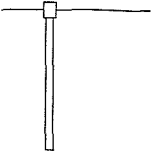
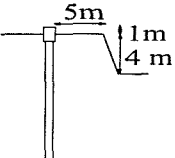
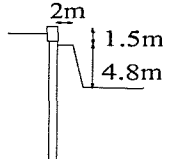
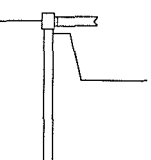
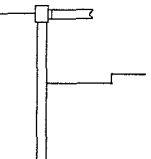
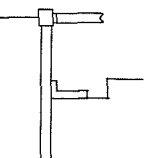
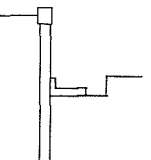
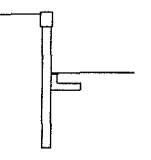
**Figure 6.1. Finite element mesh**

As stated in section 6.1, CRISP uses an incremental or tangent stiffness approach to model the non-linear stress-strain response. The unloading of elements associated with the excavation procedure and the loading/unloading of the prop needs to be divided over a number of smaller increments that the program applies in turn. In order to limit the output and the computational time taken for each analysis, a balance has to be made between the number of elements and loading increments.

In all analyses, excavation was modelled in stages as observed at the case study. The change in load associated with the removal of each layer was applied over a single increment block of between 5 & 45 equal increments. An analysis was performed which used double the number of load increments: this made no significant difference to the results. Since the only real effect of doubling the number of loading increments was to increase the size of the output file, it was decided to perform the analyses using the smaller number of increments for each increment block.

#### **6.4. Idealised Geometry for each construction phase**

The idealised geometry, Table 6.1, is symmetrical about the centre line, so that the mesh represents one half of a cross-section through the excavation. The nodes along the base of the mesh were modelled as fully pinned. The boundaries at the side of the mesh were modelled as being restrained in the horizontal direction only. The analyses commenced with the wall already in place (the effects of the wall installation process are discussed in section 6.6.3.)

Inc No	Description	Schematic	Day
	Installation of contiguous pile wall.		
1-10	First stage excavation.		0
11-25	Third stage excavation.		155
26-50	Temporary props installed and pre-loaded		192
51-65	Earth berm removed.		195
66-110	Excavation to stabilising base blinding level and construction of stabilising base.		211
111-145	Temporary props removed.		290
146-150	Road opened to traffic		577

**Table 6.1. Idealised geometry**

## 6.5. Selection of constitutive model

Back analysis is generally defined as a technique that can provide the controlling parameters of a system by analysing its output behaviour. It must be emphasised that back analysis is not simply the reverse calculation of conventional analysis, because, particularly in the modelling of weak rock, the basic assumptions could differ. In a conventional analysis a constitutive model is assumed, and the values of the material constants of the model can be determined by performing laboratory tests and/or *in situ* tests. These values are then used as input data for an ordinary analysis to calculate displacements, stresses and strains. These results represent a unique solution, at least for the given model.

In back analysis, displacements, strains and pressures have already been obtained by field measurements. A constitutive model is assumed, and the material constants and external forces can be back calculated with reference to the field measurements. Consequently, the back calculated values of the material constants depend on the assumed model. To have any confidence in obtaining a correct result in back analysis, great care should be taken in selecting the model.

In view of the findings of chapter 3 and 5, it was anticipated that an elastic constitutive law would adequately represent the behaviour of the weak rock at the case study with yield of the intact weak rock taking place according to a Mohr Coulomb failure criterion. To validate this, two analyses were undertaken. In analysis MOD1 (Figure 6.2a and 6.3a) a linear elastic constitutive law was assumed and the yield parameters taken as those of the intact weathered weak rock (i.e.  $c' = 50$  kPa and  $\phi' = 35$ ). In analysis MOD2 (Figure 6.2b and 6.3b); a linear elastic constitutive law was also assumed to govern the pre-yield stress strain behaviour of the weak rock. But this time the weak rock was modelled as linear elastic perfectly plastic material with yield parameters taken as those of a smooth joint (i.e.  $c'$  was taken as zero). It was found that even in analysis MOD2 the stresses in the weak rock did not approach their yield values (Figure 6.4). This is why the wall displacements and bending moments in Figures 6.2 and 6.3 are almost identical in the two analyses.

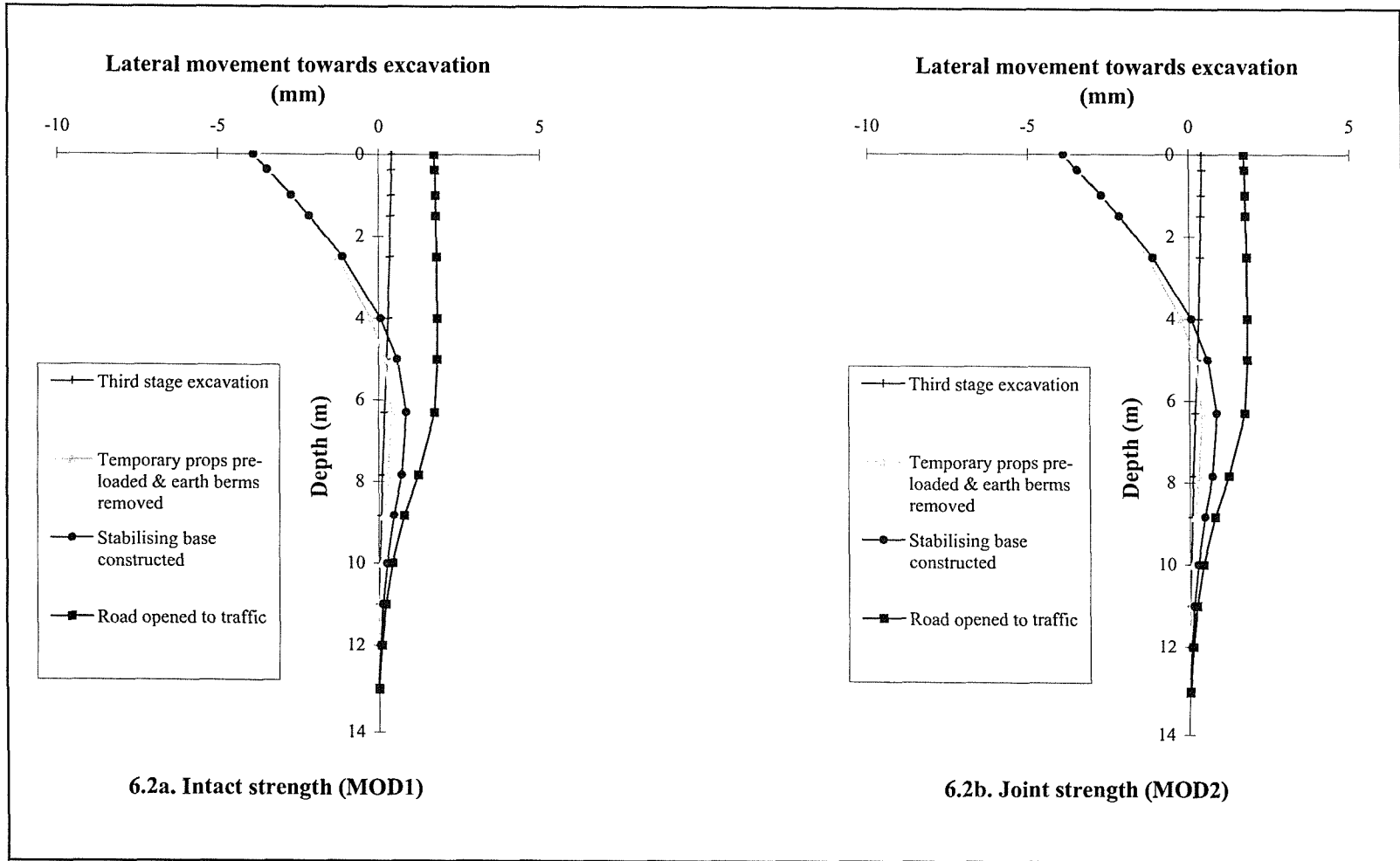


Figure 6.2. Comparison of calculated lateral wall movements

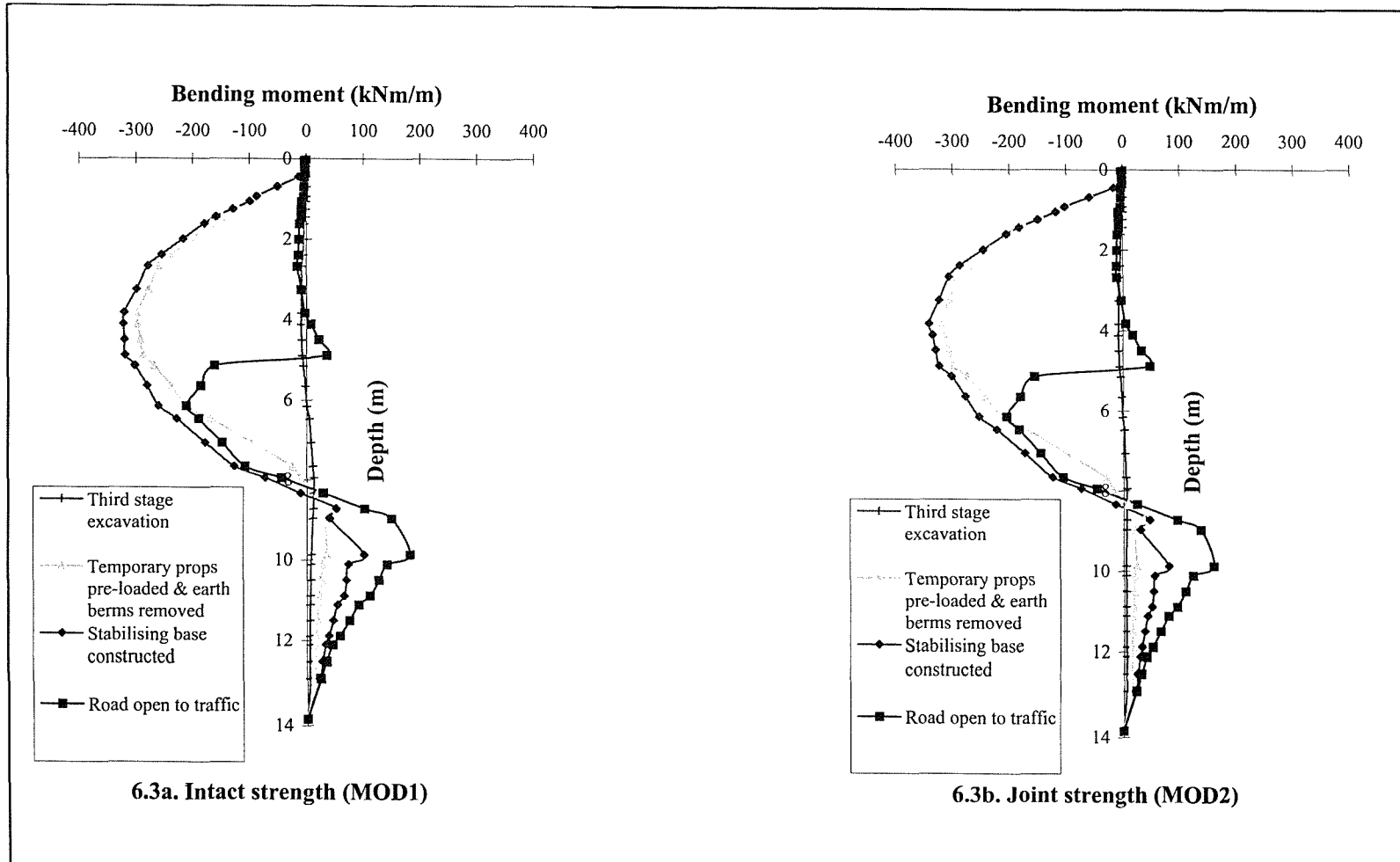
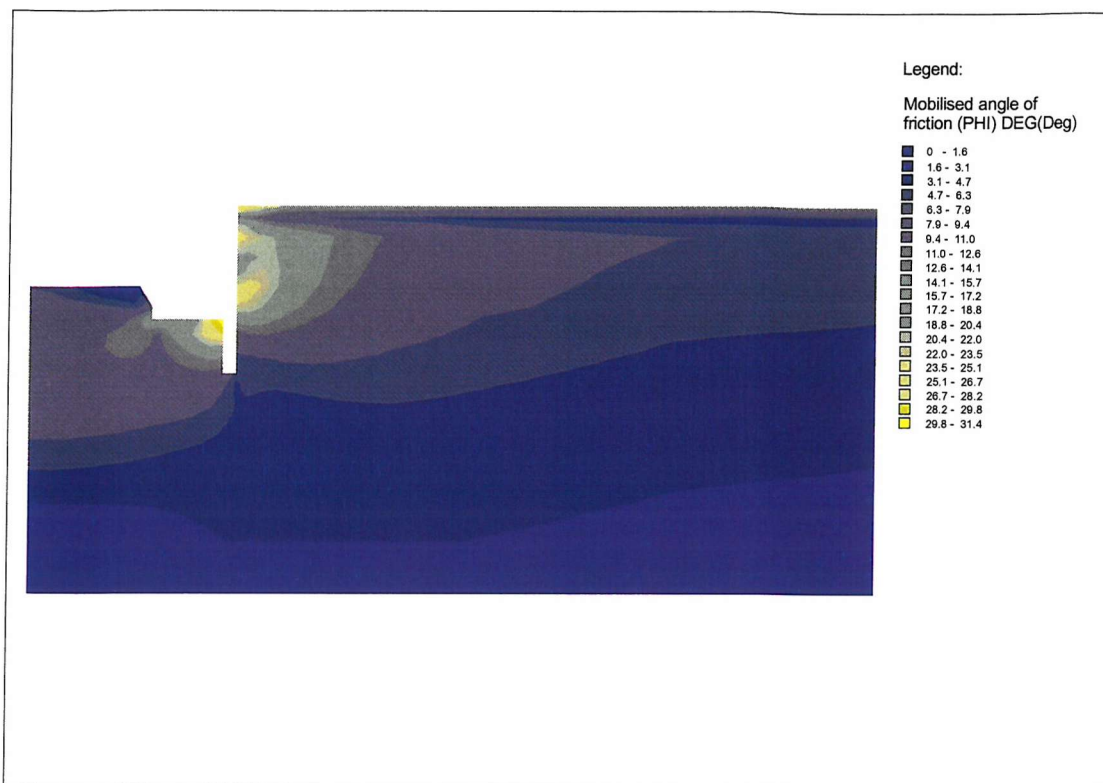


Figure 6.3. Comparison of calculated wall bending moments



**Figure 6.4. Mobilised angle of friction (analysis MOD2)**

The major potential shortcomings of using a linear elastic model is that it cannot take into account any non-linearity of stiffness with strain and it does not take into account the effect that discontinuities have on the stress distribution.

Observations in hard rocks suggest these shortcomings might be significant because:

Goodman (1976) and Bandis *et al* (1983) have showed that the introduction of a single discontinuity into a laboratory specimen of rock will give rise to a significant change in the stress displacement characteristics when compared with that of the intact rock Figure 6.5. It can be seen from Figure 6.5 that the stiffness of discontinuities in rock is stress dependent and non-linear. Figure 6.5 shows that the cycles of loading and unloading exhibited hysteresis and permanent set.

Barton (1986) has also defined three characteristic modes of load deformation behaviour associated with the orientation of the discontinuities relative to the direction of the applied load based on the dominant deformation mechanism Figure 6.6. Figure 6.6 shows the three simple rock mass models considered by



Barton (1986) subjected to a vertical applied load. The shape of the load deformation curve is non-linear in cases A and C and only linear in case B. All the load deformation curves showed hysteresis and a permanent set on unloading.

In jointed chalk the load-settlement curve from plate test is also convex (Figure 6.7). At a certain bearing pressure the compressibility of the rock mass increases significantly and settlements are not recovered upon unloading. This change in gradient of the load settlement curve that gives rise to this characteristic shape is associated with yielding of the rock mass. However, at small strains, prior to yielding the rock mass behaves in a more or less linear manner, after yield it behaves as a granular soil, (see Burland and Lord 1970, Matthews 1990). As the strains encountered around retaining walls are generally small (Mair 1993), this would suggest that a linear elastic model is suitable for a stiff weak rock.

The yielding behaviour observed in the chalk is contrary to the behaviour obtained from the laboratory tests and *in situ* loading tests in hard rock. The reasons for this difference in behaviour could be due to loading in the hard rock tests not being great enough to de-structure the intact hard rock. Nevertheless, in these hard rock tests there also appears to be a linear portion to the load settlement curve at the start of loading.

Model tests on jointed rock masses carried out by Gazier and Erlikhman (1971), have shown that the stress distribution beneath the loaded area is significantly different to that based on an elastic continuum Figure 6.8. The model tests on jointed rock masses all show that the stress distribution beneath the load area is significantly different to that based on an elastic continuum. In a real weak rock mass the situation is further complicated by the fact the style of jointing often changes with depth. It is arguable therefore whether the stress at a given point can be predicted with any accuracy.

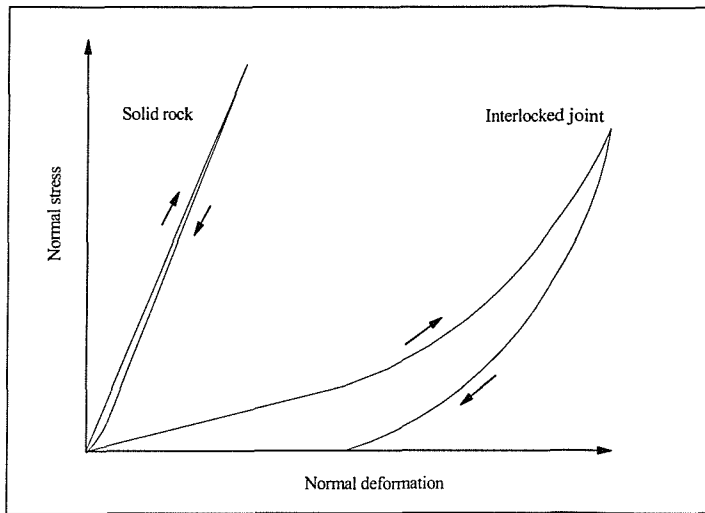


Figure 6.5. Stress-deformation behaviour of rock joints  
(after Bandis et al. 1983)

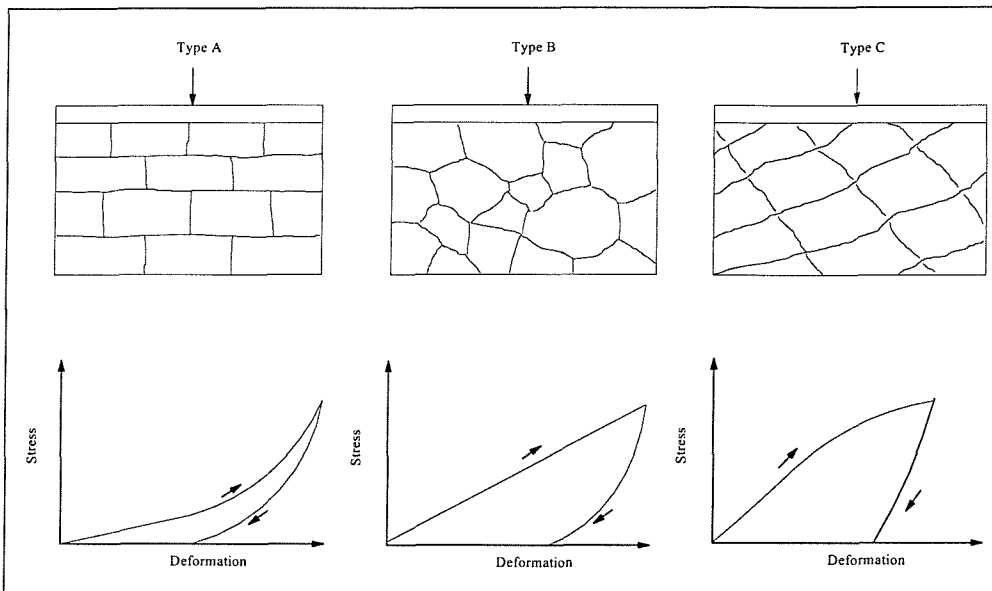


Figure 6.6. Load-deformation behaviour for rock masses (after Barton 1986)

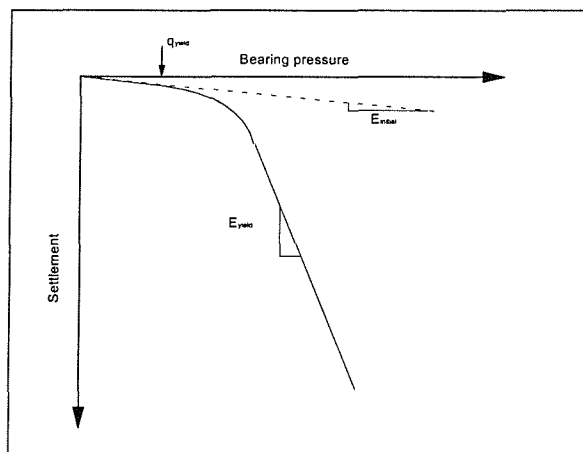
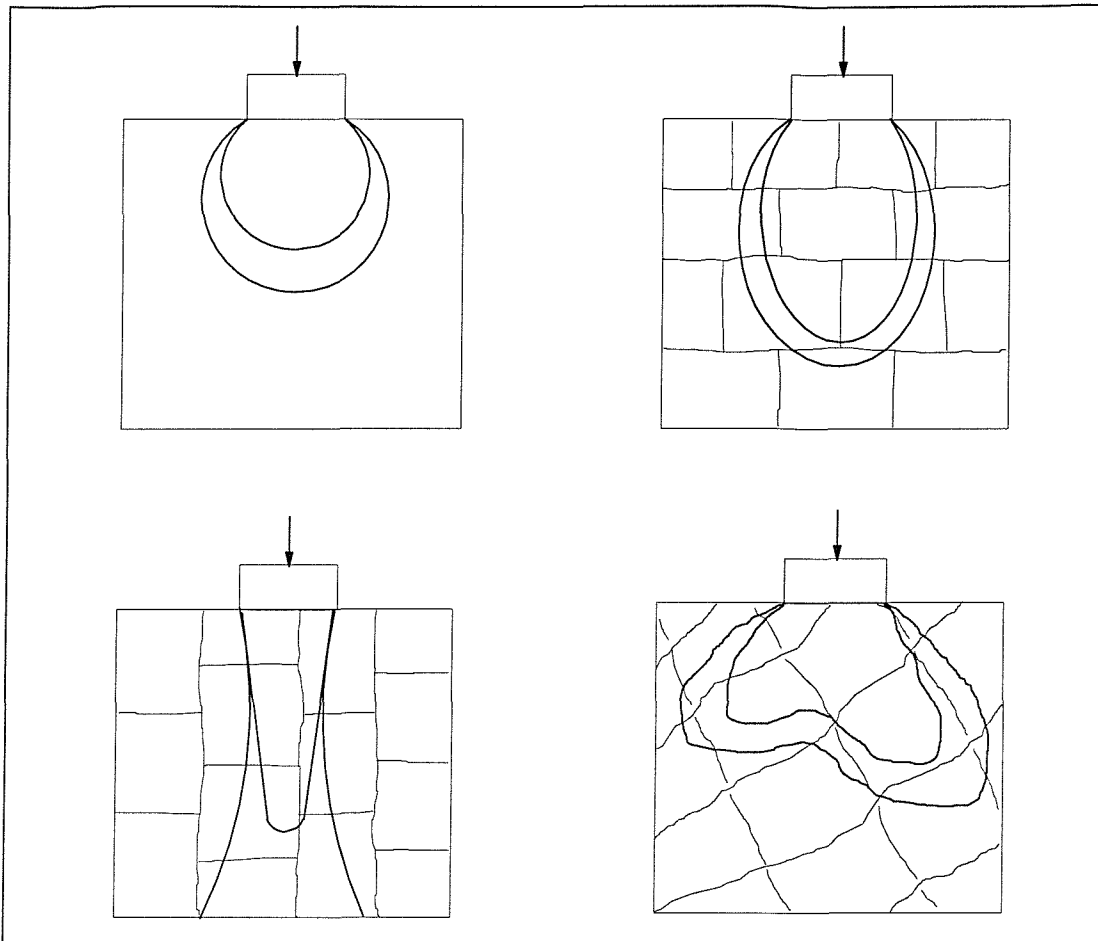


Figure 6.7. Typical deformation curve for chalk  
(after Burland and Lord 1970)



**Figure 6.8. Pressure distributions for a circular foundation on rock masses with different discontinuity set orientations (after Gaziev and Erlikhman 1971)**

## 6.6. Input parameters

The finite element analysis has been used to obtain a back calculated stiffness profile behind the instrumented wall. Initially, a sensitivity study was undertaken to assess which parameters have the greatest influence on the wall behaviour. It was found that the specified horizontal stresses, the stiffness profile and the pre-load in the temporary props were the three main parameters influencing wall behaviour. Other parameters had only a minor influence on wall behaviour.

### 6.6.1. Structural components

#### *Wall and stabilising base*

The stabilising base and the bored wall were modelled as an impermeable elastic material with the parameters listed in Table 6.2.

<b>E<sub>c</sub></b> (kN/m <sup>2</sup> )	<b>E<sub>w</sub></b> (kN/m <sup>2</sup> )	<b>ν</b>	<b>G</b> (kN/m <sup>2</sup> )	<b>γ</b> (kN/m <sup>3</sup> )
25 × 10 <sup>6</sup>	28.5 × 10 <sup>6</sup>	0.15	12.4 × 10 <sup>6</sup>	24

**Table 6.2. Material properties of wall**

Where  $E_c$  = Young's modulus of the concrete

$E_w$  = Young's modulus of the wall

$\nu$  = Poisson's ratio

$G$  = Shear modulus

$\gamma$  = Bulk unit weight

The stiffness modulus for the concrete was taken as the average suggested in BS8110, Table 7.2, for the static modulus of elasticity at 28 days for normal weight concrete. The value of the stiffness for the wall is a calculated composite modulus that includes the effect of the reinforcement.

As the wall was constructed using contiguous bored piles (so that the cross sectional area is not constant), it was not possible to model the exact geometry of the wall in the plain strain analysis. In the analyses a uniform wall thickness of 1m was used, with a reduced Young's modulus of  $15 \times 10^6$  kN/m<sup>2</sup>, which gave the same average bending stiffness (EI), per metre run as the 1m diameter piles at 1.1m centres used in reality. The connection between the wall and the slab was modelled as a rigid connection and therefore able to transmit bending moments.

### *Temporary props*

The temporary props were modelled in the analyses using 2m long bar elements with a reduced Young's modulus such that the stiffness in the axial compression per metre run was equivalent to 720 mm diameter × 8.6 mm thick props at 5m centres, spanning 11.175m (half the width of the excavation). The equivalent Young's modulus for the bar element was calculated to be  $1.84 \times 10^7$  kN/m<sup>2</sup> using Equation 6.1:

$$\frac{E_p A_p}{L_p} = \frac{E_m A_m}{L_m} \quad (6.1)$$

Where  $E_p$  = Actual Young's modulus of the prop

$A_p = A_m$  = Actual cross sectional area of prop

$L_p$  = Actual length of prop to centreline of excavation

$E_m$  = Calculated equivalent Young's modulus for bar element

$L_m$  = Length of bar element in analysis

The adjusted bar element stiffness was checked by calculating the prop load from the shortening of the props during pre-loading in the analysis, using Equation 6.2. This was found to be in agreement with the prop load applied directly in the analysis.

$$\frac{E_p A_p}{L_p} \delta = \frac{E_m A_m}{L_m} \delta = P \quad (6.2)$$

Where  $\delta$  = shortening of prop as calculated in the analysis

$P$  = Applied prop pre-load

As discussed in chapter 3, the initial load that had been applied to each prop as a pre-load reduced as adjacent props were pre-loaded. This was a three dimensional effect that could not be modelled in the analyses used in this chapter. To overcome this, the pre-load used in the analysis was taken as the measured load just after all the props had been pre-loaded. For the two monitored props P1 and

P2, these were 180 kN/m and 140 kN/m respectively. As the back analysis was very sensitive the pre-load specified, it was decided that rather than take an average of the loads, both loads should be used in separate back analyses. This therefore provided an upper and lower bound stiffness profile for the monitored retaining wall section.

### 6.6.2. Material properties

#### *Geological sequence*

The ground behind the monitored retaining wall was subdivided into three zones:

- Made ground – from ground level to a depth of 1.5m
- Highly weathered weak rock – from 1.5m to a depth of 6.3m
- Moderately to slightly weathered weak rock – from 6.3m

This profile was based on the geology observed at the instrumented section and that indicated from the geophysics tests.

#### *Made ground*

The elements representing the Made ground were modelled as a linear elastic perfectly plastic material. The soil parameters used in the finite element analysis to represent the Made ground are shown in Table 6.1.

$c' \text{ \& } \phi'$	E (kN/m <sup>2</sup> )	$\nu$	G (kN/m <sup>2</sup> )	$\gamma_b$ (kN/m <sup>3</sup> )
$c' = 0 \text{ \& } \phi' = 30$	$1.0 \times 10^4$	0.2	$8.3 \times 10^3$	20

**Table 6.3. Made ground parameters**

Where  $c'$  = Cohesion intercept

$\phi'$  = Effective angle of friction

$E$  = Young's modulus of the made ground

$\nu$  = Poisson's ratio

$G$  = Shear modulus

$\gamma_b$  = Bulk unit weight

There was no geotechnical information available from the site investigation on Made ground, so typical values quoted from Carder and Symons (1989) were used. The sensitivity of the results to these parameters was negligible, as most of the made ground behind the wall was removed during first stage excavation.

### *Bromsgrove Sandstone*

The elements representing the Bromsgrove Sandstone were modelled as linear elastic perfectly plastic material. The stiffness of the Bromsgrove Sandstone is one of the variables to be determined by the back calculation so it is not listed with the other parameters in, Table 6.4.

Description	$c'$ & $\phi'$	$\nu$	$\gamma$ (kN/m <sup>3</sup> )
Highly weathered weak rock	$c' = 5 \text{ kPa}$ & $\phi' = 35$	0.2	22
Moderately weathered weak rock	$c' = 50 \text{ kPa}$ & $\phi' = 35$	0.2	22

**Table 6.4. Bromsgrove sandstone parameters**

### 6.6.3. Ground water

As the ground water was below the retaining wall, it was not included in the analysis. The perched water table was also neglected as seepage was allowed through the wall into a drain located in front of the monitored section of retaining wall. This will have prevented any build up of pore water pressures behind the wall.

### 6.6.4. *In situ* lateral stresses

In soils mechanics the lateral stresses in a soil prior to excavation can have a considerable influence on the behaviour of a retaining wall (e.g. Powrie and Li, 1990, Gourvenec, 1998 and Gunn and Clayton 1992). In rock mechanics, the influence of the *in situ* lateral stresses on the behaviour of structures is just as important.

The horizontal earth pressures measured in the case study (see chapter 4, Figure 4.7) suggest that the effective *in situ* earth pressure coefficient ( $K_o$ ) was between 0.8 and 2. However, these were determined from pressuremeter tests that had been influenced by radial cracking, so that the validity of these measurements is questionable.

In the finite element analyses used in this chapter, the wall was cast in-place. It is commonly recognised that stress relief during the installation of a diaphragm or bored pile wall will alter the stress state of the soil, resulting in a different initial or pre-excavation lateral earth pressure coefficient, ( $K_i$ ). The magnitude of these stress changes will depend on the installation sequence and the method used to support the adjacent ground prior to pouring the concrete. During construction of the bored piles forming the instrumented wall section the ground was supported by temporary casing to the base of the made ground, below which the hole was unsupported.



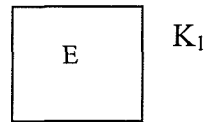
In many finite analyses in the past, stress relief during the construction of the wall has not taken into account (e.g Potts and Burland 1983). However, this approach is likely to lead to the calculation of unrealistically high loads acting on the wall and consequently unrealistic wall movements. It is preferable that stress changes due to wall installation are estimated as accurately as possible so that appropriate values can be specified for the pre-excavation earth pressure coefficient,  $K_i$ .

Experience has shown that the lateral earth pressure coefficient tends to move towards unity during the construction of a diaphragm and bored pile walls (e.g Powrie, 1986 and Tedd *et al.* 1984). However there are arguments that the stress relief that occurs during the installation of a bored pile wall is significantly less than for a diaphragm wall. This is mainly due to hoop stresses set up around the pile hole.

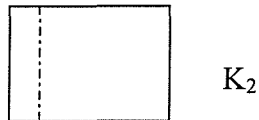
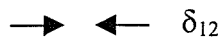
The lateral stress changes resulting from installation of the wall are not easily quantified, and since there are uncertainties concerning the initial lateral stresses, (see chapter 4), it was decided that the pre-excavation earth pressure coefficient, ( $K_i$ ), would therefore be back analysed.

Generally, when back calculating values from a monitored retaining wall it is not possible to determine both the stiffness profile and the initial lateral stresses. Normally one of these has to be assumed prior to the back analysis. The reason is that there are at least two combinations of stiffness and  $K_i$  that will produce, a given set of movements (a low  $K_i$  and a low stiffness or a high  $K_i$  and a high stiffness). However, in the case of the monitored wall presented in this thesis, it was possible to back calculate the stiffness profile and the lateral stresses. This is because the temporary prop was pre-loaded, which meant that the wall movements occurred in both directions. Hence, there is only one combination of stiffness and  $K_i$  that will produce a given set of wall movements Figure 6.9.

*At the start of the analysis*



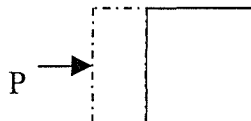
*On excavation (unload)*



$$\delta_{12} = 1/E \times (K_1 - K_2)$$

The wall movement into the excavation depends on the specified stiffness and pre-excavation stresses

*On pre-loading the prop (loading)*



$$\delta_{23} = P/E$$

**Figure 6.9. One combination of stiffness and  $K_i$  that will produce, a given set of movements**

The wall movement away from the excavation depends on the specified stiffness and pre-load of the prop (not the *in situ* stresses). As the pre-load and wall movements are known, there must be only one value of stiffness for this combination. As the stiffness has now been found, the pre-excavation stresses that allows you to obtain the initial wall movements can be found.

To demonstrate that there is only one combination of stiffness and  $K_i$  that will produce a given set of wall movements and bending moments, four analyses using a prop pre-load of 140 kN/m are presented:

- **STIFF1.** The stiffness profile used in this analysis is that used in the original design, Table 6.5, and a  $K_i = 0.92$  (this is a back calculated value of  $K_i$ , see later).

	Highly weathered rock	Moderately weathered rock
Stiffness parameters	$E = 30 \text{ MPa} + 5 \text{ MPa/m}$	$E = 100 \text{ MPa} + 20 \text{ MPa/m}$

**Table 6.5. Design stiffness parameters**

- **STIFF2.** The stiffness profile used in this analysis is based on the geophysical data, Table 6.6, with the same  $K_i$  as in analysis STIF1, ( $K_i = 0.92$ ).

	Highly weathered rock	Moderately weathered rock
Stiffness parameters	$E = 120 \text{ MPa} + 60 \text{ MPa/m}$	$E = 500 \text{ MPa} + 10 \text{ MPa/m}$

**Table 6.6. Geophysical stiffness parameters**

- **Ki0.75.** The stiffness profile used in this analysis is the same as in the STIFF1 analysis, Table 6.5, but  $K_i$  is equal to 0.75.
- **Ki1.5.** The stiffness profile used in this analysis is the same as in the STIFF2 analysis, Table 6.6, but  $K_i$  is equal to 1.5.

The stiffness profile used in STIFF1 is only slightly softer than that back calculated (see Table 6.7). The consequence of using a lower stiffness profile is

that the wall movements into the excavation are greater at the start and end of excavation (Figure 6.10). On pre-loading the wall movements are again greater. Consequently, the wall bending moments are much larger (Figure 6.11) as the wall has been allowed to move too far into the excavation before it was pre-loaded.

If a lower value of  $K_i$  is then used with the stiffness profile in **STIFF1**, as in analysis **Ki0.75**, the wall movements into the excavation prior to pre-loading are reduced (Figure 6.12). However, the wall movements increase on pre-loading. The bending moment profiles also change as a consequence of the change in wall movements (Figure 6.13).

In analysis **STIFF2**, the stiffness profile used is much stiffer than that in analysis **STIFF1**. The initial wall movements are much smaller than those measured (Figure 6.14). Consequently, so are the bending moments (Figure 6.15).

If a higher value of  $K_i$  is used with the stiffness profile in **STIFF2**, as in analysis **Ki1.5**, the wall movements into the excavation are increased (Figure 6.16). However, the wall movements decrease on pre-loading. The bending moment profiles also change as a consequence of the change in wall movements (Figure 6.17).

It can be seen from these four analyses that there is only one combination of stiffness and  $K_i$  that will produce the measured wall movements and bending moments at the instrumented wall. It is possible to have combinations of  $K_i$  and stiffness that will predict movements in one direction, but only one of these combinations work for both directions.

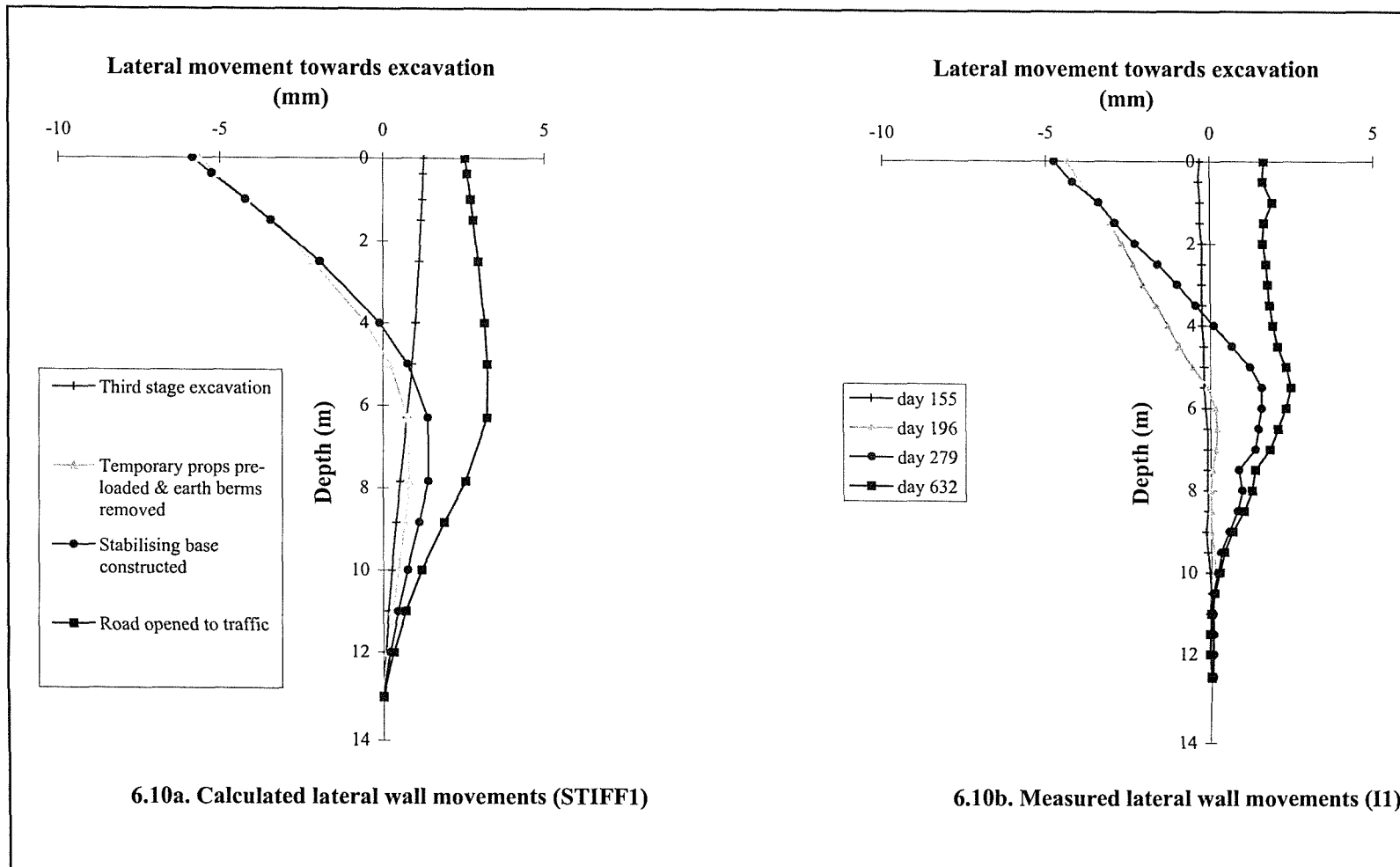


Figure 6.10 Comparison of calculated and measured lateral wall movements (STIFF1)

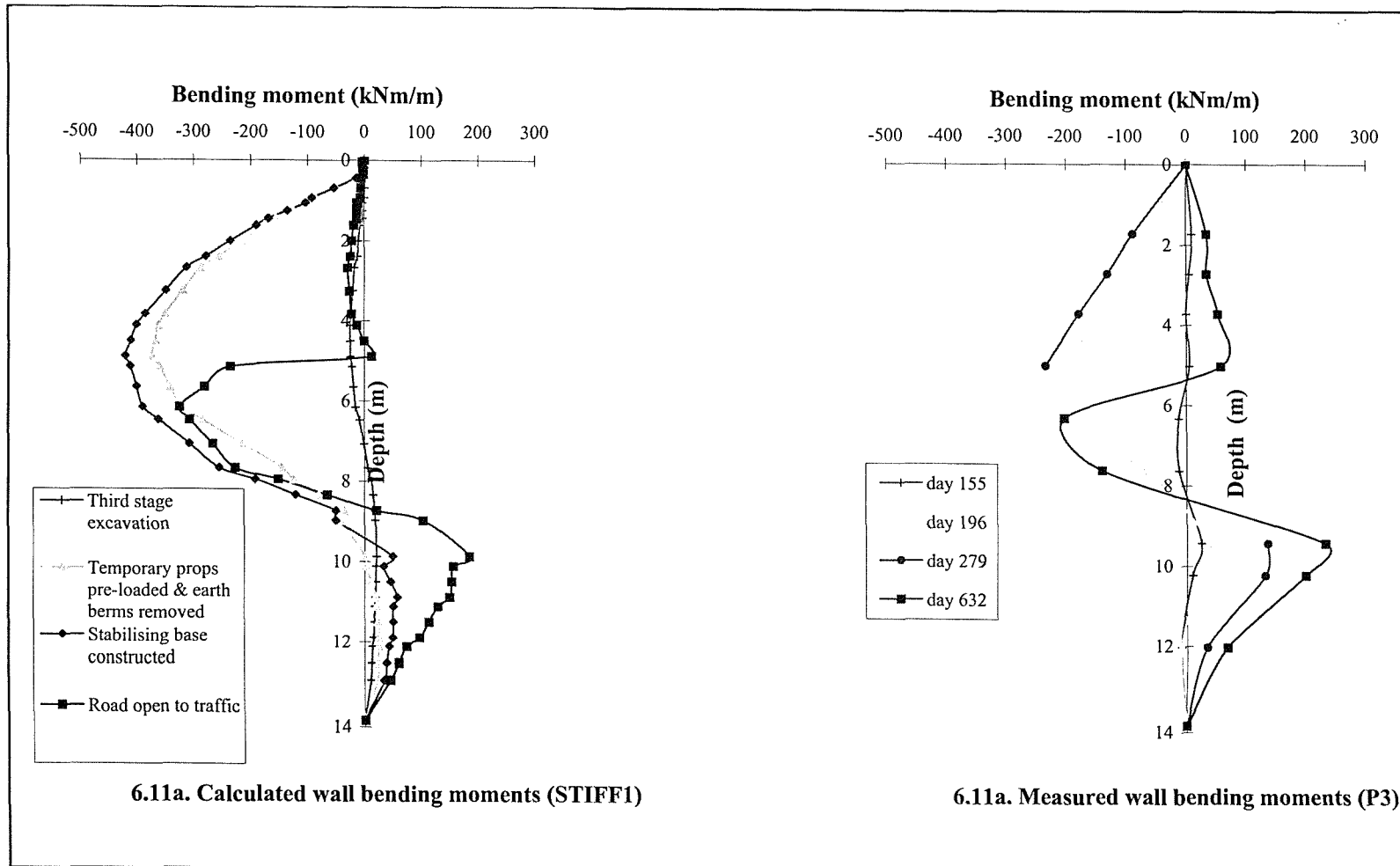
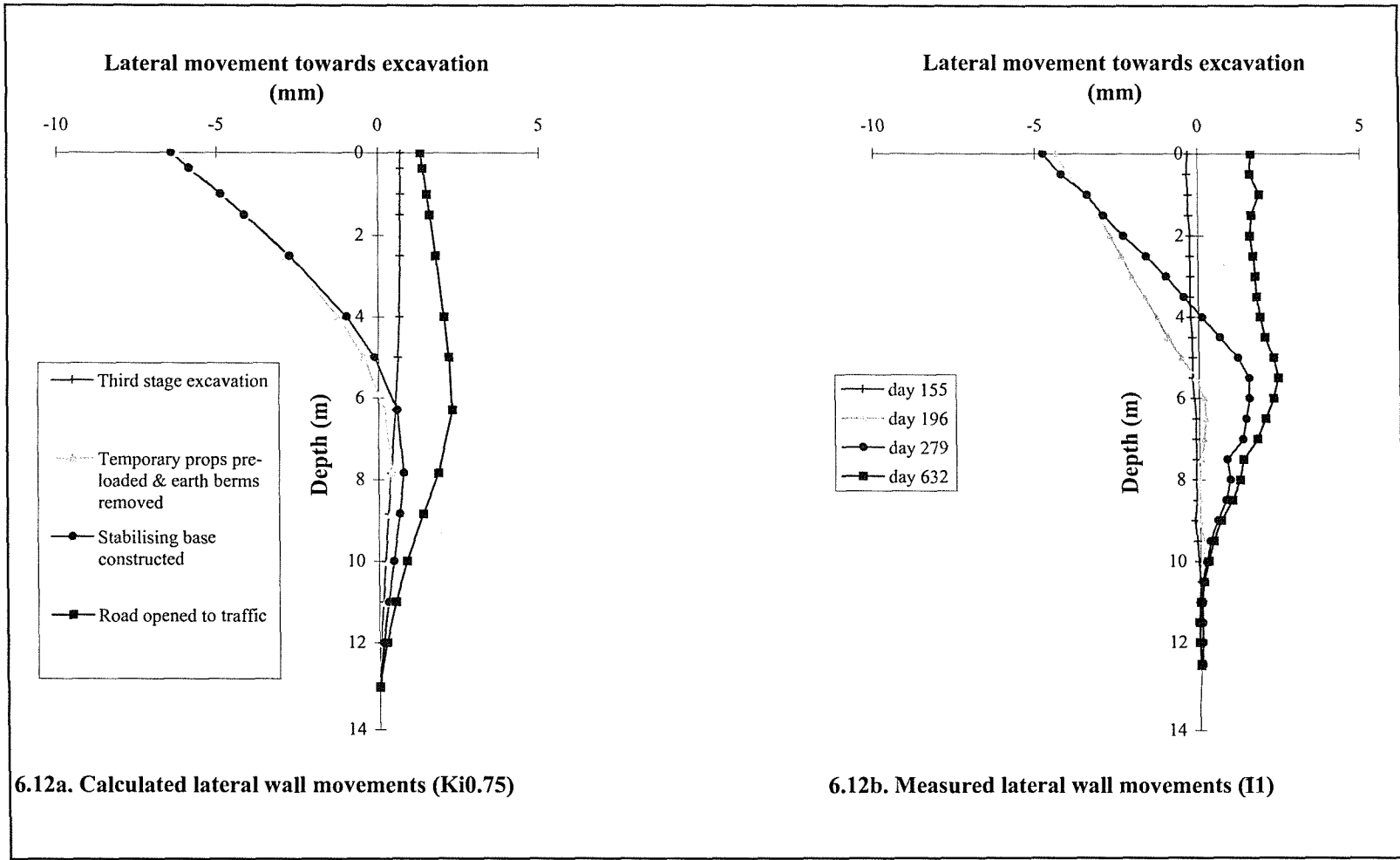


Figure 6.11 Comparison of calculated and measured wall bending moments (STIFF1)



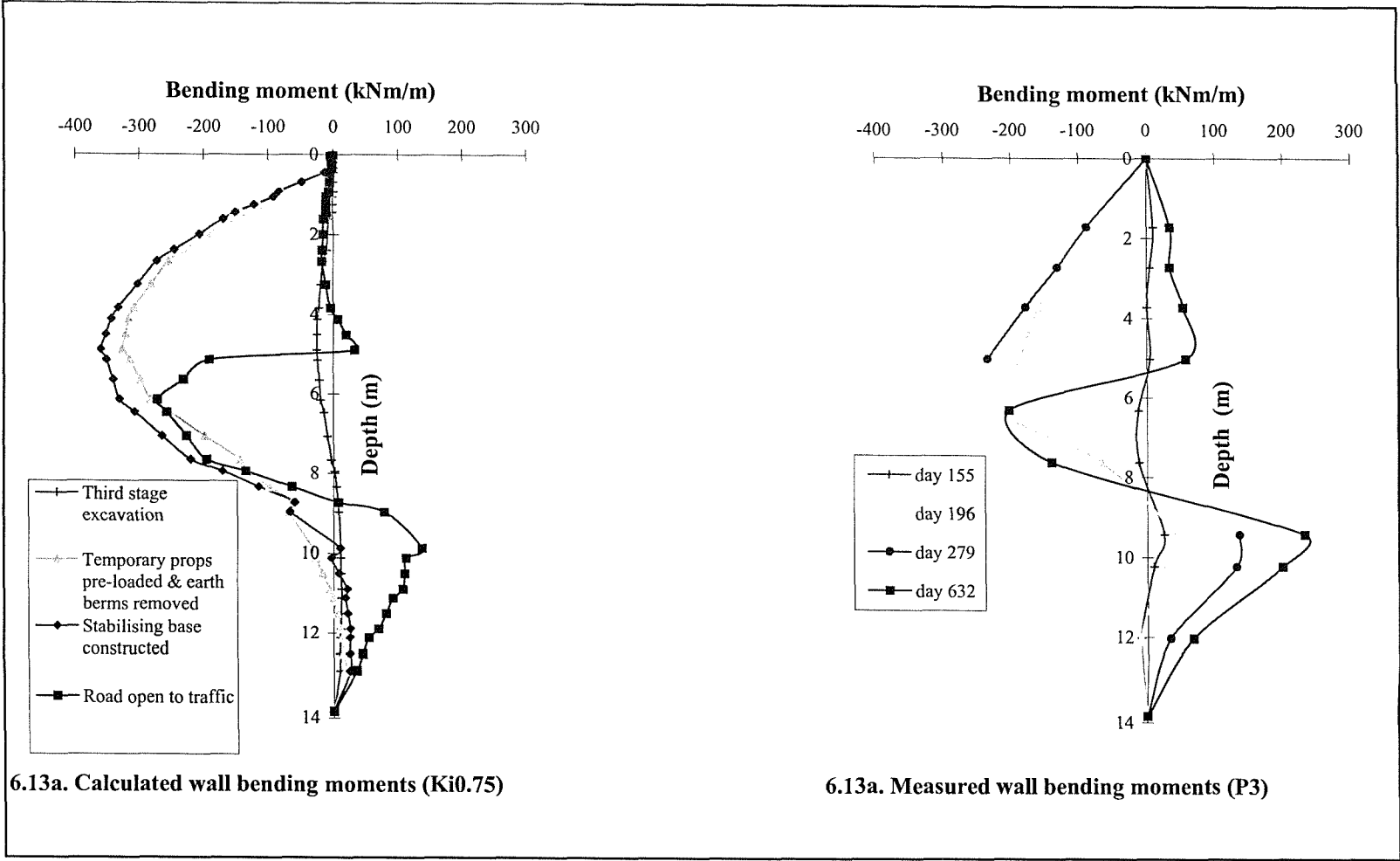
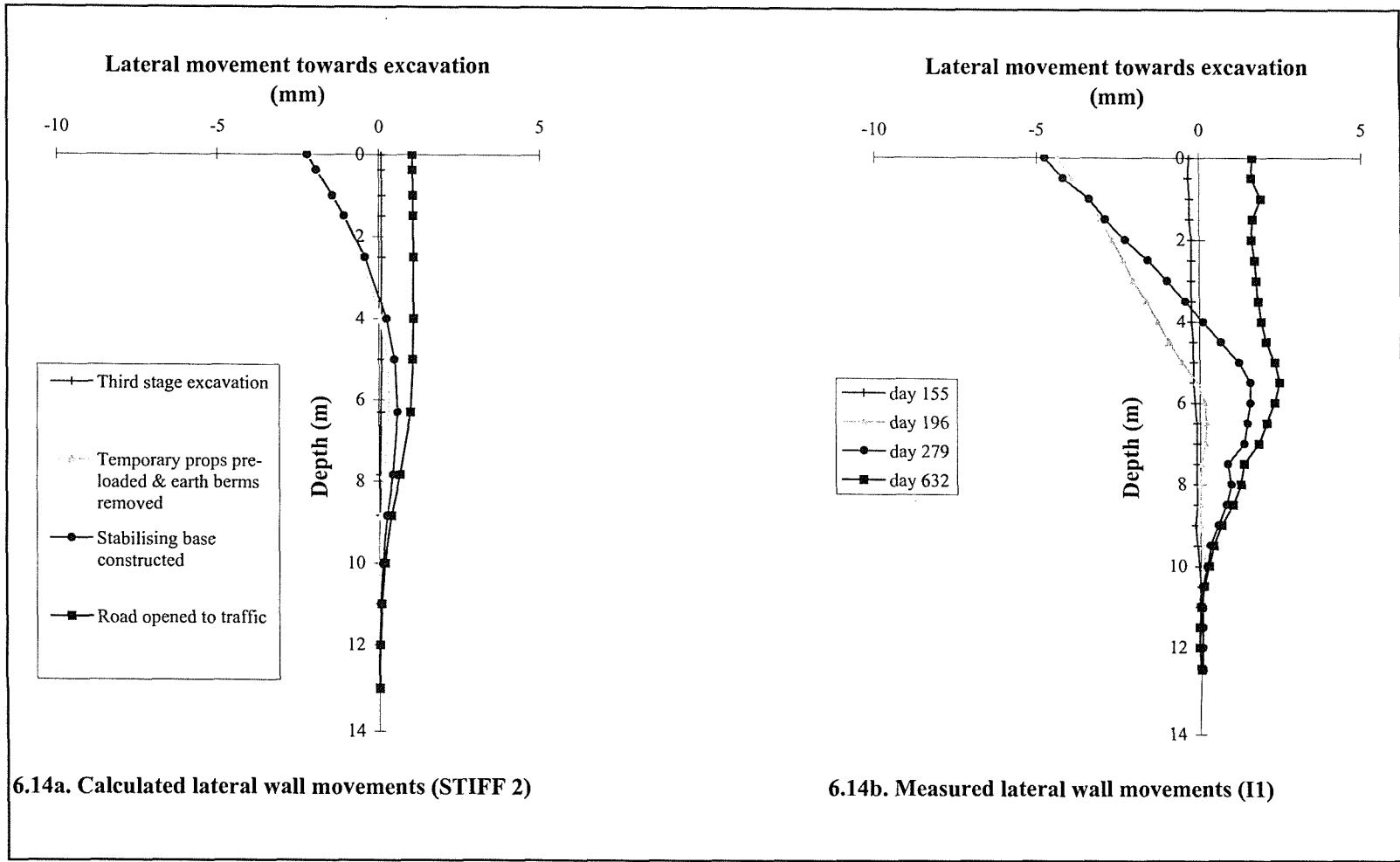


Figure 6.13. Comparison of calculated and measured wall bending moments (Ki0.75)





**Figure 6.14. Comparison of calculated and measured lateral wall movements (STIFF2)**

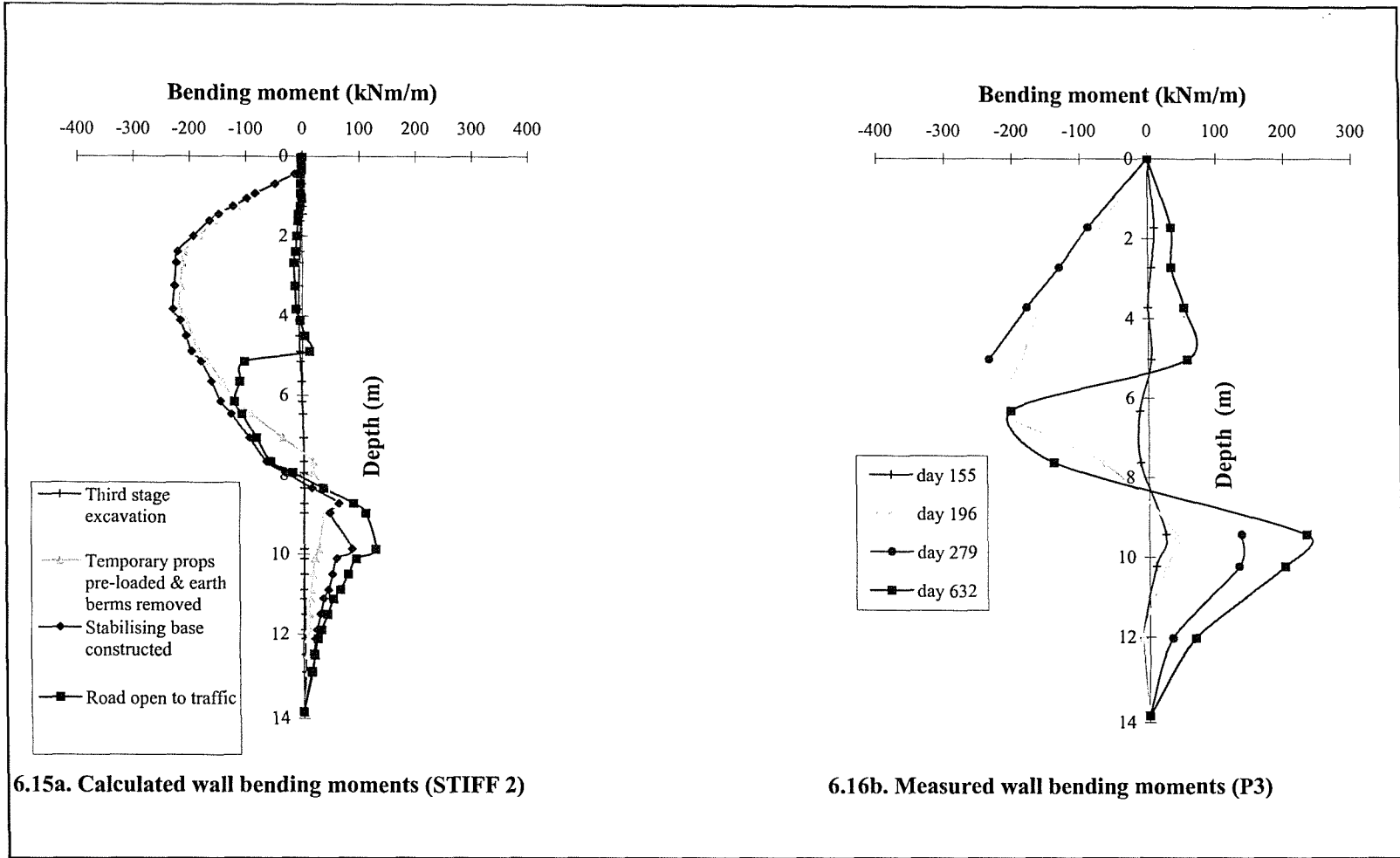


Figure 6.15. Comparison of calculated and measured wall bending moments (STIFF 2)

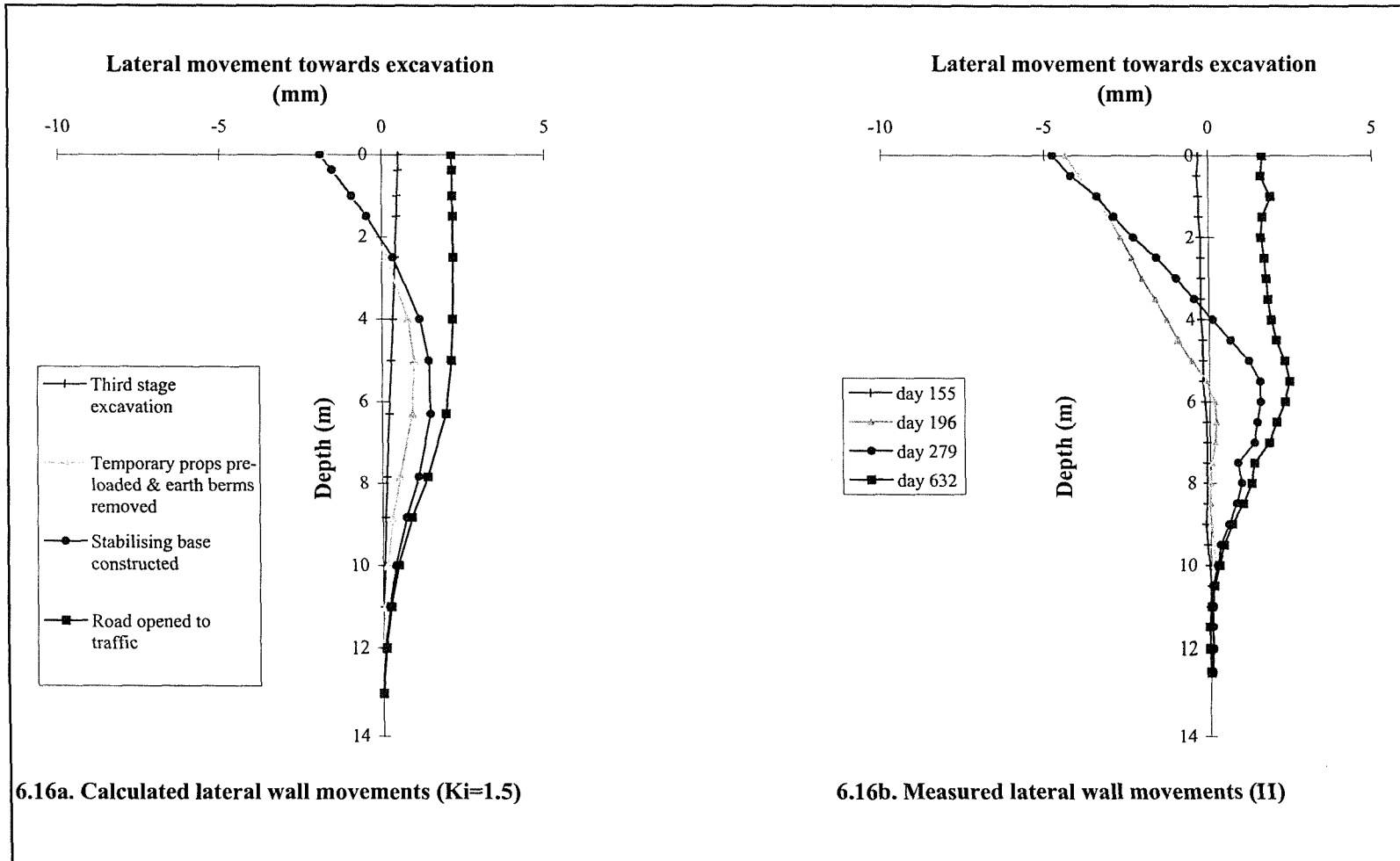
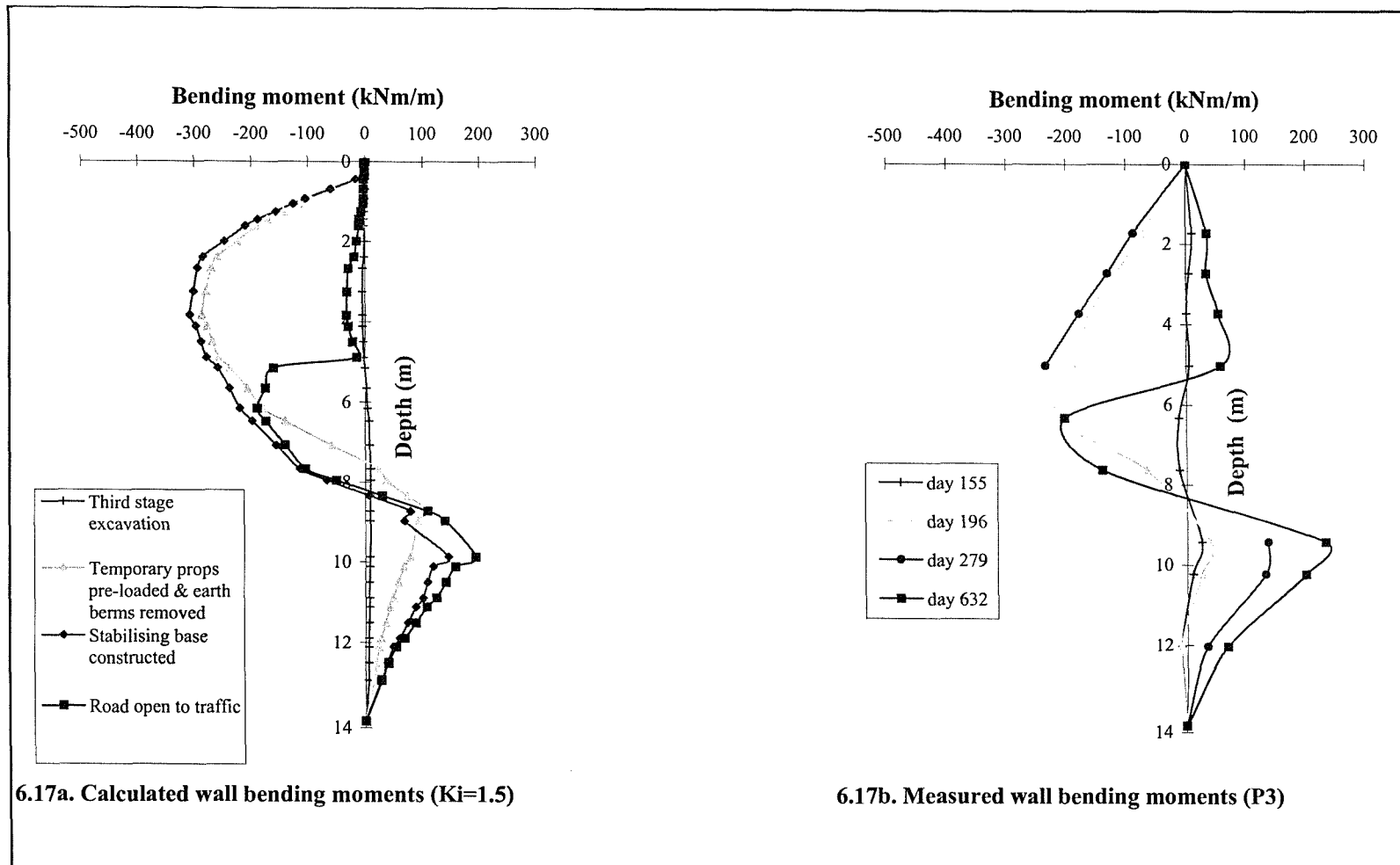


Figure 6.16. Comparison of calculated and measured lateral wall movements (Ki = 1.5)



**Figure 6.17. Comparison of calculated and measured wall bending moments (Ki=1.5)**

## 6.7. Result of analyses

The stiffness profiles and pre-excavation earth pressures,  $K_i$ , were back-calculated for the specified temporary prop pre-load. The parameters back-calculated for the 140kN/m and 180kN/m pre-load are listed in Table 6.7 and 6.8 respectively.

The parameters were determined by running a series of analyses where the stiffness profile and the pre-excavation stress state were varied until a reasonable agreement was obtained between the monitored wall behaviour and the calculated wall behaviour.

	Highly weathered rock	Moderately weathered rock
Stiffness parameters	$E = 37.2 \text{ MPa} + 24 \text{ MPa/m}$	$E = 285 \text{ MPa} + 15 \text{ MPa/m}$
Pre-excavation earth pressure	$K_i = 0.92$	$K_i = 0.92$

**Table 6.7. Parameters back calculated using a 140kN/m prop pre-load**

	Highly weathered rock	Moderately weathered rock
Stiffness parameters	$E = 50 \text{ MPa} + 31 \text{ MPa/m}$	$E = 310 \text{ MPa} + 15 \text{ MPa/m}$
Pre-excavation earth pressure	$K_i = 0.95$	$K_i = 0.95$

**Table 6.8. Parameters back calculated using a 180kN/m prop pre-load**

Figure 6.17 compares the calculated and measured lateral wall movements determined using the values in Table 6.7 and a temporary prop pre-load of 140kN/m. The wall movements that occurred during stage one excavation, (which were less than 0.5mm) are not included in Figure 6.18 (wall movements

were not measured during this stage, see Chapter 3). It can be seen from Figure 6.18 that calculated wall movements are slightly different to the measured wall movements, but they are within the tolerance of the field measurements ( $\pm 1$ mm, see Chapter 3).

Figure 6.19 compares the corresponding bending moments. Again, there are variations between the calculated and measured bending moments profiles, particularly after the props have been pre-loaded. However, there is a fair agreement between the calculated maximum values.

Figure 6.20 compares the calculated and measured stabilising toe bending moments, and Figure 6.21 compares the calculated and measured vertical stresses below the stabilising toe.

It can be seen from Figures 6.18 to 6.21 that it was not possible to obtain an exact agreement for all four monitored areas of wall behaviour, but the results of the analysis are considered to be a reasonable match, if the accuracy of the wall measurements are taken into consideration.

Similar comparisons are shown in Figures 6.22 to 6.25 for the analysis using the parameters listed in Table 6.8, with a temporary prop pre-load of 180kN/m.

Figure 6.26 shows the calculated shear strains determined using the values in Table 6.7 and a temporary prop pre-load of 140kN/m.

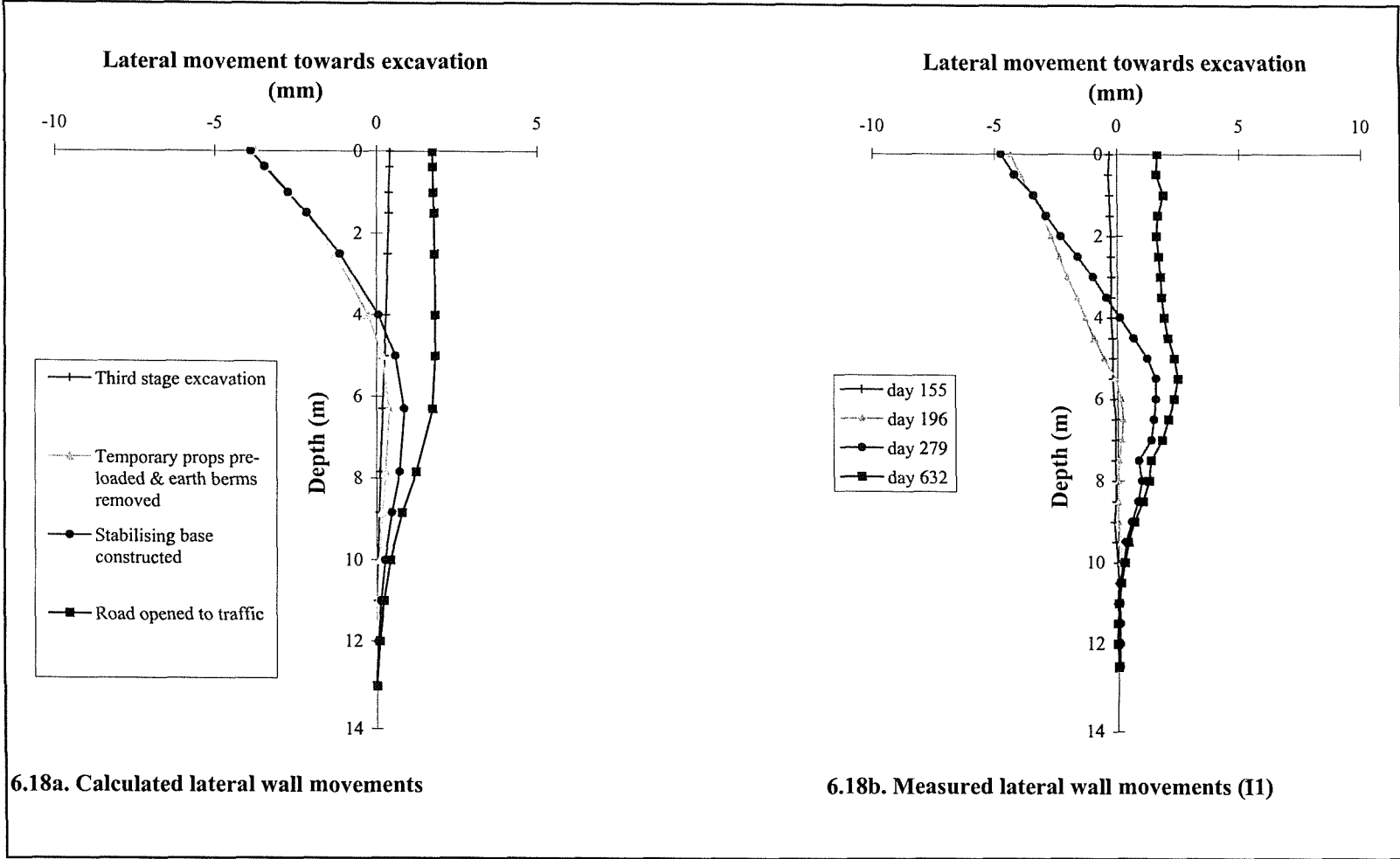
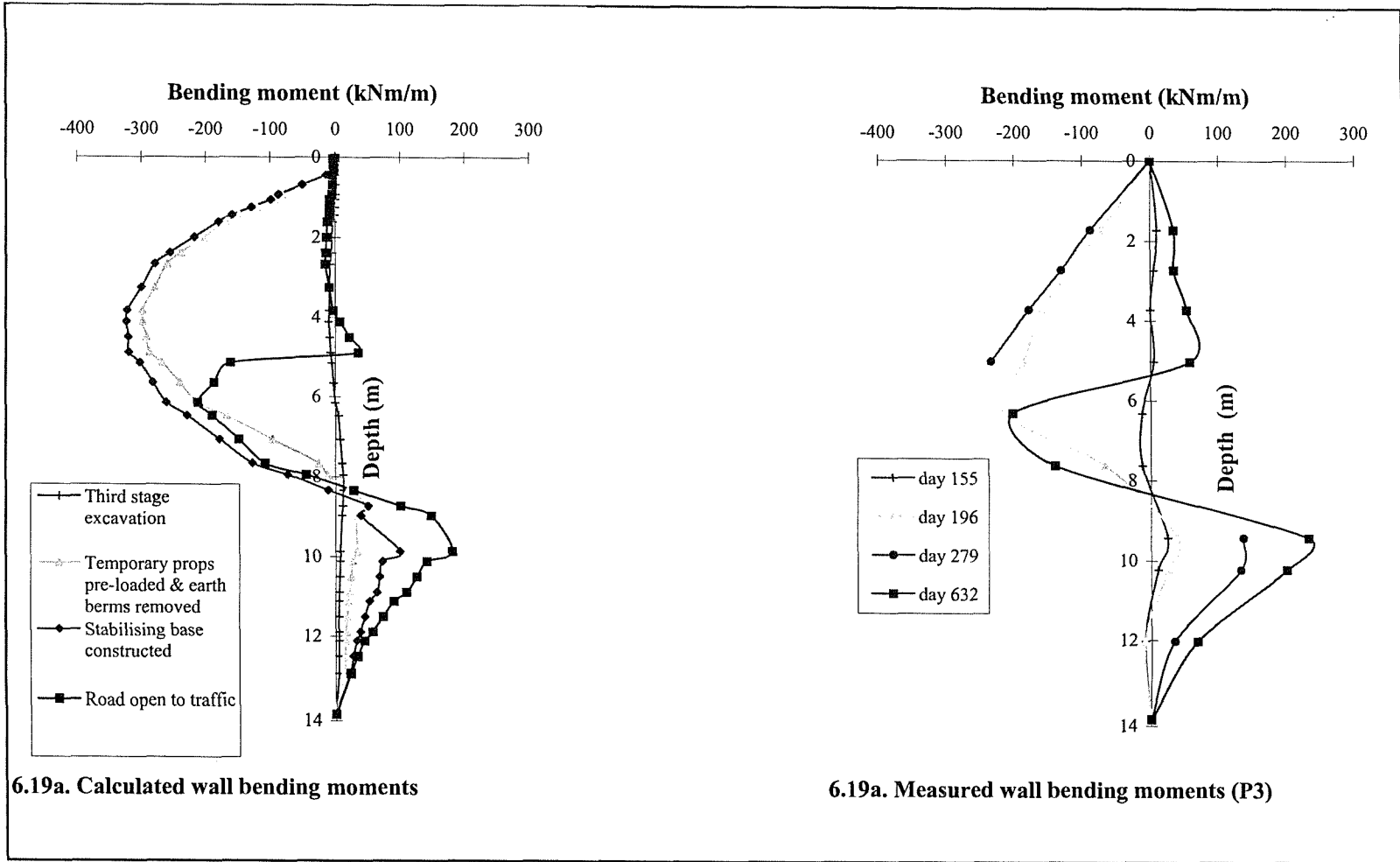


Figure 6.18. Comparison of calculated and measured lateral wall movements (prop load = 140 kN/m)



**Figure 6.19. Comparison of calculated and measured wall bending moments (prop load = 140 kN/m)**



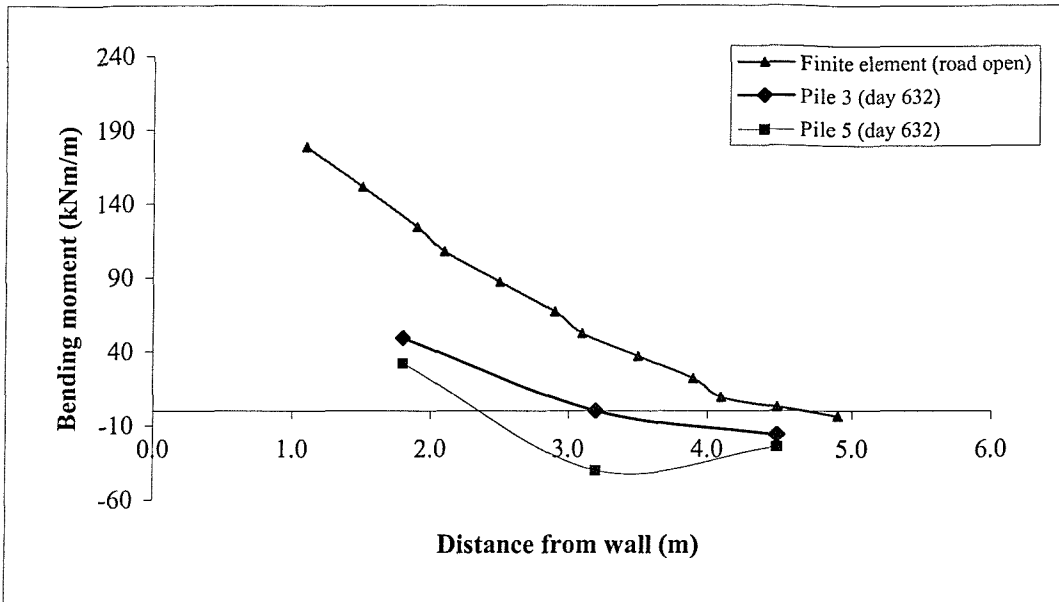


Figure 6.20. Comparison of calculated and measured toe bending moments (prop load = 140 kN/m)

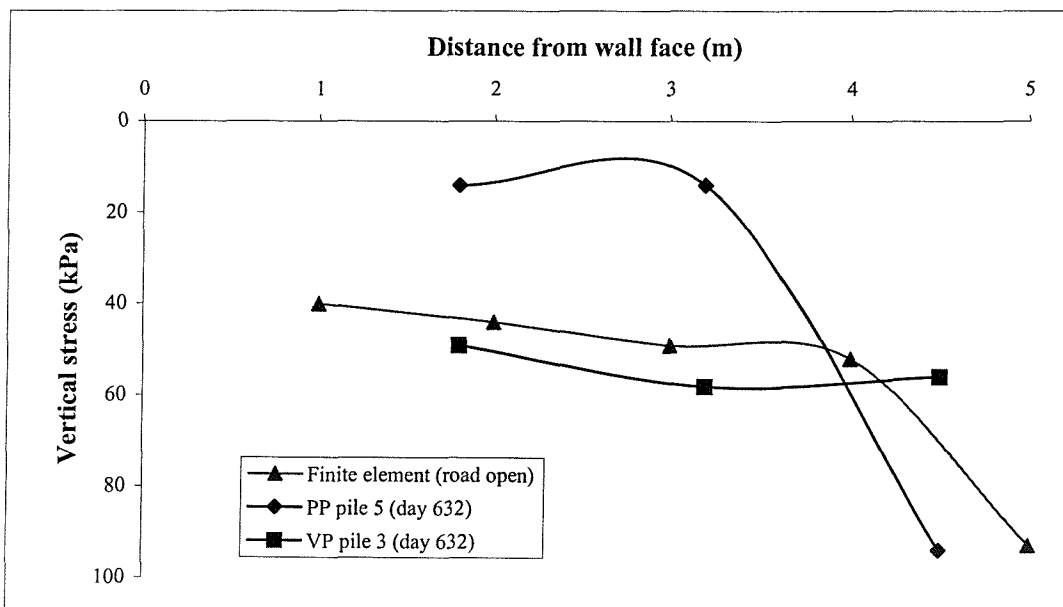


Figure 6.21. Comparison of calculated and measured vertical contact stresses (prop load = 140 kN/m)

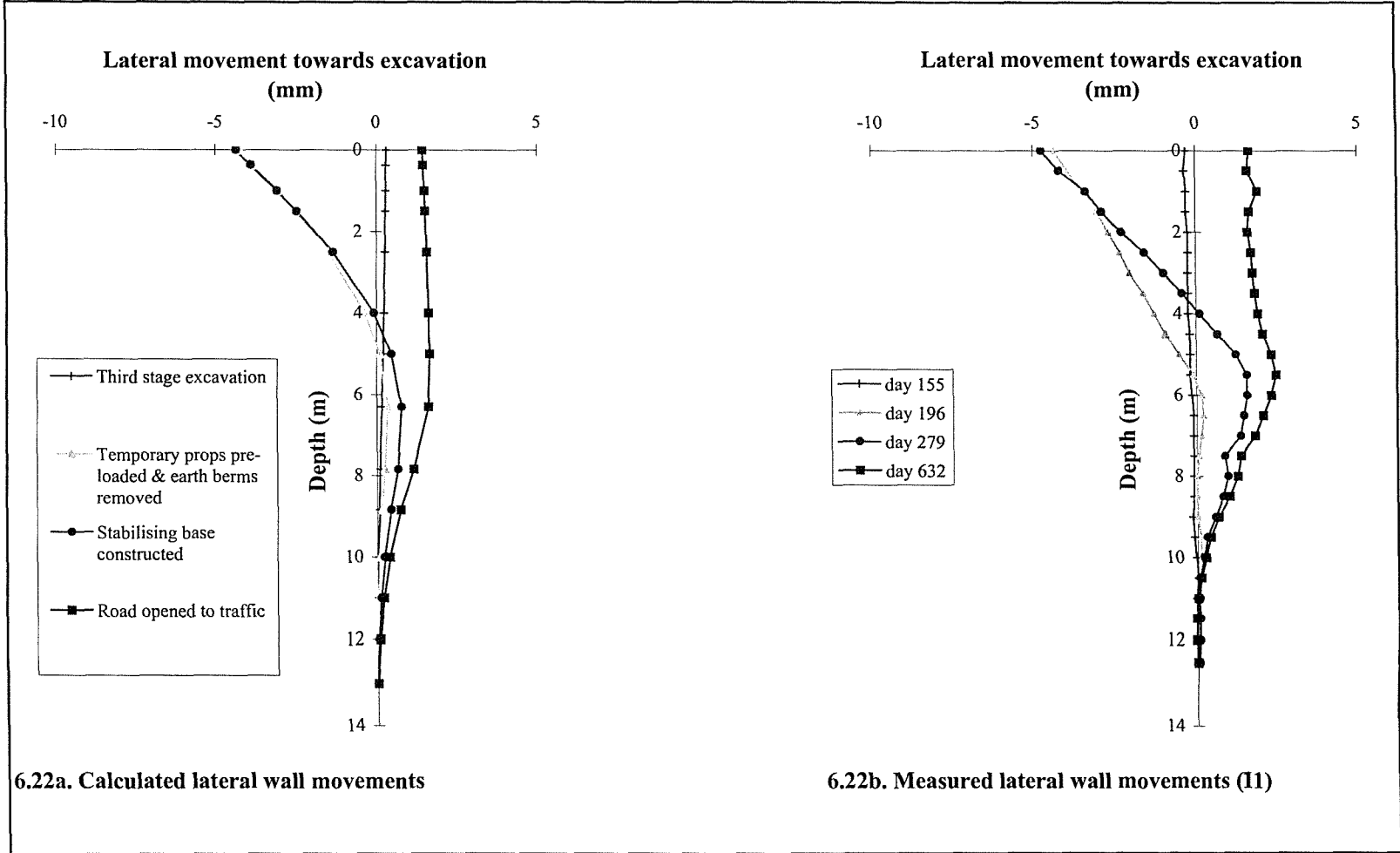


Figure 6.22. Comparison of calculated and measured lateral wall movements (prop load = 180 kN/m)

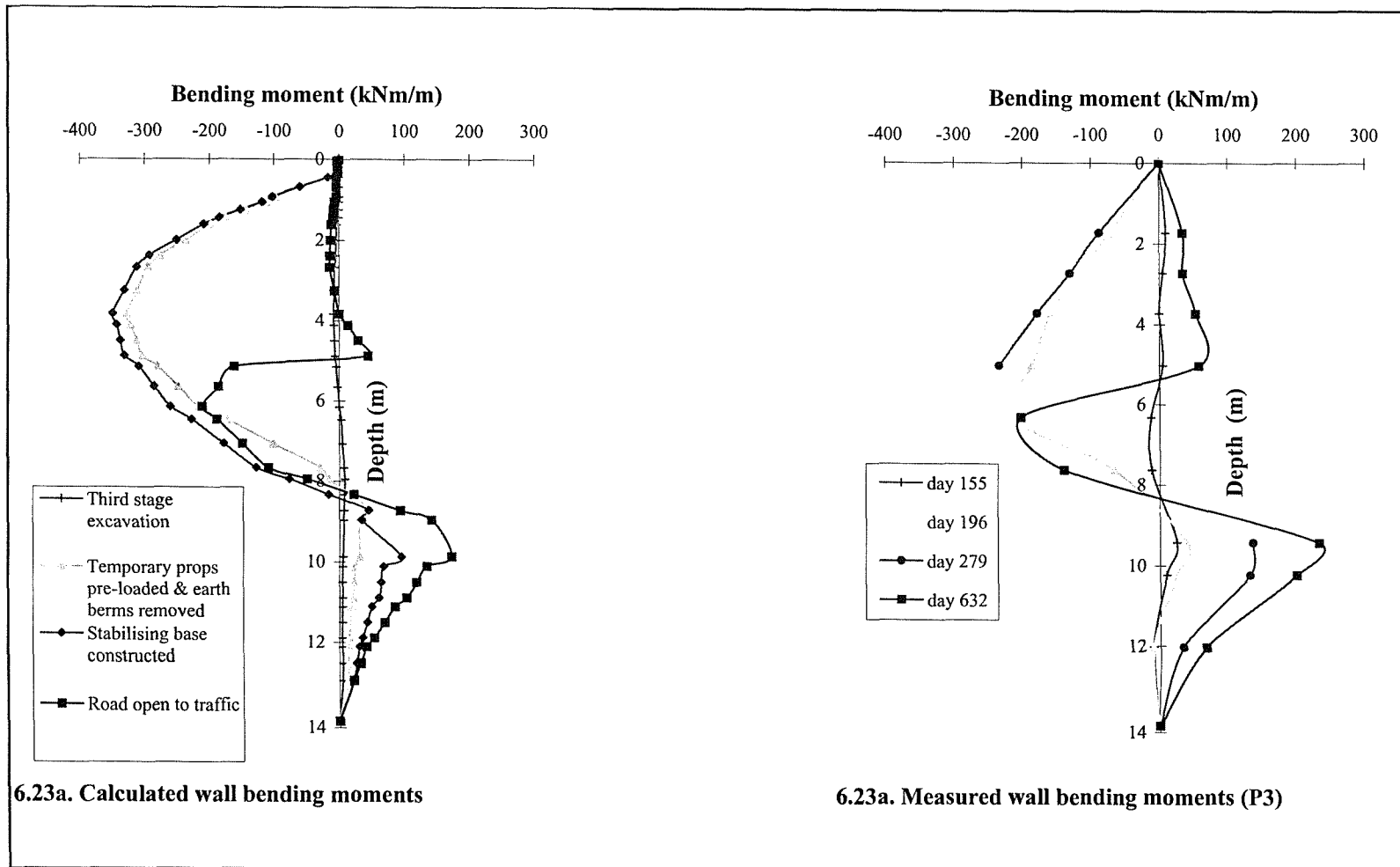


Figure 6.23. Comparison of calculated and measured wall bending moments (prop load = 180 kN/m)

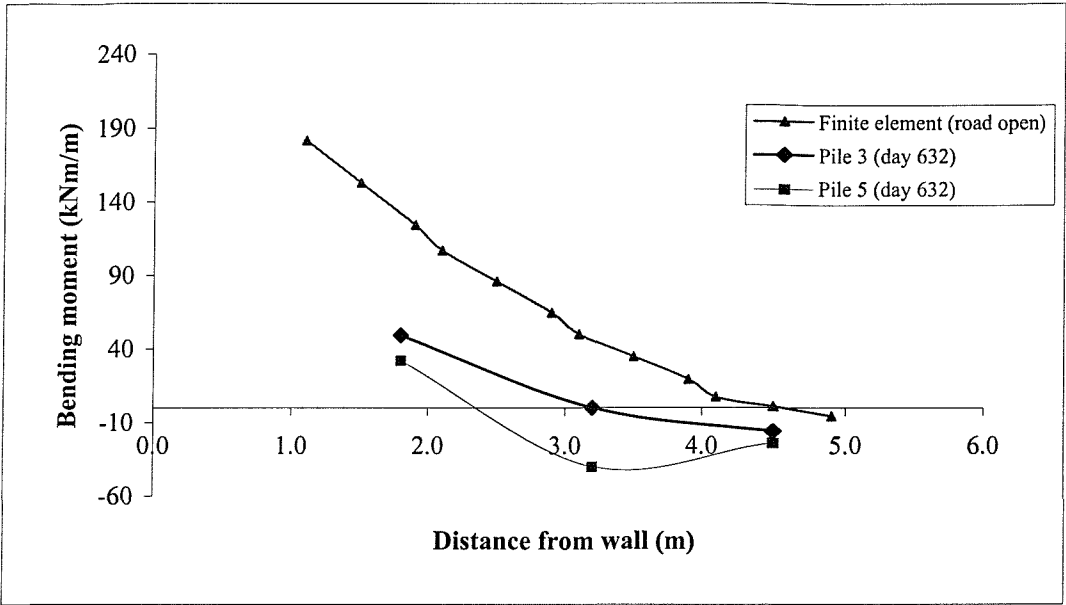


Figure 6.24. Comparison of calculated and measured toe bending moments (prop load = 180 kN/m)

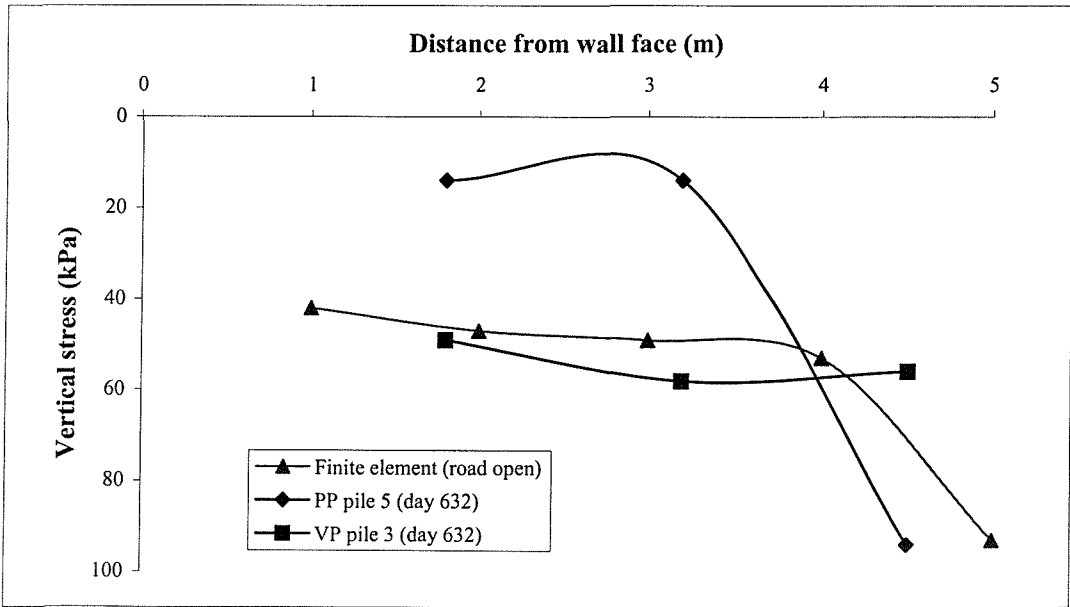
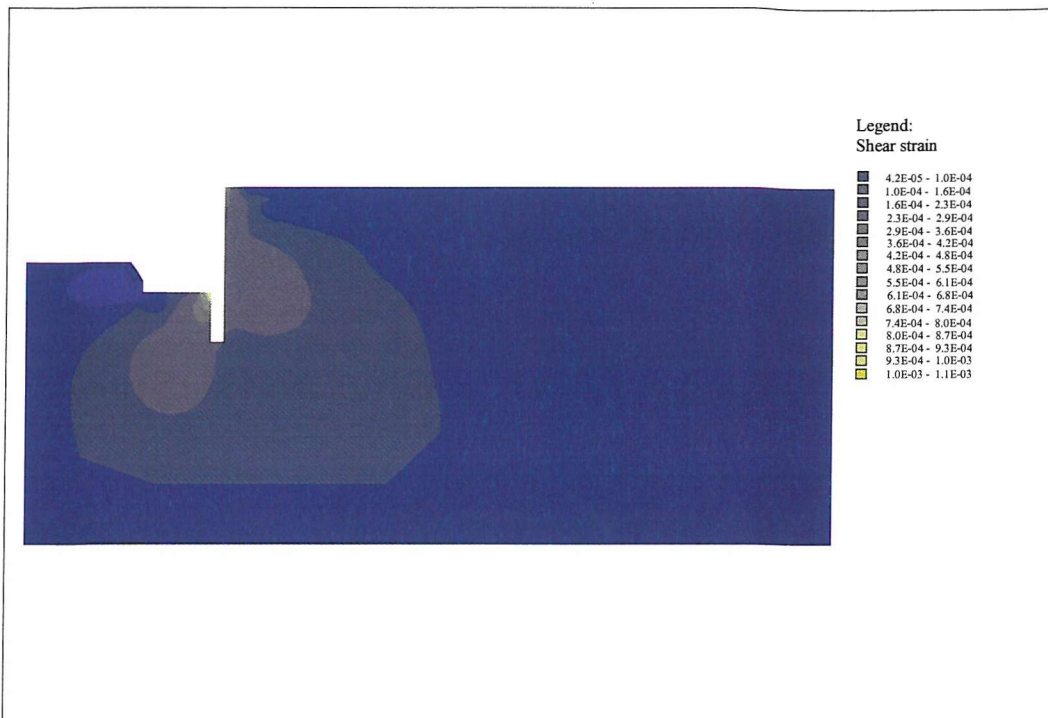


Figure 6.25. Comparison of calculated and measured vertical contact stresses (prop load = 180 kN/m)



**Figure 6.26. Shear strains around retaining wall (prop load = 140kN/m)**

## 6.8. Construction sequence

To investigate the influence of pre-loading the temporary prop on retaining wall behaviour, an analysis identical to the back-analysis using a pre-load of 140kN/m, was carried out, except that the temporary prop was not pre-loaded.

Figure 6.27 compares the calculated lateral wall movements for a retaining wall that was not pre-loaded, with those for a retaining wall that was pre-loaded. It can be seen that pre-loading the temporary prop reduces the movements of the wall into the excavation. However, pre-loading the prop causes wall movements away from the excavation and heave behind the wall that may be less desirable.

Figure 6.28 show the corresponding bending moments for the two analyses. The bending moments from the analysis where the prop was pre-loaded are much greater. This is also the case for the bending moments in the toe Figure 6.29. Therefore, the bending moments are more critical when the pile is pre-loaded.

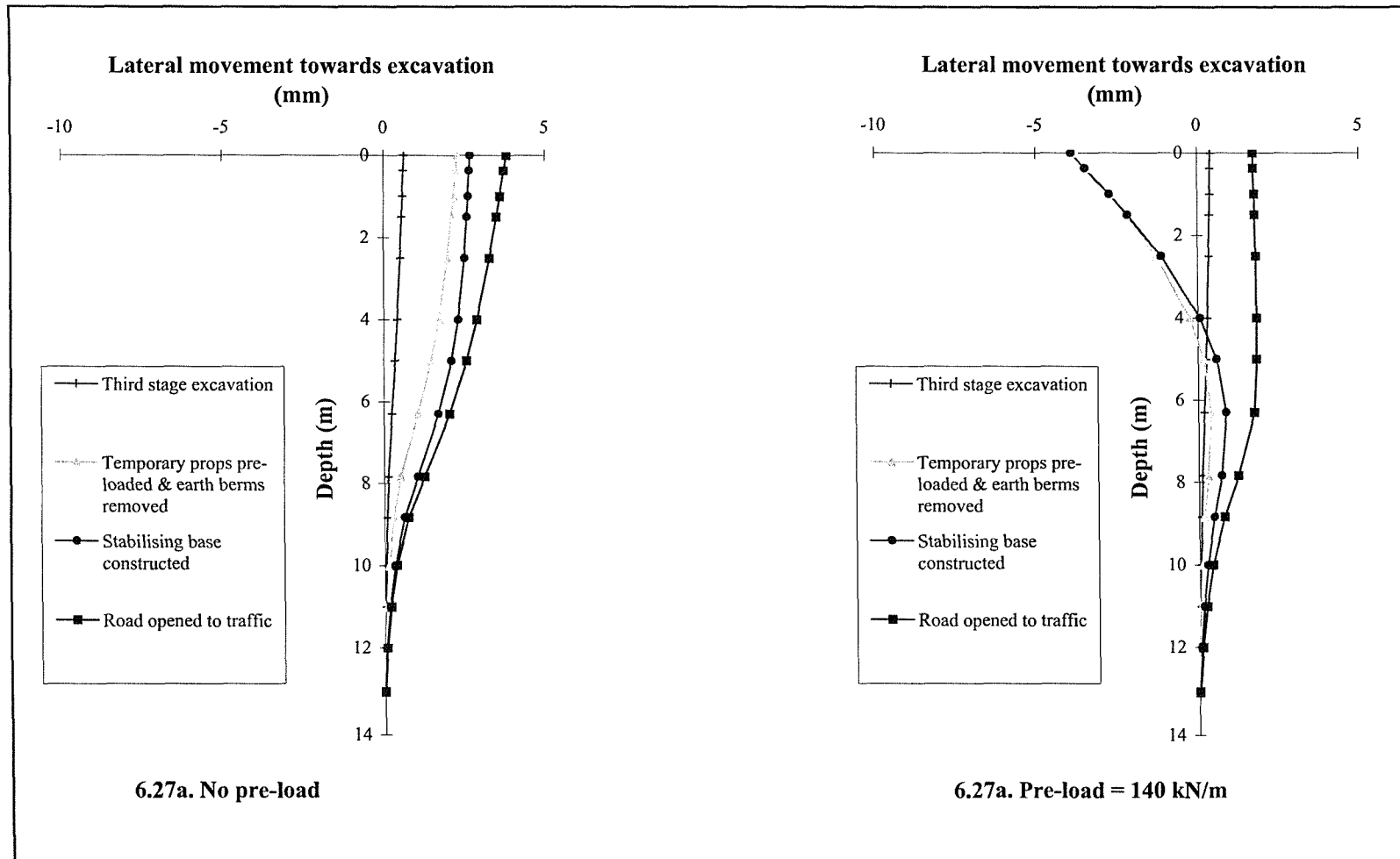


Figure 6.27. Comparison of calculated lateral wall movements

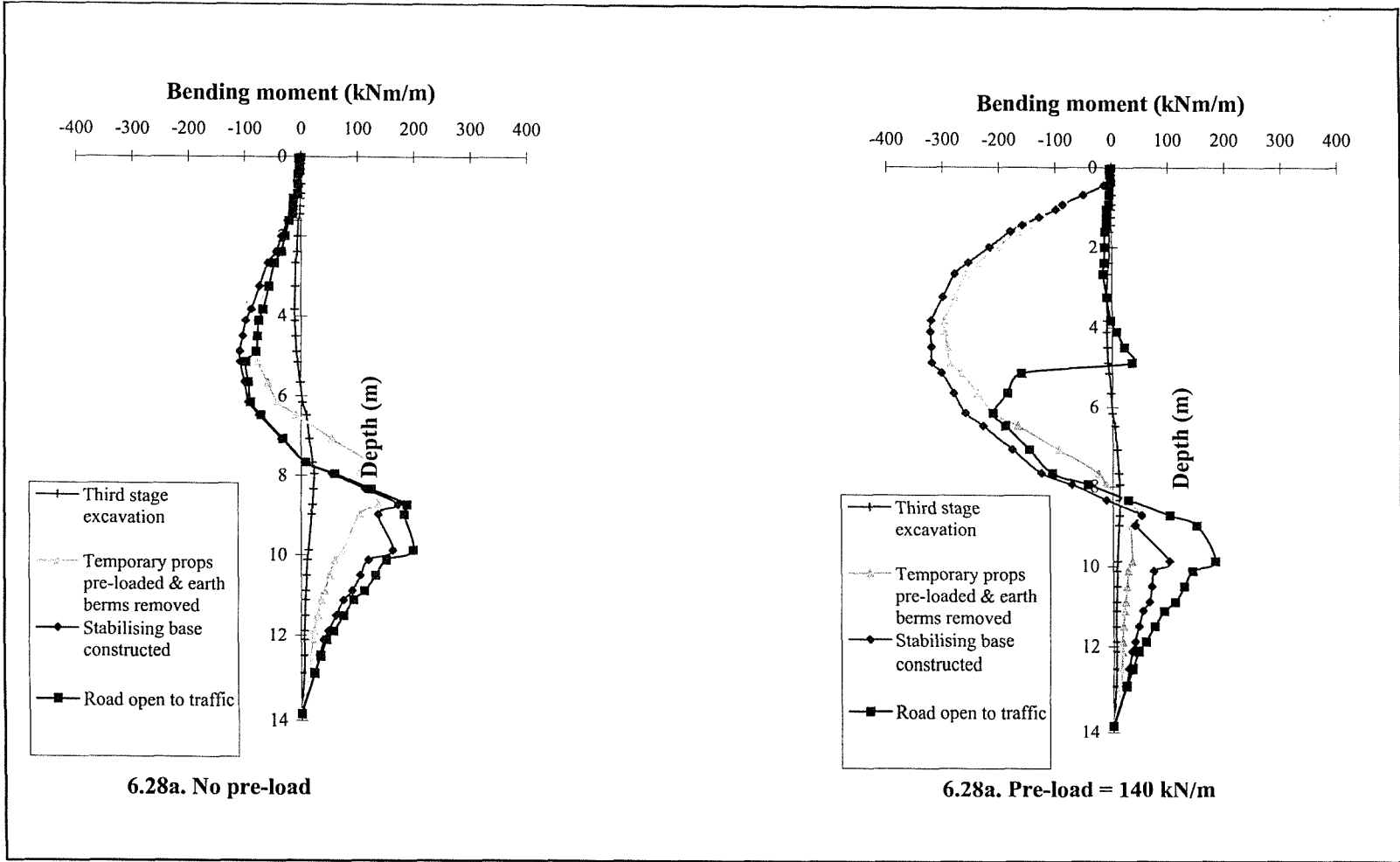


Figure 6.28. Comparison of calculated wall bending moments

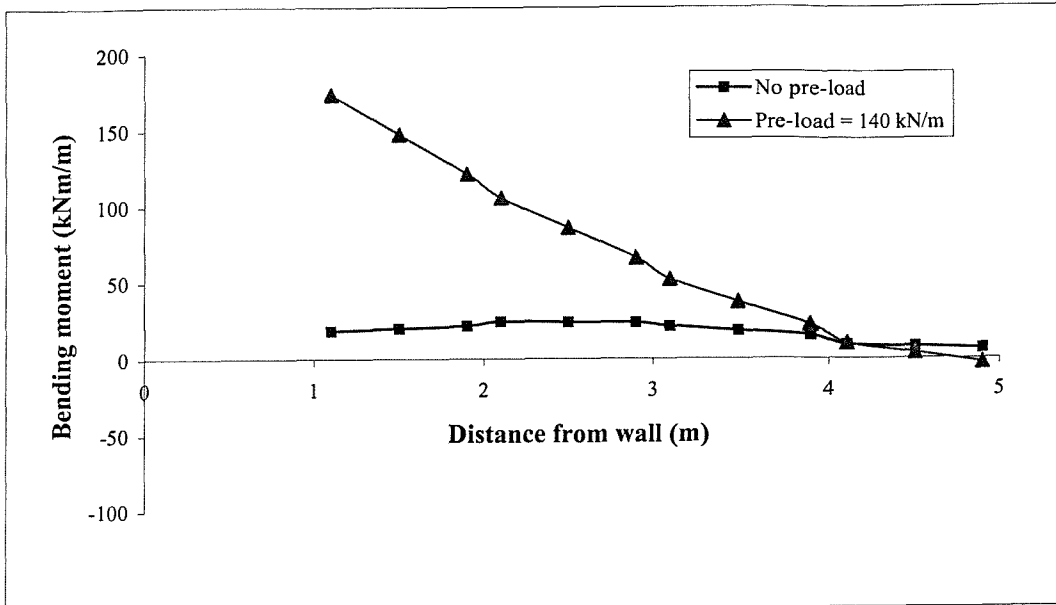


Figure 6.29. Comparison of calculated toe bending moments

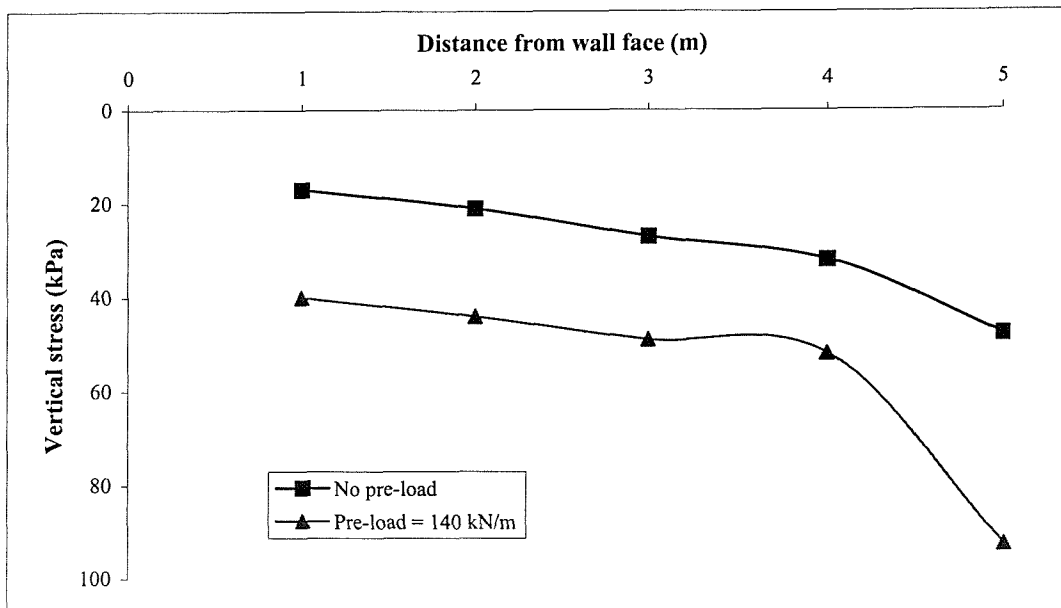


Figure 6.30. Comparison of calculated vertical contact stresses



The vertical contact stresses at the underside of the stabilising toe are also greater, with the difference between the magnitude of the vertical stresses being mainly due to the amount of pre-load (i.e if you work out the difference per metre run, it approximates to the amount of pre-load), Figure 6.30.

A further set of analyses were performed where the temporary prop pre-load was increased to 240 and 340 kN/m and these are compared to the back-analysis using a pre-load of 140kN/m. Figure 6.31 shows the influence that the pre-loading has on the horizontal stresses behind the retained wall. The figure clearly indicates that the horizontal stresses developed behind the retaining wall are dependent on the amount of pre-load. Consequently, the vertical contact stresses under the stabilising base increase with increasing temporary prop pre-load, Figure 6.32, along with bending moments developed in the toe, (Figure 6.33).

The wall movements into the excavation are slightly reduced by the increasing the temporary prop loads, Figure 6.34b. However, the wall movements away from the excavation are significantly increased, Figure 6.34a.

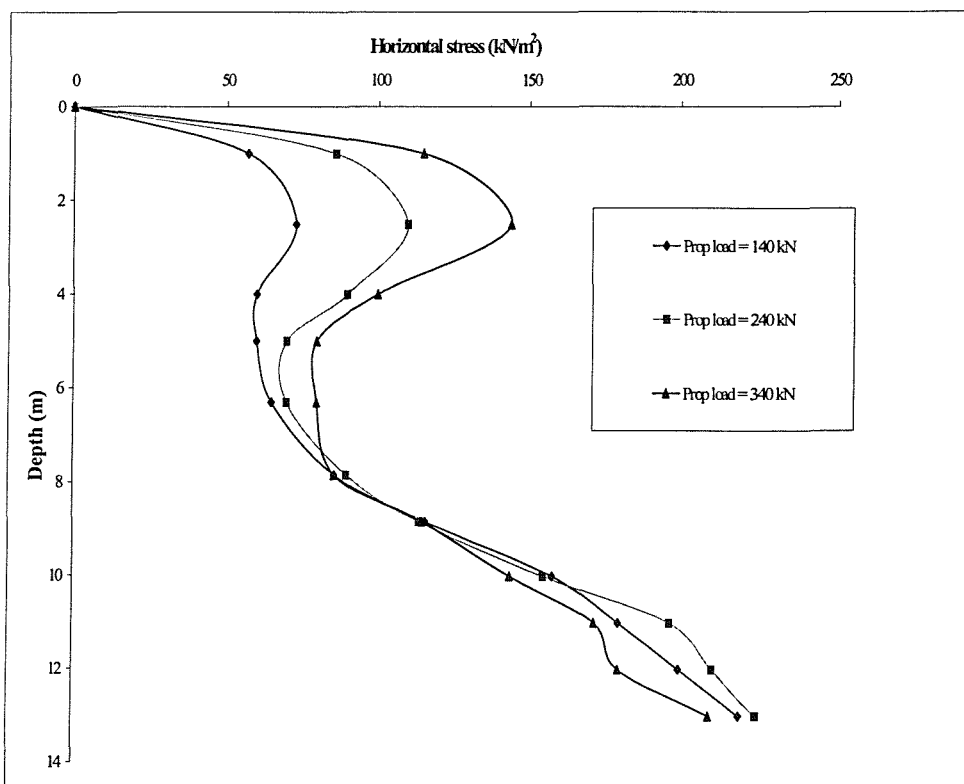


Figure 6.31. Comparison of horizontal stresses

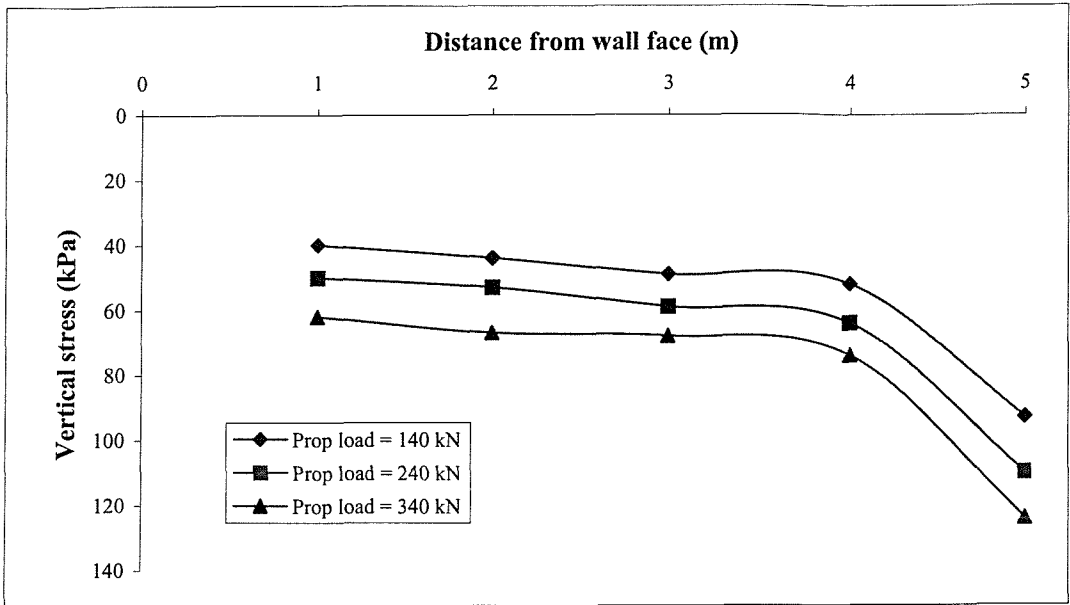


Figure 6.32. Comparison of calculated vertical contact stresses

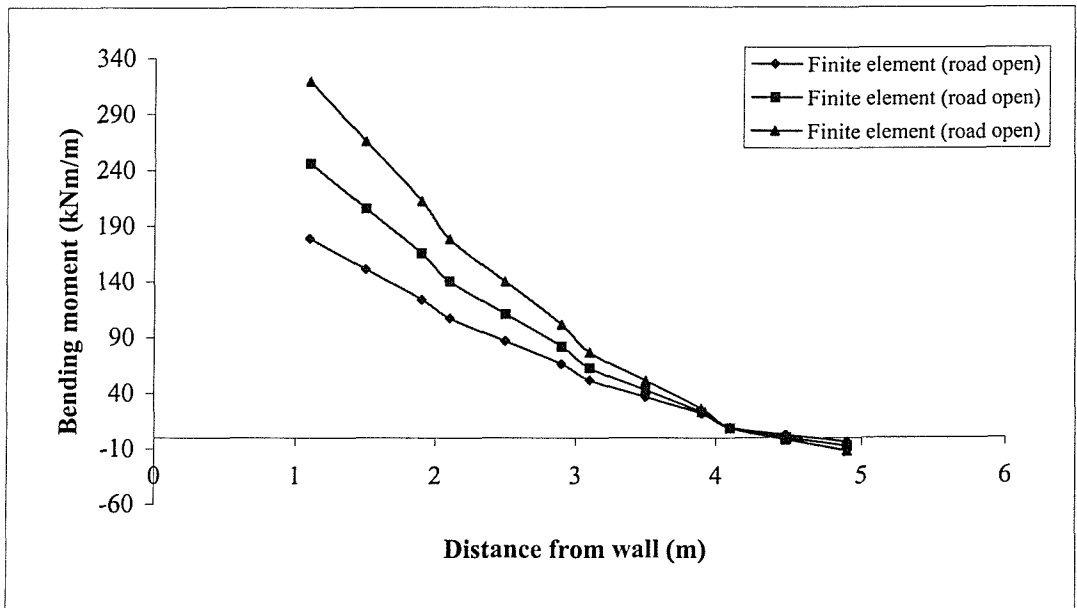
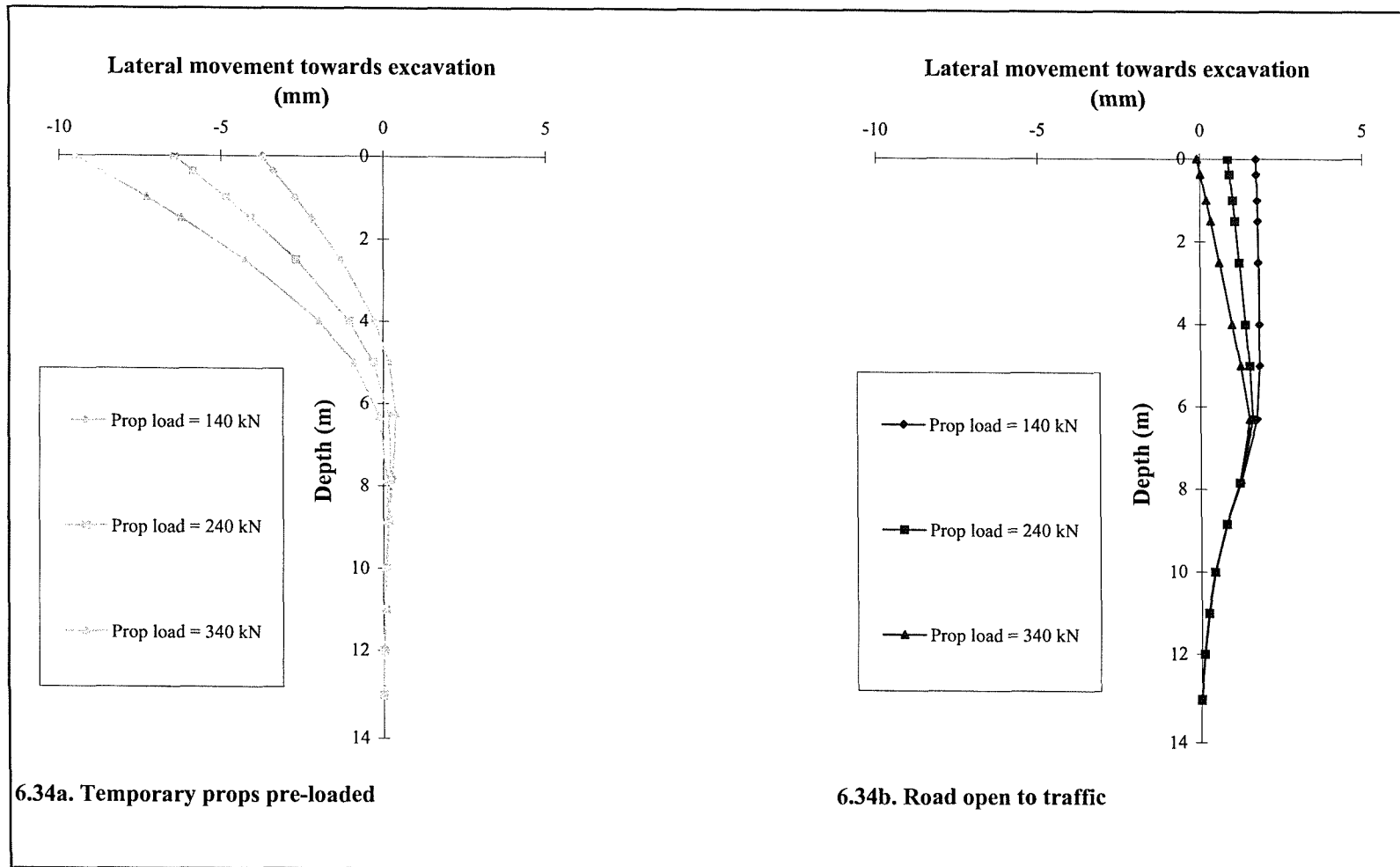


Figure 6.33. Comparison of calculated toe bending moments



**Figure 6.34. Comparison of calculated lateral wall movements**

## 6.9. Comparison of measured and back calculated stiffness

It is the discontinuities that reduce the mass stiffness of the weak rock at the case study. Discontinuity patterns in a weak rock often make the rock mass anisotropic. Such anisotropy is likely to give rise to mass modulus anisotropy with  $G_v < G_h$ . As the frequency of the horizontal joints is greater than the vertical joints at the case study, this might be significant. The only parameters that represented the mass modulus at the case study were the shear stiffness values determined from the geophysical tests. Because the shear stress applied to the ground from the geophysics tests is in the right direction to adequately simulate that applied by the retaining wall, the result from the back analysis should therefore be directly comparable.

Seismic tests apply very small strains ( $10^{-6}$  and  $10^{-4}$ ) to the materials in which they are used Auld (1997). Because of this, it has generally been considered that they give results relevant only to the linear elastic phase of the geomaterial deformation. The linear-elastic idealisation of geomaterials behaviour is attractive because of its conceptual simplicity. However, it is widely recognised that some yielding occurs inside the state boundary surface of a geomaterial (see Lerouiel and Vaughan 1990). This leads to non-linear stress-strain behaviour of geomaterials at intermediate strain levels. The limit of linear behaviour of intact weak rocks has been shown to be between  $1 \times 10^{-4}$  to  $4 \times 10^{-4}$  (Matthews 1990, Kim *et al.* 1990 and Cuccovillo and Coop 1997).

Jardine *et al.* (1986) carried out finite element analyses to examine the levels of strain around a range of construction types in a material with stiffness similar to that of a stiff clay. They found that typical shear strain levels are less than about  $1 \times 10^{-3}$ . In cases when excavations are well restrained, or in stiffer ground, typical strain levels could be even less. This is true for the case study, as the typical strain levels around the retaining wall are between  $2 \times 10^{-4}$  and  $6 \times 10^{-4}$  (see Figure 6.26). These values are very close to the threshold limit of the linear elastic behaviour of intact weak rocks. This implies that the stiffness at operational strain

levels might be only slightly lower than those derived from seismic velocity measurements.

Figure 6.35 compares the back calculated stiffness profiles for the respective prop loads with those measured from the geophysical testing. The figure shows that the stiffness profile determined from the geophysical testing is stiffer than the profiles determined from the back analyses. The stiffness derived from the geophysics is based on fundamental elastic theory and hence should be reasonably accurate for the strain levels involved (assuming the rock mass behaves as a linear elastic material). As the stiffness profile represents the mass stiffness and incorporates the effects of discontinuities on the overall behaviour of the material, it was anticipated that this profile would be similar to the one back calculated. However, there is a clear difference between the two. The question is why is there a difference between the two?

Provided the stress-strain behaviour of the weak rock mass is linear there is no reason why wall movements predicted using the geophysical profile should not show good agreement with the observed wall movements. This might suggest that the stress-strain behaviour is non-linear and therefore the back calculated stiffness is strain level dependent.

Matthews and Clayton (2000) suggest that it is entirely reasonable to estimate the operational stiffness from field geophysical results by using a reduction factor to take account of any expected strain level dependency. They suggest a factor of 0.85 for weak rocks, which they imply, is perhaps on the conservative side. However, a reduction factor of between 0.6 would be needed for the case study. This would tend to suggest that any reduction in stiffness due to non-linear behaviour of the weak rock mass is not the major factor here.

Previous work has shown that the presence of a natural discontinuity in a laboratory specimen of hard rock, perpendicular to the direction of applied load, also results in a modification to the stress-strain behaviour when compared with that of the intact rock, Figure 6.5 (Bandis *et al.* 1983). Figure 6.5 exhibit a non-linear stress-deformation curve, which indicates an increase in stiffness with

linear stress-deformation curve, which indicates an increase in stiffness with increasing load at intermediate strains. It can be seen that at intermediate strains the stiffness is strain dependent, but stiffness increases with strain. This also does not answer the above question, because it would suggest that the back calculated stiffness values should be higher than those determined from the geophysical tests.

The next possibility is that the intact weak rock in the weak rock mass was de-structured during loading and the stiffness of the weak rock mass was similar to that of a soil. Yet, this assumption would be incorrect, because it assumes that the load applied to the weak rock mass was high enough to de-structure the intact weak rock. This is most unlikely, as the applied load was much less than the unconfined compressive strength of the intact rock.

Another possible reason for the difference between the values could be due to stress relief during the construction of the retaining wall. The excavation of the bored piles is certain to have resulted in significant total stress relief, because during formation, the hole excavated was left unsupported. The total horizontal stress on the boundary of this hole will be reduced from the initial *in situ* horizontal total stress in the undisturbed weak rock to zero. This would probably have allowed the discontinuities to slightly soften, hence the softer response determined from the back analyses. This is the most probable reason for the major difference in the stiffness profiles.

The geophysical tests may in general give a more representative stiffness profile, but in this case it tends to err on the high side because the additional effects of stress relief during wall installation which are not taken into account in the back analysis. These values could therefore be used directly in design for estimating wall movements. However, it should be remembered that linear elasticity constitutes the oldest and simplest approach to modelling the stress-strain behaviour of soils and rocks under low deforming loads. But, for weak rock masses that are subject to high loads, hence large deformation, the stress strain curve is most likely to be non-linear, and any analysis based on linear elasticity may not be completely realistic.

Figure 6.35 and Figure 6.36 compares the back calculated stiffness profiles for the respective prop loads with those measured from the pressuremeter tests. Figure 6.37 shows that the stiffness profile determined from the unload/reload loop is generally stiffer than the profiles determined from the back analyses. This is not that unexpected, as the unload/reload values should represent an intact value. However, the stiffness profile determined from the initial loading stage is very similar to those back calculated Figure 6.36. These values should also represent an intact value. But as discussed in Chapter 4, the reason the shear moduli determined from the initial loading stages of pressuremeter tests are smaller than those determined from the unload/reload loops is a result of disturbance during pressuremeter insertion. Therefore, the close agreement with the back calculated values must be regard as fortuitous.

Also it was shown in Chapter 4, that most of the unload/reload values were also influenced by the initial borehole disturbance. This explains why some of the unload/reload values are also similar to those back calculated.

If unload/reload moduli from good quality pressuremeter tests are to be used in design it is likely that the wall movements will be underestimated, as the shear modulus value is likely to be representative of an intact modulus value. Except if the joint spacing is less than the  $\frac{1}{3}$  of the diameter of the probe and therefore it would represent a mass modulus (see Haberfield and Jonhston 1990).

Figure 6.38 compares the back calculated stiffness profiles for the respective prop loads with those measured from the standard penetration tests. As it was anticipated that the intact rock would dominate the penetration resistance, it was therefore likely that stiffness values obtained from the SPT tests would be stiffer than the back calculated values. However, the values determined from the SPT are much lower. There are several possible reasons for the difference in the values: from disturbance ahead of the bottom of the borehole produced by the drilling method, to the empirical nature of the correlations between N value and E being site specific. As the relationships, (Stroud 1988 and Thompson *et al.* 1988), between N value and E are based on a limited database, the use of the SPT alone

could result in misleading values. Therefore, SPT results should be treated with caution when used for the determination of design parameters for intact weak rock.

Provided the strength of the weak rock does not dominate the mass behaviour, it would appear that a continuum model is suitable for estimating wall movements and bending moments. However, if there is any mass modulus anisotropy, it is unlikely that the assumption that the rock mass behaves as an isotropic material is correct. Therefore, any ground movements predicted from this model are likely to be incorrect.

#### **6.10. Comparison of measured and back calculated *in situ* earth stresses**

The back calculated *in situ* earth pressure coefficient was approximately 1.0. The horizontal earth pressures measured in the case study (see chapter 4, Figure 4.7) indicated that the effective *in situ* earth pressure coefficient ( $K_o$ ) was between 0.8 and 2. However, these were determined from pressuremeter tests that had been influenced by borehole disturbance, so that the validity of these measurements is questionable. Also, in the finite element analyses used in this chapter, the wall was cast in-place. It is recognised, (e.g Powrie, 1986 and Tedd *et al.* 1984), that stress relief during the installation of a bored pile wall will alter the stress state of the soil, resulting in a different initial or pre-excavation lateral earth pressure coefficient, ( $K_i$ ). The magnitude of these stress changes will depend on the installation sequence and the method used to support the adjacent ground prior to pouring the concrete. During construction of the bored piles forming the instrumented wall section the ground was supported by temporary casing to the base of the made ground, below which the hole was unsupported. The excavation of the bored piles is certain to have resulted in significant total stress relief, because during formation, the hole excavated was left unsupported. The total horizontal stress on the boundary of this hole will be reduced from the initial *in situ* horizontal total stress in the undisturbed weak rock to zero. In soils the total stress acting on the soil is often taken as the pressure applied by wet concrete.



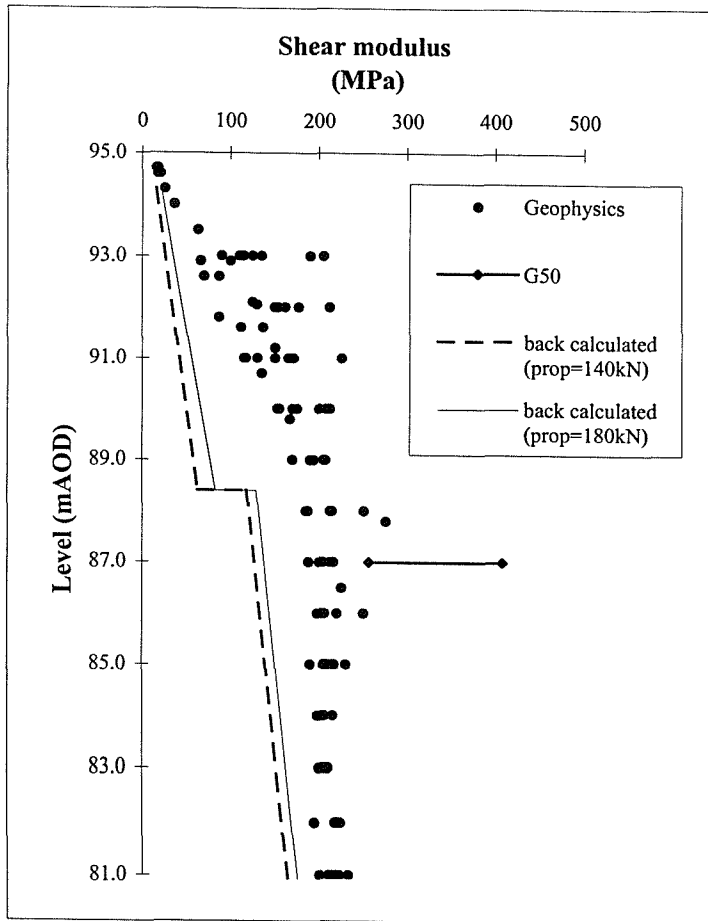


Figure 6.35. Comparison of back calculated and geophysical stiffness values

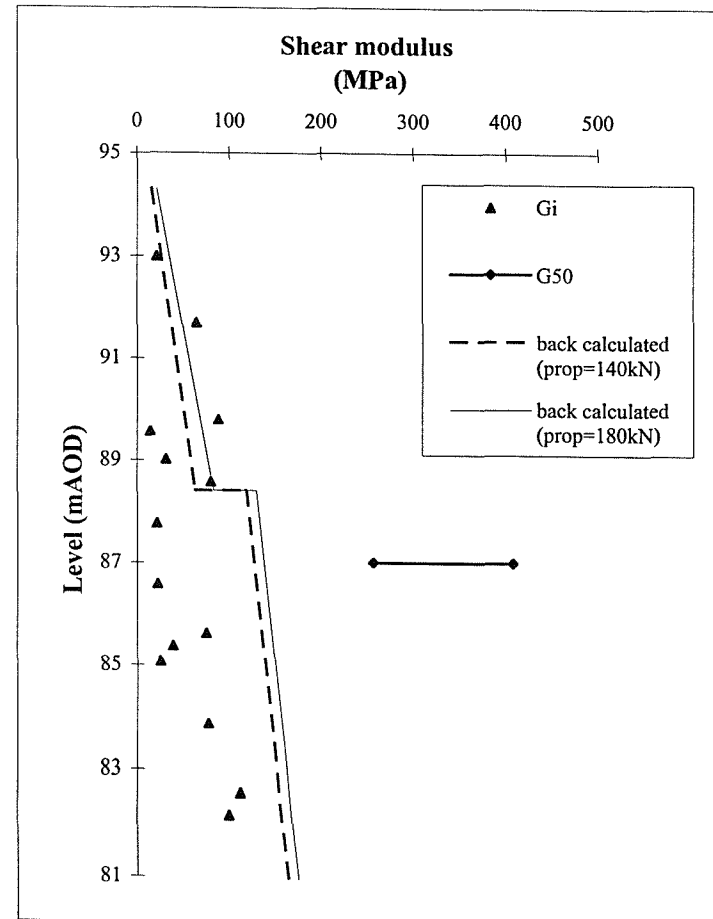


Figure 6.36. Comparison of back calculated and initial pressuremeter stiffness values

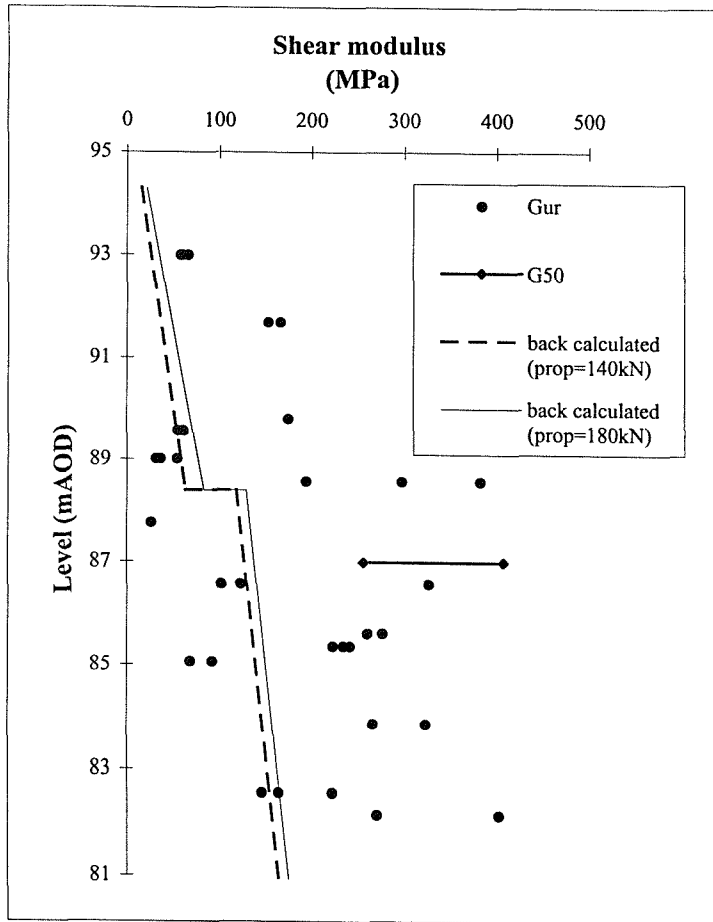


Figure 6.37. Comparison of back calculated and unload/reload pressuremeter stiffness values

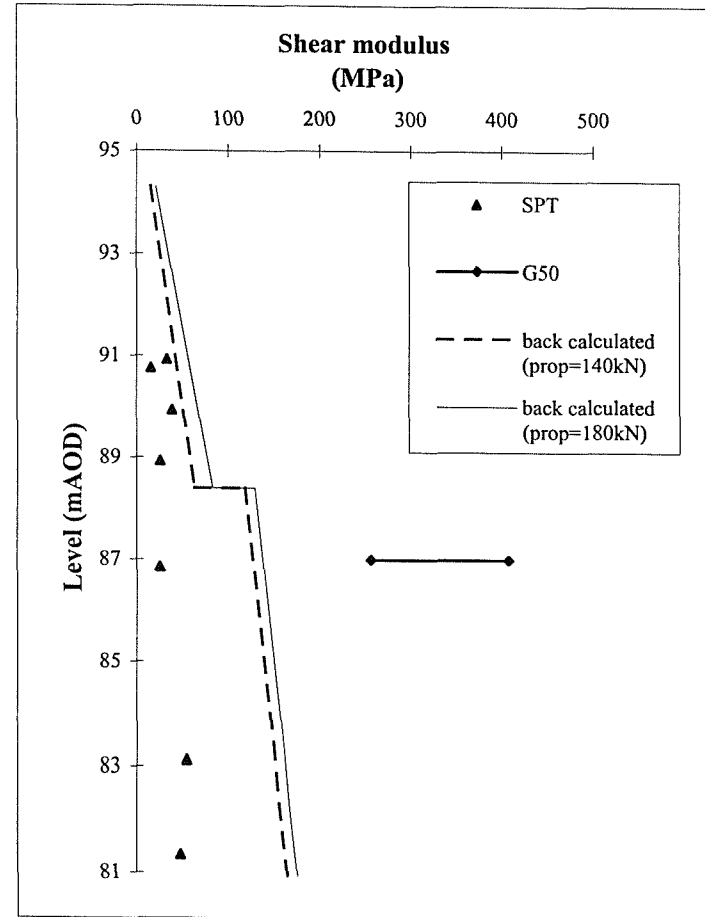


Figure 6.38. Comparison of back calculated and SPT stiffness values

This appears to be also the case for the weak rock mass at Coventry and might suggest that this assumption should also be made for similar situations.

### 6.11. Summary

It has been demonstrated that it is possible to determine both the stiffness profile and the pre-excitation stresses if a retaining wall rotates into and away from the excavation.

The pre-excitation horizontal stresses and the stiffness profiles for the two temporary prop pre-loads at the instrumented wall have been back calculated, and these are summarised in Table 6.9

<b>Prop pre-load (kN/m)</b>	<b>Parameter</b>	<b>Highly weathered rock</b>	<b>Moderately weathered rock</b>
<b>140</b>	<b>Stiffness parameters</b>	$E = 37.2 \text{ MPa} + 24 \text{ MPa/m}$	$E = 285 \text{ MPa} + 12 \text{ MPa/m}$
<b>140</b>	<b>Pre-excitation earth pressure</b>	$K_i = 0.92$	$K_i = 0.92$
<b>180</b>	<b>Stiffness parameters</b>	$E = 50 \text{ MPa} + 31 \text{ MPa/m}$	$E = 310 \text{ MPa} + 12 \text{ MPa/m}$
<b>180</b>	<b>Pre-excitation earth pressure</b>	$K_i = 0.95$	$K_i = 0.95$

**Table 6.9. Summary of back calculated properties**

For stabilising base retaining walls, it has been demonstrated that the pre-loading of the temporary props will help to reduce the wall movements into the excavation. However, pre-loading results in wall movements away from the excavation, hence heave and greater bending moments during the construction phase. These impacts should also be taken into consideration at the design stage.

The stiffness derived from geophysical tests is based on fundamental elastic theory and hence, should be reasonably accurate for the strain levels involved.

Provided the small strain stress-strain behaviour of the rock mass is not significantly non-linear there is no reason why wall movements predictions made using this method should not show good agreement with observed movements. However, they tend to underestimate wall movements if the additional effects of stress relief during wall installation are not taken into account.

In weak rock with closely spaced discontinuities it is unlikely that a representative volume of the rock mass is tested by a pressuremeter. Therefore if the mechanical disturbance of the test zone is not very significant, the stiffness values obtained from pressuremeter tests are more most likely to represent an intact value. If these are used to predict wall movements, it is likely that the wall movements will be underestimated.

The SPT does not measure stiffness and hence correlations proposed by various authors between SPT N value and E have no fundamental basis whatsoever. The relationships are purely empirical and hence rely to a large extent on the scope of the database which forms the basis for the relationship. In general these databases are too limited for weak rock to enable any reliable stiffness parameters to be obtained for use in design in weak rock.

It is recognised that excavation and concreting during the installation of a bored pile wall will alter the stress state of the soil, resulting in a different initial or pre-excavation lateral earth pressure coefficient, ( $K_i$ ). During construction of the bored piles forming the instrumented wall section the ground was supported by temporary casing to the base of the made ground, below which the hole was unsupported. The finite element analysis has shown that the lateral earth pressure coefficient tends to move towards unity during the construction of a bored pile wall. This is also the assumption used in many soil mechanics problems (e.g Powrie, 1986 and Tedd *et al*, 1984). It would appear that this assumption may also be used in weak rock problems, if installation is not modelled.

Provided the strength of the weak rock does not dominate the mass behaviour, it would appear that a continuum model is suitable for estimating wall movements and bending moments.

## ***CHAPTER 7***

### ***CONCLUSIONS***

#### **7.1. Introduction**

This research has generated a high-quality case record of a retaining wall embedded in weak rock (Bromsgrove Sandstone) at Coventry. The field data have been used to investigate suitable geotechnical parameters and models for use in the design of walls embedded in weak rock. In addition, the research has identified some of the advantages and disadvantages of the construction method used in this case, and highlighted some issues concerning the use of field instrumentation for stabilised base retaining walls. The major results and findings are summarised in this chapter and recommendations for further work is suggested.

## 7.2 The objectives

The overall aim of the research was to investigate suitable models, geotechnical parameters and methods of analysis for use in the design of walls embedded in weak rock. The specific objectives of the research were:

- i. To monitor in detail the performance of a retaining wall embedded in weak rock, during and shortly after construction.
- ii. To obtain geotechnical parameters for the weak rock involved, using conventional *in situ*, seismic and laboratory testing techniques.
- iii. To compare the range of stiffness parameters obtained using *in situ*, seismic and laboratory techniques, with those suggested by a back analysis of the behaviour of the wall.
- iv. To investigate suitable models, geotechnical parameters and methods of analysis for use in the design of walls embedded in weak rock, with reference to the data obtained from the case study.

## 7.3. Field monitoring

High-quality records of wall movements, bending moments, temporary prop loads, and vertical contact stresses under the permanent stabilising base of the instrumented retaining wall were obtained. Independent wall movement measuring techniques ensured that consistent sets of wall movement data were obtained for the case study. In addition, lines of instruments at different locations confirm the agreement between the measurements. Equilibrium analyses of the wall suggest that there is a consistency between the different measurements of prop load, vertical contact stress and base bending moments.

The field monitoring has reaffirmed:

- the desirability of datalogging the output from field instrumentation, which enables a continuous record to be obtained; and
- the necessity of recording temperatures when the measurements being made are temperature sensitive.

Temperatures changes have an influence on the prop loads and readings taken from fluid filled pressure cells. It has been shown that these can both be compensated for if a temperature compensation factor is obtained over a period of time when no construction activity is taking place.

#### **7.4. *In situ* field tests**

Geotechnical parameters for the weak rock involved (Bromsgrove sandstone), were obtained using conventional *in situ*, seismic and laboratory testing techniques.

It was shown that the shear moduli determined from the initial loading stages of the pressuremeter tests were smaller than those determined from the unload/reload loops. This was not unexpected, as generally the initial loading curve from a pressuremeter test is influenced by drilling disturbance. However, it would appear that unload/reload parameters obtained from the pressuremeter tests at Coventry are also influenced by the initial drilling disturbance. The shear parameters obtained from the pressuremeter tests at Coventry are therefore not representative of the intact value of the weak rock, but are more likely to represent a disturbed value.

The stiffness parameters deduced from empirical correlations with SPT blowcount were very low. This was likely to be due to disturbance ahead of the bottom of the borehole produced by the drilling method and the empirical correlations between N value and E being site specific. The relationships between N and E are purely empirical, and hence rely on the scope of the database which forms the basis for the relationship. The

database is too limited to enable any reliable stiffness parameters to be obtained from SPT blowcount for weak rock.

The shear modulus parameters determined from the geophysical tests were the only parameters obtained from all the tests that were representative of the mass stiffness of the weak rock at Coventry.

### **7.5. Significance of results for engineering practice**

It is clear that the selection of a design approach for a retaining wall in weak rock should depend primarily on the presence and nature of the discontinuities. It follows that a detailed discontinuity survey should form part of the site investigation for an excavation in weak rock. The pattern and nature of the discontinuities would then influence the design methodology. as follows

- where discontinuities are included in a rock mass but do not influence the overall stability of the excavation, an equivalent continuum analysis may be used in which the stiffness profile is determined from field tests involving a volume of material sufficient to represent the behaviour of the mass. This has been demonstrated to be the case at the monitored section of wall.
- where discontinuities are included in a rock mass with a dip angle that is greater than the relative shear strength of the discontinuity, the discontinuities will control the design and a method that explicitly takes into account the properties of the discontinuity (e.g. limit equilibrium or discrete element analysis) should be used.

The findings from the back analysis suggest that:

- The stiffness parameters derived from geophysical tests seem to be appropriate for the strain levels involved with normal, in service retaining wall movements. Provided the small strain stress-strain behaviour of the rock mass is not significantly non-linear there is no reason why wall movements predictions made using this method should not show good agreement with observed movements. However, wall



movements will tend to be underestimated if the additional effects of stress relief during wall installation are not taken into account.

- In weak rock with closely spaced discontinuities it is unlikely that a representative volume of the rock mass is tested by a pressuremeter. If the mechanical disturbance of the test zone is not very significant, the stiffness values obtained from pressuremeter tests are more likely to represent an intact value. If these are used to predict wall movements, it is likely that the wall movements will be underestimated.
- The SPT does not measure stiffness and hence correlations proposed by various authors between SPT N value and E have no fundamental basis whatsoever. The relationships are purely empirical and rely to a large extent on the scope of the database which forms the basis for the relationship. In general these database are too limited for weak rock to enable any reliable stiffness parameters to be obtained for use in design.

It is recognised that excavation and concreting during the installation of a the bored pile wall will alter the stress state of the weak rock, resulting in a different initial or pre-excavation lateral earth pressure coefficient, ( $K_i$ ). During construction of the bored piles forming the instrumented wall section the ground was supported by temporary casing to the base of the made ground, below which the hole was unsupported. The finite element analysis has suggested that the lateral earth pressure coefficient tends to move towards unity in the ground adjacent to the wall, during the construction of a bored pile wall. This is also the assumption used in many soil mechanics problems (e.g Powrie, 1986 and Tedd *et al*, 1984). It would appear that this assumption might also be used in weak rock problems, if installation is not modelled.

## **7.6. Construction sequence effects**

For stabilising base retaining walls, it has been demonstrated that pre-loading the temporary props will help to reduce the wall movements into the excavation. However, pre-loading results in wall movements away from the excavation and greater bending moments during the construction phase. These impacts should also be taken into consideration at the design stage.

## **7.7. Further research**

Generally, when a research project is completed, it does not mean that the research into the problem investigated has also been completed. Suggestions for further research can usually be made. On the basis of the research described in this thesis the following suggestions for further work might be made.

- A test programme looking into the stress strain behaviour of jointed weak rock masses is required to confirm that weak rock masses behave as a linear elastic material for the strain levels involved with normal, in service retaining wall movements. This could possibly be carried out using large diameter plate loading/unloading test studies on different weak rock types. However, the test method might need to be improved, in order to obtain data at the strain levels involved with normal, in service retaining wall movements.
- Further case studies are required to confirm the behaviour of retaining walls, for the situation where the discontinuity dip direction dominates the stability of the excavation. In this case, it is most likely that the properties of the joints will dominate the behaviour of the retaining wall. It is therefore very important that stiffness and strength data of the discontinuities are obtained at any such case study, so they could be directly used in the discrete element method when back analysing any such retaining wall.
- The SPT database for the empirical correlations between N value and E need to be improved for weak rock in the UK. Any new correlations should include a

description of the weak rock it applies to. This might help to find correlations that are more general for the different types of weak rock encountered in the UK.

- A better technique is required for installing weak rock pressuremeters in order to reduce the amount of borehole disturbance. Otherwise, this type of testing is likely to yield disturbed stiffness parameters. Alternatively, the bedding/disturbance might be overcome if the tests are performed at higher pressures than those for the majority of the tests carried out at the case study in this thesis. However, further work is required to confirm this.

- Askegaard, V. (1961).** Measurements of pressure between a rigid wall and a compressible medium by means of pressure cell. Acta Polytechnica Scandinavica, Civil Eng. and Building Construction Series, No 11. Copenhagen: Technical University of Denmark.
- Auld, B. (1997).** Cross-hole and down-hole  $V_s$  by mechanical impulse. Journal of Geotechnical Engineering, ASCE, 103, 3, 545-562.
- Bandis, S.C., Lumsden, A.C., and Barton N.R (1983).** Fundamentals of rock joint deformation. Int. Journal Rock Mech. Min. Sci. & Geomech, 20, 249-268.
- Barton, N. (1986).** Deformation phenomena in jointed rock. Geotechnique, 36, 2, 147-167.
- Batten, M. (1998).** Prop loads in two large braced excavations. PhD Thesis University of Southampton.
- Bieniawski, Z.T. (1973).** Engineering classification of jointed rock masses. The Civil Engineer in South Africa, 15, 335-343.
- Bieniawski, Z.T. (1989).** Engineering Rock Mass Classifications. J.Wiley & Sons, New York.
- British Standards institution (1994).** Code of practice for earth retaining structures BS8002. British Standards Institution, London.
- British Standard institution, Anon (1981).** Code of practice for site investigations BS5930. British Standards Institution, London.
- Britto, A.M. and Gunn, M.J. (1987).** Critical state soil mechanics via finite elements. Ellis Horwood, Chichester.

**Brown, E.T. (1993).** The nature and fundamentals of rock engineering. Comprehensive rock engineering, Pergamon Press Ltd, Oxford.

**Burland, J.B. (1990).** On the compressibility and shear strength of natural clays. Geotechnique, 40, 3, 329-378.

**Burland, J.B. and Kalra, J.C. (1986).** Queen Elizabeth II conference centre: geotechnical aspects. Proc. Instn. Civil Eng., 80, 1479-1504.

**Burland, J.B. and Lord, J.A. (1970).** The load deformation behaviour of the middle Chalk at Mundford, Norfolk: a comparison between full-scale performance and in situ and laboratory measurements. Proc. Conf. on In situ Investigations in Soils and Rocks, BGS, London, 3-15.

**Carder, D.R. (1998).** Personal communication.

**Carder, D.R. (2000).** Personal communication.

**Carder, D.R. and Krawczyk, J.V. (1975).** Performance of cells designed to measure soil pressure on earth retaining structures. TRL Report 766. Transportation and Road Research Laboratory, Crowthorne.

**Carder, D.R. and Symons, I.F. (1989).** Long term performance of a propped retaining wall embedded in stiff clay. TRL Report 273. Transportation and Road Research Laboratory, Crowthorne.

**Chandler, R.J. (1969).** The effect of weathering on shear strength properties of Keuper Marl. Geotechnique, 19, 3, 321-334.

- Clarke, B.G. (1995).** Pressuremeters in geotechnical design. Blackie Academic & Professional, Glasgow.
- Clarke, B.G. and Allan, P.G. (1989).** A self-boring pressuremeter for testing weak rock. Proc. 12<sup>th</sup> Int. Conf. SMFE, Brazil, 1, 211-213.
- Clayton, C.R.I. (1990).** The mechanical properties of the chalk. Keynote address. Proc. Int. Symp.on chalk, Brighton. 213-238. Thomas Telford, London.
- Clayton, C.R.I. (1995).** The standard penetration test (SPT): methods and use. CIRIA Report 143, Construction Industry Research & Information Association, Butterworths, London.
- Clayton, C.R.I. and Bica, A.V.D. (1993).** The design of diaphragm-type boundary total stress cells. Geotechnique, 43, 4, 523-535.
- Cuccovillo, T. and Coop, M.R. (1997).** Yielding and pre-failure deformation of structured sands. Geotechnique, 47, 3, 491-508.
- Cuccovillo, T. (1995).** Shear behaviour and stiffness of naturally cemented sands. PhD thesis. University of London.
- Cundall, P.A. (1971).** A computer model for simulating progressive large scale movements in blocky rock systems, Rock Fracture, Proc. Int. Symp. Rock Fracture, Nancy, papers 2-8.
- Davies, T.J. and Barton M.E. (1998).** Precise geological characterisation for the wider application of high quality site data. Proc. 1<sup>st</sup> Int. Conf on Site Characterisation, Atlanta, USA, 1, 133-138.

- Deere, D.U. (1967).** Design of surface and near surface construction in rock, Failure and Breakage of rock. Proc. 8<sup>th</sup> Symp. Rock Mech. American Int. of Mining, Metall. & Petro. Eng.,, 237-276.
- Duncan, J.M. and Goodman, R.E. (1968).** Finite element analyses of slopes in jointed rock. Report S-68-3, U.S. Army Engineers waterways Experiment Station, Vicksburg.
- Ervin, M.C., Burman, B.C. and Hughes, J.M.O. (1980).** The use of a high capacity pressuremeter for design of foundations in medium strength rock. Proc. Int. Conf. on Structural Foundations in Rock, Sydney, 9-16.
- Exploration Associates Ltd (1989).** Coventry North-South, Phase II. Factual report on preliminary and main ground investigations, No E7482/8.
- Exploration Associates Ltd (1993).** Coventry North-South, Phase II. Supplementary site Investigations, No 113333.
- Exploration Associates Ltd (1994).** Coventry North-South, Phase II. Interpretative report on ground investigations, No E7482/14.
- Gaziev, E. and Erlikhman, S. (1971).** Stresses and strains in anisotropic foundations, Rock Frature, Proc. Int. Symp. Rock Fracture, Nancy, paper 2-1.
- Gerrard, C.M. (1982).** Equivalent elastic moduli of a rock mass consisting of orthorhombic layers. Int.J.Rock.Min.Sci & Geomech. 19, 5-23.
- Gibson, R.E. and Anderson, W.F. (1961).** Insitu measurement of soil properties with the pressuremeter. Civ. Engg. Wks. Rev. 56: 615-618.

- Goodman, R.E. (1976).** Methods of geological engineering in discontinuous rock. West, New York.
- Goodman, R.E. (1989).** Introduction to rock mechanics. 2<sup>nd</sup> edition, John Wiley & Son, New York.
- Goodman, R.E., Taylor, R.L. and Brekke, T.L. (1968).** A model for the mechanics of jointed rock. Journal of Soil Mech. & Found. Div., ASCE, 94, 637-659.
- Gourvenec, S. (1998).** Three dimensional effects of diaphragm wall installation and stage construction sequences. PhD Thesis, University of Southampton.
- Gunn, M.J. and Clayton, C.R.I., (1992).** Installation effects and their importance in the design of earth retaining structures. Geotechnique, 42, 1, 137-141.
- Harberfield, C.M. and Johnston, I.W. (1990).** A numerical model for pressuremeters testing in weak rock. Geotechnique, 40, 4, 569-580.
- Harberfield, C.M. and Johnston, I.W. (1993).** Factors influencing the interpretation of pressuremeters in soft rock. Geotechnology conference on hard soils-soft rocks, Athens, 1, 525-531.
- Hoek, E. and Bray, J.W. (1981).** Rock Slope Engineering. 3<sup>rd</sup> edition, Institution of Mining and Metallurgy, E & FN Spon, London.
- Hoek, E. and Brown, E.T. (1980).** Empirical strength criterion for rock masses. Journal of Geotech. Eng. Div., ASCE, 106, 1013-1035.
- Hoek, E. and Brown, E.T. (1988).** The Hoek-Brown failure criterion-a update. Proc. 15<sup>th</sup> Candian. Rock Mech. Symp., Toronto, 31-38.



- Hope, V., Sutton, J.A. and Clayton, C.R.I. (1997).** The use of seismic geophysics in the characterisation of a weak rock site. Proc. 1<sup>st</sup> Int. Conf on Site Characterisation, Atlanta, USA, 1, 479-484.
- Hudson, J.A. (1989).** Rock mechanics principles in engineering practice. CIRIA Report TA 706, Construction Industry Research & Information Association, Butterworths, London.
- International Society for Rock Mechanics (1981).** Rock characterization, testing and monitoring: ISRM suggested methods, Site Characterization, Pergamon Press, Oxford.
- International Society for Soil Mechanics and Foundation Engineering (1985).** Technical committee report on undisturbed and Laboratory testing of soft rocks and indurated soils. ISSMFE.
- Jardine, R.J., Potts, D.M., Fourie, A.B. and Burland, J.B. (1986).** Studies of the influence of non-linear stress-strain characteristics in soil-structure interaction. Geotechnique, 36, 3, 377-396.
- Jewell, R.J. and Fahey, M. (1984).** Measuring properties of rock with high pressure pressuremeter. Proc. Australia-New Zealand Conf. on Geomechanics, Perth, 2, 535-539.
- Johnston, I.W. & Novello, E.A. (1994).** Soil mechanics and soft rock technology. Proc ICE, Geotechnical Eng. 107, 1, 3-9.
- Kim, Y.S., Ochi, K. and Tatsuoka, F. (1990).** Strength and deformation properties of mudstones in triaxial compression. Proc. 8<sup>th</sup> Japanese Symp. on Rock Mech. 357-362.

- Kulhawy, F.H. (1975).** Stress deformation properties of rock and rock discontinuities. *Engineering Geology*, 9, 327-350.
- Kulhawy, F.H. (1978).** Geomechanical model for rock foundation settlement. *Journal of the Geotechnical Engineering Division, ASCE*, 104.
- Leach and Thompson (1979).** The design and performance of large diameter bored piles in weak mudstones rocks. *Proc 7<sup>th</sup> Euro. Conf. On Soil Mech. & Found. Eng.*, Brighton, 101-108.
- Leroueil, S. and Vaughan, P.R. (1990).** The general and congruent effects of structure in natural soils and weak rocks. *Geotechnique*, 40, 3, 467-488.
- Lo, K.Y. (1970)** The operational strength of fissured clays. *Geotechnique* 20, 1, 57-74.
- Mair, R.J. (1993).** Developments in geotechnical engineering research: application to tunnels and deep excavations. *Unwin Memorial Lecture, Proc. of ICE Civil Eng.*, 93, 27-41.
- Mair, R.J. and Wood, D.M. (1987).** In situ pressuremeter testing: methods testing and interpretation. *CIRA Report, Construction Industry Research & Information Association, Butterworths, London.*
- Marsland, A. (1972).** Clays subjected to in situ plate tests. *Ground Engineering*, 5, 24-31.
- Markland, J.T. (1972).** A useful technique for estimating the stability of rock slopes when the rigid wedge slide type of failure is expected. *Imperial College Rock Mechanics Research Report, No 19.*

- Matthews, M.C. (1993).** The mass compressibility of fractured chalk. PhD thesis. University of Surrey.
- Matthews, M.C. and Clayton, C.R.I. (1992).** Compressibility of jointed rock with special reference to the chalk. Proc. I.S.R.M. Symposium on Rock Characterisation (Eurock 92). British Geotechnical Society, 445-450.
- Matthews, M.C, Clayton, C.R.I. & Russell, C.S. (1993).** Assessing the mass compressibility of chalk from visual description. The engineering geology of weak rock, 337-345, Balkema, Rotterdam.
- Old, R.A, Bridge, D.McC and Rees, J.G.(1990).** Geology of the Coventry area. British Geological Survey Technical Report WA/89/29.
- Potts, D.M. and Burland, J.M. (1983).** A numerical investigation of the retaining walls of the Bell Common Tunnel. TRL Report 783, Transportation and Road Research Laboratory, Crowthorne.
- Powrie, W.P. (1986).** The behaviour of diaphragm walls in clay. PhD Thesis, Cambridge University.
- Powrie, W. and Li. E.S.F. (1991).** Finite element analysis of an in situ wall propped at formation level. Geotechnique, 41, 4, 499-514.
- Richards, D.J., Holmes, G.J., and Beadman, D. (1999).** Measurement of Temporary prop loads during the construction of the Mayfair Underground Car Park, London. Proc. Inst. Of Civil Eng., 137, 165-174.
- Rowe, P.W. (1972).** The relevance of soil fabric to site investigation practice. Geotechnique 22, 2, 195-300.

- Schuil-Brewer, T.J (2001).** Future PhD Thesis.
- Serafim, J.L. and Pereira, J.P. (1983).** Considerations of the geomechanical classification of Bieniawski. Proc. Int. Symp. on Eng. Geology and Under Ground Construction, Lisbon, 1, 33-42.
- Skempton, A.W., Schuster, R.L. & Petley, D.J. (1969).** Joints and fissures in the London clay at Wraybury and Edgware. Geotechnique 19, 2, 205-217.
- Singh, B. (1973).** Continuum characterisation of jointed rock masses. Int. Journal. Rock. Mech. Min. Sci. & Solids, 23, 371-394.
- Stroud, M.A. (1988).** Introduction to papers 1 to 8. Geotechnology conference on penetration testing in the U.K. ICE, Birmingham.
- Tatsuoka, F., Kohata, Y., Ochi, K., Kim, Y. and Shi, D. (1993).** Measuring small strain stiffness of soft rocks. Geotechnical Engineering of Hard Soils-Soft Rocks, 809-816, Balkema, Rotterdam.
- Taylor, D.W. (1947).** Pressure distribution theories, earth pressure cell investigation and pressure distribution data. Vicksburg: US Army Engineer Waterways Experiment Station.
- Tedd, P., Chard, B.M., Charles, J.A. and Symons, I.F., (1984).** Behaviour of a propped embedded retaining wall in a stiff clay at Bell Common. Geotechnique, 34, 4, 513-532.
- Terzaghi, K. (1936).** Stability of slopes of natural clay. Proc. 1<sup>st</sup> Int. Conf. Soil Mech. Found. Eng, Cambridge, Mass., 1, 161-165.

**Thompson, R.P. and Leach, B.A. (1988).** The application of the SPT in weak sandstone and mudstone rocks. Geotechnology conference on penetration testing in the U.K. ICE, Birmingham.

**Trollope, D.H. and Lee, I.K. (1961).** The measurement of soil pressures. Proc. 5<sup>th</sup> Int. Conf. On Soil Mech., Paris, 2, 493-499.

**Twine, D. and Roscoe, H. (1999).** Temporary propping of deep excavations-guidance on design. CIRIA Publication C517, London.

**Ward, W.H., Samuels, S.G. & Butler, M.E. (1959).** Further studies of the properties of London clay. Geotechnique 9, 1, 33-138.

**Wood L.A. and Perrin A.J. (1984).** Observations of a strutted diaphragm wall in London clay: a preliminary assessment. Geotechnique, 34, 4, 563-579.

**Zienkiewicz, O.C. and Pande, G.N. (1977).** Time dependent multilaminate model of rocks – A numerical study of deformation and failure of rock masses. Int. Jour. Numer. Anal. Meth. Gemech, 1, 219-247.